256p.

mfs

N64-176[illegible] *

CODE-1

CR-55929

[redacted]

OTS PRICE

XEROX $ 16.50 ph

MICROFILM $ 2.88 mf.

REPUBLIC
AVIATION CORPORATION

RAC 1333
SSD-1027
17 June 1963

t SYNCHRONOUS METEOROLOGICAL SATELLITE (SMS) STUDY,

Final Report, Feb. - May 1963

Volume 4

Attitude and Station Control

(NASA CR-55929; RAC 1333; SSD-1027) OTS: $---

auth 17 Jun. 1963 256p refs

Prepared for
NATIONAL AERONAUTICS AND SPACE ADMINISTRATION
Goddard Space Flight Center
Greenbelt, Maryland

under
NASA Contract ~~No.~~ NAS5-3189

1948322 REPUBLIC AVIATION CORPORATION
Farmingdale, ~~L.I.~~, N.Y.

NASA CR 55427

FOREWORD

This final report on Contract NAS 5-3189 is presented by Republic Aviation Corporation to the Goddard Space Flight Center of the National Aeronautics and Space Administration and consists of the seven volumes listed below. The period of the contract work was February through May, 1963.

The sub-titles of the seven volumes of this report are:

1 Summary and Conclusions
2 Configurations and Systems
3 Meteorological Sensors
4 Attitude and Station Control
5 Communications, Power Supply, and Thermal Control
6 System Synthesis and Evaluation
7 Classified Supplement on Sensors and Control

Except for Volume 7, all of these are unclassified. Volume 7 contains only that information on specific subsystems which had to be separated from the other material because of its present security classification. Some of these items may later be cleared for use in unclassified systems.

Volumes 3, 4, and 5 present detailed surveys and analyses of subsystems and related technical problems as indicated by their titles.

In Volume 2, several combinations of subsystems are reviewed as complete spacecraft systems, including required structure and integration. These combinations were selected primarily as examples of systems feasible within different mass limits, and are associated with the boosters to be available.

Volume 6 outlines methods and procedures for synthesizing and evaluating system combinations which are in addition to those presented in Volume 2.

Volume 1 presents an overall summary and the principal conclusions of the study.

TABLE OF CONTENTS

Section	Title	Page
1	INTRODUCTION	1-1
2	ATTITUDE CONTROL	2-1
	A. Attitude Reference Sensor Survey	2-1
	1. Radio Frequency Attitude Sensing	2-1
	2. Optical Attitude Sensing	2-2
	3. Map Matching	2-4
	4. Infrared Horizon Sensors	2-5
	a. Advanced Technology Laboratories	2-5
	b. Barnes Engineering Co.	2-6
	c. Honeywell, Boston	2-6
	5. Star Tracking	2-7
	6. Sun Tracking	2-7
	7. Magnetometers	2-8
	8. Differential Gravity Gradient Sensing	2-8
	9. Stellar Drift Sensing	2-9
	10. Gyro Rate Sensing	2-9
	11. Selected Attitude Reference Sensors	2-10
	a. Infrared Horizon Sensors	2-10
	b. Star Tracking	2-14
	c. Sun Tracking	2-15
	d. Gyro Rate Sensing	2-16
	12. Conclusions	2-18
	13. Areas of Future Study	2-19
	a. Gyroscopes	2-19
	b. Polaris Tracker	2-19
	c. High Accuracy Laser Attitude System	2-19
	d. Horizon Sensors	2-19
	e. Map Matching	2-19
	f. Earth's Magnetic Field at Synchronous Altitude	2-19

TABLE OF CONTENTS (Continued)

Section	Title	Page
B.	Torquers	2-20
1.	Reaction Wheels	2-20
2.	Reaction Sphere	2-20
3.	Gyro Torquing Devices	2-22
a.	GLOPAC	2-22
b.	Twin Gyro Controller	2-23
1)	Weight	2-25
2)	Power	2-26
3)	Size	2-28
4.	High Pressure Cold Gas	2-28
5.	Solid Subliming Gas	2-29
6.	Cap Pistol	2-30
7.	Electric Propulsion	2-30
a.	Plasma Pinch Engine	2-30
b.	Electrostatic (Ion) Engine	2-30
8.	Hot Gas Systems	2-31
9.	Magnetic Torquers	2-32
10.	Vaporjet	2-32
11.	Diffusion of Hydrogen through Palladium	2-32
12.	Brushless DC Motor	2-33
13.	Conclusions	2-33
C.	Disturbance Torques	2-35
1.	Introduction	2-35
2.	Disturbance Torque Calculations	2-35
a.	Predictable Solar Torques	2-35
1)	Pressure Due to Incident Radiation and Reflection on a Flat Plate	2-36
2)	Diffuse Reradiation Analysis Based on Lambert's Cosine Law	2-37
3)	Radiation Normal to the Axis of a Circular Cylinder	2-40
4)	Inclined Cylinder (Angle Between the Incident Radiation and the Axis of the Cylinder is 90-ϕ)	2-41

TABLE OF CONTENTS (Continued)

Section | Title | Page

5) Spin Stabilized Vehicles 2-45
6) 3-Axis Stabilized Vehicle 2-47
7) Gravity Gradient Vehicle 2-56
b. Gravity Gradient Torque 2-57
c. Magnetic Torques Due to Interaction with the Earth's Field 2-57
d. Equipment Dependent Disturbances 2-57
1) Vidicon Equipment 2-59
2) Infrared Systems 2-59
3) Disturbance Torque Due to Rotation of Solar Paddles 2-60
e. Orbit Coupling Torque 2-61
f. Attitude Disturbance Torque during Ascent 2-62
3. Disturbance Torque Model 2-64
4. Areas for Future Study 2-64
a. Solar Disturbing Torques 2-64
b. Magnetic Torque Disturbances 2-69
c. Final Equipment Design 2-69
D. System Descriptions 2-70
1. 3-Axis Stabilized Spacecraft 2-70
a. Control Logic Functions 2-72
1) Priority Logic 2-72
2) Acquisition and Reacquisition 2-72
3) Dumping Logic 2-72
4) Injection Velocity Correction Logic 2-72
5) Station Keeping Logic 2-72
b. Operational Modes 2-72
1) Automatic Solar Paddle Drive Control 2-72
2) Command Rate Control 2-73
3) Command Control of Pitch and Roll Bias 2-73
c. Alternate 3-Axis Systems 2-73

TABLE OF CONTENTS (Continued)

Section	Title	Page
	2. Gravity Gradient Spacecraft	2-74
	a. Earth Tracking Mode	2-74
	b. Earth Acquisition Mode	2-74
	3. Spin Stabilized Spacecraft	2-76
	a. Spin System Control Modes	2-76
	1) Acquisition and Reacquisition Mode	2-77
	2) Earth Tracking Mode	2-78
	4. Control and Stabilization Performance Summary	2-78
E.	Earth Tracking-Dynamic Analysis and Simulation	2-79
	1. Discrete - Continuous Controller	2-79
	a. Introduction	2-79
	b. Analysis	2-80
	1) Single Axis	2-80
	2) Coupled System	2-84
	c. Analog Computer Simulation	2-88
	2. Gyrocompass Yaw Control System	2-96
	a. Introduction	2-96
	b. Discussion	2-96
	1) The Gyrocompass Principle	2-96
	2) Application of Gyrocompass to Yaw Control	2-98
	c. Dynamic Analysis	2-99
	1) General	2-99
	2) Yaw Alignment	2-102
	3) Tracking Mode	2-102
	4) Pitch Wheel Spin-Up	2-102
	d. Analog Simulation	2-104
	1) General	2-104
	2) Pitch Wheel Spin-Up	2-104
	e. Summary of Parameters	2-110

TABLE OF CONTENTS (Continued)

Section	Title		Page
	f.	Effects of Actual Horizon Scanner Characteristics	2-111
		1) Effect of Horizon Scanner Noise	2-111
		2) Effect of Horizon Sensor Dead Zone	2-111
3.	Discrete Controller		2-113
	a.	Ion Engine Control System	2-113
	b.	Hardware	2-113
	c.	Sensors	2-118
	d.	Plasma Engine Control System	2-118
4.	Continuous Noncoupling Systems		2-118
	a.	Summary	2-118
	b.	Discussion	2-119
		1) Limit Cycle Criteria	2-119
	c.	Pulse Logic Mechanizations	2-122
		1) Introduction	2-122
		2) Rate Stable Pulsing	2-122
		3) Pseudo-Rate Pulsing	2-122
		4) Error Pulsing without Rate Information	2-123
	d.	Application of Pseudo Rate to SMS	2-126
		1) Introduction	2-126
		2) Acquisition Mode	2-126
		3) Limit Cycle Operation	2-130
	e.	Reaction Jet Characteristics in Pulsed Mode Operation	2-131
		1) Introduction	2-131
		2) Cold Gas	2-131
		3) Liquid Hypergolics	2-131
		4) Hydrogen Peroxide	2-131
5.	Gravity Gradient Controller		2-131
	a.	Introduction	2-131
	b.	Vehicle Control System Analysis	2-132

TABLE OF CONTENTS (Continued)

Section	Title	Page
	6. Spin Controller	2-145
	a. Introduction	2-145
	b. Impulse Torquer Requirements	2-147
	F. Earth Acquisition and Reacquisition	2-148
	1. Introduction	2-148
	2. Attitude Stabilization during Transfer Ellipse	2-148
	a. Spin Stabilization	2-148
	b. 3-Axis Spacecraft Stabilization	2-150
	c. Conclusions	2-151
	3. Acquisition and Reacquisition for Various Vehicle and Control System Configurations	2-151
	a. Earth Acquisition of the 3-Axis Stabilized Spacecraft	2-152
	b. Earth Acquisition for Gravity Gradient Spacecraft	2-154
	c. Earth Acquisition for Spin Controlled Spacecraft	2-155
3	ORBIT GETTING AND STATION KEEPING	3-1
	A. Ascent, Orbit Injection, and Correction	3-1
	1. Summary	3-1
	2. Introduction	3-1
	3. Low Altitude Waiting Trajectory	3-2
	a. General	3-2
	b. Phasing Requirements	3-2
	4. High Altitude Waiting Trajectory	3-6
	5. Injection Errors	3-8
	a. The Effect of Orbit Element Errors on the Subsatellite Pattern	3-8
	b. Correction of the Given Injection Errors (Impulsive)	3-9
	c. Correction of the Given Injection Errors (Nonimpulsive)	3-10
	d. Correction Technique for Low Altitude Waiting Ascent	3-10

TABLE OF CONTENTS (Continued)

Section — Title — Page

- e. Correction Technique for High Altitude Waiting Ascent 3-10
  - 1) Eastward Drift 3-10
  - 2) Westward Drift 3-11
  - 3) Intermediate Drift Correction 3-11
- 6. Propulsion Requirements 3-13
  - a. Apogee Kick Maneuver 3-13
  - b. Injection Error Correction 3-13
- 7. Conclusions 3-13

B. Perturbations 3-15

- 1. Summary 3-15
- 2. General 3-15
- 3. Earth Oblateness and Extra-Terrestrial Perturbations 3-15
  - a. General 3-15
  - b. Semimajor Axis 3-16
  - c. Eccentricity 3-18
  - d. Argument of Perigee 3-18
  - e. Right Ascension of the Ascending Node 3-18
  - f. Inclinations 3-18
  - g. Perigee Passage 3-19
  - h. Summary of Drift Perturbations for an Equatorial Orbit 3-19
  - i. Inclined Orbit 3-19
- 4. Terrestrial Perturbations - Tesseral and Sectorial Harmonics 3-20
  - a. General 3-20
  - b. Large Angle Longitude Excursions 3-20
  - c. Nodal and Inclination Perturbations 3-21
  - d. Small Angle Excursions for an Indirect Orbit 3-22
  - e. Ideal Station Keeping Requirements 3-25
- 5. Injection Altitude Correction 3-26
  - a. General 3-26
  - b. Polar Flattening 3-26

TABLE OF CONTENTS (Continued)

Section	Title	Page
	c. Lunar-Solar Gravitation	3-26
	d. Nodal Regression	3-27
	e. Summary of Altitude Errors	3-28
	6. Conclusions	3-28
	C. Station Keeping	3-30
	1. Introduction and Summary	3-30
	2. Station Keeping Against Terrestrial Gravitational Disturbances	3-32
	a. Equations of Motion	3-32
	b. Guidance Approach	3-32
	c. System Simulation on the Analog Computer	3-35
	d. Analog Computer Analysis	3-35
	1) Effects of Thrust Forces on the Orbit	3-35
	2) Effects of the Equatorial Ellipticity of the Earth	3-36
	3) Initial Guidance Study	3-41
	4) Parametric Variations of System Components	3-47
	5) Injection Error Study	3-47
	6) Orbit Eccentricity Caused by Constant Thrusting	3-48
	3. Conclusions	3-51
	D. List of Symbols	3-53
	E. References	3-55
4	CONTROL AND STATION KEEPING SYSTEM IMPLEMENTATION	4-1
5	SYSTEM IMPLICATIONS OF ATLAS-AGENA INJECTION ERRORS	5-1
	A. Injection Error Correction	5-1
	B. Attitude Control	5-2
	C. References	5-4

TABLE OF CONTENTS (Continued)

Section	Title	Page
Appendix A	DERIVATION OF COMPLETE MOMENT EQUATIONS	A-1
	A. Introduction	A-1
	B. Satellite Equations of Motion for Earth Tracking	A-1
	C. List of Symbols	A-5
Appendix B	ANALYTICAL SIMPLIFICATION	B-1
	A. Simplification of Tracking Equations	B-1
	B. Numerical Example of Simplification	B-1
Appendix C	THE INFLUENCE OF THE EARTH'S EQUATORIAL ELLIPTICITY ON THE NODAL AND INCLINATION PERTURBATIONS OF AN INCLINED 24-HOUR ORBIT	C-1

LIST OF ILLUSTRATIONS

SECTION 2

Figure	Title	Page
2-1	OGO Dual Tracker Casting	2-13
2-2	High Accuracy SMS Horizon Sensor Head	2-13
2-3	Bendix Sun Sensor Type 1771858	2-17
2-4	Honeywell GE159 Rate Gyro	2-17
2-5	Typical Reaction Wheel	2-21
2-6	Reaction Wheel Torque - Speed Curves	2-21
2-7	GLOPAC Gyro Orientation	2-24
2-8	Twin Gyro Controller	2-24
2-9	(a) High Pressure Cold Gas System	2-29
	(b) Solid Subliming Low Pressure Gas System	2-29
2-10	Torques Due to Solar Radiation - Spin Stabilized 1000 lb Vehicle - Winter Solstice	2-48
2-11	Torques Due to Solar Flare - Spin Stabilized 1000 lb Vehicle - Winter Solstice	2-48
2-12	Torques Due to Solar Radiation - 3-Axis Stabilized 1000 lb Vehicle - Winter Solstice	2-48
2-13	Torques Due to Solar Flare - 3-Axis Stabilized 1000 lb Vehicle - Winter Solstice	2-50
2-14	Torques Due to Solar Radiation - Gravity Gradient 1000 lb Vehicle - Winter Solstice	2-50
2-15	Torques Due to Solar Flare - Gravity Gradient 1000 lb Vehicle - Winter Solstice	2-58
2-16	Solar Torques - Spin Stabilized 500 lb Vehicle Shown for One Year	2-58
2-17	Block Diagram - 3-Axis Stabilized Control System	2-71
2-18	Block Diagram - Gravity Gradient Control System	2-75
2-19	Block Diagram - Spin Stabilized Control System	2-77
2-20	Block Diagram - Single Axis Reaction Wheel System	2-79
2-21	Typical Servomotor Reaction Wheel Characteristics	2-83
2-22	Typical "Flat" Reaction Wheel Characteristics	2-83
2-23	Attenuation Phase Margin Diagram	2-83
2-24	Horizon Scanner Dead Zone Characteristics	2-85
2-25	Describing Function for Horizon Scanner Dead Zones	2-85
2-26	Nichols Plot of Horizon Scanner Describing Function	2-85

LIST OF ILLUSTRATIONS (Continued)

SECTION 2 (Continued)

Figure	Title	Page
2-27	Block Diagram - Coupled Yaw-Roll System	2-87
2-28	Roll Angle Time History	2-87
2-29	Calculated Roll Reaction Wheel Momentum Time History	2-87
2-30	Block Diagram of Yaw-Roll Axes with Decoupling Computer	2-89
2-31	Computer Run of Vehicle Roll Attitude and Rate for Various Dumping Torque Levels	2-89
2-32	Peak Roll Attitude Excursion During Dump Interval as a Function of Dump Torque Magnitude	2-90
2-33	Peak Roll Rate During Dump Interval as a Function of Dump Torque Magnitude	2-90
2-34	Plot of Dump Time for Various Dump Torque Levels	2-90
2-35	Impulse Necessary to Dump at Various Torque Levels	2-90
2-36	Computer Run of Vehicle Attitude and Dump Time for a Horizon Scanner Dead Zone of 0.05°	2-91
2-37	Computer Run of Vehicle Attitude and Dump Time for a Horizon Scanner Dead Zone of 0.5°	2-92
2-38	Plot of Vehicle Attitude Error vs Horizon Scanner Dead Zone	2-93
2-39	Computer Run of 3-Axis Coupled System Response to a Steady Disturbance Torque	2-94
2-40	Computer Run of Yaw-Roll Coupled System Subjected to Sinusoidal Disturbance at Orbital Frequency	2-95
2-41	Computer Run of Yaw-Roll Coupled System Subjected to Sinusoidal Disturbance at Orbital Frequency (Orbital Rate Coupling Term ω_0 Removed)	2-99
2-42	Gyrocompass Yaw Attitude Control System - Proportional Control	2-105
2-43	Gyroscope Yaw Attitude Control System - Reaction Wheel with Auxiliary Dumping	2-106
2-44	Initial Yaw Alignment with Proportional Noncoupling Control Torques and Wheel Initially Up to Speed	2-107
2-45	Transient Response of Yaw-Roll Gyrocompass System for Initial Small Yaw Misalignment - No Yaw Damper	2-108
2-46	Initial Yaw Alignment while Accelerating Wheel Up to Speed (Proportional Noncoupling Control Torques)	2-109

LIST OF ILLUSTRATIONS (Continued)

Figure	Title	Page
	SECTION 2 (Continued)	
2-47	Gyrocompass System-Horizon Scanner Noise Effect on Tracking Accuracy	2-212
2-48	Power Required for Ion Engine 3-Axis Control System	2-114
2-49	Weight of Power Supply for Ion Engine 3-Axis Control System	2-116
2-50	Parametric Plot of Station Keeping System Characteristics - Ion Engine	2-117
2-51	Experimental Systems for Low Rate Limit Cycle Attitude Control	2-117
2-52	Block Diagram - Attitude Control System with Pseudo-Rate Compensation	2-124
2-53	Characteristic Switching Line Established by the Sum of Attitude and Pseudo-Rate	2-124
2-54	Block Diagram for Pseudo-Rate Mechanization	2-125
2-55	Phase Plane Diagram of Mercury System Switching Lines	2-125
2-56	Typical Trajectory - Mercury Type Switching Line	2-127
2-57	Phase Plane Diagram of Pseudo-Rate Control System for Different Values of Acceleration	2-127
2-58	Phase Plane Diagram of Pseudo-Rate Control System for Different Values of Time Constant	2-128
2-59	Phase Plane Diagrams of Pseudo-Rate Control System for Different Values of Gain (K)	2-128
2-60	Phase Plane Diagram of Pseudo-Rate Control System with Disturbance Torques	2-129
2-61	Phase Plane Diagram of Simple ON-OFF Control System	2-129
2-62	Loss of Specific Impulse vs Pulse Size	2-133
2-63	Typical System Configuration for a Gravity Gradient Controlled Space Vehicle	2-133
2-64	Single Axis Pitch, Roll, Gravity Gradient Control Loop	2-134
2-65a	Plot of Vehicle Length (r) vs Rate Loop Gain (K) for Various Values of Rate Loop Damping for Vehicle of Mass $M_1 = 3.11$ Slug	2-136
2-65b	Plot of Steady State Vehicle Attitude Error vs Constant Disturbance for Various Lengths of Vehicle Mass $M_1 = 3.11$ Slug	2-136

LIST OF ILLUSTRATIONS (Continued)

SECTION 2 (Continued)

Figure	Title	Page
2-65c	Plot of Peak Vehicle Attitude Error vs Sinusoidal Disturbance Torque for Various Lengths of Vehicle of Mass $M_1 = 3.11$ Slug and Damping Coefficient $\xi = 0.65$	2-137
2-65d	Plot of Peak Vehicle Rate vs Sinusoidal Disturbance Torques for Various Lengths of Vehicle of Mass $M_1 = 3.11$ Slug and Damping Coefficient $\xi = 0.65$	2-137
2-65e	Plot of Peak Vehicle Attitude Error vs Radius of Vehicle of Mass $M_1 = 3.11$ Slug and Damping Coefficient $\xi = 0.65$ for Various Sinusoidal Disturbance Torques	2-138
2-65f	Plot of Peak Vehicle Rate vs Radius of Vehicle of Mass $M_1 = 3.11$ Slug and Damping Coefficient $\xi = 0.65$ for Various Sinusoidal Disturbance Torques	2-138
2-66a	Plot of Vehicle Length (r) vs Rate Loop Gain (K) for Various Values of Rate Loop Damping for Vehicle of Mass $M_2 = 15.55$ Slug	2-139
2-66b	Plot of Peak Vehicle Attitude Error vs Constant Disturbance for Various Lengths of Vehicle of Mass $M_2 = 15.55$ Slug	2-139
2-66c	Plot of Peak Vehicle Attitude Error vs Sinusoidal Disturbance Torque for Various Lengths of Vehicle of Mass $M_2 = 15.55$ Slug and Damping Coefficient $\xi = 0.65$	2-140
2-66d	Plot of Peak Vehicle Rate vs Sinusoidal Disturbance Torque Torque for Various Lengths of Vehicle of Mass $M_2 = 15.55$ Slug and Damping Coefficient $\xi = 0.65$	2-140
2-66e	Plot of Peak Vehicle Attitude Error vs Radius of Vehicle of Mass $M_2 = 15.55$ Slug and Damping Coefficient $\xi = 0.65$ for Various Sinusoidal Disturbance Torques	2-141
2-66f	Plot of Peak Vehicle Rate vs Radius of Vehicle of Mass $M_2 = 15.55$ Slug and Damping Coefficient $\xi = 0.65$ for Various Sinusoidal Disturbance Torques	2-141
2-67a	Plot of Vehicle Length vs Rate Loop Gain for Various Values of Rate Loop Damping for Vehicle of Mass $M_3 = 31.10$ Slug	2-142
2-67b	Plot of Steady State Vehicle Attitude Error vs Constant Disturbances for Various Lengths of Vehicle of Mass $M_3 = 31.10$ Slug	2-142
2-67c	Plot of Peak Vehicle Attitude vs Sinusoidal Disturbance Torques for Various Lengths of Vehicle Mass $M_3 = 31.10$ Slug and Damping Coefficient $\xi = 0.65$	2-143

LIST OF ILLUSTRATIONS (Continued)

SECTION 2 (Continued)

Figure	Title	Page
2-67d	Plot of Peak Vehicle Rate vs Sinusoidal Disturbance Torques for Various Lengths of Vehicle of Mass M_3 = 31.10 Slug and Damping Coefficient $\xi = 0.65$	2-143
2-67e	Plot of Peak Vehicle Attitude Error vs Radius of Vehicle of Mass M_3 = 31.10 Slug and Damping Coefficient $\xi = 0.65$ for Various Sinusoidal Disturbance Torques	2-144
2-67f	Plot of Peak Vehicle Rate vs Radius of Vehicle of Mass M_3 = 31.10 Slug and Damping Coefficient $\xi = 0.65$ for Various Sinusoidal Disturbance Torques	2-144
2-68	Spin Vehicle Momentum Vector Diagram	2-146
2-69	Geometrical Arrangement of Basic Spin Control Components	2-146
2-70	Spacecraft Spin Rate Requirement During Transfer Orbit	2-149
2-71	Apogee Motor Thrust Vector Misalignment	2-150
2-72	Spin Vehicle Sensor Geometry	2-156

SECTION 3

Figure	Title	Page
3-1	Ascent Schematic	3-3
3-2	Ability to Alter Station Longitude Based on an Off-East Launch Azimuth	3-5
3-3	Earth Track of Low Altitude Wait Ascent Mode	3-5
3-4	High Altitude Waiting Orbit - Circularization Characteristics	3-7
3-5	High Altitude Waiting Orbit - Drift Characteristics	3-7
3-6	High Altitude Waiting Trajectory - Latitude-Longitude Trace	3-12
3-7	Satellite Semimajor Axis - Perturbation vs Time	3-16
3-8a	Satellite Eccentricity Perturbations $(\Omega + \omega)_o = 0$	3-17
3-8b	Satellite Eccentricity Perturbations $(\Omega + \omega)_o = 45°$	3-17
3-9	Satellite Argument of Perigee Perturbation	3-12
3-10	Satellite Longitude of Node-Perturbation vs Time	3-17
3-11	Satellite Inclination Perturbation	3-19
3-12	Satellite Perigee Passage - Perturbation vs Time	3-19
3-13	Long Period Oscillation for a Satellite Injected into a Synchronous Equatorial Orbit at 90°W Longitude	3-21
3-14	Geometry Schematic	3-23
3-15	SMS Station Drift	3-25

LIST OF ILLUSTRATIONS (Continued)

Figure | Title | Page

SECTION 3 (Continued)

3-16 Approximate Station Keeping Pattern 3-34
3-17 Horizontal Thrust Case - Typical Computer Run 3-37
3-18 Vertical Thrust Case - Typical Computer Run 3-37
3-19 Horizontal Thrust for One Day - Typical Computer Run 3-38
3-20 Removal of 5° Station Error - Typical Computer Run 3-39
3-21 Longitude Drift Rate Caused by Second Sectorial Harmonic vs Time for Various Relative Longitudes 3-40
3-22 Longitude Limit Value of 2° - Typical Computer Run 3-42
3-23 Impulse and Duty Cycle for Mean Motion Station Keeping Method 3-44
3-24 Cumulative Velocity Impulse vs Time for Peak to Peak λ Excursions 3-44
3-25 Peak to Peak Variation in Longitude vs Impulse 3-45
3-26 Relative Longitude of -52.5° - Typical Computer Run 3-46
3-27 Impulse Time vs Initial Drift Rate or Velocity Error 3-48
3-28 Longitude Excursion while Nulling Initial Drift Rate 3-48
3-29 Eccentricity vs Impulse for Various Thrust Acceleration Levels 3-50
3-30 Disturbing Accelerations on the Satellite Caused by the Earth's Equatorial Ellipticity 3-51

SECTION 4

4-1 500-lb 3-Axis Stabilized Nozzle Geometry 4-4

SECTION 5

5-1 Single and Double Impulse Maneuver Boundaries 5-3

LIST OF ILLUSTRATIONS (Continued)

Figure	Title	Page
	APPENDIX A	
A-1	Coordinate Reference System	A-2
	APPENDIX B	
B-1	Block Diagram - Simplification of Earth Tracking Equations	B-2

SECTION 1 - INTRODUCTION

Volume 4 presents the studies conducted in the areas of attitude control, orbit getting, and station keeping. Attitude control is presented first. The subject is treated in detail due to its relative importance as indicated by the work statement and the NASA Project Officer. The results of analytical studies (including automatic computer simulations) and hardware surveys are presented.

The orbit getting and station keeping studies are presented next. These studies are not carried out in as much detail as those of attitude control, since they were not as important for the purposes of this study.

In order to decide how to apportion the total effort to be expended in the area of attitude control, it was necessary to make relative judgements of the applicability to the SMS of the various possible control techniques. This section presents the judgements made and the factors considered. The various control technique discussions are presented below in order of increasing importance.

Spin Stabilized - In order to accomplish the SMS mission, the RMS rates which the meteorological sensors can tolerate are about 0.001°/sec maximum for a nominal performance level, with lower rates desired for improved resolution. If the SMS were to be spun at only 1 rpm (about 6°/sec) an image motion compensation (IMC) scheme with a basic accuracy of approximately 1 part in 60, 000 would have to be evolved. The development of such a system which would be both light and reliable would be a major task. Furthermore, it would be impossible to forecast whether such an IMC system could be developed in the 1966-68 time period. For these reasons, it was decided that a minimal effort would be devoted to this control technique. The material presented in other sections of this volume for this system is primarily illustrative and does not represent the results of a detailed synthesis effort.

Gravity Gradient - The use of gravity gradient control appears to be best suited to applications where relatively low performance requirements in terms of rate stabilization and pointing accuracy are coupled with a requirement for long life. These requirements permit the use of passive control techniques, which are logically associated with a gravity gradient controller. These techniques do not, however, appear to be well suited to situations where rate stabilization requirements are stringent, as in the SMS mission. If high quality stabilization is to be achieved, then active damping is probably required, and active concepts must be utilized.

The problems associated with erecting a gravity gradient configuration in orbit have not yet been completely solved, so that further development effort is required in this area.

In view of the foregoing considerations, it was decided to give this attitude control technique a relatively brief treatment rather than to study it in detail at the expense of other techniques deemed more promising in terms of estimated availability in the 1966-68 time period.

Discrete Control - This control method is typified by electric propulsion systems. This type of system was studied in detail in Republic's 'Proposal for Studies of Synchronous Meteorological Satellite Systems Problems" (Republic Aviation Corporation Report No. RAC 826, 23 July 1962). The studies are updated in this document.

Continuous Noncoupling Control - This type of control utilizes torquers operated in a discontinuous manner. An example of this method is the use of high pressure cold gas torquers. Logic is included in the controller to minimize limit cycling and thereby prevent excessive fuel consumption. The results of a Minneapolis-Honeywell study of this type of system are presented in this volume. It is felt that this control concept is promising and that future studies in this area might be quite rewarding.

Discrete-Continuous and Gyro Compassing Controllers - These control techniques appear to be the most promising for the time period of interest, i.e., 1966-68. For this reason they are the subject of rather detailed studies, utilizing both analytical and analog computation techniques.

SECTION 2 - ATTITUDE CONTROL

A. ATTITUDE REFERENCE SENSOR SURVEY

A preliminary survey was made of attitude sensing devices which could be used on the synchronous meteorological satellite (SMS). Included were sensors ranging from those fully developed to those under developmental study for possible future applications. The attitude sensors could be grouped in the following categories:

(1) Radio frequency attitude sensing
(2) Optical attitude sensing
(3) Map matching
(4) Infrared horizon sensing
(5) Star tracking
(6) Sun tracking
(7) Magnetometers
(8) Differential gravity gradient sensing
(9) Stellar drift sensing
(10) Gyro rate sensing

1. Radio Frequency Attitude Sensing

RF radiation can be used for attitude measurement of the satellite. One crude method that is considered for the gravity gradient vehicle seeks to determine if the sensor portion of the vehicle is pointed in the hemisphere containing the Earth instead of the hemisphere away from the Earth. This information is necessary before the vehicle is extended to its final configuration, to ensure the vehicle will stabilize finally with the sensors pointed at the Earth, not away from it. The course direction of the sensor end of the vehicle can be determined by using an antenna with a conical beam having a solid angle of 120 to 160° and aligned with the Z axis of the vehicle. This antenna, instead of the normal antenna, could be connected by ground command to the output of the data transmitter. When the sensor frequency signal is received on the Earth, the vehicle is in the proper orientation for extension.

Another method having greater accuracy is to transmit an RF beam covering the Earth from a plane polarized antenna mounted on the satellite aligned to the Y axis. A plane polarized receiving antenna on the ground can be used to measure the direction of polarization of the beam by maximizing the received signal, which for the SMS would be the yaw attitude. This method would have an accuracy of 3 to 5°, because direction is obtained by maximizing the received signal. A more accurate method would be to receive the signal on two plane polarized antennas orthogonally positioned in a plane normal to the beam and to servo the antenna until equal signals are received. With this method, an accuracy of 1 to 2° could be obtained. However, both of these methods would be ambiguous and additonal information would be required to resolve the ambiguity. The meteorological pictures could be used for this purpose. The frequency of transmission would be selected to minimize the Faraday rotation of the beam as it passes through the atmosphere.

A method which can be used to measure roll and pitch attitude uses a transmitter with a circularly polarized antenna mounted on the satellite, with the beam covering the Earth and directed along the Z axis. When this signal is received on a rotating plane polarized antenna, the direction of the center of the beam can be determined. The receiving antenna is servoed in roll and pitch until equal signal strength is received throughout a complete revolution, by a system similar to a conventional conical scan radar system. When the signal is equal for a complete revolution, the plane of the antenna is normal to the centerline of the line beam.

Yaw orientation of the satellite must be obtained by another means to relate the beam attitude to the satellite roll and pitch attitude. In addition, the positions of the satellite and the receiving station must be known, and a computation made to convert the measured angles to satellite attitude angles. Accuracy of this method is in the order of 3 to 5°, because the error signal is a function of the cosine of the angle.

Another method of measuring roll and pitch attitudes involves the use of a ground transmitter and a standard monopulse or interferometer receiving system on the satellite. Accuracies of one mil or better can be obtained in measuring the angles to the transmitter. However, to convert these angles to roll and pitch errors requires a computation involving the position of the ground station and the position and yaw angle of the satellite. The computation could be made either on the ground or in the satellite. For reliability reasons it would be better to transmit the measured angles to the ground, perform the computation, and transmit the attitudes or attitude errors back to the satellite. In either case, the final attitude accuracy would depend upon the accuracy of the yaw angle measurement.

The need for measuring yaw angle can be eliminated by using two ground stations with a large base line between them and two receiving systems on the satellite. If the receiving system could acquire both ground stations, it could be time shared and only one would be needed.

The use of RF attitude sensing for a backup system is desirable. Its use as a primary attitude reference is limited by its accuracy, or by the satellite equipment and computation required for a more accurate system. If attitude sensing can be obtained from an RF link which is used for another purpose (such as telemetry), then it is desirable to make use of it. An example of this would be obtaining yaw attitude from the existing telemetry link. A system which can be used, even with degraded performance, in case of a malfunction of the primary system should be considered, provided it does not require the addition of much equipment on the satellite.

2. Optical Attitude Sensing

Optical methods of attitude sensing were investigated for use in the SMS because of the high accuracies attainable with these methods. The simplest method would be to track the SMS with two large aperture high resolution telescopes and determine the actual attitude from the observed relative attitude of the vehicle by correcting for the location of the telecopes. This method is not practical because of the size of the satellite and its altitude. The satellite could be located and tracked, as was done with Syncom, but there would be insufficient detail for any possible attitude measurements. Syncom appeared as a 17th magnitude star, (approximately) and although the SMS will be brighter because it is larger, there is little possibility of determining any information about its attitude (except rotation, due to changes in brightness).

Another method that was considered required installing a narrow beam laser on board the satellite. Acquisition of this beam on the ground would be difficult for any practical size detector. A wider beam would simplify the acquisition problem, but would reduce accuracy and greatly increase the power required.

The Perkin-Elmer Corporation has been studying methods of measuring attitude by optical means. One device they are investigating consists of a spherical mirror and lens which reflects light in the same direction as it is received. The polarization of the reflected light is shifted in a direction proportional to the angle of incidence. By measuring the polarization of the reflected light with respect to the transmitted light, the angle of incidence can be determined. To utilize this device for the SMS, a light source is required which has sufficient power to make a round trip. Although this may not be practical at this time, laser development is progressing so rapidly that it may be practical within a few years.

Another system being considered by Perkin-Elmer which is within the present state of the art of lasers uses one-way transmission to the satellite. In this system, two or more laser light sources are located in relatively cloud free areas. (The number of sources exceeding two depends on the probability of at least two being in cloud free conditions with a sufficient base line for accurate triangulation.) The satellite equipment required with this system is a simple optical detector which measures the roll and pitch signals from both beams. These signals could be measured simultaneously or in sequence to an accuracy in the order of arc seconds. The signals are then transmitted to the ground over the telemetry link, and the three vehicle attitudes are computed by using these signals and the triangulation data from the laser ground transmitters. The necessary attitude commands are generated and sent to the satellite over the normal command link.

With the addition of a modulation detector in the satellite and a modulated laser on the ground, the laser beam could be used as a command link, and all command information could be transmitted to the satellite by means of this beam. A possible means of 1-axis attitude sensing is that of detecting the polarization of the ground laser beam at the satellite. This method has an advantage in that corrections of the vehicle's attitude can be made by rotating the polarization of the ground laser. Attitude sensing by optical means has the advantages of small, passive satellite equipment and high accuracy. However, the system has the disadvantage that it cannot be used when clouds cover the laser transmitter. In addition, it cannot be used for initial acquisition of the Earth by the satellite and therefore requires a secondary or coarse attitude system to bring the satellite orientation within the limits of the optical system. The telemetry, command, and computer requirements make the overall system more complex than other less accurate systems. This would prohibit its use unless attitude accuracies of 0.1° or better are required.

3. Map Matching

The main purpose of the control system on the SMS is to provide for stabilization and pointing of the meteorological sensors. The maximum stabilization rates are determined by the rates which would smear the cloud pictures at the best resolution of the meteorological sensors, while pointing accuracy is necessitated by the accuracy required for geographic location of the cloud pictures. The cloud pictures can be used at the same time to determine the pointing accuracy of the meteorological sensors because the Earth is not entirely cloud covered. There is a high probability that the full Earth pictures will always contain some clear areas showing prominent continental features such as coast lines, peninsulas, gulfs, etc. By knowing the exact position of the satellite, which will be available from tracking stations, and determining the positions of two recognizable landmarks with respect to the picture outline, the attitude of the satellite can be computed.

Since the full Earth pictures will include the Earth's horizon, accurate roll and pitch vehicle attitude can be determined when at least half of the horizon plus one geographic landmark at a distance from the satellite's nadir are present. The landmark is used to measure yaw angle in order to resolve the roll and pitch errors (determined from the picture) to roll and pitch in satellite coordinates.

Instead of using landmarks and the horizon for attitude sensing, the terminator (the band between daylight and darkness on the Earth which is located geographically at local sunrise and sunset times) may be used. The terminator will always be present in the full Earth pictures except for a period of approximately 1 hour at 0000 and 1200 Local Mean Time at the nadir of the satellite. The terminator will always provide yaw and pitch attitude information, and except for a few hours at 0600 and 1800 during the equinoxes, it will also provide roll information. If the terminator and the horizon are both included in a picture, all three attitudes of the satellite can be obtained.

One method of extracting three axis attitude information from the photographs is to use a properly scaled overlay showing the prominent geographic features of the Earth. The overlay is rotated in yaw and moved in pitch and roll with respect to the frame until it aligns with the landmarks on the picture. If the angles are small, these motions can be directly converted to the desired angles. The same overlay and basic method can be used when the horizon is the reference. The overlay method can also be used when the terminator is the reference, but now a large number of overlays are required, depending on the time of the day and the day of the year.

A second method, which is more versatile, consists of using a scale model of the Earth with prominent geographic features, a light source representing the Sun (which can be positioned to simulate time and days of the year), and an optical system simulating the meteorological sensors which can be positioned about the three axes. An optical comparator is included to permit alignment of the Earth's picture with the image of the Earth's model. This method of matching would include all possible references obtainable from the pictures (as described previously) and would read out the three attitudes directly.

Attitude information derived from the meteorological pictures is not recommended for use as a primary attitude sensor but as a backup system. The reason for this is that rates of attitude error are used for damping, and they can be derived best from attitude sensors aboard the satellite. Two main areas in which attitude information derived from pictures will be used are: first, to bias any steady state errors due to drift or misalignment of the satellite sensors; and second, to serve as a backup system for the horizon sensor. In case of failure of the horizon sensor, rate gyros on the satellite will be used for damping, and commanded attitude derived from picture information will be used for aiming the satellite.

4. Infrared Horizon Sensing

Information about horizon sensors proposed to NASA Goddard for development of a reliable Earth sensor was received from the following companies:

(1) Barnes Engineering Co.
(2) Bendix, Eclipse Pioneer Division
(3) Electro-Optical Systems
(4) General Electric, Light Military Electronics Department
(5) Honeywell, Aeronautical Division, Boston

The information received is considered sufficient to appraise a number of different approaches to the problem. Until a contract is given for the development of this sensor, the NASA specification will be used for evaluation. The specification classifies this sensor as one of lightweight, small size and power, low accuracy, and high reliability.

In addition to reviewing horizon sensors proposed as reliable Earth sensors, the following sensors produced by Advanced Technology Laboratories, Barnes Engineering, and Minneapolis Honeywell were reviewed.

a. Advanced Technology Laboratories

The conical scanning sensors used on the Discover vehicle contained two identical scanning heads, each rotating to produce a conical surface in space. Pitch is measured by the angles at which the line of sight of either head enters and leaves the Earth. Roll is measured by the difference of the fraction of time the line of sight of one head spends within the Earth compared to the fraction of time spent by the line of sight of the other head within the Earth.

The principal advantages of this system are its ability to operate over a wide range of pitch and roll, and to respond rapidly. The disadvantages include: needing high speed rotating parts with bearings to produce the conical scan, with resulting lubrication and reliability problems; being susceptible to interference from spurious infrared radiation far from the horizon; and having a relatively wide signal bandwidth, which decreases the signal to noise ratio, resulting in the use of large infrared optical systems.

Advanced Technology Laboratories' OGO horizon point tracker is applicable for use in the SMS; and it will be discussed under "Selected Attitude Reference Sensors."

The horizon sector scan system (which is used on Agena D and Gemini) is more accurate because a large horizon section is used, instead of a few fixed points. A single tracking head is mounted so that its scan plane can be continuously rotated in azimuth in a reciprocating motion while tracking the horizon in elevation. Time variations of the elevation angle to the horizon are used to measure the roll and pitch attitude errors. Its disadvantages are its inability to measure large values of pitch and roll at high altitudes, and reduced reliability because of the continuous scan motion.

b. Barnes Engineering Co.

The conical scan horizon system used on the Mercury vehicle consisted of two identical self-contained sensor heads, each mounted to measure attitude angles about a given axis. The scan is produced by rotating a prism which rotates the instantaneous field of view in a conical pattern at a rate of 33 cps and a full cone angle of 110°. This system has a short life because of the rotating parts; and it is also subject to large errors due to cold clouds.

A four-beam horizon sensor using thermopile detectors is in production. This sensor is designed for altitudes below 100,000 feet and is not applicable for SMS.

A lunar and planetary horizon scanner is being developed by Barnes Engineering Co. for Jet Propulsion Laboratories. The scanning is accomplished by sampling an array of thermopiles with light-actuated photoconductive switches. A five-element thermopile subtending 3° in elevation tracks the horizon in each of four quadrants. The four optical heads which contain these thermopiles and spherical mirrors are positioned by a stepper motor which is actuated only by attitude changes. The accuracy estimated on Earth is less than 1 minute of arc, and although this sensor must be more versatile and complex than necessary for the SMS, a simplified version may be used.

For the SMS application, Barnes Engineering Co. proposed a completely static horizon sensor using one spherical mirror and thermopile array edge detectors. Details on this unit will be given in "Selected Attitude Reference Sensors."

c. Honeywell, Boston

A sensor system has been built for the Applied Physics, Laboratory of John Hopkins University. It uses a bolometer array and an inverted conical reflector in front of the optics to provide a wide field of view for low altitude applications.

Honeywell, Boston has developed an improved sensor which has no moving parts. A wide field of view is provided by a reflecting cone in front of the optics, and the infrared energy is electronically modulated by a germanium modulator. However, the reflecting cone optics system is not applicable for use in the SMS.

A lunar and planetary horizon sensor which utilizes an edge sensing scheme which is independent of thermal surface anomalies and dependent only upon the detection of positive thermal gradients is being developed. The attitude signals are linear over a ±10° range, and the null accuracy is estimated to be better than 0.2°. Scanning is done with mirrors mounted on flex-free pivots.

The Honeywell sensor recommended for use in the SMS will be described in "Selected Attitude Reference Sensors."

5. Star Tracking

Bendix and Kollsman two-gimballed OAO star trackers were investigated. Both have a freedom of ±60° on each axis and an accuracy of approximately 20 arc seconds. Bendix uses electronic scanning and responds to stars of magnitude +2.5 and brighter, while Kollsman uses mechanical scanning and responds to stars of magnitude +2.0 or brighter. Gimballed trackers were not investigated in detail, since they cannot be generally utilized in an Earth-oriented vehicle without continuous programming and extensive computation.

A boresight tracker which can track Polaris is more applicable to the SMS orientation. Two ITT Federal Laboratories boresight trackers currently in production were investigated. One has an 8° square acquisition, and the other a 1° square acquisition. Both trackers use electronic scans, and can track stars dimmer than Polaris. The 8° acquisition is applicable to SMS and is described in "Selected Attitude Reference Sensors."

The possibility of developing a Polaris tracker for the SMS application was discussed with Bendix. They estimated that a unit with a 5 x 5 x 3 in. tracking head and a 3 in. diameter, 5 in. long electronics package weighing less than 10 lb and requiring 7w of power would be able to track Polaris, and it would have an electronic offset bias to correct for the 55 arc minutes deviation of Polaris from the Earth's polar axis.

6. Sun Tracking

A 180° field of view Sun sensor proposed by Sperry Gyroscope Co. comprises a 180° Pacific Optical Company lens and a radiation tracking transducer manufactured by Micro-Systems, Inc. The resolution of the sensor for a signal to noise ratio of one is computed to be 1 arc second. Linearity of 5% can be obtained within 20° of the boresight axis, and an overall accuracy of 1° can be obtained by electrical compensation of the distortion due to the 180° lens when operating out of this region.

Electro Optical Systems, Inc. also proposed a 180° field of view Sun sensor using a Pacific Optical Company lens and a radiation tracking transducer. The error due to drift is calculated to be less than 0.75° when the Sun is near the boresight axis. Linearization of the radiation tracking transducer can be accomplished by using: 1) multiple contacts; 2) prisms in front of the cell; and 3) a graded attenuator in front of the cell. All of these methods have been successfully tried.

The Bendix 180° Sun sensor will be described in "Selected Attitude Reference Sensors."

7. Magnetometers

Honeywell's Aeronautical Division has proposed a 3-axis saturable reactor (flux gate) type of magnetometer for another space application. The device weighs approximately 5lb, is approximately 70 cu. in. and has a sensitivity of 200 gamma in a 20000 gamma field. Since the Earth's field at synchronous altitude is estimated as being approximately 300 gamma, a lower threshold of measurement is required. Honeywell is presently working under a Navy contract to develop a new magnetometer of greater accuracy. A measurement accuracy of 1 gamma in a field of 300 gamma with 1/4 gamma noise at a 2 cps bandwidth is attainable. With this accuracy, the direction of the magnetic field can be measured to 1/5°.

Dalmo Victor also confirmed that a sensitivity of 1 gamma could be obtained with a 1/4 gamma noise by using a saturable reaction type of magnetometer. The threshold for this type of magnetometer is usually 1% of full scale. Using this figure, the direction of the magnetic field can be measured to 3/5° By using another 3-axis magnetometer as a basis, they can develop a 3-axis magnetometer weighing 4 lb and requiring 1.5w of power for use at synchronous altitude.

The use of the Earth's magnetic field as a means of sensing attitude cannot be recommended for use in the SMS. Very little data is available on the Earth's field at synchronous altitude, and use of it as an attitude reference cannot be considered until its intensity, direction, and variations are known. A more probable use of magnetometers is in conjunction with magnetic torquers for unloading wheels or torquing the satellite when more information on the Earth's field is available.

8. Differential Gravity Gradient Sensing

The Ford Instrument Company is developing a new type of sensitive accelerometer which uses an unbalanced rotating disc supported on air bearings and driven by a constant torque at low speeds. By using a light system and radial slots at the edge of the disc, the time required by the disc to rotate through each of four quadrants can be accurately measured. If the instrument is subjected to acceleration, the time required for the disc to rotate through a quadrant in the direction of acceleration will be greater than in the opposite quadrant where it rotates against the acceleration. Acceleration along two vehicle axes can be measured with this device.

A feasibility model has been made, and accuracies in the order of 10^{-6}g have been obtained. Work has started on the preliminary design of a unit with an estimated sensitivity of 10^{-11}g.

This accelerometer was originally considered for use in sensing the gravity gradient; however, it has been dropped because of the problem of separating gravity gradient accelerations from control and disturbance accelerations.

9. Stellar Drift Sensing

Both Kollsman and Honeywell have made studies of stellar drift sensors. Kollsman investigated tracking any suitable star in the field of view and Honeywell considered tracking the star field with an image dissector tube.

Advanced Technology Laboratories started building a prototype stellar drift sensor under contract and continued the development with in-house funds. Its rate accuracy is estimated to be 1%, but there is a ±5% cross coupling effect in rates which prohibits its use in the SMS.

Investigation of a stellar drift sensor was dropped, since a satisfactory working system was not located.

10. Gyro Rate Sensing

Rate gyros manufactured by Honeywell, Nortronics and Sperry Gyroscope Co. were reviewed. Because of the long life requirements, hydrodynamic gas spin motor bearings offer the best reliability; and because of the low rate threshold requirements, integrating rate gyros operated in the rate mode were selected for use in the SMS. Nortronics is developing a miniature gyro meeting these requirements; but characteristics of this gyro were not made available. Both Sperry Gyroscope Co. and Honeywell are developing gyros of this type. The Sperry gyro is classified, and its description will be in the selected sensors section of the classified supplement; the Honeywell gyro will be described in "Selected Attitude Reference Sensors."

Sperry Gyroscope Co. is also developing a fluid sphere gyroscope which could possibly be used because of its unique characteristics. In principle, the fluid sphere gyroscope is a device whereby angular momentum is provided by a mass of liquid contained in a spherical cavity that is rotating. When an angular input is applied, the liquid body spin axis tends to retain its pointing direction in space while the cavity axis is moved away. Because of the spherical symmetry, this occurs for inputs about any axis normal to the spin axis. In order to detect the internal deflection angle, a differential microphone is used to sense a spin frequency differential pressure which is found to occur between a pair of ports 45° to the cavity axis. Two pairs of ports are used to measure deflection about two axes.

When the spin axes are not aligned, there is a relative angular velocity between the cavity and the liquid body. This results in viscous shear torques which act to precess the liquid body spin axis back into alignment with the cavity spin axis. The gyroscope is therefore a two-degree-of-freedom rate type which can have a relatively long time constant so that it acts somewhat like a displacement gyroscope. An advantage of the device is its simplicity; and although it has spin bearings, the motor and bearings are external to the gyro and can be made in almost any desired form. The cavity is rotated at relatively low speeds (6000 RPM) which further simplifies this problem.

Over fourteen units have been built for different applications without a failure. Random drifts of 0.02°/hr have been obtained. For the SMS application, a 1-1/2 in. cavity unit would have the following characteristics:

Size: 3 in. diameter by 3-1/2 in. long
Weight: 2 lb
Random Drift: 0.01°/hr
Resolution: below 0.01°/hr
Saturation: 15°/sec
Electronics: 6 cu. in., 1/2 lb
Power: 400 cps 10w starting, 2w running

Predicted reliability: 95% probability of continuous 1 yr operation.

Since each unit measures rates about two axes, three units would provide completely redundant rates.

11. Selected Attitude Reference Sensors

a. Infrared Horizon Sensors

The OGO horizon sensor which is produced by Advanced Technology Laboratories was selected for use in the SMS because it is an existing unit having the required characteristics. Further development of this system in the next four years will improve its reliability. The system uses four trackers: three are required to derive roll and pitch; and one is redundant. Each tracker contains a single infrared telescope whose line of sight can be moved vertically in a plane. Electronic circuitry causes the line of sight to move slowly through the entire range of 90° in the plane until the horizon is encountered. When this occurs, the search motion stops and the line of sight locks on to the horizon and continues to track it with a high speed dither motion of ±1° from the center of the horizon gradient. The average angle of the line of sight during the dither cycle is measured electrically and then summed to produce roll and pitch signals.

The optical motion needed in this system is produced by a specially designed device called a "Positor." This unit consists of a mirror mounted on a crossed spring suspension. The mirror is rotated electromagnetically while at the same time a precision differential transformer type of resolver measures the mirror's angle.

Two identical tracking systems are mounted in one casting, as shown in Figure 2-1. Two such castings and one central electronics unit form a complete system. Incoming infrared radiation from the horizon of the Earth passes through a coated germanium window which serves the dual purpose of protecting the interior of the instrument from dust and restricting the optical passband to wavelengths greater than 8 microns. The telescope consists essentially of a single germanium miniscus (objective) lens, a germanium-immersed thermistor bolometer detector, and a thermally compensated lens spacer.

In order to provide 0.1° accuracy in angle measurement when working with the Earth's infrared horizon, the OGO system was designed to lock on to the inflection point of the gradient. It does not seek a particular level of infrared, but locks on to and tracks the particular point on the horizon gradient where the curve of radiation versus angle inflects. This technique eliminates large errors that can occur when a fixed level seeking device is used and the level threshold drifts due to cold clouds or changes in vehicle temperature.

The OGO sensor has a built-in Sun detector which provides a "tracker failed" indication when the Sun appears in the tracker field of view. The OGO trackers will continuously track the Sun without damage. (This has been demonstrated on the ground by tracking the Sun for an extended period of time.) The "tracker failed" signal from the Sun alarm causes the affected tracker to be removed from the computation, and complete, undegraded pitch and roll outputs to be provided from the remaining three trackers.

A summary of the system characteristics follows:

Size: Two tracking heads, each 9-1/2 x 6-1/2 x 2-1/2 in. Electronics unit, 7-1/4 x 5-3/4 x 3-1/4 in.

Weight: System weight - 12.47 lb

Power: Search mode - 11.4w. Track mode - 8.5w from plus and minus 20 VDC with 1.5% regulation. Ripple - less than 1% with transients up to 0.5V peak. Negligible power required at 5V, 2461 cps.

Output voltage characteristics: The pitch and roll outputs are 2461 cps phase reversing AC at a scale factor of 400MV RMS per degree of tilt. The scale factor is linear with ±4% out to 25° tilt. In addition, the tilt must not exceed about 1/3 the total subtended angle of the Earth, or the system will loose track. Null accuracy is ±0.1°.

Acquisition: Initial acquisition - less than 40 seconds from the time power is applied. Reacquisition - 4 seconds from the time track is lost until track is regained (power continuously applied during this period).

Noise:

3 db points, 0 to 0.2 cps	8.5 MV RMS
0.2 to 0.4 cps	11.8 MV RMS
0.4 to 0.8 cps	7.9 MV RMS
0.8 to 1.6 cps	11.6 MV RMS
1.6 to 8.0 cps	11.6 MV RMS
8 to 100 cps	5.7 MV RMS
24 to 100 cps	5.7 MV RMS

Reliability: The probability of successful operation for one year in orbit is 0.86. This is based on Space Technology Laboratories and Martin Denver failure rates. The 0.86 reliability for one year takes into account both detectable and undetectable failure modes. Other reliability analyses have indicated considerably lower figures because of the large number of parts in the system. As more experience is gained in use of the system, a more realistic realiability figure will be determined.

The Barnes Engineering Company proposed a horizon sensor for use in the SMS which has no moving parts, and is light and compact (Figure 2-2). Acquisition can be accomplished when aimed within 16° of the center of the Earth, and the tracking accuracy is calculated to be better than ±10 seconds of arc with gross temperature differences across the Earth's disc.

The 4 in. diameter spherical mirror has an aperture of 2 in. at F/1.5 with 25% obscuration. It is made of uncoated lithium fluoride and makes use of the "Reststrahlen" effect in the 15 to 35 micron region, which averages about 70% reflectivity. This almost totally removes the apparent Earth temperature inhomogeneities.

The Earth horizon at synchronous attitude subtends an angle of 17.3°. To detect this horizon, four 40-element thermopile array edge detectors are placed in the image plane. Each detector covers a 40° of the horizon and is spaced 50° apart.from its neighbouring detectors. One pair of opposing detectors is used to measure roll, and the other pair, pitch. The signals are amplified with low noise transistor preamplifier and photomodulator circuits employing neon lamps in conjunction with cadmium selenide photoswitches. The lamps are used in a relaxation oscillator circuit to chop the DC signal from the thermopile. This circuit has been successfully tested over typical space ambient temperature variations; and the tests indicate stability of 0.1 MV over the range.

The electronics package will operate from + 28 VDC and will consume less than 1/2 w of power. The package will be less than 7 x 2 x 1-1/2 in. in volume and will weigh less than 1.2 lb. If packaged as an integral part of the sensor head, the entire system package will be 4-1/2 in. in diameter x 8 in. long and will weigh 2.2 lb.

Although this unit appears applicable to the SMS as proposed, there are some necessary modifications which must be made. The linear range of the proposed system is 2.7 milliradians. This must be increased to a minimum of 1° before it is acceptable. The addition of eight more thermopile arrays, similar to the lunar and planetary scanner, can be used to increase the linearity. The additional thermopiles would also produce the required acquisition signal. A Sun alarm, to indicate when the Sun is in the vicinity of the detectors (in order to prevent false signals) is required.

The additional requirements will increase the complexity, weight, size, and power of the sensor, and reduce its accuracy, but it still has the possibility of being very accurate and light in weight. Since it is related to the lunar and planetary sensor, developments on that program will produce information of use in the SMS application.

The Honeywell Aeronautical Division proposed a horizon sensor using four optical tubes that each contain a solid state germanium modulator. The 4-element optics are focused in two orthogonal axes on one detector. The modulation

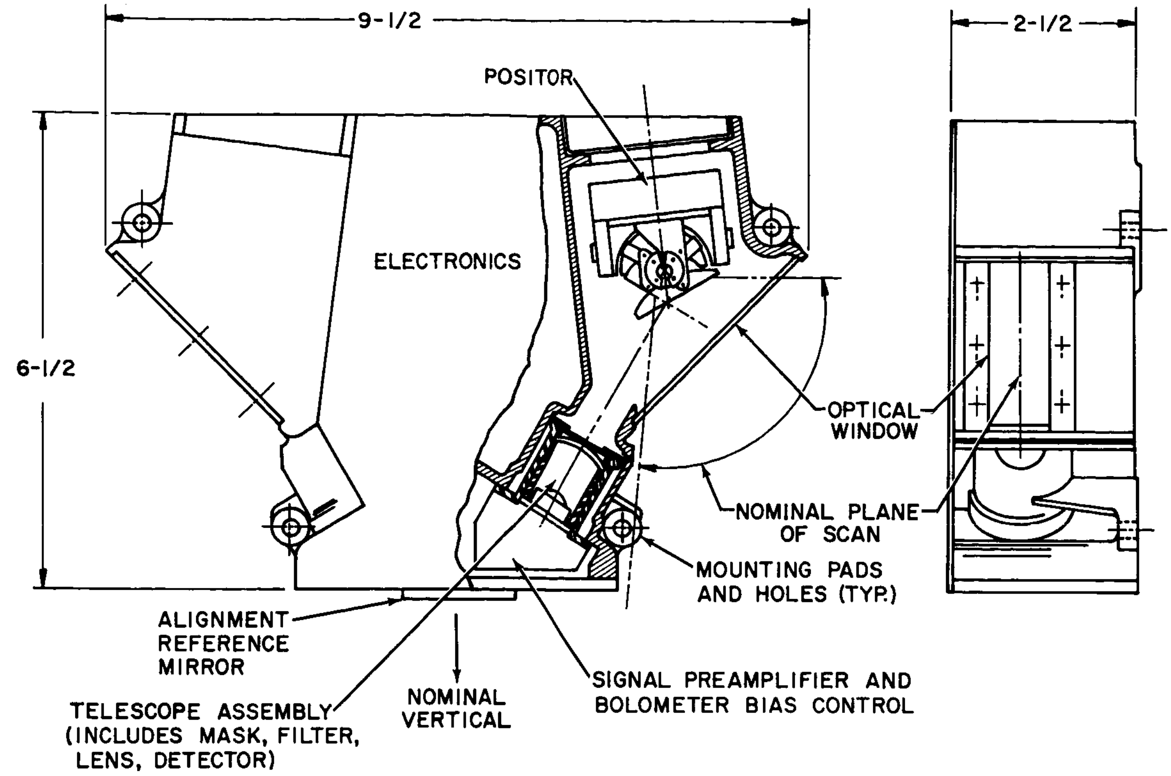
9-1/2
2-1/2
POSITOR
ELECTRONICS
6-1/2
OPTICAL WINDOW
NOMINAL PLANE OF SCAN
MOUNTING PADS AND HOLES (TYP.)
ALIGNMENT REFERENCE MIRROR
TELESCOPE ASSEMBLY (INCLUDES MASK, FILTER, LENS, DETECTOR)
NOMINAL VERTICAL
SIGNAL PREAMPLIFIER AND BOLOMETER BIAS CONTROL

Figure 2-1. OGO Dual Tracker Casting

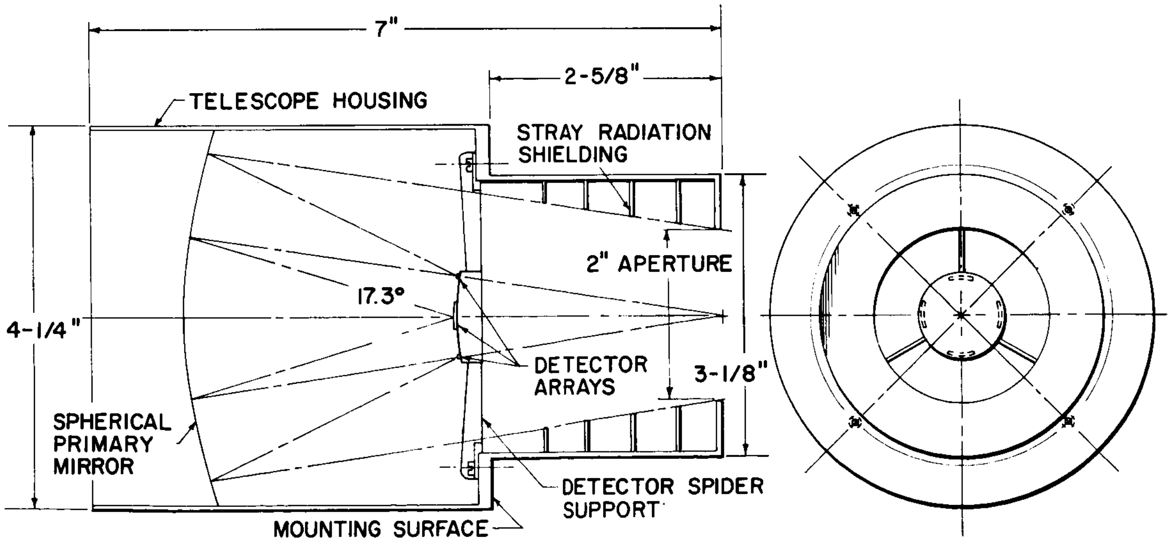
7"
2-5/8"
TELESCOPE HOUSING
STRAY RADIATION SHIELDING
2" APERTURE
17.3°
4-1/4"
DETECTOR ARRAYS
3-1/8"
SPHERICAL PRIMARY MIRROR
DETECTOR SPIDER SUPPORT
MOUNTING SURFACE

APPROXIMATE WEIGHT : 1 LB

Figure 2-2. High Accuracy SMS Horizon Sensor Head

provides synchronous detection of the attitude signals, channel separation, and time sharing of the electronics. The detector is a single thermistor bolometer in a bridge circuit. The thermistor is maintained at 27°C by the use of a thermoelectric heat pump. The current through the heat pump is reversible so that it can be used as a cooler or as a heater.

The germanium modulator (GEM) is a Honeywell developed component which is being used as a radiation chopper in several infrared communications systems. It was selected for a fusing system because of its inherent reliability. For the sensor application, the GEM is operated in one of two electrical modes only, that of zero applied current and voltage or that of a forward conducting germanium diode. The quiescent mode of modulation operation is zero current and maximum transmission. When the modulation is pulsed with a current of 0.5 ampere, it becomes opaque.

The characteristics of the system are summarized as follows:

Size: Packaged as either one or two units less than 200 cu. in. (total)

Weight: Less than 6 lb

Field of View: ± 12° by ± 3° in each of two orthogonal sensing axes

Power: 6 W from 28 ± 6 VDC

Linearity: Better than 10% in a ± 6° range

Noise Content: Single frequency noise at 40 cps and 1 KC. White noise (RMS) corresponding to less than 0.1° signal voltage.

Null Accuracy: Null uncertainty is approximately 0.1°

Saturation: Output is saturated at ± 6°, remains saturated out to ± 16°, then decreases linearly to null at 22°

Bandwidth: 1 rad/sec; can be made wider to 10 rad/sec with increase in noise

Spectral Range: 14 to 16 microns

b. Star Tracking

Tracking Polaris is particularly attractive for the SMS, because it is located 55 arc minutes from the desired orientation of the pitch axis. The difficulty in using this mode is the problem of acquisition. Since Polaris is not a very bright star (+ 2.1 magnitude), magnitude alone cannot be used to discriminate it from other stars. However, the closest star to the pole within 1/2 magnitude of Polaris is Kochab (+ 2.2 magnitude), which is located approximately 16° from the pole. A tracker with a 1/2 magnitude discrimination could acquire Polaris, if aimed or scanned in such a manner as to include Polaris and exclude Kochab from its field of view. Thus, a tracker with a field of view less than 16° could acquire Polaris if aimed at it with an accuracy of 1/2 of its field of view.

ITT Federal Laboratories is currently fabricating two boresight star trackers. The optics of these trackers focus the radiant energy on the photocathode of an image tube combined with a 16-stage multiplier section with the screen of the image tube replaced by a small aperture. The photocathode converts the optical image to an electron image which is magnetically scanned in the image tube section to produce square waves at the multiplier output as the electron image passes over the aperture. When the image does not lie along the optical reference axis of the tube, the time asymmetry of the square waves gives rise to a component at the fundamental sweep frequency. This component is the error signal. Synchronous gating circuits switch the output of the phototube alternately to the two attitude outputs. A vertical and horizontal crossed-line sweep is used with the intersection of the line falling in the center of the aperture, when the target is in perfect alignment. For a centered target, the error signal is an 800 cps signal;but with an off-center target, the pairs of pulses differ in duration, giving a 400 cps error component at the phototube output.

The characteristics of the tracker suitable for use in the SMS are as follows:

Size: 5 in. diameter x 10 in. long
Weight: 9 lb
Power: 6.5 W acquisition, 7.9 W track
Field of View: 8° square, acquisition; 16 arc minutes square, track
Bandwidth: 5 cps
Error Gradient: 0.69 V/arc min, track
RMS Noise: 1.59 MV/radian/second
Lens: Diameter 2 in., focal length 75 mm f1.5
Recognizable Star Magnitude: + 3.0
Tracking Accuracy: 45 arc seconds
Maximum Rates: Star presence; acquisition, 20°/sec
Error signal; acquisition, 8°/sec
Error signal; track, 1.3°/sec

c. Sun Tracking

The Bendix Sun sensor Type 1771858, which was selected for use in the SMS, is shown in Figure 2-3. In the upper left is shown the quad cell structure used to sense the 20° solid cone angles. These cells are mounted behind a square aperture plate, lying to the right of the quad cell structure. To the right of the aperture plate is the glass dome which seals the entire unit.

On the lower left is shown the unit with the aperture plate in place. Also visible are some of the peripheral cells which are mounted at right angles to the quad cell structure on the aluminum casting which forms the body of the unit. The completely assembled device is shown in the lower right hand corner.

The Sun sensor views a solid hemisphere, and provides two DC output signals proportional to the azimuth and zenith angles of the Sun's position relative to the reference. The signals are linear within a 20° cone of the boresight. For angles greater than ± 10°, the output increases as an approximate cosine function up to ± 90°.

The quad cells produce increasing outputs to 35° and then decrease, reaching zero output at 70°. The peripheral cells are placed so that their outputs increase as those of the quad cells fall, to produce a combined output which smoothly increases out to 90° from the boresight axis. To reduce errors caused by reflected sunlight from the Earth, Moon or vehicle, the peripheral cells can be disconnected from the quad cells after track has been attained. Light entering the sensor outside the 20° cone would then produce a smaller error and beyond a 140° cone, no error.

The characteristics of this sensor are as follows:

Size: 2 in. diameter x 1-7/8 in. long

Weight: 3 oz.

Power: none

Linear Range: ± 10° on each output

Gradient: 100 ohm load, simulated sunlight, 10,000 ft candles. 0.18 Ma/° in linear range. Approximate cosine function beyond linear range ± 90° output - 4.7 Ma

d. Gyro Rate Sensing

The Honeywell miniature integrating gyro GG 159 (Figure 2-4) is one of the two gyros selected for use in the SMS. This gyro has hydrodynamic gas spin bearings, ceramic construction, hydrostatic gimbal suspension, moving coil signal and torque generator, and a spin motor running detector.

The hydrodynamic gas spin bearing is a self-activating device which supports the motor on a thin film of gas without any external aid, such as pressure lines or gas supplies. Since the bearings are frictionless, infinite running life should be attained. Wear damage occurs only during start and stop cycles of the motor, and this is reduced by proper material selection. Extensive wear tests on various platings and materials have shown conclusively that alumina ceramics are superior to any nonceramic material, both from the standpoint of wear resistance and dimensional stability. Wear characteristics are further reduced by proper gas bearing design in cases where the motor becomes gas borne at very low speed and light load conditions. Honeywell gas bearings have repeatedly been subjected to thousands of start-stop cycles with no detectable damage or degradation of performance.

Ceramic construction is not only used for the spin bearing support surface, but it is also extended to the gimbal structure. The choice of ceramic construction permits mass stabilities previously

The hydrostatic gimbal suspension is obtained by causing the damping and flotation fluid to flow symmetrically about the gimbal, entering at the center with equal axial flows along the gimbal in both directions.

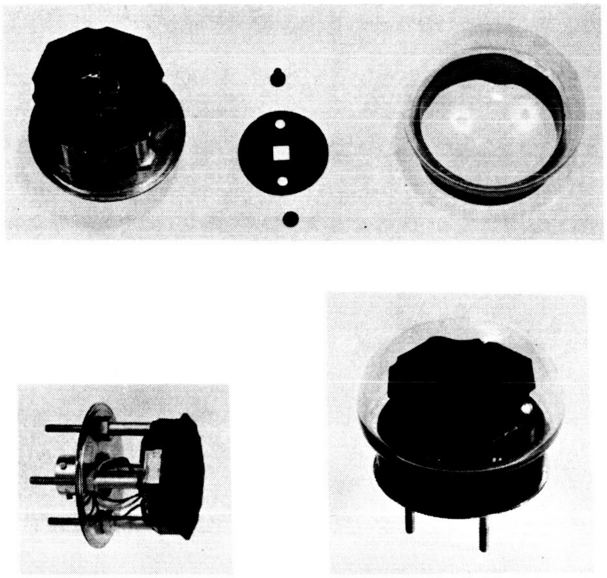

Figure 2-3. Bendix Sun Sensor Type 1771858

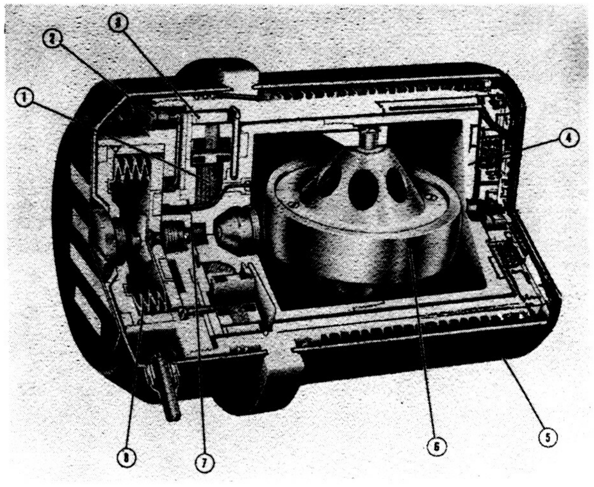

1. SIGNAL GENERATOR
2. TERMINAL
3. PERMANENT MAGNET TORQUER
4. FLOATED GIMBAL
5. CASE
6. GYRO MOTOR
7. BELLOWS
8. MICROVERNIER BALANCE CAPSULE

Figure 2-4. Honeywell GG 159 Rate Gyro

Symmetrical restrictions in the flow path develop symmetrical pressure drops which, in turn, hold the gimbal at the developed pressure center. Since the gimbal has a neutral buoyancy in the field, the centering forces need only be sufficient to keep the gimbal centered in the presence of disturbing forces. The required pressure and flow are provided by a small positive displacement pump at one end of the gyro. The pump is a solenoid-actuated piston working against a spring return, with two small ball-check valves.

The moving coil signal and torque generator provides signals and torquing functions with extremely low reaction torques. The signal generator is suitable for high frequency operation to 30 KC. The torque generator requires no bias excitation, and provides extremely linear torquing characteristics with high scale factor stability because of its Alnico V magnet.

The spin motor running detector has been included in the design of the gyro for operational checkout procedures. A small magnet is imbedded in the outer wheel periphery, and a coil is mounted external to the hermetic seal on the gyro case. Wheel rotation causes a change in the coil flux linkage, and generates a voltage output at the frequency of the wheel rotation.

A summary of the characteristics of this gyro is as follows:

Size: 2-1/8 in. diameter x 3 in. long

Weight: 0.85 lb

Power: Signal generator - 12.0 V, 150 MA, 7200 cps
Spin Motor - 26 V, 255 MA, 800 CPS 3 phase
Heater - 28 W, 28 V
Sensor - 780 ohms
Gimbal suspension - 110 V, 25 MA, 60 cps

Signal Generator Sensitivity: 25 MV/milliradian

Torque Generator Scale Factor: 80°/hr/MA

Maximum Torquing Rate: 8000°/hr

Gyro Transfer Function: 250 MV/milliradian (max)

Time Constant: 8 milliseconds (max)

Random Drift: 0.003°/hr

Additional information on classified gyro rate sensing equipment is given in Volume VII.

12. Conclusions

Attitude sensors are available now that provide nominal levels of performance and reliability. It is desirable that better sensors be developed for the 1966-1968 period to fulfill tighter design requirements for the SMS stabilization system. Additional development is also desirable to provide greater accuracy and reliability with instruments of lighter weight and lower power requirements. This optimization would be better accomplished by developing instruments specifically for the SMS application, instead of using those which have the necessary characteristics but were developed for other applications.

13. Areas of Future Study

There are several attitude sensor areas that warrant further study. A brief listing of these areas follows:

a. Gyroscopes

The effect of space environment on the life and the change of drift characteristics in zero g conditions requires more detailed investigation.

b. Polaris Tracker

Since a precise Polaris tracker (with compensation for its 55 arc minutes offset) can be used for precise yaw and roll attitude measurement, further investigation of such a device should be made. The two major problems are acquisition and compensation for the 55 arc minute offset.

c. High Accuracy Laser Attitude System

A laser attitude system offers the most precise means of measuring a 3-axis of attitude angle with a small amount of equipment on the satellite. Detailed definition of a system is required.

d. Horizon Sensors

Continued study of horizon sensors is necessary to determine the optimum sensor design for the SMS requirements.

e. Map Matching

Further investigation of full Earth picture matching techniques is necessary to determine feasibility of attitude bias corrections for the satellite, and geographic corrections for the cloud pictures.

f. Earth's Magnetic Field at Synchronous Altitude

More information is required on the nature of the Earth's magnetic field at synchronous altitude, in order to determine if it is feasible to use the magnetic field for attitude measurement or torquing.

B. TORQUERS

A survey was made of the various torquers that might be applicable to the synchronous meteorological satellite (SMS) project. Based on this survey, those torquers that looked promising were studied in more detail. Sizing and performance characteristics as applied to the SMS satellite were obtained or generated based on information obtained from the component manufacturers. This survey included the following torquers:

(1) Reaction wheels

(2) Reaction sphere

(3) Gyro systems
  (a) Glopac
  (b) Twin gyro

(4) High pressure cold gas

(5) Solid subliming low pressure gas

(6) Cap pistol

(7) Electric propulsion
  (a) Plasma pinch engine
  (b) Electrostatic ion engine

(8) Hot gas

(9) Magnetic torquing

(10) Vaporjet low pressure gas

(11) Diffusion of hydrogen through palladium

(12) Brushless DC motors

1. Reaction Wheels

Reaction wheels are angular momentum storage devices that are used for satellite attitude control,(see Figures 2-5 and 2-6). Since angular momentum of the vehicle and wheel combined must be conserved in the absence of external disturbing torques, angular momentum can be transferred only between the satellite and the wheel. Thus, a change in wheel speed, with the resulting momentum change, will effect an equal but opposite change in satellite angular momentum. Motor torque, accelerating or decelerating the wheel, is transmitted through the unit mounting pads to the satellite structure to maintain vehicle attitude in the presence of disturbing torques.

The wheel motor can continue to apply torque to the vehicle until a maximum speed somewhat below the motor synchronous speed is reached. The wheel must then be "unloaded," or returned to a speed in the neighborhood of zero by the application of an opposite torque to the vehicle, e.g., by cold gas reaction jets. Cyclic disturbing torques of equal positive and negative variations will not cause wheel saturation, provided they are within the wheel limits, because the wheel will be alternately accelerated and decelerated Predominantly unidirectional disturbing torques will eventually result in wheel saturation unless the stored momentum is dumped (wheel unloaded). Sections E1 and E2 provide detail wheel characteristics for the SMS vehicle.

The advantages of the reaction wheel are its ability to provide fine control and to compensate for cyclic disturbing torques without the expediture of propellant.

2. Reaction Sphere

The Bendix Corporation has conducted a development program on the concept of combining three reaction wheels into a single unit, an electric

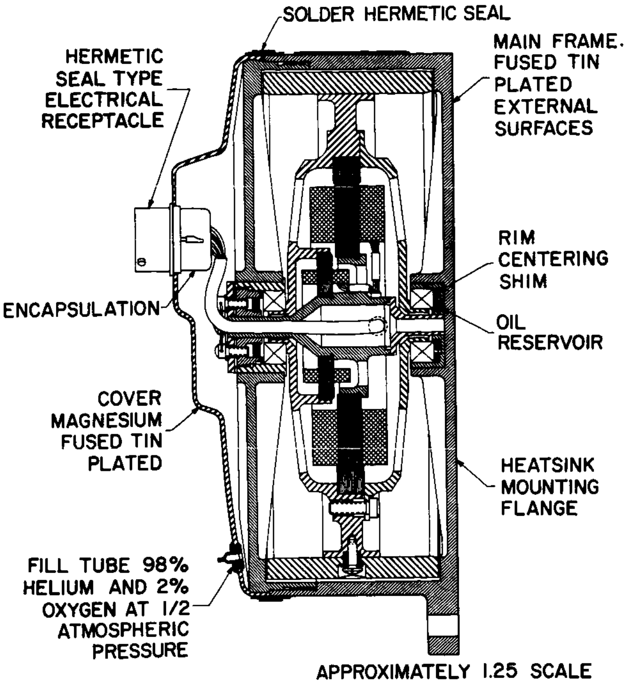
SOLDER HERMETIC SEAL
HERMETIC SEAL TYPE ELECTRICAL RECEPTACLE
MAIN FRAME. FUSED TIN PLATED EXTERNAL SURFACES
RIM CENTERING SHIM
ENCAPSULATION
OIL RESERVOIR
COVER MAGNESIUM FUSED TIN PLATED
HEATSINK MOUNTING FLANGE
FILL TUBE 98% HELIUM AND 2% OXYGEN AT 1/2 ATMOSPHERIC PRESSURE
APPROXIMATELY 1.25 SCALE

Figure 2-5. Typical Reaction Wheel

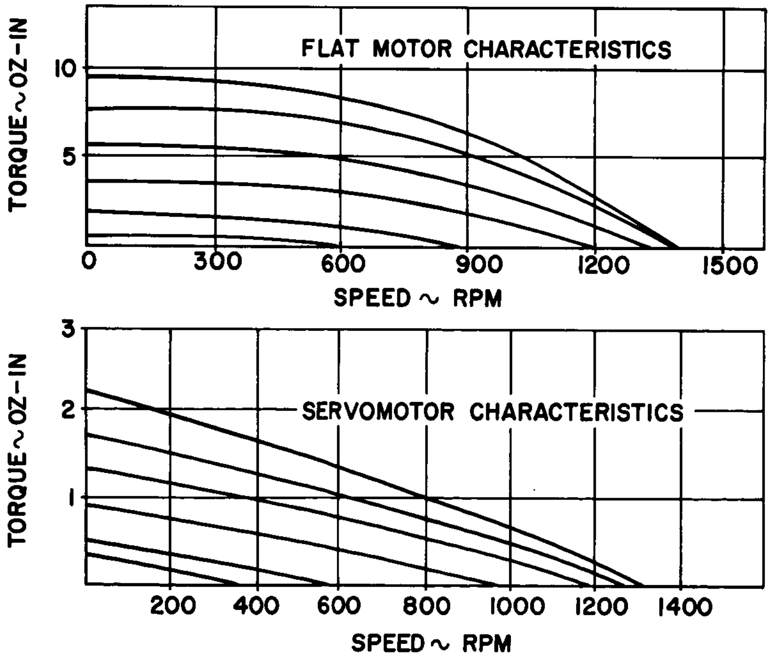

Figure 2-6. Reaction Wheel Torque-Speed Curves

motor having a sperical rotor which can be accelerated in any direction. An electrostatic suspension system is used to support the rotor, and this not only enhances inherent reliability by the minimization of moving parts but decouples the single moving part from all effects of friction.

Like the reaction wheel system, the reaction sphere is an inertial torquing device for controlling the attitude of a space vehicle. At the same time, the reaction sphere eliminates gyroscopic cross coupling effects which exist when three wheels are used. Three stators surround the sphere in the orthogonal axes; these may be excited singly, or in combination to induce a torque to accelerate the sphere in any desired direction. The reaction to the applied torque accelerates the vehicle. When the component of the sphere speed in the plane of a stator reaches its maximum value, the sphere is "unloaded" in that plane through the application of an opposite torque to the vehicle, e.g., by reaction jets. The unit incorporates speed sensors in each stator plane for initiating this action.

3. Gyro Torquing Devices

Use of a gyro as a torquing device is another inertial control concept. Like the reaction wheel, the gyro operates on the principle of conservation of momentum and, as such, is a momentum transfer device. In the gyro concept, use is made of the torque generated when a high speed wheel is forced to precess about an axis other than its spin axis. The prime advantage of using a gyro rather than a reaction wheel is that lower control power is required for the gyro (theoretically, by a factor of several orders of magnitude, neglecting the power required to spin the gyro). The torque exerted by the gyro on the vehicle is many times the input torque; in comparison, the input torque to a reaction wheel must equal the torque to be exerted on the vehicle. The torque gain of the gyro is a function of the ratio of angular momentum to gimbal damping. Two gryo systems which have been mechanized and appear feasible for attitude control are General Electric's Gyroscopic Lower Power Attitude Control (GLOPAC) system and Ling-Temco-Vought's "Twin Gyro" system.

Both of these systems use single axis (one gimbal) gyros. The gyro is forced to turn about its output axis (forced precession), causing a torque to be exerted on the vehicle about the input axis. As the gyro is precessed away from its null or zero axis, the control torque has one component about the desired axis and another undesired component about a perpendicular axis. Thus, as the gimbal angle becomes larger, the control torque output decreases and the cross coupling torque increases. The cross coupled impulse becomes equal in magnitude to the control impulse when the gimbal angle reaches 90°. In addition, a given precession velocity, or torque input, results in decreasing torque response about the control axis as the gimbal angle increases. Consequently, the gimbal angle must be limited to something less than 90°.

a. GLOPAC

GLOPAC is a four gyro, 3- axis system using the momentum changes of its gyros to control the orientation of a vehicle in space. The control system consists of three major functional elements: the attitude sensors, the four body mounted power gyros, and the gyro computer. The attitude sensors are discussed elsewhere in this report. The power gyros are single-degree-of-freedom, bodybound, high speed wheels. The gyro gimbal axis is oriented by a torque motor and its angular orientation is read out by a resolver. The gyro computer contains circuitry necessary for gyro torquing and reset control. The computer outputs, which are the commands to the gyro torque motors, change the angular orientation of the gyros in a manner which produces corresponding gyro precession torques in the proper direction to maintain vehicle attitude in the presence of disturbing torques. The addition of the fourth gyro increases the maximum momentum capability or saturation limit of the attitude control and decreases the frequency of reset. A saturation limit of approximately 3H (H is the momentum of one gyro) can be obtained with the GLOPAC system. This is seven times the saturation value of the conventional three-gyro system and is a significant improvement over the saturation limit of the reaction wheel control. The extra gyro provides redundancy to improve the overall system reliability. Thus, the use of a fourth gyro has a dual advantage. This configuration of the four gyros, shown on Figure 2-7, was developed to simplify the control torque computations resulting from the gyro system equations.

The GLOPAC four gyro momentum transfer system can provide the desired pointing accuracy for the SMS (accuracies of less than a minute of arc are possible). The weight of the gyros (2 in.-lb-sec) at 3.15 lb per gyro, is 12.6 lb. The computer weight including the power converter is 3.5 lb.

The stabilization rates of the gyroscopic momentum transfer system depend on the gyro threshold, which is a function of the gimbal bearings used. The threshold of the 2 in.-lb sec gyro is approximately 2°/hr (or 5.5 x 10^{-4}/sec) in a 1g environment. The threshold in zero g conditions will be lower, but the actual magnitude has not been determined. A zero g threshold of one-half the 1g value appears to be a reasonable value. Based on this assumption, the stabilization rates of the 2 in.-lb-sec gyro in a zero g environment is 2.7 x $10^{\circ -4}$/sec.

The GLOPAC hardware described could be ready for the first flight by mid-1965. The equipment considered is four power gyros, the gyro electronics, and the necessary power conversion equipment.

b. Twin Gyro Controller

The Twin-Gyro Controller consists essentially of two identical single axis gyroscopes gimbaled to a common frame as illustrated in Figure 2-8. The frame is torqued about one axis by the controller. Thus, three controllers (six gyros) will be required to control the attitude of the satellite about its three axes. The twin gyros will eliminate the most significant cross coupling effects. This is accomplished by turning the two gyro rotors mounted to the same frame (for each axis) in opposite directions and precessing their gimbals simultaneously in opposite directions. The control components of the torques generated will be in the same direction and will add, while unwanted components will be in opposite directions and will cancel. The gimbal drive motor torques will be in opposite directions and will also cancel. The only cross coupling torque that will not cancel is that due to rotation about an axis orthogonal to the control and gimbal axes. Since this torque is a sine function of the gimbal angle, it will be small if the gimbal angle is small.

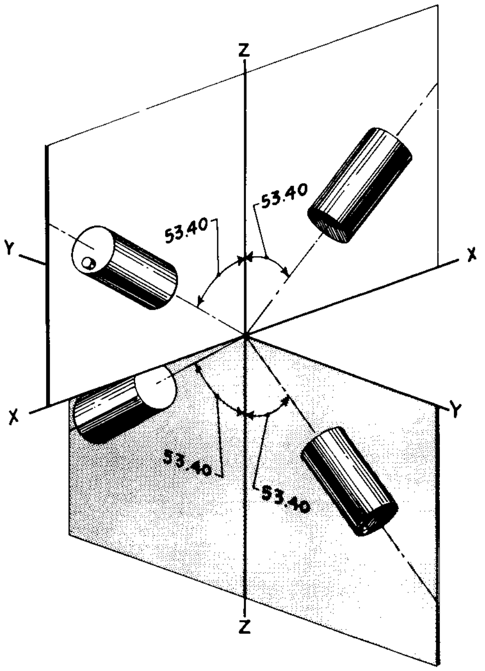
Z
Y
X
53.40
53.40
X
Y
53.40
53.40
Z

Figure 2-7. GLOPAC Gyro Orientation

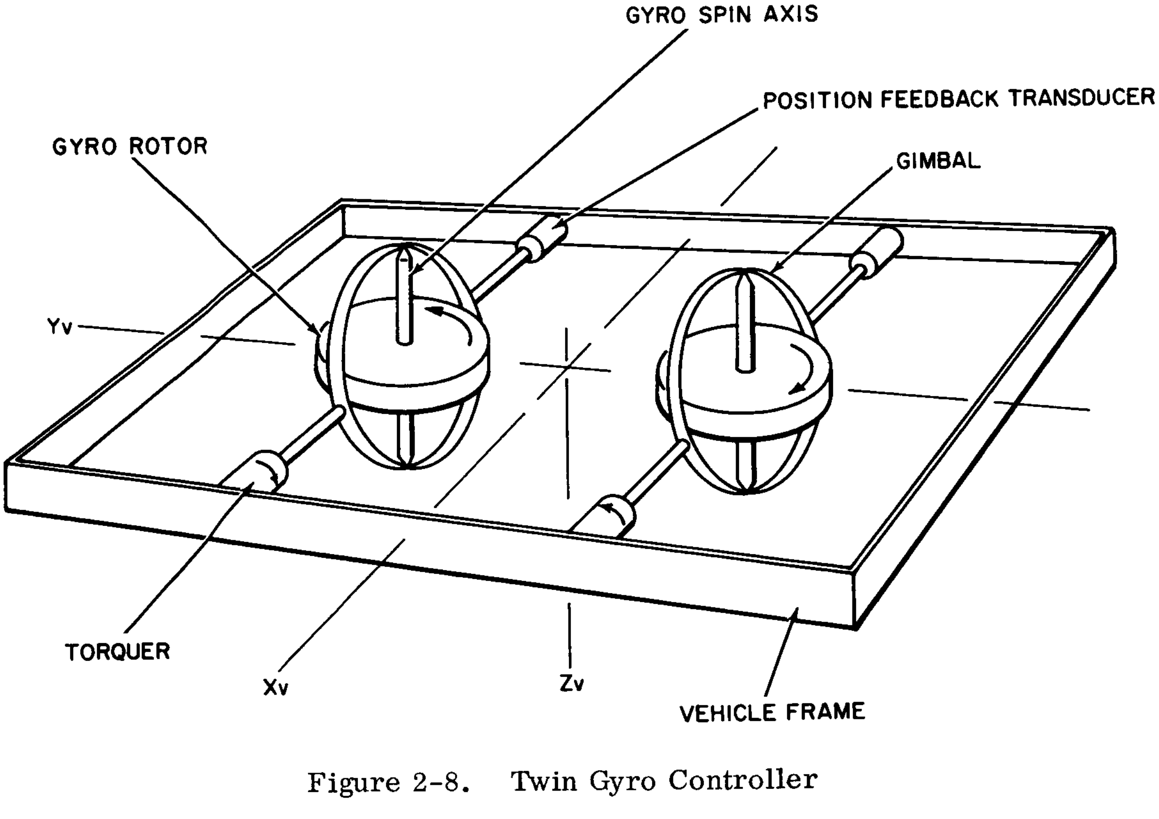
GYRO SPIN AXIS
POSITION FEEDBACK TRANSDUCER
GYRO ROTOR
GIMBAL
Yv
TORQUER
Xv
Zv
VEHICLE FRAME

Figure 2-8. Twin Gyro Controller

The weight, power and size for the Twin Gyro Controller for the SMS are based on 3.6 to 3.7 x 10^6 cm^2/sec angular momentum wheels in all axes. These characteristics are summarized below.

1) Weight.

a) Single Wheel System-Present. The following breakdown assumes the use of present state of the art technology in off the shelf items now in production.

Unit	Weight (lb)	Remarks
Rotor Assembly	1.70	Includes rotor, motor, sealed housing, and bearing. Weight is average of weights obtained from three companies.
Torque Motor	0.06(0.95oz)	Kearfott CMO-0218 motor.
Followup Synchro	0.07(1.13oz)	Kearfott CMO-1002 synchro.
Gear Train	0.20	Includes sealed bearing, irreversible output, and lubrication.
Structure Assembly	0.24	Average per wheel for a 3-axis assembly.
Amplifier	0.12	Average per wheel for a six amplifier package.
Total	2.39	
Total-3-Axis Controller	14.34	

The foregoing values were obtained from supplier catalogs or from vendors in response to direct questions. The weights for the gear train, assembly structure, and amplifier are based upon layouts by Temco and are consistent with values derived by ratioing actual weights from previously built Twin Gyro Controller designs.

b) Single Wheel System-Future. The following breakdown assumes the design to be achieved in 2 years with development time and funds allotted for optimizing the controller for minimum weight. These weights would be realizable objectives based upon present trends and new developments presently in research.

Unit	Weight (lb)
Rotor Assembly	1.40
Torque Motor	0.05
Synchro (size 8)	0.06
Gear Train	0.15
Assembly Structure	0.20
Amplifier	0.09
Total	1.95
Total 3-Axis Controller	11.70

The above values were derived in the same manner as those for the present state of the art equipment. It must be kept in mind that to realize the above unit weights, development effort will be required on each item since, none are currently off the shelf. Using present approaches, it should be possible to achieve the above goals within 2 years with development effort.

c) General Comments on Weight. The weights given are for a single structural assembly for the controller and amplifiers. If it is more desirable for space utilization, each wheel or controller axis can be located separately. The structural weight totals will increase by about 0.60lb for the three axes if the controller is separated into three assemblies, and by about 1.40lb if separated into six assemblies.

One method for reducing the structural weight would be to incorporate the controller structure as part of the vehicle structure, since location is not critical. With this method, precise alignment of the controller axes with the sensor axes could also be aided by the use of precision machined structure for the vehicle.

The synchro listed in the present state of the art tabulation is not adequate in accuracy for the 1000 lb vehicle where very low stabilization rates are required. However, a special unit of the same weight will be substituted for the size 8 listed.

If disturbance torques are found to be greater than those used to size this rotor a different size rotor will be required. The weights of the rotor and structure will vary approximately proportionally to angular momentum. The weights of other items will be constant over a wide range of momentum values.

2) Power

a) Requirements for a 3-Axis System-Present. The following breakdown assumes the use of present state of the art technology in off the shelf items now in production.

Unit	Power (W)	Remarks
Rotor Power	36.0 - running	Uses of a hysteresis - ring type motor.
Excitation Power	17.2	
Amplifier Power	15	
Total	68.2	

Most existing rotor designs are based upon short runup time. Since in the SMS application run up time is not critical, a minor design change would allow (under existing technology) a reduction in running power to about 3.0 w/rotor. This would require a 30 minute starting time to come to the synchronization speed of the rotor, and would allow a total rotor power of 18 W with a total power of 50.2 w for a 3-axis assembly. Although a rotor of this type is available, it is not currently in production.

The excitation power listed is for the motor used in the analysis work done previously for the SMS. Later analysis indicates that another motor of lower wattage may be used but the analysis of motor parameters indicates that further work should be done before there is assurance that it can be used, since its use may necessitate special compensation in the servo loops. This appears to be a promising approach, when it is considered that the excitation wattage would be only 9.0 w with an amplifier power of 6 w. With this potential torquer motor, the total controller power would be 33 w for a 3-axis assembly.

The power to the rotors should be 115V, 400 cps single or three phase. Use of three phase power saves the weight of a phase shifting capacitor. A frequency of 400 cps appears to be the best choice for now and the near future, however, 800 cps or higher is usable. Trade-offs indicate that other frequencies usually are not worth the possible reliability problems they introduce, since unproven designs would be involved. Excitation power would be 26 V AC, single phase, preferrably 400 cps, and the amplifier would use regulated DC of at least 28 V. It would probably be most efficient as concerns parts, weight, and reliability to have + and - 28 VDC for the amplifiers.

b) Requirements for a 3-Axis System-Future. The following breakdown assumes the design is made in about 2 years with development required for reduction of power. This power breakdown would be realizable objectives based upon present trends and known approaches.

Unit	Power (W)
Rotary Power	12(2W/wheel)
Excitation Power	7
Amplifier Power	4
Total	23

The use of a synchronous hysteresis motor which is possible in the future would allow a reduction in rotor power optimized for lower running power. This power reduction is achieved with special starting provisions, which require additional ground starting equipment. This will not add weight or lower system reliability.

The excitation power reduction would be effected by the use of a special motor with lower fixed field steady power requirements. The amplifier power reduction would be obtained principally by use of a more efficient amplifier tuned to the power level requirements of the torquer rather than stall conditions. The torque output requirements of the torquer are very near the no-load requirements, while most existing designs are based upon power efficiency near the stall torque output of the motor.

It should be noted that the amplifier power required is that for torquing all wheels at the maximum gimbal angular rate for the torque conditions specified. This condition is not expected to occur continuously, so the total power listed is more of a peak load, while the continuous load will be about 70% of the total listed.

3) Size.

Using Present Components

3-Axis Controller	7.0 x 7.0 x 7.0 in.
1-Axis Controller (output torque axis through 7 x 3.5 side)	7.0 x 7.0 x 3.5 in.
1-Wheel System (output torque axis through 6.0 x 3.5 side)	6.0 x 3.5 x 3.5 in.

Using Special Components Within Present State of the Art

3-Axis Controller	6.0 x 6.0 x 6.0 in.
1-Axis Controller	6.0 x 6.0 x 3.1 in.
1-Wheel System	5.0 x 3.1 x 3.1 in.

Future Systems - Designed within 2 years with Special Components

3-Axis Controller	No appreciable change from present
1-Axis Controller	
1-Wheel System	

4. High Pressure Cold Gas

The compressed cold gas system is most attractive for low thrust, low total impulse space missions. It is extremely simple, with an associated high reliability, and involves the least extension of the present state of the art. Cold gas systems have been used in the Mariner, Ranger, and other space programs, resulting in a large fund of knowledge and experience with this type of system. The system is illustrated schematically in Figure 2-9.

The storage tank is initially charged with dry nitrogen at 3000 psia. From the storage tank the gas flows through a two stage regulator to the shut-off valves and thrust nozzles. The storage tank filler and all valves will have built-in filters at their inlet ports. Nitrogen is employed in many operational systems and is superior to helium because of storage advantages and lighter system weight. Helium is prone to leakage; and because it weighs less than nitrogen it requires a larger, and hence, heavier, storage tank. The use of gases other than nitrogen has recently been the subject of investigation. Vacuum specific impulse and gas weight are not the only considerations because the tank weight is usually of the same order of magnitude. The specific gas to be used should be determined at the time hardware is designed by reviewing the overall weight (tank plus propellant), performance, thermal characteristics, storability, and stability of the various gases.

5. Solid Subliming Gas

The cold gas reaction control systems which have first gained acceptance for satellite attitude control use nitrogen gas. This system requires high pressure, leading to leakage problems, heavy storage tanks, and the necessity of using pressure regulators. The solid subliming system developed by Rocket Research Corporation uses low pressures and requires no pressure regulators, see Figure 2-9. The propellant is stored in the solid state and sublimes as required. Storage of the propellant in the condensed state enables low volume, lightweight tanks to be used, and the system is self-feeding. Sublimation is the direct conversion from a solid to vapor. This change is accompanied by an absorption of heat. A solid can be completely vaporized without the intervention of a liquid phase, provided that the pressure of the vapor is not allowed to exceed that of the triple point. If the triple point is high, it is a simple matter to maintain this sublimation at a high rate, which is desirable.

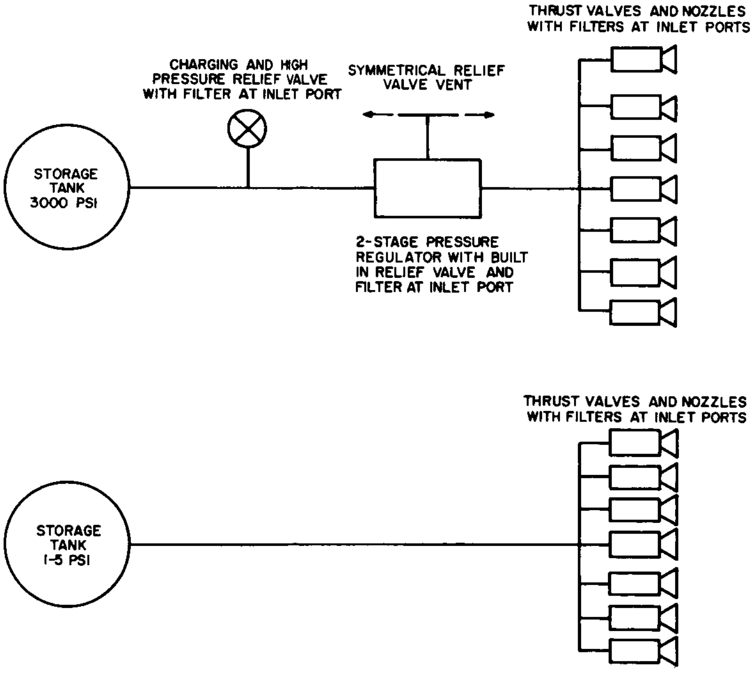
THRUST VALVES AND NOZZLES WITH FILTERS AT INLET PORTS
CHARGING AND HIGH PRESSURE RELIEF VALVE WITH FILTER AT INLET PORT
SYMMETRICAL RELIEF VALVE VENT
STORAGE TANK 3000 PSI
2-STAGE PRESSURE REGULATOR WITH BUILT IN RELIEF VALVE AND FILTER AT INLET PORT
THRUST VALVES AND NOZZLES WITH FILTERS AT INLET PORTS
STORAGE TANK 1-5 PSI

Figure 2-9. (a) High Pressure Cold Gas System
(b) Solid Subliming Low Pressure Gas System

6. Cap Pistol

Curtiss-Wright's "Cap Pistol" is a series of small bits of solid propellant imbedded in a plastic tape. Each bit is actually a self-contained solid rocket, having its own nozzle, propellant charge, and ignition system. These tiny rockets move into firing position in much the same manner as the rounds of ammunition fed through a machine gun.

7. Electric Propulsion

a. Plasma Pinch Engine

This engine, developed by Republic Aviation, is discussed in Volume 7.

b. Electrostatic Ion Engine

Basically, the Hughes electrostatic engine involves the ionization of the propellant which is then accelerated electrostatically. The ion engine has the highest potential specific impulse, upwards of 10,000 seconds, and as a matter of fact, cannot operate efficiently below a specific impulse of about 5000 seconds.

Four major subsystems comprise the ion engine: propellant storage and handling subsystem, ionization subsystem, ion acceleration subsystem, and beam neutralization subsystem.

The propellant handling system must provide an accurately metered propellant supply at low flow rates. The propellant used in the Hughes Cesium surface- contact ion engine is cesium which is kept liquid by the application of heat. The ionized propellant is produced by passing the cesium through a porous, heated, tungsten ionizer. Power must be supplied to heat the ionizer approximately 30 seconds before each firing. In general, since the duty cycle associated with an attitude control system is low, warming the ionizer for each firing is more economical from a power standpoint than continuous heating at operating temperature.

The ion acceleration and beam neutralization subsystems have been subjected to intensive research and development. The accel-decel principle of acceleration has been widely accepted. This concept allows high beam current density with a reasonable exhaust velocity, and the difference in potential between the accel and decel areas prevents the beam neutralizing electrons from flowing back to the ion source. Of major consideration is the prevention of ion impingement on the electrodes with its accompanying decrease in electrode operating life. It is generally accepted that a solution has been arrived at for beam neutralization. Beam neutralization is required to prevent the buildup of a positive space charge which will cause succeeding ions to "stall" and be turned back. Neutralization is accomplished by addition of electrons to the beam, which may introduce problems. Flight test of this system is scheduled for 1963.

The characteristics of the Hughes ion engine are summarized below.

Station Keeping System Characteristics
(E-W correction)

Satellite Mass (lb)	Duty Cycle (%)	Thrust Internal (min)	Average Power Reqts (W)	Solar Cell Wt (lb)	Energy Storage Reqt (W-hr)	Battery Wt (lb)	Total Power Supply Wt (lb)
100	0.05	0.66 one per day	0.22	0.03	5.2	1.9	1.9
500	0.23	3.3 one per day	1.1	0.14	26	3.8	3.9
1000	0.46	6.6 one per day	2.2	0.28	52	7.6	7.9

P/T = 267 KW/lb

ηpc = 85%

P = 470 W (including power conditioning)

T = 1.5 m lb

System Weights (lb)

System Components	Present	Target
Engine Stations (4)	52	45
Engines (3 per station) -3		
Feed system (loaded with 3 yr cesium supply)-8		
rotator - 2		
Power Conditioning Equipment	26	20
Power Control System	5	2.5
Overall System Controls	5	2.5
Cabling	5	5
Signal Conditioning	2	2
Totals	95	77

8. Hot Gas Systems

A bipropellant system utilizes a hypergolic propellant combination which is ignited in a combustion chamber. The typical bipropellant attitude control system consists of three subsystems: a pressurization subsystem, a propellant feed and storage subsystem, and a subsystem of thrust chamber assemblies.

The pressurization subsystem provides high pressure nitrogen gas for expelling the propellants and actuating the propellant valves. The propellant feed and storage subsystem includes fuel and oxidizer storage tanks from which the propellants are discharged, by high pressure nitrogen, into the propellant feed lines to the thrust chambers. The thrust chamber assemblies include on-off propellant valves for sequencing of fuel and oxidizer to the thrust chambers. The thrust chamber assemblies produce thrust by burning the fuel and oxidizer combination. Starting is effected by the hypergolic ignition of the fuel and oxidizer.

Liquid monopropellant systems use a stored liquid to generate and expell hot gases. In operation, actuation of a squib start valve allows nitrogen gas from a storage bottle to pressurize the propellant tank. Upon command, solenoid operated propellant valves open, permitting hydrogen peroxide (or another propellant) to flow through a catalyst bed in the thrust chamber. The catalytic reaction causes decomposition. In the case of hydrogen peroxide, decomposition forms steam and oxygen which exhausts through the rocket nozzle, providing thrust.

Small solid propellant rockets have certain major disadvantages, notably limited burning time and inability to restart. For these reasons, solid propellants are not practical for attitude control. The Curtiss-Wright "Cap Pistol" concept, discussed previously, uses many one shot rockets to circumvent these shortcomings.

9. Magnetic Torquers

By controlling the currents in a group of three orthogonal coils fixed to the body of a satellite, a useful attitude control torque can be produced by reaction with the Earth's magnetic field. Such magnetic torquing can provide direct control of the vehicle momentum or indirect control by removing the momentum accumulated in reaction wheels. Of course, no torque can be generated about an axis aligned with the Earth's magnetic field. This concept is primarily applicable to low orbits and should not be considered for the SMS until information is available on magnetic fields at synchronous orbital altitudes.

10. Vaporjet

The Vaporjet (Advanced Technology Laboratories) is a reaction device in which thrust is obtained by the expulsion of a vapor through a nozzle. In this system, the working fluid is a vapor generated from its liquid phase at constant temperature and pressure. ASD Technical Report 61-471, "Design and Development of a Vaprojet Attitude-Control System for Space Vehicles," discusses Advanced Technology Laboratories' work on these systems.

11. Diffusion of Hydrogen Through Palladium

An interesting cold gas system being developed by Advanced Technology Laboratories uses hydrogen as the propellant. Its diffusion rate through an alloy of palladium-silver is regulated by controlling the temperature of the palladium silver. Although this work is in a preliminary status, it is worth following up for possible future application. Advanced Technology Laboratories first phase report, "Research on Diffusion of Hydrogen Through Palladium," ATL-D-943, Dec. 21, 1962, discusses some of the work done in this area

12. Brushless DC Motor

Kearfott's brushless DC motor development was briefly reviewed. It was felt that for this particular program, considering the present state of development of these motors, AC motors would be more applicable.

13. Conclusions

Cold gas systems have been in use for some time both in space and other applications. Therefore, they have been more fully developed than the other reaction jet type systems. Their basic simplicity, plus the large amount of development work already accomplished, has resulted in reliable systems.

Solid subliming systems are potentially simpler (fewer valves and lower gas pressures), lighter, and more reliable, and merit serious consideration after more operating experience has been obtained with these systems.

The electric propulsion systems, i.e., the plasma pinch and ion engines, offer very high specific impulse with corresponding light propellant systems. However, the impulse requirements must be sufficient to justify the heavier engine weight and relatively high electrical power requirements. Also, more development work must be accomplished before this type system can be fully evaluated.

Angular momentum transfer or storage devices, reaction wheels, reaction spheres, and gyro systems are of prime advantage where fine control of the satellite is required and/or where the cyclic distrubing torques contribute significantly to the total impulse required. These devices can compensate for these cyclic disturbing torques without mass expenditure. The reaction wheels are the most fully developed of these devices and therefore, are probably the most reliable. The reaction sphere, when developed to the point where reliable flight hardware is available, will be a desirable torquer, since the cross coupling effects inherent in a 3-axis reaction wheel system do not exist. Gyro systems, although not as fully developed as systems as are reaction wheels, offer several possible advantages which justify their consideration. Gyros have been built for this purpose, tested, and refined over a long period of time. Lower control power is required for the gyro and the torque exerted by the gyro on the vehicle is many times the input torque.

Information for this survey of torquers was obtained from the following companies by exchange of visits and/or correspondence.

1.	Reaction wheels	Bendix-Eclipse Pioneer
2.	Reaction sphere	Bendix-Eclipse Pioneer
3.	Glopac	General Electric, Light Military Electronics Dept.

4.	Twin Gyro	Temco Electronics
5.	High pressure cold gas	Walter Kidde Co., Inc. Whittaker Controls & Guidance Sterer Engineering Mfg. Co. Bendix-Eclipse Pioneer
6.	Low pressure cold gas	
	a) Solid Subliming Microrocket	Rocket Research Corp.
	b) Vaporjet	Advanced Technology Laboratories
7.	Cap pistol	Curtiss-Wright Corp.
8.	Plasma Engines	Republic Aviation Corp. Rocket Research Corp.
9.	Ion engines	Hughes Research Labs Electro Optical
10.	Hot gas	The Marquardt Corp. Rocket Research Corp. Aerojet General Vickers, Inc.
11.	Magnetic torquing	Westinghouse Electric Corp.
12.	Diffusion of hydrogen through palladium	Advanced Technology Laboratories

C. DISTURBANCE TORQUES

1. Introduction

The purpose of this analysis is to estimate anticipated disturbance torques and provide a torque model which can be used to size control system torque devices. In addition, attitude stabilization performance must be assessed under the influence of these disturbances.

The satellite lifetime of one year in orbit requires that constant attitude disturbing torques be reduced to the minimum value possible. A lack of alignment of the principal axes with the stabilized axes will cause a constant disturbing torque due to differential gravity which will have a very significant effect on control gas requirements. A design requirement of 1/2° error angle between principal and body axes will suitably minimize such gas consumption requirements.

The solar effect torques (solar radiation and solar flare) will vary sinusoidally. These torques will have components with a one year period and daily and twice daily periods. The control system will have to compensate for a steady bias due to inequality of positive and negative daily torque-time areas. The reaction wheel system is not sized to compensate for the bias effect, which will be corrected for by the cold gas wheel momentum dumping system. For vehicles with solar paddles, shadowing effects may increase the peak value of the torques which vary daily, but the average value of the yearly torque-time areas will still be zero.

Magnetic interaction with the Earth's field can be made negligible by arrangement of conductors carrying DC so as to minimize loop areas. Magnetic devices in the vehicle will use shielding to reduce the effects of stray fields. The random effect of the Sun's magnetic field is not known, but is expected to be negligible.

The equipment-dependent torques are found to be small and generally consist of spaced torque square pulses with equal negative and positive torque-time areas for short time periods; hence, they impose only a minor burden on the attitude control system.

2. Disturbance Torque Calculations

a. Predictable Solar Torques

The purpose of this subsection is to develop the analytical expressions which describe satellite disturbance torques due to solar pressure and solar flare. The analyses of solar pressure effects involving specular reflection, absorption, and diffuse reradiation, as well as solar flare effects, are performed for flat plates and circular cylinders. The results of the analyses are applied to the following vehicle configurations:

(1) Spin stabilized vehicle (cylinder spinning about the long pitch axis).

(2) Three-axis stabilized vehicle (cylindrical body with flat plate paddles).

(3) Gravity gradient stabilized vehicles (coaxial cylinders).

The analyses performed for the spin-stabilized vehicle and the gravity gradient stabilized vehicle assume that the center of gravitational attraction and the geometric center of the vehicles coincide. The 3-axis stabilized vehicle with flat plate paddles was analyzed using the assumption that the paddle axis and the geometric center of the vehicles coincide, but that the center of gravitational attraction is displaced along roll, pitch, and yaw body axes. The shadowing effect of the paddles on the cylindrical body of the 3-axis vehicle is not considered but shadow effects are compensated for in the study of the gravity gradient stabilized vehicle.

The solar pressure parametric study assumes coefficients of specular reflection (R_1, R_2, R_3) are known for various surfaces in the space environment, and that absorbed incident radiation is diffusely re-emitted in accordance with Lambert's cosine law. Solar flare is treated as a phenomenon involving inelastic collision of particles with the satellite surfaces, and both reflection and reradiation effects are considered negligible.

1) Pressure Due to Incident Radiation and Reflection on a Flat Plate. The basic equations of solar pressure and solar flare interaction are shown below. It should be noted that assumptions made are consistent with present practices within the field.

The incident solar energy is considered to be equivalent to a matter wave where the mass can be derived from $E = mc^2 = h\nu$. For complete absorption of sunlight by a surface, the momentum change of the absorbing surface = $mc = \frac{h\nu}{c}$. Since the change in momentum per unit time is a force ($\frac{d}{dt}(mv) = F$); $F = \dot{m}c$ and the impulse equals $\dot{m}ct$. If the incident solar energy is expressed as "S" energy per unit time, per unit area at a given distance from the sun,

$$S = \frac{\text{Energy}}{At} = \frac{mc^2}{At}$$

$$m = \frac{ASt}{c^2} \quad ; \quad \dot{m} = \frac{AS}{c^2}$$

$$\dot{m}_{\text{per unit area}} = \frac{S}{c^2}$$

$$F_{\text{unit area}} = \dot{m}c = \frac{S}{c}$$

If the incident energy is not completely absorbed, but is partially reflected specularly and an angle of incidence exists, then the force on the surface due to radiation pressure is:

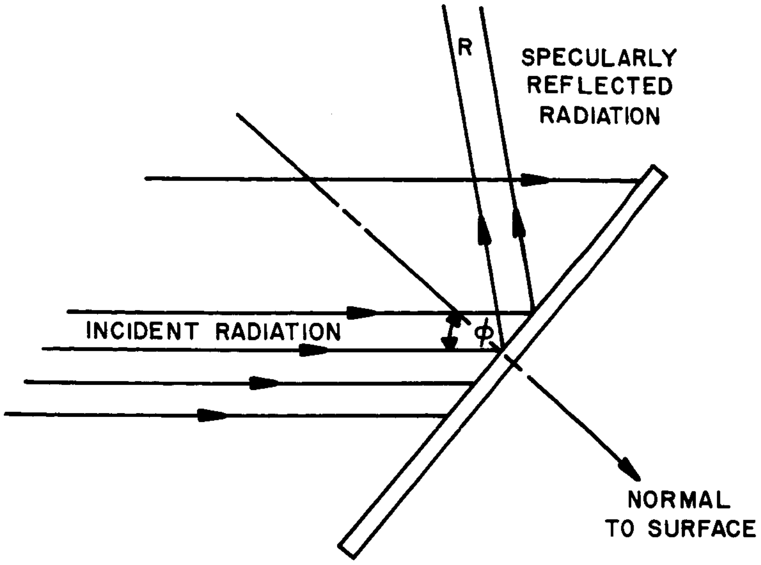
R
SPECULARLY REFLECTED RADIATION
INCIDENT RADIATION
ϕ
NORMAL TO SURFACE

Force Normal to Surface } $(1+R)\frac{S}{c}\cos^2\phi\ (A)$

Force Tangent to Surface } $(1-R)\frac{S}{c}\cos\phi\sin\phi\ (A)$

R = fraction of incident radiation reflected where the incident pressure per unit area is $\frac{S}{c}\cos\phi$

The solar energy is either converted to electrical energy and stored or reradiated diffusely. If the surface temperatures on the vehicle are constant, the reradiated energy will produce zero net force. If the value of R is not high, and the surface temperature is much higher than that of the rest of the satellite, then the diffuse reradiation from the surface will add to the force on the surface.

2) Diffuse Reradiation Analysis Based on Lambert's Cosine Law. Emitted radiation pressure from a diffuse surface (based on Lambert's law of radiation; $I = I_o \cos\psi$)

$I = I_o$ normal to emitting area

$I = I_o \cos\psi$ in any direction "ψ"

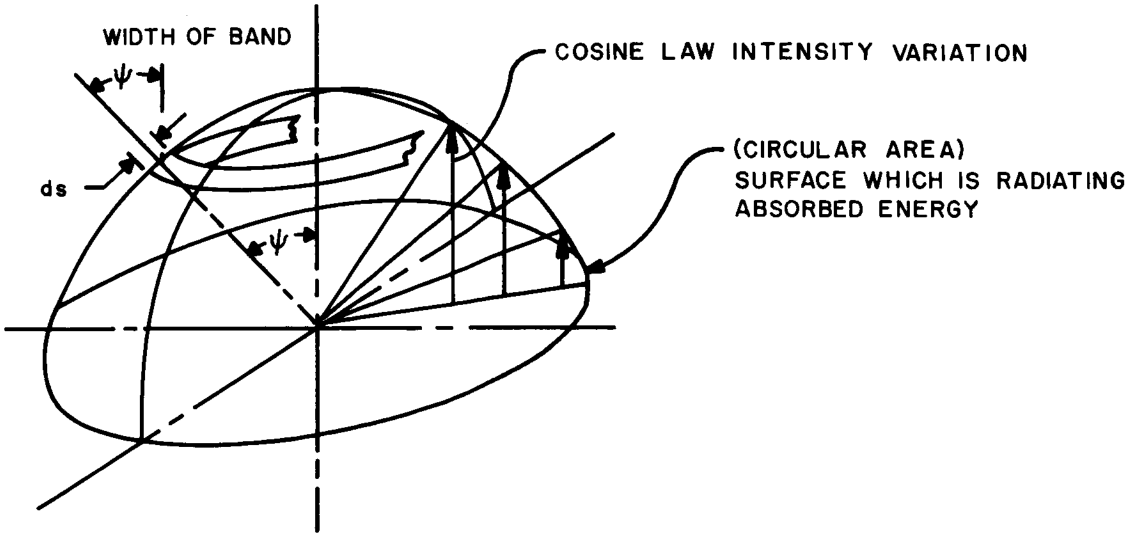
WIDTH OF BAND
ψ
ds
ψ
COSINE LAW INTENSITY VARIATION
(CIRCULAR AREA) SURFACE WHICH IS RADIATING ABSORBED ENERGY

Area of each differential band of the intensity sphere of radius "r": $dA = 2\pi(r\sin\psi)\,ds$, where $ds = r\,d\psi$

$dA = 2\pi\,(r^2)\,(\sin\phi)\,d\psi$

differential radiation component normal to emitting surface for each band

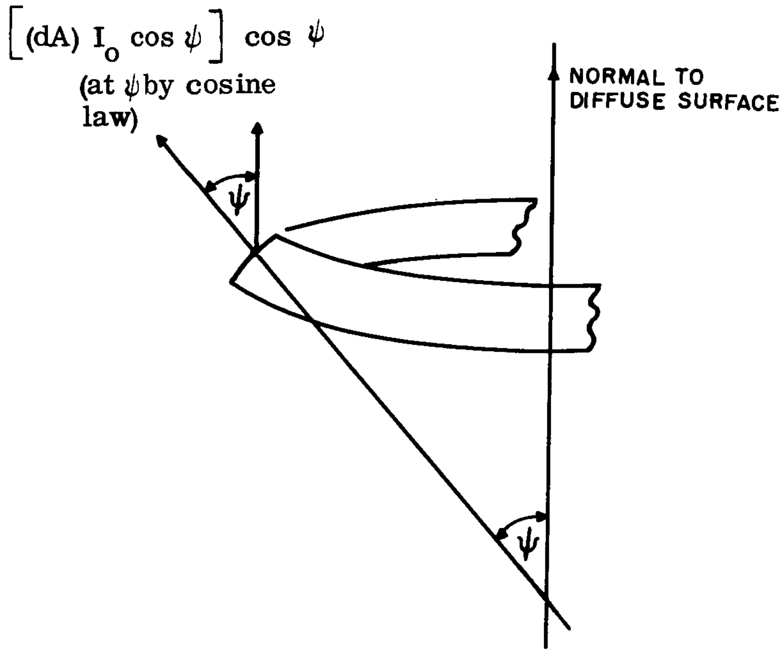

$\left[(dA)\, I_o \cos\psi\right] \cos\psi$
(at ψ by cosine law)
NORMAL TO DIFFUSE SURFACE
ψ
ψ

Total component of emitted radiation normal to plane on which differential area source lies

$$2\pi r^2 I_o \int_0^{\pi/2} \sin\psi \cos^2\psi \, d\psi = 2\pi r^2 I_o \left[- \frac{\cos^3\psi}{3} \right]_0^{\pi/2}$$

$$= + \frac{2\pi}{3} r^2 I_o$$

$$= \left[\frac{2}{3}\,\frac{S}{c}\right]$$

Total pressure is "P"

Area of Hemisphere

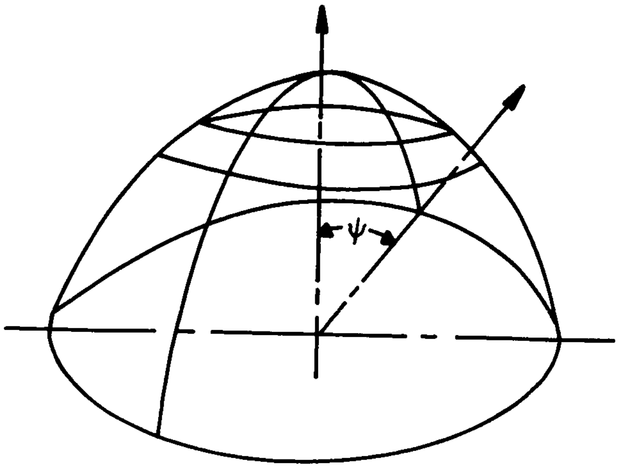

$$A = 2\pi r^2 \left[-\cos\psi \right]_0^{\pi/2}$$

$$A = 2\pi r^2$$

$$P = \left[(1 - R)(1 - \gamma) \right] \frac{S}{c} \cos\phi$$

$$dA = 2\pi r \sin\psi \, ds$$

$$A = 2\pi r^2 \int_0^{\pi/2} \sin\psi \, d\psi$$

$$I = I_o \cos\psi$$

$$P = \int I \, dA$$

$$P = 2\pi r^2 I_o \int_0^{\pi/2} \sin\psi \cos\psi \, d\psi$$

$$P = 2\pi r^2 I_o \left[\frac{1}{2} \sin^2\psi \right]_0^{\pi/2}$$

$$P = \pi r^2 I_o$$

$$I_o = \frac{P}{\pi r^2}$$

Due to Solar radiation pressure

The Total Normal Force Becomes:

$$N = (A) \frac{S}{c} \cos\phi \left[(1 + R) \cos\phi + \frac{2}{3} (1 - R)(1 - \gamma) \right]$$

The Tangential or Shearing Force Remains

$$T = (A) \left(\frac{S}{c} \cos\phi \right) \left[1 - R \right] \sin\phi$$

where $\frac{S}{c} = 1 \times 10^{-7} \text{ lbs/ft}^2$

The mechanism of solar flare involves inelastic collision between particles and surface, and $R = 0$, $\gamma = 0$. Diffuse reradiation is neglected.

Using $\left[\frac{S_f}{c}\right]$ for solar flare (max) $= 75 \times 10^{-7}$ lbs/ft^2

Solar Flare

$$\text{Normal Force} = (A)\left[\frac{S_f}{c}\right] \cos^2 \phi$$

$$\text{Shear Force} = (A)\left[\frac{S_f}{c}\right] \cos \phi \sin \phi$$

The solar flare inputs would be added to the solar pressure effects. Both solar radiation pressure and particle effects caused by solar flare are subject to shadowing and reflection effects of paddles, satellite overhangs, etc. A complete analysis requires the use of a digital computer program and study.

The satellite configurations considered consist of flat surfaces and cylinders. The effect of solar radiation and solar flare on cylinders is discussed below.

3) Radiation Normal to the Axis of a Circular Cylinder.

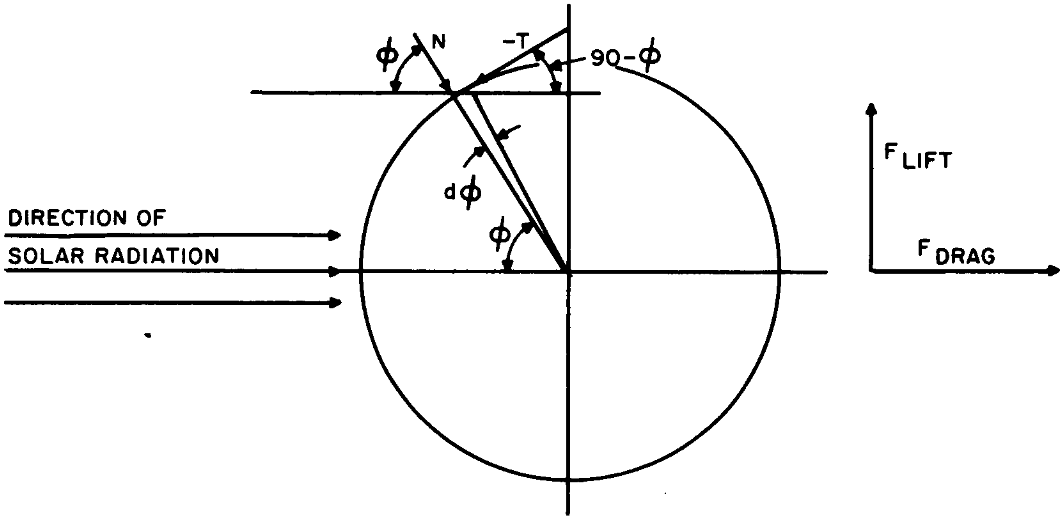

Normal and tangential forces on differential area of cylinder which approximates flat plate

$$dN = dA \frac{S}{c} \cos \phi \left[(1+R) \cos \phi + \frac{2}{3}(1-R)(1-\gamma)\right]$$

$$dT = dA \frac{S}{c} \cos \phi \ (\sin \phi)(1-R)\ )$$

where $dA = (r\ell)\, d\phi$

$$F_D = \int_{-\pi/2}^{\pi/2} N \cos \phi + \int_{-\pi/2}^{\pi/2} T \sin \phi$$

$$F_D = 2\left(\frac{S}{c}\right)(r)(\ell)\left\{\int_0^{\pi/2} \left[(1+R)\cos^3 \phi + \frac{2}{3}(1-R)(1-\gamma)\cos^2 \phi\right] d\phi + \int_0^{\pi/2} (1-R)\cos \phi \sin^2 \phi \, d\phi\right\}$$

$$F_D = 2\left(\frac{S}{c}\right) r\ell \left[\underbrace{\frac{(1+R)}{3}\sin\phi\,(\cos^2\phi+2)}_{\text{surface normal term}} + (1-R)\left[\underbrace{\frac{2}{3}(1-\gamma)\left(\frac{1}{2}\phi + \frac{1}{4}\sin 2\phi\right)}_{\text{re-radiation}} + \underbrace{\frac{\sin^3\phi}{3}}_{\text{surface tangent term}} \right]_0^{\pi/2}$$

$F_L = 0$ (By symmetry)

$$F_D = (2)\,\frac{S}{c}\,(r\ell)\left[\left(\frac{1+R}{3}\right)2 + (1-R)\left[\frac{2}{3}(1-\gamma)\left(\frac{\pi}{4}\right) + \frac{1}{3}\right]\right]$$

Solar Radiation Pressure

$$F_D = 2\,\frac{S}{c}\,r\ell\left[\frac{2}{3} + \frac{2R}{3} + \frac{1}{3} - \frac{1}{3}R + (1-R)\,\frac{\pi}{6}\,(1-\gamma)\right]$$

$1 + \frac{R}{3}$ Due to re-radiation

$$F_D \approx 2\,\frac{S}{c}\,r\ell\left[1 + \frac{\pi}{6} + \frac{R}{3} - \frac{R\pi}{6} - \frac{\gamma\pi}{6}\right]$$

Additional terms due to re-radiation

Solar Flare

$R = 0$; Re-radiation = 0

$$F_D = 2\,\frac{S}{c}\,r\ell$$

Normal to cylinder axis

4) Inclined Cylinder (Angle Between the Incident Radiation and the Axis of the Cylinder is 90-ϕ).

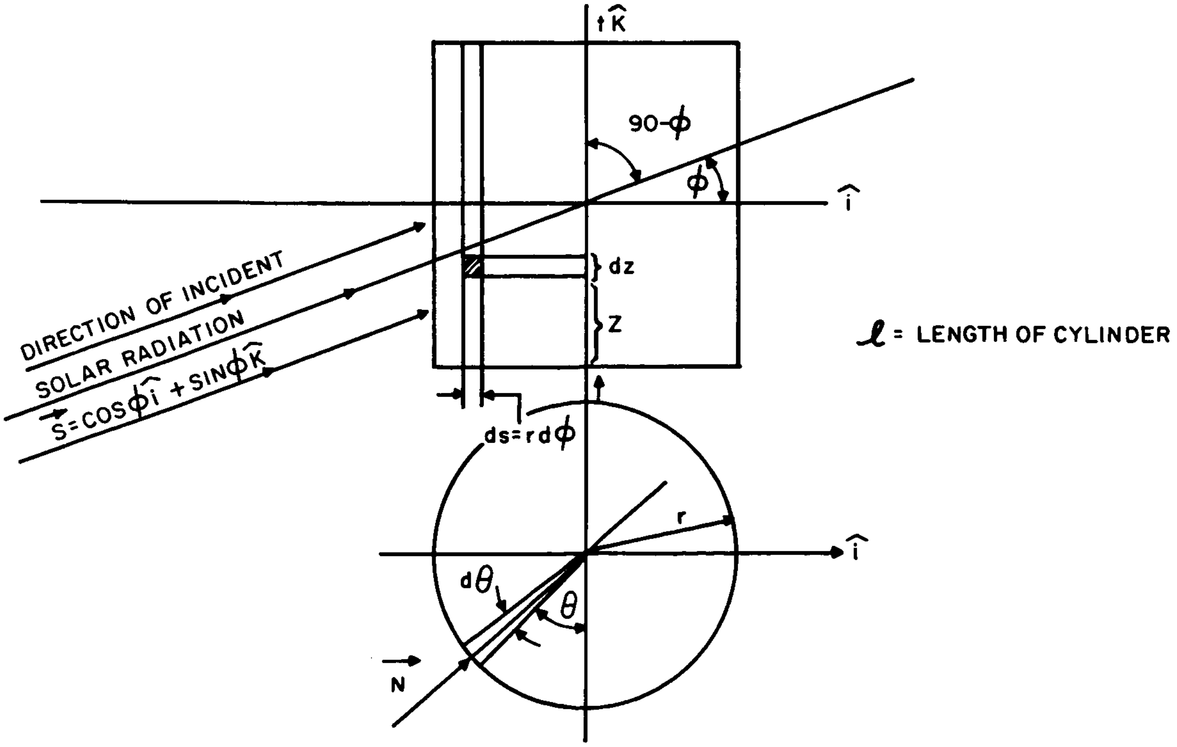

$\hat{K}$
90-ϕ
ϕ
$\hat{i}$
dz
Z
DIRECTION OF INCIDENT SOLAR RADIATION
$\vec{S} = \cos\phi\,\hat{i} + \sin\phi\,\hat{K}$
ℓ = LENGTH OF CYLINDER
ds=rdϕ
r
$\hat{i}$
dθ
θ
$\vec{N}$

$$\vec{T} = \vec{N} \times (\vec{S} \times \vec{N})$$

$\vec{S} \times \vec{N}$ Components

$\hat{i}$	$\hat{j}$	$\hat{k}$
$\frac{-\sin\phi\cos\theta}{\sqrt{1-\cos^2\phi\sin^2\theta}}$	$\frac{\sin\phi\sin\theta}{\sqrt{1-\cos^2\phi\sin^2\theta}}$	$\frac{\cos\phi\cos\theta}{\sqrt{1-\cos^2\phi\sin^2\theta}}$

$\vec{T}$ Components

$\frac{(\cos^2\theta)\cos\phi}{\sqrt{1-\cos^2\phi\sin^2\theta}}$	$\frac{-\sin\theta\cos\theta\cos\phi}{\sqrt{1-\cos^2\phi\sin^2\theta}}$	$\frac{\sin\theta^2\sin\phi + \cos^2\theta\sin\phi}{\sqrt{1-\cos^2\phi\sin^2\theta}}$

$\vec{S}$ defines the direction of the incident radiation

$\vec{N}$ defines the normal to the "flat" differential area dA

$dA = ds\,dz = r\,d\theta\,dz$

For each dA shown projected on plane formed by $\vec{N}$ and $\vec{S}$

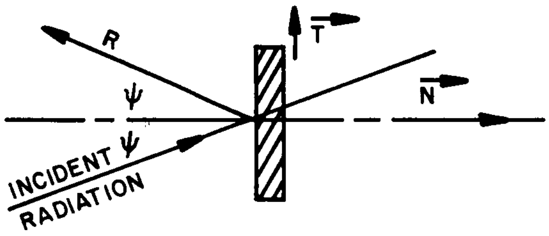

ψ is angle between $\vec{N}$ and $\vec{S}$

R = Reflectivity

The forces on each differential area are

$$dN = dA\left(\frac{S}{c}\right)\cos\psi\left[(1+R)\cos\psi + (1-R)\frac{2}{3}(1-\gamma)\right]$$

$$dT = dA\,\frac{S}{c}\cos\psi\left[(1-R)\sin\psi\right]$$

where ψ can be determined by $\cos\psi = \cos\phi\sin\theta$.

When integrating $\vec{N}$ and $\vec{T}$ and combining terms, it can be noted that the only terms in z are dz, so that $\int dz = \ell$ and the equations are

$$d\vec{N} = (r\ell d\theta)\,\frac{S}{c}\left[(1+R)\cos^2\phi\ \sin^2\theta + \frac{2}{3}[(1-R)(1-\gamma)]\sin\theta\cos\phi\right]\left[n_x\hat{i},\ n_y\hat{j},\ n_z\hat{k}\right]$$

$$d\vec{T} = (r\ell d\theta)\,\frac{S}{c}\ [1-R]\ \sqrt{1-(\cos^2\phi\ \sin^2\theta}\ \ \cos\phi\ \sin\theta\left[t_x\hat{i}, t_y\hat{j}, t_z\hat{k}\right]$$

Integrating $\vec{N}$ and $\vec{T}$ and combining components

$$\vec{N} = \left[r\ell\frac{S}{c}\cos\phi\right]\left[n_x\hat{i}, n_y\hat{j}, n_2\hat{k}\right]$$

$n_x = \sin\theta$

$$\hat{i} = (1+R)\cos\phi\int_0^\pi \sin^3\theta\ d\theta + \frac{2}{3}\left[(1-R)(1-\gamma)\right]\int_0^\pi \sin^2\theta\ d\theta$$

$$(1+R)\cos\phi\left[-\frac{1}{3}\cos\theta(\sin^2\theta+2)\right]_0^\pi + \frac{2}{3}\left[(1-R)(1-\gamma)\right]\left[\frac{\pi}{2}\right]$$

$$\left[(1+R)\cos\phi\,\frac{4}{3} + \frac{\pi}{3}[1-R-\gamma]\right] r\ell\,\frac{S}{c}(\cos\phi) = \hat{i}\text{ comp. of }\vec{N}\quad\text{(complete with factor)}$$

$n_y = \cos\theta$

$$\hat{j} = (1+R)\cos\phi\int_0^\pi \sin^2\theta\ \cos\theta\ d\theta + \frac{2}{3}\left[(1-R)(1-\gamma)\right]\int_0^\pi \sin\theta\cos\theta\ d\theta$$

$$\left[\frac{\sin^3\theta}{3}\right]_0^\pi = 0 \qquad\qquad \left[\frac{1}{2}\sin^2\theta\right]_0^\pi = 0$$

$n_z = 0$

$\therefore$ only $\hat{i}$ component of $\vec{N}$ remains

$$\vec{T} = r\ell\frac{S}{c}\ [1-R]\cos\phi\ [\text{components}]$$

$$\hat{i} = \int \frac{\sin\theta\cos^2\theta\ \cos\phi\sqrt{1-\cos^2\phi\ \sin^2\theta}}{\sqrt{1-\cos^2\phi\ \sin^2\theta}} \qquad d\theta = \cos\phi\int\cos^2\theta\ \sin\theta\ d\theta$$

$$= -\cos\phi\left[\frac{\cos^3\theta}{3}\right]_0^\pi$$

$$= -\cos\phi\left[-\frac{1}{3}-\frac{1}{3}\right]$$

$$= \frac{2}{3}\cos\phi$$

$\hat{i}$ comp. of $\vec{T}$, complete with factor $= r\ell\frac{S}{c}\ [1-R]\cos^2\phi\,(\frac{2}{3})$

$$\hat{j} \cos \phi \int -(\sin \theta^2) \cos \theta \, d\theta = \cos \phi \left[+ \frac{\sin^3 \theta}{3} \right]_0^{\pi} = 0$$

$$\hat{k} \sin \phi \int \sin \theta \, d\theta = \sin \phi \left[- \cos \theta \right]_0^{\pi}$$

$$= \sin \phi \; [+2]$$

$\vec{K}$ component of $\vec{T}$

$$r\ell \frac{S}{c} [1-R] \cos \phi \sin \phi \; (2)$$

Combining $\vec{N}$ and $\vec{T}$ components

$$\hat{i} = \frac{S}{c} (2r\ell) \cos^2 \phi \left[\frac{[1-R]}{3} + \frac{2}{3} [1+R] \right]$$

$$+ \frac{S}{c} (2r\ell) \cos \phi \left[\frac{\pi}{6} \right] \left[(1-R)(1-\gamma) \right]$$

(due to re-radiation diffusely)

$$\hat{j} = 0$$

$$\hat{k} = \frac{S}{c} [2r\ell] \cos \phi \sin \phi 1-R]$$

therefore, for a cylinder with the angle between $\vec{S}$ and the axis of the cylinder equal to (90-ϕ), the forces acting on the cylinder are

F normal to axis $= \frac{S}{c} (2r\ell) \cos^2 \phi \left[1 + \frac{R}{3} \right]$

$$+ \frac{S}{c} (2r\ell) \cos \phi \; \frac{\pi}{6} \left[(1-R)(1-\gamma) \right] \Big\} \text{ Diffuse re-radiation term}$$

F parallel to axis, acting as a shear =

$$\frac{S}{c} [2r\ell] \cos \phi \sin \phi \; (1-R)$$

where $2r\ell$ = projected area of cylinder on plane parallel to axis

$\frac{S}{c}$ = solar pressure, complete absorption

5) Spin Stabilized Vehicles. Solar radiation pressure and solar flare effects are simple to compute for a spin stabilized vehicle where the vehicle is a cylinder spinning about its axis which is parallel to the spin axis of the Earth. If the spin rate is high enough, diffuse reradiation force becomes negligible.

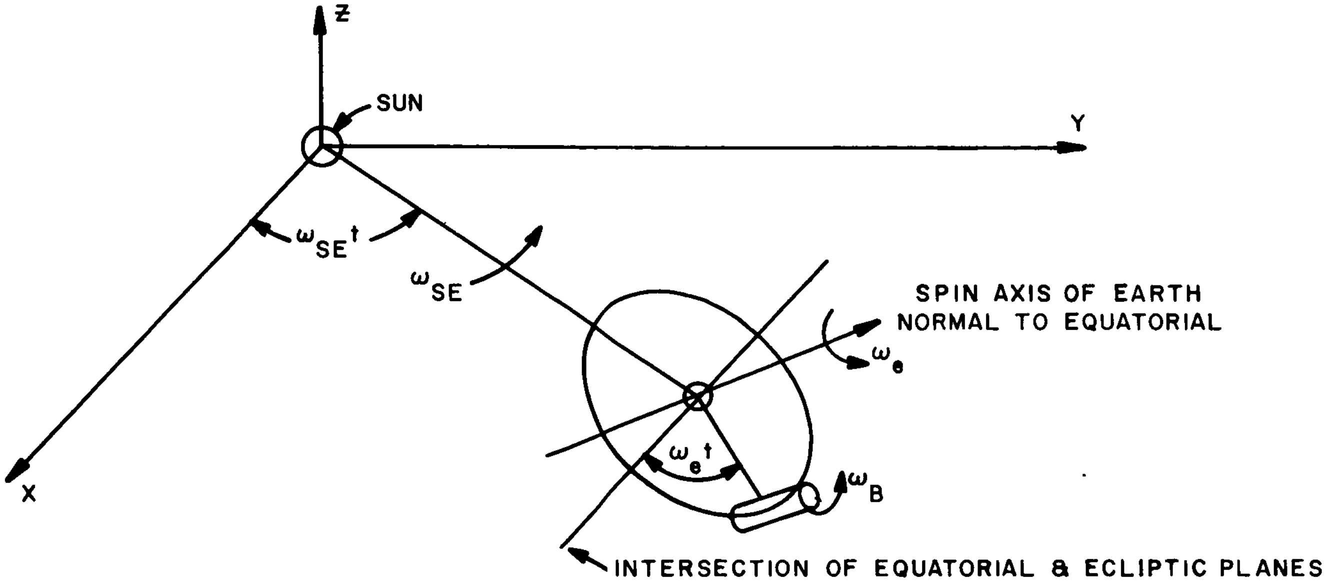
Z
SUN
Y
$\omega_{SE}t$
ω_{SE}
SPIN AXIS OF EARTH NORMAL TO EQUATORIAL
ω_e
$\omega_e t$
ω_B
X
INTERSECTION OF EQUATORIAL & ECLIPTIC PLANES

ω_{SE} = angular orbital rate of earth about sun

ω_e = angular rate of satellite about earth

ω_B = spin rate of satellite

All rates are with respect to the inertial reference.

The Sun-to-Earth vector (which is for all purposes, also the Sun-to-satellite vector) has direction cos $\omega_{SE}t\ \hat{i}$, sin $\omega_{SE}t\ \hat{j}$, $0\,\hat{k}$. The Earth-to-satellite vector has direction cosines cos $\omega_e t\,\hat{i}$, $\sin \omega_e t \sin \alpha\,\hat{j}$, $-\sin \omega_e t \cos \alpha\,\hat{k}$. The pitch axis has direction cosines: $0\hat{i}$, $-\cos \alpha\,\hat{j}$, $-\sin \alpha\,\hat{k}$. The rotating orthogonal body axes can be described by

(A) $-\cos \omega_B t\ \hat{i}$, $-\sin \omega_B t \sin \alpha\,\hat{j}$, $+\sin \omega_B t \cos \alpha\,\hat{k}$ (Yaw)

(B) $-\sin \omega_B t\ \hat{i}$, $\cos \omega_B t \sin \alpha\,\hat{j}$, $-\cos \omega_B t \cos \alpha\hat{k}$ (Roll)

The total solar radiation torque can be expressed as a function of the angle between the incident radiation and the satellite spin axis.

$$F_{T_1} = \frac{S}{c}(2r\ell)\,|\cos\xi\,|\sin\xi\,(1-R_1)$$

$$F_{N_1} = \frac{S}{c}(2r\ell)\,|\cos\xi\,|\cos\xi\,\left(1+\frac{R_1}{3}\right)$$

$$F_{T_2} = \frac{S}{c}(\pi r^2)\,|\sin\xi\,|\cos\xi\,(1-R_2)$$

$$F_{N_2} = \frac{S}{c}(\pi r^2)\,|\sin\xi\,|\sin\xi\,(1+R_2)$$

$$\cos(90-\xi) = \sin\xi = -\sin\omega_{SE}t\,(\cos\alpha)$$

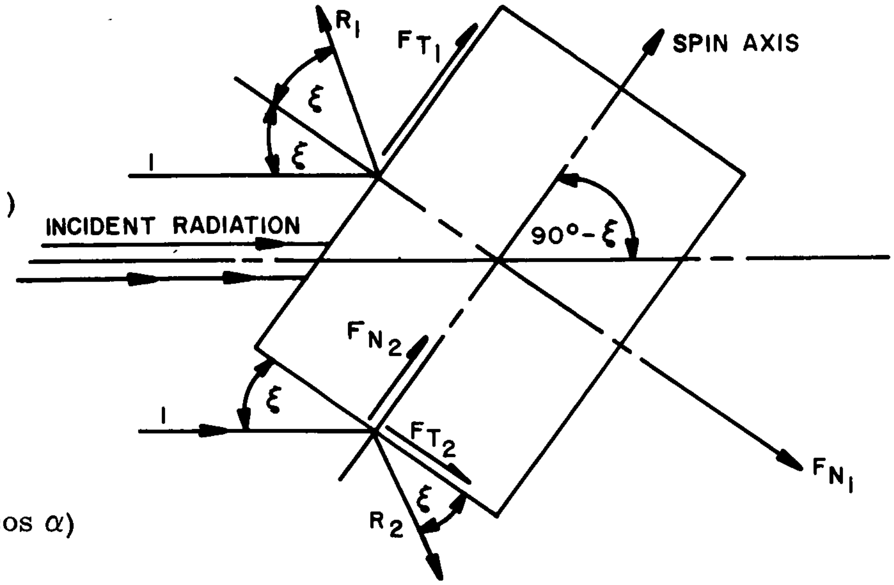

Where the mass center coincides with the centroid of the cylinder the torque depends only on the tangential (shear) components. Taking the direction of positive torque as spin axis × $\vec{SE}$:

The torque magnitude is

$$F_{T_1}r - F_{T_2}\frac{\ell}{2} = \frac{S}{c}\left[2r^2\ell\,|\cos\xi\,|\sin\xi\,(1-R_1) - \pi r^2\frac{\ell}{2}\,|\sin\xi\,|\cos\xi\,(1-R_2)\right]$$

or

$$\frac{S}{c}r^2\ell\cos\xi\sin\xi\left[2(1-R_1) - \frac{\pi}{2}(1-R_2)\right]$$

$$2 - 2R_1 - \frac{3.14}{2} - \frac{3.14}{2}R_2$$

$$|M_o| = +\frac{S}{c}r^2\ell\cos\xi\,\sin\xi\left[.43-2R_1+1.57R_2\right] = \frac{S}{c}r^2\ell\left[2\,|\cos\xi\,|\sin\xi\,(1-R_1) - \frac{\pi}{2}\,|\sin\xi\,|\cos\xi\,(1-R_2)\right]$$

where $\sin\xi = +\cos\alpha\sin\omega_{SE}t$ $\cos\xi = \sqrt{1-\cos^2\alpha\sin^2\omega_{SE}t}$

The direction cosines of the shear torque are

Spin Axis × SE

$$\frac{-(\sin\alpha)(\sin\omega_{SE}t)}{\sqrt{1-\cos^2\alpha\sin^2\omega_{SE}t}} \qquad \frac{(\sin\alpha)(\cos\omega_{SE}t)}{\sqrt{1-\cos^2\alpha\sin^2\omega_{SE}t}} \qquad \frac{+(\cos\alpha)(\cos\omega_{SE}t)}{\sqrt{1-\cos^2\alpha\sin^2\omega_{SE}t}}$$

The torque can be decomposed along the rotating orthogonal body axes by taking the dot product of the torque along axis "A" and axis "B" respectively.

$$M \text{ about } B_{(\text{roll})} = \vec{M} \cdot \vec{B}$$

$$\frac{|M_o|}{\sqrt{1-\cos^2\alpha \sin^2\omega_{SE}t}} = \sin\omega_{SE}t\,(\sin\alpha)(\sin\omega_B t) + \cos\omega_{SE}t(\cos\omega_B t)\left[\sin^2\alpha - \cos^2\alpha\right]$$

$$M_{B_{(\text{roll})}} = -\frac{S}{c}r^2\ell\cos\alpha\,\sin\omega_{SE}t\left[.43-2R_1+1.57R_2\right]\Big\{\sin\omega_{SE}t\,(\sin\alpha)\,\sin\omega_B t$$
$$+\cos\omega_{SE}t\,(\cos\omega_B t)\left[\sin^2\alpha - \cos^2\alpha\right]\Big\}$$

$$M_{A_{(\text{Yaw})}} = +\frac{S}{c}r^2\ell\cos\alpha\,\sin\omega_{SE}t\left[.43-2R_1+1.5R_2\right]\Big\{\sin\omega_{SE}t\,\sin\alpha\,\cos\omega_B t$$
$$+\cos\omega_{SE}t\,(\sin\omega_B t)\,(\cos^2\alpha - \sin\alpha)\Big\}$$

The torque expressions for solar flare can be obtained by eliminating terms containing the reflectivities R_1 and R_2, and using $\left[\frac{S_f}{c}\right]$ instead of $\frac{S}{c}$. Figures 2-10 and 2-11 show torques computed for solar radiation and solar flare for winter and autumn. Figure 2-12 shows the yearly variation in the gross torque causing precession of the spin axis. The reflectivity of the curved portions of the cylinder is 0.20, the reflectivity of the ends used was 0.22. The preliminary body dimensions were taken as diameter 90 in., length 72 in. (1000 lb vehicle).

6) 3-Axis Stabilized Vehicle. The 3-axis stabilized vehicle configuration consists of a cylinder, which has its axis oriented along yaw, and a pair of solar paddles, which are mounted on a shaft that coincides with the vehicle pitch axis. The positive sense of the roll axis is along the orbital velocity vector. The negative sense of the pitch axis is along the Earth's spin axis and is defined by $o\hat{i}$, $-\cos\alpha\,\hat{j}$, $-\sin\alpha\,\hat{k}$ (pitch). The orthogonal axes are

$$-\sin\omega_e t\,\hat{i}, +(\cos\omega_e t)(\sin\alpha)\hat{j}, -\cos\omega_e t\cos\alpha\,\hat{k} \quad (\text{Roll})$$

$$-\cos\omega_e t\,\hat{i}, -(\sin\omega_e t)(\sin\alpha)\hat{j}, +\sin\omega_e t\cos\alpha\,\hat{k} \quad (\text{Yaw})$$

The positive yaw direction = Roll × Pitch. The direction of the sun radiation (and solar flare) is: $\cos\omega_{SE}t\,\hat{i}$, $\sin\omega_{SE}t$, $o\hat{k}$.

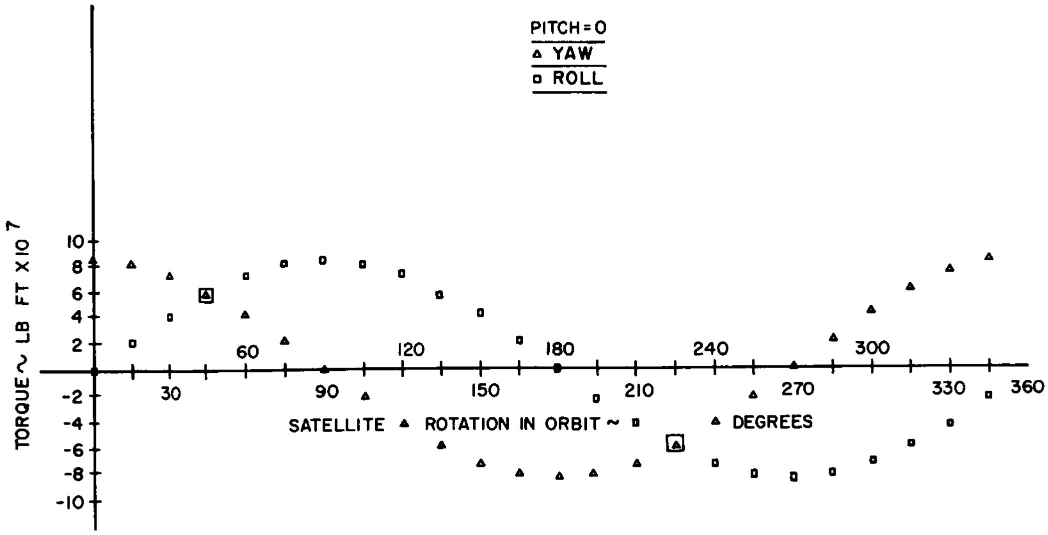

Figure 2-10. Torques Due to Solar Radiation - Spin Stabilized 1000 lb Vehicle - Winter Solstice

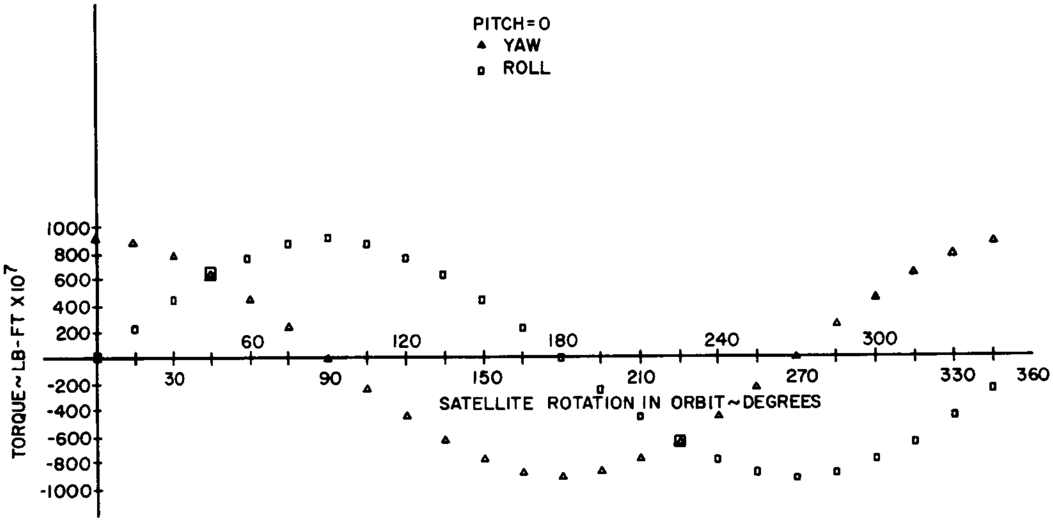

Figure 2-11. Torques Due to Solar Flare - Spin Stabilized 1000 lb Vehicle - Winter Solstice

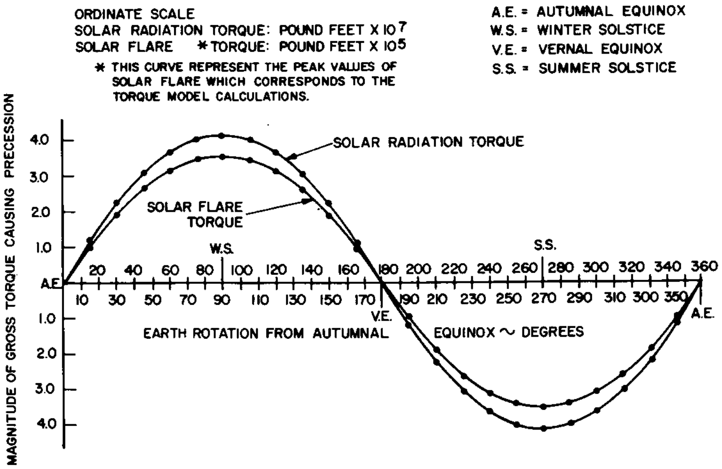

Figure 2-12. Torques Due to Solar Radiation - 3-Axis Stabilized 1000 lb Vehicle - Winter Solstice

The torques on a 1000 lb vehicle with a 90 in. diameter and 72 in. length are plotted as Figures 2-13 and 2-14 for solar radiation and solar flare during winter. The curves take into effect eccentricity of the cylinder centroid and mass center of the vehicle. The paddle axis is assumed to pass through the cylinder centroid. The eccentricities used are: 0.707 in. yaw, 0.5 in. pitch, and 0.5 in. roll. The reflectivities are: 0.22 for all surfaces except the solar cells, which have R = 0.20. The paddle area is 48 sq ft.

a) Cylindrical Body. The torques on the 3-axis stabilized configuration in the absence of an eccentricity between the centroid of the cylinder, axis of the paddle shaft, and center of mass (gravitational attraction) are due to the shear force components of the cylinder. This can be derived in a manner similar to that shown for the spin stabilized vehicle, except that the cylinder axis lies along the yaw axis. The torque can be decomposed along roll and pitch. The forces normal to the surfaces of the cylinder contain the diffuse reradiation terms, but the shear forces do not, so that the expression for the gross torque is

$$|M_o| = \frac{S}{c} r^2 \ell \cos\phi \sin\phi \,[.43 - 2 R_1 + 1.57 R_2]$$

where $\sin\phi = -\,[(\cos\omega_e t)(\cos\omega_{SE} t) + (-\sin\omega_e t)(\sin\alpha)(\sin\omega_{SE} t)]$

The direction cosines of the gross torque unit vector by Yaw Axis $\times \vec{SE}$.

$$\begin{array}{lll} Y_y S_z - Y_z S_y & -\sin\omega_e t \cos\alpha \sin\omega_{SE} t & \hat{i} \\ Y_z S_x - Y_x S_z & \sin\omega_e t \cos\alpha \cos\omega_{SE} t & \hat{j} \\ Y_x S_y - Y_y S_x & -\cos\omega_e t (\sin\omega_{SE} t) + \sin\omega_e t (\sin\alpha)\cos\omega_{SE} t & \hat{k} \end{array}$$

All divided by

$$\sqrt{\sin^2\omega_{SE} t + \sin^2\omega_e t(1 - \sin^2\alpha \sin^2\omega_{SE} t - \sin^2\omega_{SE} t}$$

The torque components along the satellite axes:

Yaw component = zero

Pitch component = $T_c\,(-(\sin\omega_e t)(\cos\omega_e t) + \sin\alpha\,\omega_e t \sin\omega_{SE} t)$

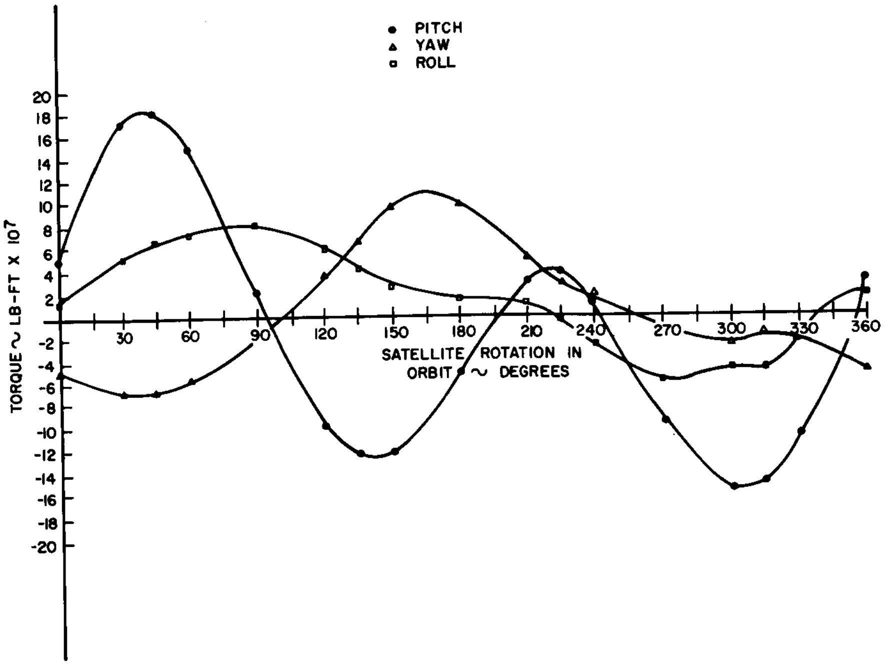

Figure 2-13. Torques Due to Solar Flare - 3-Axis Stabilized 1000 lb Vehicle - Winter Solstice

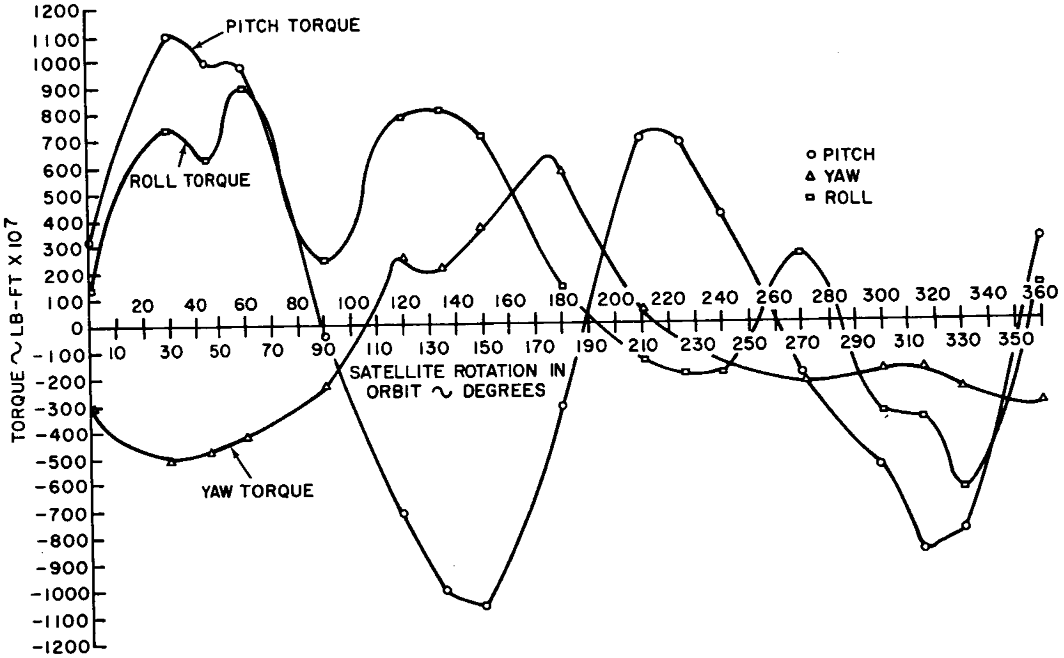

Figure 2-14. Torques Due to Solar Radiation - Gravity Gradient 1000 lb Vehicle - Winter Solstice

Roll component

$$T_c \left\{ \cos\alpha \;\; \sin\omega_{SE} t \right\}$$

$$\text{where} \quad T_c = \frac{\frac{S}{c} r^2 \ell \cos\phi \;\; \sin\phi \, [.43 - 2R_1 + 1.57R_2]}{\sqrt{\sin^2\omega_{SE} t + \sin^2\omega_e t \, [1 - (\sin^2\omega_{SE} t)(1 + \sin^2\alpha)]}}$$

$$[\text{For solar flare, use} \left[S_f/c\right]; R_1 = R_2 = 0]$$

When the center of mass (gravitational attraction) and the centroid of the cylinder do not coincide, a torque due to both normal and shear forces exists. The normal force component will include the diffuse re-radiation terms for solar radiation pressure. The additional torque components due to an eccentricity $\vec{r}$, will be $(\vec{r} \times \vec{F})$ taken as a dot product along the body axes. $\vec{F}$ is the vector sum of the normal and shear forces acting on the cylinder.

$$F_{T_1} = \frac{S}{c} (2r\ell) \cos\phi \; \sin\phi \, (1 - R_1)$$

$$F_{N_1} = \frac{S}{c} (2r\ell) \cos\phi \left[[1 + \frac{R_1}{3}] \cos\phi + \frac{\pi}{6} [(1 - R_1)(1 - \gamma)] \right]$$

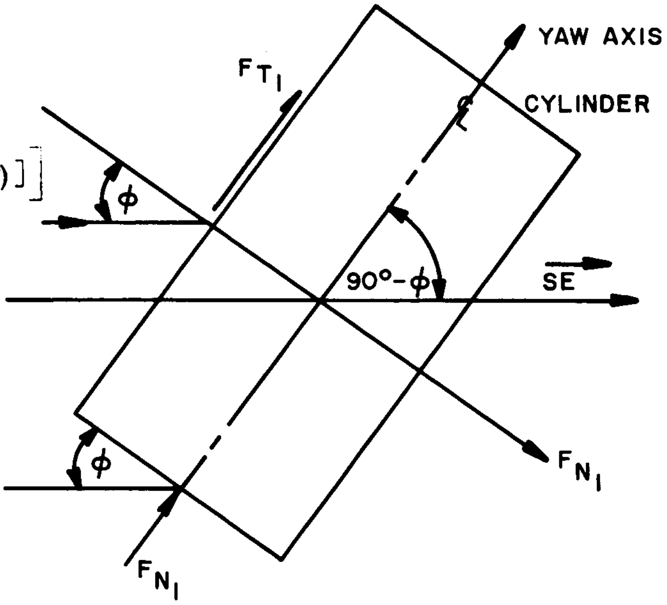

$$F_{T_2} = \frac{S}{c} (\pi r^2) \sin\phi \cos\phi \, (1 - R_2)$$

$$F_{N_2} = \frac{S}{c} (\pi r^2) [1 + R_2] [\sin^2\phi]$$

where R_1 = cylinder reflectivity

R_2 = end reflectivity

γ = fraction of absorbed radiation converted to stored electrical energy

F_A = forces F_{T_1} and F_{N_2}, acting along the yaw axis direction $\begin{array}{l} -\cos \omega_e t\,\hat{i} \\ -\sin \omega_e t \sin \alpha\,\hat{j} \\ +\sin \omega_e t \cos \alpha\,\hat{k} \end{array}$

F_B = forces F_{N_1} and F_{T_2}, acting along the direction $(\vec{Yaw} \times \vec{SE}) \times \vec{Yaw}$

which has direction cosines:

$$\frac{\cos \omega_{SE} t\,(\sin^2 \omega_e t) - \sin \omega_{SE} t\,(\sin \alpha)(\cos \omega_e t)(\sin \omega_e t)}{\sqrt{\sin^2 \omega_{SE} t + \sin^2 \omega_e t\,[1 - (\sin^2 \omega_{SE} t)\,(1 + \sin^2 \alpha)\,]}}$$

$$\frac{\sin \omega_{SE} t\,[1 - \sin^2 \omega_e t\,(\sin^2 \alpha)] - \cos \omega_{SE} t (\sin \alpha)\,(\sin \omega_e t)(\cos \omega_e t)\;\hat{j}}{\sqrt{\sin^2 \omega_{SE} t + \sin^2 \omega_e t\,[1 - (\sin^2 \omega_{SE} t)\,(1 + \sin^2 \alpha)\,]}}$$

$$\frac{\sin \omega_{SE} t\,(\sin \alpha)(\cos \alpha)(\sin^2 \omega_e t) + (\cos \omega_{SE} t)(\sin \omega_e t)(\cos \omega_e t)\;\hat{k}}{\sqrt{\sin^2 \omega_{SE} t + \sin^2 \omega_e t\,[1 - (\sin^2 \omega_{SE} t)\,(1 + \sin^2 \alpha)\,]}}$$

The vector sum of the forces acting at the centroid of the cylinder:

$$F_A(-\cos \omega_e t) + F_B \frac{(\cos \omega_{SE} t)(\sin^2 \omega_e t) - \sin \omega_{SE} t (\sin \alpha)(\cos \omega_e t)(\sin \omega_e t)\,\hat{i}}{\sqrt{\sin^2 \omega_{SE} t + \sin^2 \omega_e t\,\{1 - (\sin^2 \omega_{SE} t)(1 + \sin^2 \alpha)\,\}}} = \vec{f}_x$$

$$\vec{F} \quad F_A(-\sin \omega_e t \sin \alpha) + F_B \frac{(\sin \omega_{SE} t)[1 - \sin^2 \omega_e t (\sin^2 \alpha)] - (\cos \omega_{SE} t)[(\sin \omega_e t)(\cos \omega_e t)(\sin \alpha)\,]\,\hat{j}}{\sqrt{\sin^2 \omega_{SE} t + \sin^2 \omega_e t\,\{1 - (\sin^2 \omega_{SE} t)(1 + \sin^2 \alpha)\,\}}} = \vec{f}_y$$

$$F_A(\sin \omega_e t \cos \alpha) + F_B \frac{\sin \omega_{SE} t (\sin \alpha)(\cos \alpha)(\sin^2 \omega_e t) + \cos \omega_{SE} t (\cos \alpha)(\sin \omega_e t)(\cos \omega_e t)\;\hat{k}}{\sqrt{\sin^2 \omega_{SE} t + \sin^2 \omega_e t\,\{1 - (\sin^2 \omega_{SE} t)\,(1 + \sin^2 \alpha)\,\}}} = \vec{f}_z$$

The mass eccentricity $\vec{r}$ can be expressed as components Δ_p, Δ_r, Δ_y along the pitch, roll, and yaw axes, respectively. If the negative directions are taken,

$$\vec{r} = \left[- \sin \omega_e t(\Delta r) - \cos \omega_e t \, \Delta y\right] \hat{i} = \vec{r}_x$$

$$\left[- \cos \alpha \, \Delta p + \cos \omega_e t(\sin \alpha) \, \Delta r - \sin \omega_e t \sin \alpha \, \Delta y\right] \hat{j} = \vec{r}_y$$

$$\left[- \sin \alpha \, \Delta p - \cos \omega_e t (\cos \alpha) \, \Delta r + (\sin \omega_e t) \cos \alpha \, \Delta y\right] \hat{k} = \vec{r}_z$$

The gross torque, $\vec{r} \times \vec{F}$ can be expressed as:

$$(r_y f_z - r_z f_y) \ \hat{i} = \vec{T}_x$$

$$(r_z f_x - r_x f_z) \ \hat{j} = \vec{T}_y$$

$$(r_x f_y - r_y f_x) \ \hat{k} = \vec{T}_z$$

This can be decomposed along the body axes of the vehicle, so that the torques about each of the body axes are as follows:

Pitch: $- \cos \alpha \ T_y \quad - \sin \alpha \ T_z$

Roll: $- \sin \omega_e t \ T_x + \sin \alpha \cos \omega_e t \ T_y - \cos \alpha \cos \omega_e t \ T_z$

Yaw: $- \cos \omega_e t \ T_x - \sin \alpha \ \sin \omega_e t \ T_y + \cos \alpha \sin \ \omega_e t \ T_z$

which are torques due to solar radiation or solar flare; (depending on $\frac{S}{c}$) where $R_1 = R_2 = 0$ and diffuse reradiation is deleted for solar flare.

b) Solar Paddles. The solar paddles are mounted on a shaft which coincides with the pitch axis, and the paddles are rotated so that the maximum paddle area is exposed to sunlight. The paddle normal can be defined by stating that the paddle plane always contains the pitch axis and at least one line ℓ' parallel to the ecliptic plane which is perpendicular to the Sun's radiation.

$$\vec{SE} = \cos \omega_{SE} t \ \hat{i} + \sin \omega_{SE} t \ \hat{j} + o \hat{k}$$

$$(\vec{\ell}') = - \sin \omega_{SE} t \ \hat{i} + \cos \omega_{SE} t \ \hat{j} + o \hat{k}$$

$$\text{Pitch Axis} = o\hat{i} - \cos \alpha \ \hat{j} - \sin \alpha \ \hat{k}$$

The direction of the normal to the paddle plane is,

$\pm\vec{\ell}\,' \times \vec{\text{Pitch}}$

$$\frac{\vec{N}_o}{|N|} = \frac{+\sin\alpha\cos\omega_{SE}t}{\sqrt{1-\cos^2\alpha\cos^2\omega_{SE}t}}\,\hat{i} + \frac{+\sin\alpha\sin\omega_{SE}t}{\sqrt{1-\cos^2\alpha\cos^2\omega_{SE}t}}\,\hat{j} + \frac{-\cos\alpha\sin\omega_{SE}t}{\sqrt{1-\cos^2\alpha\cos^2\omega_{SE}t}}$$

The direction of the shear force $\vec{T}_p$ can be obtained by $\vec{N}_p \times (\vec{SE} \times \vec{N}_p)$

$$t_x = \frac{\cos\alpha\sin\omega_{SE}t\cos\omega_{SE}t}{\sqrt{1-\cos^2\alpha\cos^2\omega_{SE}t}}$$

$$t_y = \frac{\cos\alpha\sin^2\omega_{SE}t}{\sqrt{1-\cos^2\alpha\cos^2\omega_{SE}t}}$$

$$t_z = \frac{+\sin\alpha}{\sqrt{1-\cos^2\alpha\cos^2\omega_{SE}t}}$$

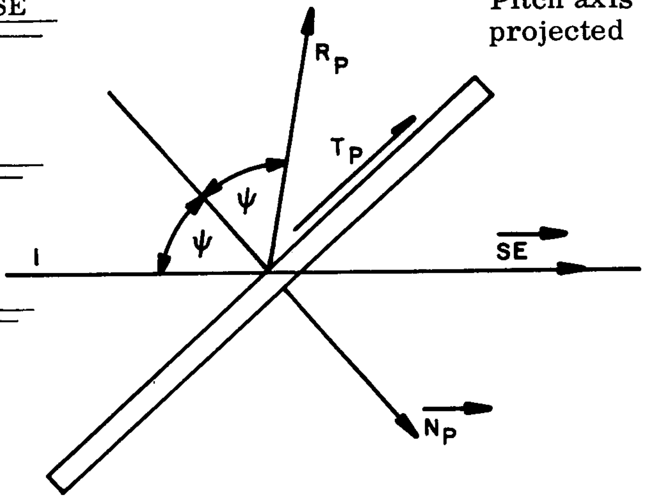

Pitch axis trace, not projected

$\vec{T}_p = t_x\hat{i} + t_y\hat{j} + t_z\hat{k}$

unit vector

The forces on the paddle are:

$$\vec{T}_p = A_p\frac{S}{c}(1-R_p)\cos\psi\sin\psi$$

$$\vec{N}_p = A_p\frac{S}{c}\cos\psi\left[(1+R_p)\cos\psi + \frac{2}{3}(1-R_p)(1-\gamma)\right]$$

$\cos\psi = \vec{SE}\cdot\vec{N}$ (both are unit vectors)

where $\cos\psi = \dfrac{\sin\alpha}{\sqrt{1-\cos^2\alpha\cos^2\omega_{SE}t}}$

The torque on the vehicle due to paddles is zero unless the center of gravitational attraction is not at the centroid of the paddles. If the same $\vec{r}$ is assumed as that used for the cylindrical body of the satellite, then the components of the paddle force can be added to the forces on the cylindrical body in the torque expression.

Considered separately, the torque components due to the paddles are

$$(r_y f_{pz} - r_z f_{py})\ \hat{i} = T_x$$

$$(r_z f_{px} - r_x f_{yz})\ \hat{j} = T_y$$

$$(r_x f_{py} - r_y f_{px})\ \hat{k} = T_z$$

Components of torque expressed in body system:

Pitch: $-\cos\alpha\ T_y - \sin\alpha\ T_z$

Roll: $-\sin\omega_e t\ T_x + \sin\alpha\cos\omega_e t\ T_y - \cos\alpha\cos\omega_e t\ T_z$

Yaw: $-\cos\omega_e t\ T_x - \sin\alpha\sin\omega_e t\ T_y + \cos\alpha\sin\omega_e t\ T_z$

Paddle Forces

$$\left\{\begin{aligned}
f_{px} &= \left[N_p \frac{\sin\alpha\cos\omega_{SE}t}{\sqrt{1-\cos^2\alpha\cos^2\omega_{SE}t}} + T_p \frac{\cos\alpha(\sin\omega_{SE}t)\cos\omega_{SE}t}{\sqrt{1-\cos^2\alpha\cos^2\omega_{SE}t}}\right] \\
f_{py} &= \left[N_p \frac{\sin\alpha\sin\omega_{SE}t}{\sqrt{1-\cos^2\alpha\cos^2\omega_{SE}t}} + T_p \frac{\cos\alpha\sin^2\omega_{SE}t}{\sqrt{1-\cos^2\alpha\cos^2\omega_{SE}t}}\right] \\
f_{pz} &= \left[-N_p \frac{\cos\alpha\sin\omega_{SE}t}{\sqrt{1-\cos^2\alpha\cos^2\omega_{SE}t}} + T_p \frac{\sin\alpha}{\sqrt{1-\cos^2\alpha\cos^2\omega_{SE}t}}\right]
\end{aligned}\right.$$

$$|N_p| = A_p \frac{S}{c} \cos\psi\left[(1+R_p)\cos\psi + \frac{2}{3}(1-R_p)(1-\gamma)\right]$$

*

$$|T_p| = A_p \frac{S}{c} (1-R_p)\cos\psi\sin\psi$$

For solar flare, $R_p = 0$, and the diffuse radiation term = 0.

7) Gravity Gradient Vehicle. The gravity gradient vehicle, like the spin stabilized vehicle, will require that the center of gravitational attraction be held to precise limits. Assuming that the center of gravitational attraction and centroid coincide, the torque on the gravity gradient configuration is as follows:

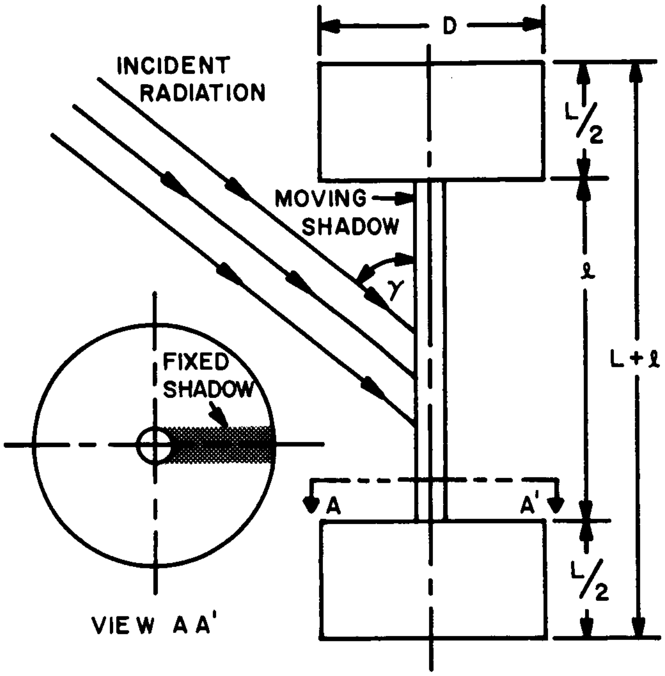

$D > d \qquad \ell >> L$

Torque on vehicle where geometric center of of vehicle and center of mass coincide.

From previously derived formulae:

Pitch Torque

$$T_c\left[(-\cos \omega_{SE}t) \sin \omega_e t + \sin \alpha (\cos \omega_e t) \sin \omega_{SE} t\right]$$

Yaw Torque = Zero

Roll Torque

$$T_c\left[(\cos \alpha) \sin \omega_{SE} t\right]$$

$$\cos \gamma = + \left[(\cos \omega_e t)(\cos \omega_{SE} t) + (\sin \omega_e t) \sin \alpha (\sin \omega_{SE} t)\right]$$

where

$$T_c = \frac{S}{c} \frac{\sin \gamma \cos \gamma}{\sqrt{P}} \left\{(1-R_2) \frac{\pi}{8} (D^2 L + d^2 \ell + \frac{(D-d)\, d(2) \ell}{\pi}\right.$$

$$- \frac{1}{2}\left[(1-R_1)(D^2 L) - (1-R_3)(d^2)(\ell - \tan \gamma \frac{(D-d)}{2}\right]$$

$$\left. - \frac{1}{4} (1 + \frac{R_3}{3}) \left[(D-d)d\right]\left[\ell - \tan \gamma \frac{(D-d)}{2}\right]\right\}$$

which includes significant shadow effects.

$$\sqrt{P} = \sqrt{\sin^2 \omega_{SE} t + \sin^2 \omega_e t \left[1 - (\sin^2 \omega_{SE} t)(1 + \sin^2 \alpha)\right]}$$

For solar flare, $R_1 = R_2 = R_3 = 0$. Diffuse reradiation effect is approximately zero, since this only exists where normal force components contribute to torque.

The actual torque will be different due to the eccentricity of the centroid of the vehicle and the center of gravitational attraction.

Figures 2-15 and 2-16 show computed torques on the 1000 lb vehicle with the following dimensions: D = 90 in., L = 72 in., d = 3 in., ℓ = 100 ft, 200 ft or 300 ft. The surface reflectivities used were R = 0.20 for solar cells, R = 0.22 for other surfaces.

b. Gravity Gradient Torque

The body pitch and roll gravity gradient torques, T_y and T_x, respectively, can be expressed in terms of the vehicle, roll, pitch, and yaw moments of inertia namely, I_x, I_y, and I_z, the orbital rate ω_o, the angle between roll principal and body axes $\Delta\phi$, the angle between the pitch principal and body axes, $\Delta\theta$.

$$T_y = -\frac{3}{2}\omega_o^2 (I_x - I_z) \sin 2(\Delta\theta)$$

$$T_x = -\frac{3}{2}\omega_o^2 (I_y - I_z) \sin 2(\Delta\phi)$$

The body and principal axis angle errors are estimated as $\Delta\phi = \Delta\theta = 1/2°$. The maximum torque values for the 500 lb, 3-axis stabilized vehicle are

Pitch $T_y = -4.62 \times 10^{-9}$ ft-lb

Roll $T_z = -9.65 \times 10^{-9}$ ft-lb

c. Magnetic Torques due to Interaction with the Earth's Field

A recent study conducted by Republic on the OSO vehicle indicated that by careful design, torques due to magnetic interaction could be virtually eliminated. A conservative estimate of the magnetic interaction effect can be obtained by considering all the power consumed by the vehicle within a single direct current loop which would produce maximum torque. Dividing the resulting magnetic moment by a factor of 300 yields disturbance torque levels that can be easily matched in a final design.

Using a magnetic flux density of 0.081×10^{-6} Weber/(meter)^2 at 22,300 miles, a current carrying loop area equal to the satellite length times diameter, and a current of $\frac{500\ W}{28\ V}$ for the 500 lb satellite, a conservative yaw torque of 1.17×10^{-9} ft-lb is obtained. Pitch and roll components can be neglected.

d. Equipment Dependent Disturbances

The infrared and vidicon equipment will use scanning mirrors and gimbaled indexing mirrors. The solar paddles will require an unwind cycle if slip rings are not used. The rapid acting shutters which will protect infrared and vidicon sensors from looking directly into the sun will be of a double-acting

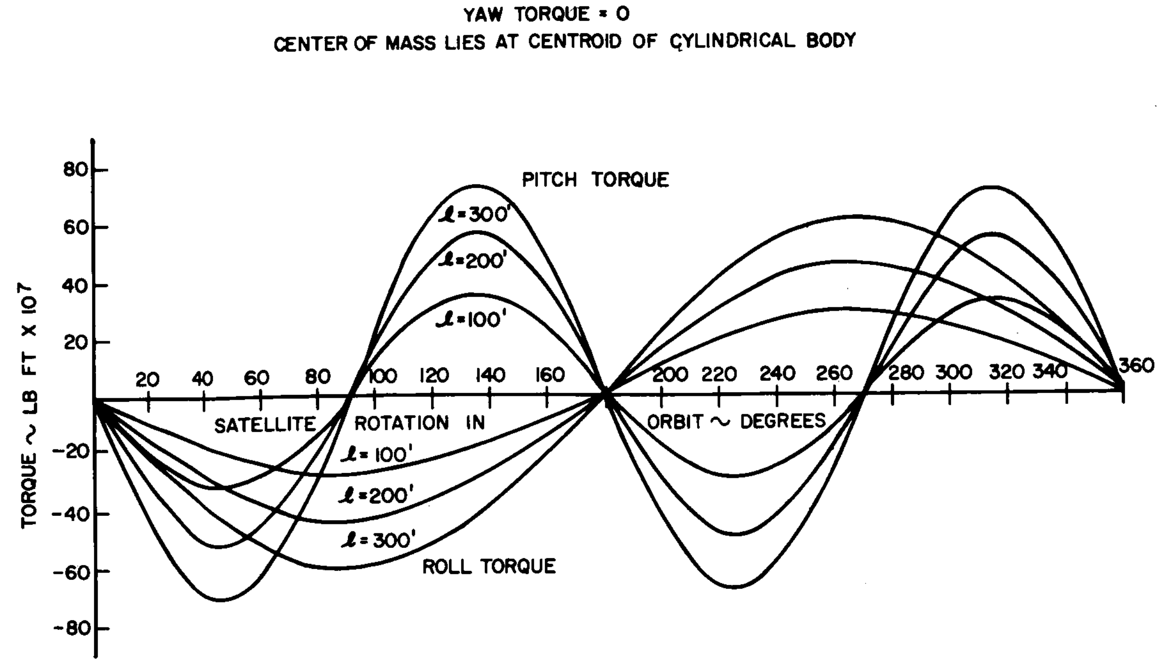

Figure 2-15. Torques Due to Solar Flare - Gravity Gradient 1000 lb Vehicle - Winter Solstice

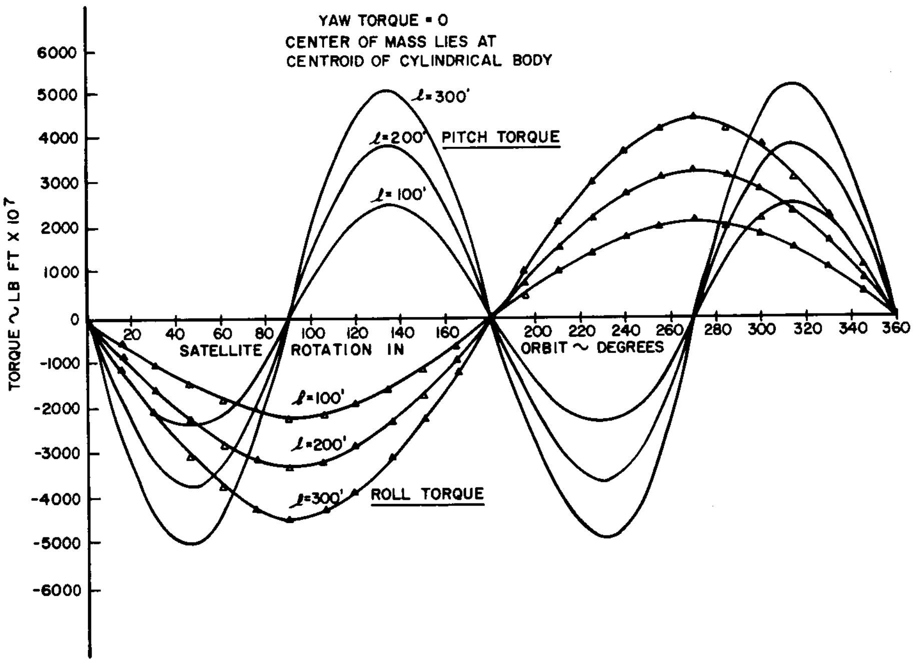

Figure 2-16. Solar Torques - Spin Stabilized 500 lb Vehicle Shown for One Year

type which will have two moving elements so that the mass center of the vehicle remains unchanged. The effect of the moment of inertia change and principal axis shift will be negligible.

1) Vidicon Equipment.

a) Filter Wheel. The filter wheel has an $I \approx 3.5 \times 10^{-3}$ slug ft^2 and rotates 2π radians in one second.

$$\text{Hence, torque, } T = \frac{2I\theta}{t^2} = \frac{(2)(3.5) \times 10^{-3}(\pi)}{(1/2)^2} = 3.5 \times 10^{-3}(3.14)\,(8)$$

or $T = 0.088$ ft-lb

It is conservative to assume two alternating pulses with 1/2 second duration and amplitude. $T = \pm 8.8 \times 10^{-2}$ occurring twice daily for sensor protection (1 cycle).

b) Scanning Mirror. The scanning mirror has an $I \approx 0.035$ slug ft^2 with a maximum of 25 steps of motion conservatively taken as 8° maximum excursion in 60 sec, once per hour.

$$\text{Hence, torque, } T = 2\,\frac{(4/57.3)(0.035)}{(30/25)^2} = 3.35 \times 10^{-3} \text{ ft-lb}$$

This can be regarded as 50 alternating rectangular pulses of $\pm 3.35 \times 10^{-3}$ ft-lb and 1.2 sec duration occurring every hour.

2) Infrared Systems.

a) Indexing Mirror. The indexing mirror has an $I \approx 0.05$ slug ft^2 and an 8° rotation in a 100 sec period.

$$\text{Hence, torque, } T = \frac{0.05\left(\frac{4 \times 2\pi}{360}\right)^2}{(50)^2}$$

or $T = 2.78 \times 10^{-6}$ foot pound with a 100 sec period, four times per hour

b) Rotating Multimirror Drum. The drum has an $I \approx 0.05$ slug ft^2 and performs two rotations in 20 sec with an angular velocity $\omega = \frac{4\pi}{20} = 0.628$ rads/sec.

Now torque, $T = \frac{I\omega}{t}$; if 2 sec is permitted for acceleration

$$T = 1/2(0.05)(0.628) = 0.015 \text{ lb-ft}$$

3) Disturbance Torque Due to Rotation of Solar Paddles (3-Axis Stabilized Vehicle and Gravity Gradient Stabilized Vehicle, if Paddles are Used). The solar paddles are so oriented that the largest possible area is directed normal to the sun line by rotation about the vehicle pitch axis. The synchronous orbiting vehicle rotates once per day with respect to the sun, so that a compensating daily rotation of the paddles is required. In order to compensate for the motion of the Earth about the Sun, the paddles must rotate one additional time per year with respect to the sun.

The relative angular position change of the paddle normal with respect to the vehicle is $(\omega_e - \omega_{SE})\Delta t$, where Δt is the time interval of interest. Since this is a constant rate, the paddles and shaft exert zero torque on the vehicle except for bearing and slip ring friction between the vehicle and paddle axis, which is overcome by the driving motor.

The slip rings used to transmit power from the solar paddles will increase the friction which the driving motor must overcome. At the present time, slip rings are being considered in preference to flexible leads which require a daily rewind cycle, during which time the power output from the solar paddles is reduced from its nominal value.

If flex leads are used, the angular disturbance to the vehicle during paddle rewind would depend on the ratio of the paddle and vehicle inertias. If the product of inertia effects of paddle rotation are neglected, and only rotation about the pitch axis is considered, then the torque exerted on the paddles by the rewind motor will react on the vehicle body in an opposite direction but with equal magnitude.

Assuming that the paddle unwind must take place in less than 1 hour, with a minimum angular velocity requirement, the disturbance will be a pair of square pulses of equal area. Considering peak torque at the motor = 1 lb-ft $\int T dt = \Delta(I_p \omega_p)$

$$\omega_p = \frac{\theta}{\Delta t} = \frac{2\pi}{3000 \text{ sec}} = 2.09 \times 10^{-3} \text{ rad/sec}$$

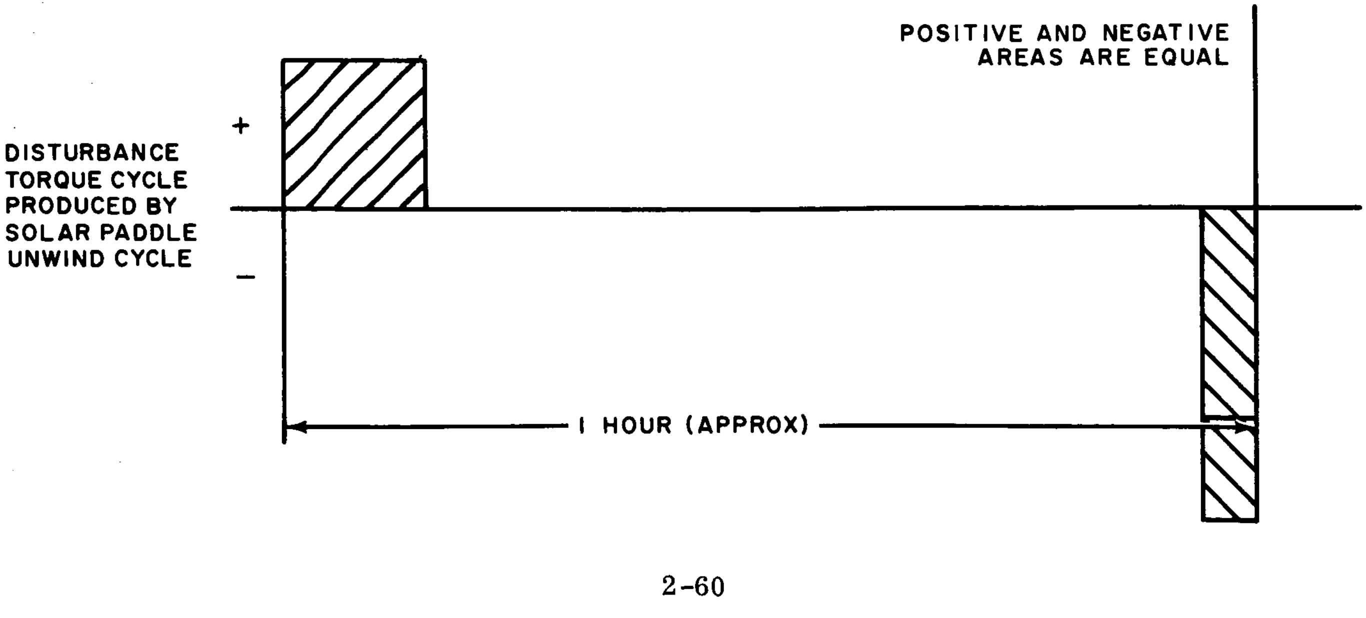

and for a paddle inertia of 6.30 slug ft^2, dt (the time in seconds during which paddles are accelerated) is $\frac{(6.30)(2.09 \times 10^{-3})}{1} = 1.32 \times 10^{-2}$ sec.

If minimum torque on the paddle shaft were a requirement, the torque pulses would follow each other and

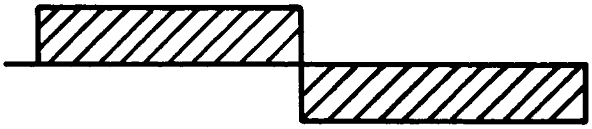

$$\theta = \frac{\alpha}{2} t^2$$

$$\pi = \frac{\alpha}{2} (30 \times 60)^2$$

$$\frac{2\pi}{(1800)^2} = \alpha \text{ (angular acceleration)}$$

$$\frac{6.28}{(1.8)^2 \times 10^6} = \alpha = 1.94 \times 10^{-6} \text{ rad/sec}^2$$

Therefore, the minimum torque for rotation of paddles for the 500 lb and 1000 lb 3-axis stabilized vehicles would be

$$T_{min} = I\alpha = (6.3)\ 1.94 \times 10^{-6}$$

$$= 1.22 \times 10^{-5} \text{ ft-lb}$$

e. Orbital Coupling Torque

If the vehicle orbit is noncircular, the orbit eccentricity, e, makes it necessary to provide a pitching acceleration to maintain the vehicle Z axis along a line to the center of the Earth at one focus of the ellipse. The value of this angular pitching acceleration, $\ddot{\theta}$, can be obtained from the expression

$$\ddot{\theta} = - \frac{2GM_e (1 + e \cos \theta)^3 \ e \sin \theta}{a^3 (1 - e^2)^3}$$

where θ = true anomaly

e = orbit eccentricity (0.025 maximum)

a = length of semi major axis of synchronous orbit

G = universal gravitational constant

M_e = mass of the Earth

The maximum value of required acceleration occurs, for the value of eccentricity chosen, when $\theta = 86°$. For a synchronous orbit, it is found that $\ddot{\theta}$ max is equal to 2.6×10^{-10} rad/sec^2. The torque required to produce this maximum acceleration for the 500 lb vehicle is 1.21×10^{-8} ft-lb (maximum). This torque is periodic with orbital frequency.

f. Attitude Disturbance Torque during Ascent

During the transfer ellipse, the effects of external disturbing torques are minimized by spin stabilization. The magnitude of the disturbing torque will determine the spin rate required for stabilization. The magnitude of the disturbing torque should not, however, be overestimated because of the associated weight penalty and complexity of the despin mechanism required.

The disturbing torque selected was based on the action of solar flare during the Hohmann transfer ellipse trajectory. For simplicity, the transfer orbit is assumed to lie in the ecliptic plane. Since the period of time during which the transfer takes place is small, it is assumed that the angle between the incident solar flare particles and the spin axis of the vehicle is a constant. The torque acting on the vehicle contains an expression involving an arbitrary angle (90° - ϕ) between the spin axis of the vehicle and the incident solar flare. The torque equation is analyzed to determine the value of ϕ which produces the largest torque. The time, measured from equinox, which produces the critical value of (90° - ϕ) can be determined by the following equations

Sun-Earth unit vector, $\vec{SE} = \cos \omega_{SE} t\,\hat{i} + \sin \omega_{SE} t\,\hat{j} + 0\hat{k}$

Spin axis unit vector, $\vec{P} = \sin (\omega_p t)\,\hat{i} - \cos (\omega_p t)\,\hat{j} + 0\,\hat{k}$

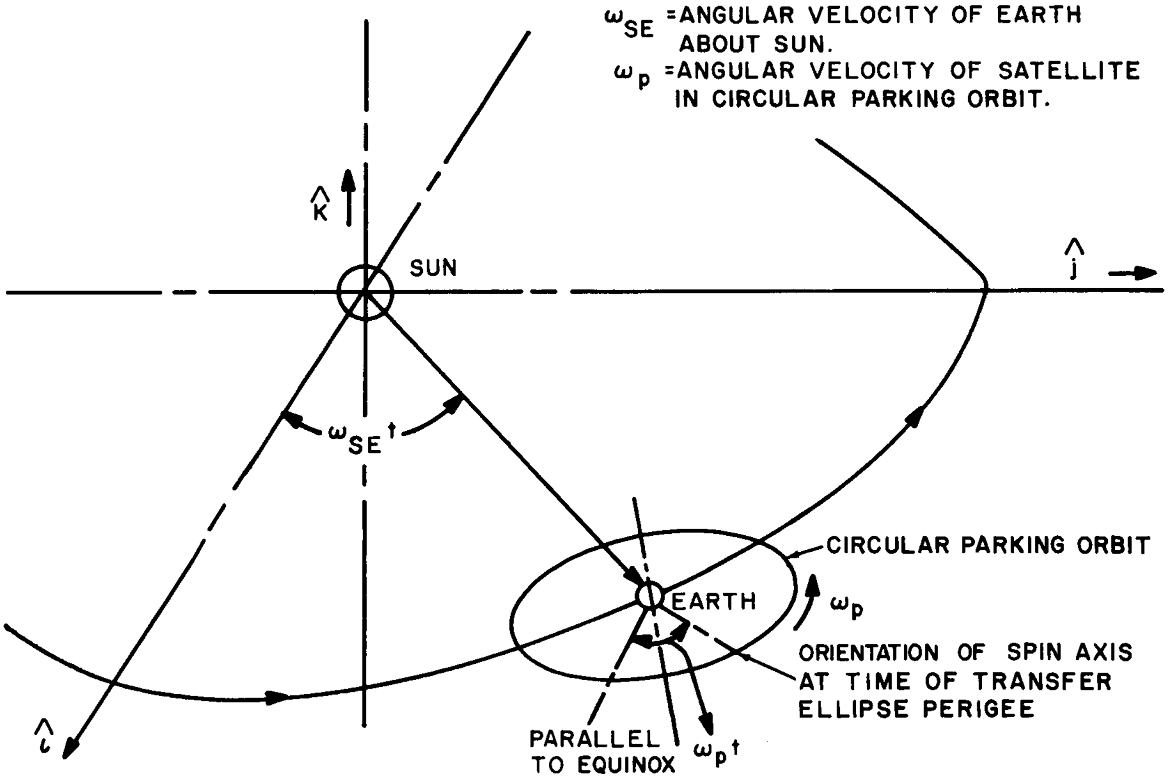
ω_{SE} =ANGULAR VELOCITY OF EARTH ABOUT SUN.
ω_p =ANGULAR VELOCITY OF SATELLITE IN CIRCULAR PARKING ORBIT.
$\hat{K}$
SUN
$\hat{j}$
$\omega_{SE}t$
CIRCULAR PARKING ORBIT
EARTH
ω_p
ORIENTATION OF SPIN AXIS AT TIME OF TRANSFER ELLIPSE PERIGEE
$\hat{i}$
PARALLEL TO EQUINOX
$\omega_p t$

Thus, $\cos (90 - \phi) = (\cos \omega_{SE} t)(\sin \omega_p t) - (\sin \omega_{SE} t)(\cos \omega_p t)$

where $(90 - \phi)$ = angle between spin axis and $\vec{SE}$

The torque can be expressed as follows, assuming that the cylindrical satellite with paddles folded can be approximated by a cylinder.

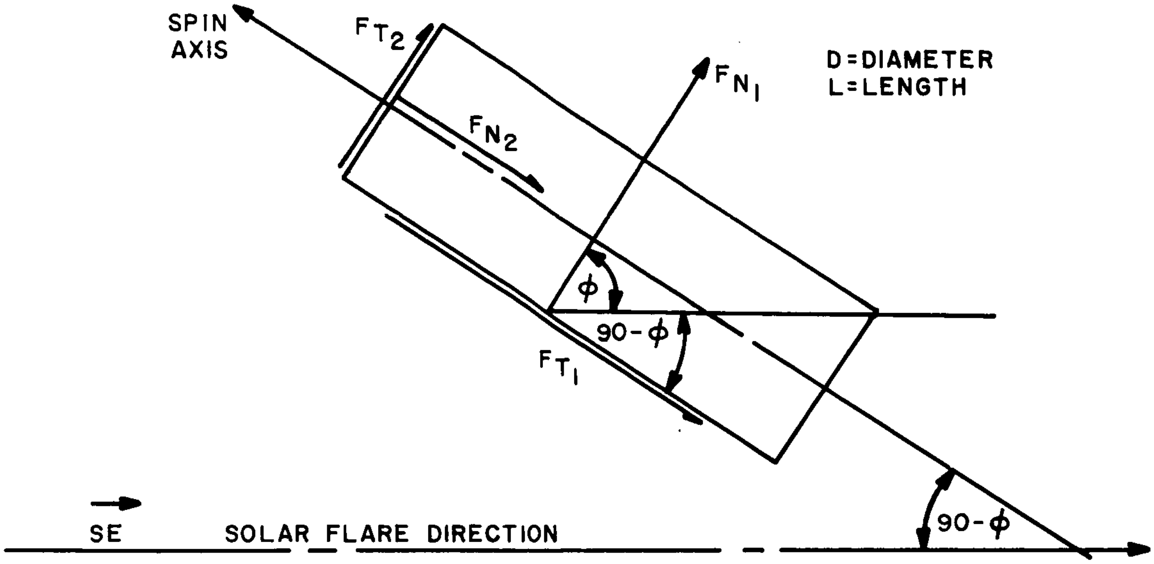
SPIN AXIS
F_{T_2}
F_{N_1}
D=DIAMETER
L=LENGTH
F_{N_2}
ϕ
$90-\phi$
F_{T_1}
SE
SOLAR FLARE DIRECTION
$90-\phi$

The torque which exists in the absence of an eccentricity between the center of mass and the cylinder centroid is expressed as

$$|T_o| = F_{T_2}\left(\frac{L}{2}\right) - F_{T_1}\left(\frac{D}{2}\right)$$

In the presence of an eccentricity (ΔL) of the center of mass and with the cylinder centroid along the spin axis, an additional torque T_e exists

$$|T_e| = (F_{N_1} + F_{T_2})\,\Delta L$$

For the case of a solar flare

$$F_{N_1} = \left(\frac{S_f}{c}\right) DL \cos^2\phi$$

$$F_{T_1} = \left(\frac{S_f}{c}\right) DL \cos\phi \sin\phi$$

$$F_{T_2} = \left(\frac{S_f}{c}\right)\left(\frac{\pi D^2}{4}\right) \cos\psi \sin\phi$$

$\left(\frac{S_f}{c}\right)$ is taken as 75×10^{-7} lb/ft^2

For the 500 lb vehicle: $D = 50$ in. $= 4.16$ ft; $L = 84$ in. $= 7$ ft; and $\Delta L = 0.5$ in. $= 0.0416$ ft

Therefore, $T_o = -(\frac{S_f}{c})(\frac{D^2 L}{2})\left[1 - \frac{\pi}{4}\right](\cos\phi)(\sin\phi) = (\cos\phi)(\sin\phi)\ 9.75\text{x}10^{-5}$ lb-ft

and $T_e = (\frac{S_f}{c})(\Delta L)\left[DL\cos^2\phi + \frac{\pi D^2}{4}\cos\phi\sin\phi\right]$

$$= 0.907\text{x}10^{-5}\cos^2\phi + 0.424\text{x}10^{-5}\cos\phi\sin\phi$$

Combining T_o and T_e for maximum torque,

$$|T_o| + |T_e| = 10.2\text{x}10^{-5}\cos\phi\sin\phi + 0.907\text{x}10^{-5}\cos^2\phi$$

The value of ϕ for which the torque is maximum is close to 45°. The peak value of solar flare torque is then $\approx 5.55\text{x}10^{-5}$ ft-lb for the 500 lb vehicle.

3. Disturbance Torque Model

Tables 2-1 through 2-3 summarize the results of disturbance torque calculations. Table 2-4 presents the resulting disturbance torque model representing a simplified summation of all significant torques.

4. Areas for Future Study

a. Solar Disturbing Torque

It is necessary that torques due to solar effects be computed for a final configuration considering shadows as "negative" solar pressures. No shadowing occurs during an equinox; maximum shadowing occurs during a solstice.

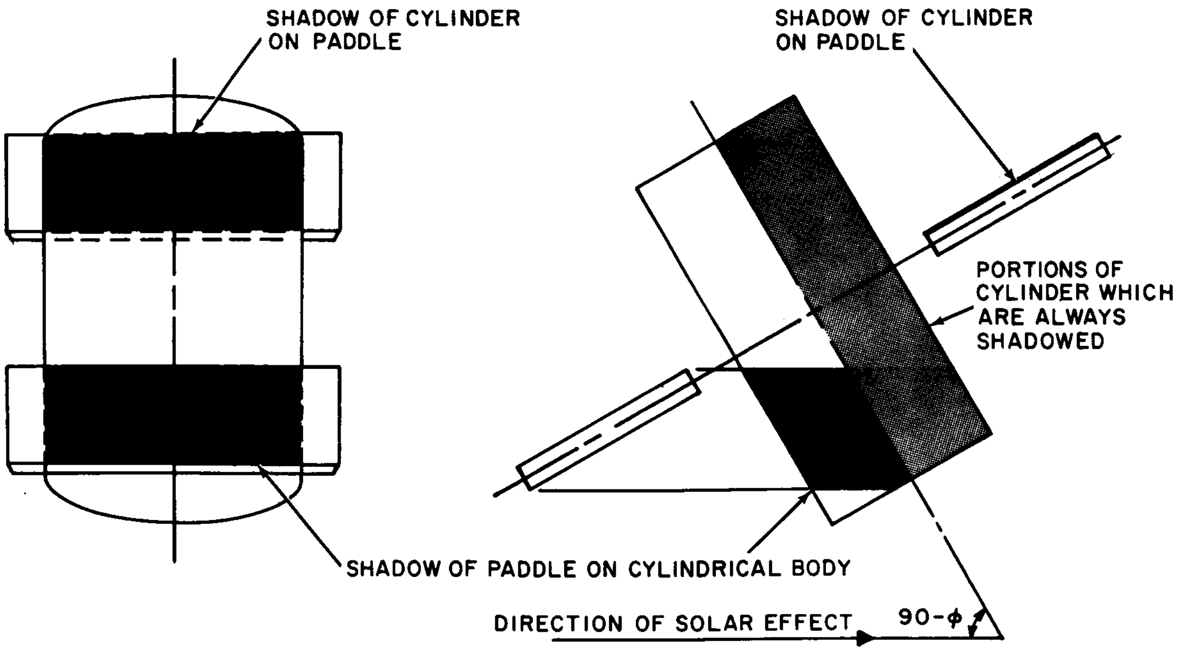
SHADOW OF CYLINDER ON PADDLE
SHADOW OF CYLINDER ON PADDLE
PORTIONS OF CYLINDER WHICH ARE ALWAYS SHADOWED
SHADOW OF PADDLE ON CYLINDRICAL BODY
DIRECTION OF SOLAR EFFECT
90-ϕ

TABLE 2-1
SOLAR DISTURBANCE TORQUE* SUMMARY FOR 3-AXIS AND GRAVITY GRADIENT CONTROLLED VEHICLES

		During Transfer Ellipse	During Orbit					
Vehicle		Solar Flare	Solar Radiation			Solar Flare		
			Yaw	Pitch	Roll	Yaw	Pitch	Roll
3-Axis Stabilized	100	Constant $\pm 0.18\text{x}10^{-5}$ lb-ft	$1.0\text{x}10^{-7}\sin 2\omega_e t$	$2.0\text{x}10^{-7}\sin 2\omega_e t$	$1.0\text{x}10^{-7}\sin \omega_e t$	$0.7\text{x}10^{-5}\sin 2\omega_e t$	$1.0\text{x}10^{-5}\sin 2\omega_e t$	$0.9\text{x}10^{-5}\sin \omega_e t$
	500	Constant $\pm 5.55\text{x}10^{-5}$ lb-ft	$9.7\text{x}10^{-7}\sin 2\omega_e t$	$16.5\text{x}10^{-7}\sin 2\omega_e t$	$7.5\text{x}10^{-7}\sin \omega_e t$	$4.9\text{x}10^{-5}\sin 2\omega_e t$	$8.3\text{x}10^{-5}\sin 2\omega_e t$	$6.8\text{x}10^{-5}\sin \omega_e t$
	1000	Constant $\pm 15.0\text{x}10^{-5}$ lb-ft	$13\text{x}10^{-7}\sin 2\omega_e t$	$22\text{x}10^{-7}\sin 2\omega_e t$	$10\text{x}10^{-7}\sin \omega_e t$	$6.5\text{x}10^{-5}\sin 2\omega_e t$	$11\text{x}10^{-5}\sin 2\omega_e t$	$9\text{x}10^{-5}\sin \omega_e t$
**Gravity Gradient Stabilized (ℓ = 100 ft)	100	Constant $\pm 0.18\text{x}10^{-5}$ lb-ft	** Zero	$15\text{x}10^{-7}\sin 2\omega_e t$	$10.5\text{x}10^{-7}\sin \omega_e t$	** Zero	$10.5\text{x}10^{-5}\sin 2\omega_e t$	$9.5\text{x}10^{-5}\sin \omega_e t$
	500	Constant $\pm 5.55\text{x}10^{-5}$ lb-ft	** Zero	$25\text{x}10^{-7}\sin 2\omega_e t$	$18\text{x}10^{-7}\sin \omega_e t$	** Zero	$18\text{x}10^{-5}\sin 2\omega_e t$	$15.5\text{x}10^{-5}\sin \omega_e t$
	1000	Constant $\pm 15.0\text{x}10^{-5}$ lb-ft	** Zero	$35\text{x}10^{-7}\sin 2\omega_e t$	$25\text{x}10^{-7}\sin \omega_e t$	** Zero	$25\text{x}10^{-5}\sin 2\omega_e t$	$22\text{x}10^{-5}\sin \omega_e t$

* All torques expressed in ft-lb.

** Center of mass assumed at centroid of vehicle.

TABLE 2-2

SOLAR DISTURBANCE TORQUE* SUMMARY FOR SPIN-STABILIZED VEHICLES

	During Transfer Ellipse	During Orbit			
Vehicle	Solar Flare	Solar Radiation		Solar Flare	
		Gross Torque T_G, Causing Precession of Spin Axis:		Yaw Torque: $T_Z = T_G \sin \omega_B t$ Roll Torque: $T_X = T_G \cos \omega_B t$	
		Peak	Continuous	Peak	Continuous
100	Constant $\pm 0.18 \times 10^{-5}$ lb-ft	**1.25×10^{-7}	$1.36 \times 10^{-7} \left[\sin \omega_{SE} t\right] \sqrt{1-.16 \sin^2 \omega_{SE} t}$	**1.08×10^{-5}	$1.17 \times 10^{-5} \left[\sin \omega_{SE} t\right] \sqrt{1-.16 \sin^2 \omega_{SE} t}$
500	Constant $\pm 5.55 \times 10^{-5}$ lb-ft	**4.15×10^{-7}	$4.52 \times 10^{-7} \left[\sin \omega_{SE} t\right] \sqrt{1-.16 \sin^2 \omega_{SE} t}$	**3.56×10^{-5}	$3.87 \times 10^{-5} \left[\sin \omega_{SE} t\right] \sqrt{1-.16 \sin^2 \omega_{SE} t}$
1000	Constant $\pm 15.0 \times 10^{-5}$ lb-ft	**11.6×10^{-7}	$12.6 \times 10^{-7} \left[\sin \omega_{SE} t\right] \sqrt{1-.16 \sin^2 \omega_{SE} t}$	**9.86×10^{-5}	$10.7 \times 10^{-5} \left[\sin \omega_{SE} t\right] \sqrt{1-.16 \sin^2 \omega_{SE} t}$

* All torques expressed in ft-lb.

** Peak values during solstice.

TABLE 2-3
SUMMARY OF ADDITIONAL DISTURBANCE TORQUES*

Vehicle		Gravity Gradient Torque Pitch	Gravity Gradient Torque Roll	Magnetic Interaction with Earth's Field Roll and Yaw	Orbital Coupling (Inclination, etc.)	Solar Paddle Unwind Cycle*** (Rectangular torque of 1 hr period occurring once per day)	Equipment Torques Applicable to all Vehicles. All Waveforms are Rectangular Torques Acting About Each Axis
Spin Stabilized	100	Zero	$**8.29x10^{-10}$	$**2.0x10^{-10}$	N. A.	N. A.	Vidicon Equipment Filter Wheel $8.8x10^{-2}$, 1 sec period twice daily Scanning Mirror $3.35x10^{-3}$ft-lb, 50 alternating pulses, 1.2 sec duration, once per hr Infrared Equipment Mirror $2.78x10^{-6}$, 100 sec period four times per hr Multimirror Drum $1.5x10^{-2}$, 2 sec duration, 20 sec between positive and negative pulses, twice hourly
	500	Zero	$**8.85x10^{-9}$	$**1.0x10^{-9}$	N. A.	N. A.	
	1000	Zero	$**6.08x10^{-9}$	$**2.0x10^{-9}$	N. A.	N. A.	
3-Axis Stabilized	100	$4.52x10^{-10}$	$4.14x10^{-10}$	Yaw Only $2.52x10^{-10}$	$0.143x10^{-8} \sin \omega_e t$	$\pm 0.97x10^{-6}$	
	500	$-4.62x10^{-9}$	$-9.65x10^{-10}$	$1.17x10^{-9}$	$1.21 \ x10^{-8} \sin \omega_e t$	$\pm 1.22x10^{-5}$	
	1000	$3.24x10^{-9}$	$4.96x10^{-9}$	$2.52x10^{-9}$	$4.88 \ x10^{-8} \sin \omega_e t$	$\pm 1.22x10^{-5}$	
Gravity Gradient Stabilized	100	NA	NA	$2.5 \ x10^{-9}$	$86.0 \ x10^{-8} \sin \omega_e t$	$\pm 0.50x10^{-6}$	
	500	NA	NA	$1.2 \ x10^{-8}$	$101.5 \ x10^{-8} \sin \omega_e t$	$\pm 0.61x10^{-5}$	
	1000	NA	NA	$2.5 \ x10^{-8}$	$120.0 \ x10^{-8} \sin \omega_e t$	$\pm 0.61x10^{-5}$	

* All torques expressed in ft-lb

** Torque acts along both Roll and Yaw body axes

Roll Component $= T \sin \omega_B t$ Yaw Component $= T \cos \omega_B t$

*** Solar Paddle unwind applicable only if slip rings are not used.

Rectangular pulses taken to be of form: 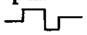

TABLE 2-4
COMPOSITE TORQUE* MODEL FOR ALL DISTURBANCES
(For Bi-Annual Solar Flare Effects, Increase Steady & Cyclical Values by 75)

Vehicle		**Steady Torques			Cyclical Torques			***Intermittent Torques All Axes(These rectangular waveform torques are conservatively taken as applicable to all vehicles)
		Yaw	Pitch	Roll	Yaw	Pitch	Roll	
Spin Stabilized	100	Zero	Zero	Zero	$1.25\times10^{-7}\sin\omega_B t$	$2.0\times10^{-10}\sin\omega_B t$	$1.25\times10^{-7}\cos\omega_B t$	8.8×10^{-2}, 1 sec period, twice daily 3.35×10^{-3}, 50 alternating pulses, 1.2 sec duration, hourly 2.78×10^{-6}, 100 sec period, four times per hour 1.5×10^{-2}, 2 alternating pulses, 2 sec duration, 20 sec between positive and negative pulses, twice hourly 1.22×10^{-5}, one hour period, once per day, pitch only 3-axis & gravity gradient vehicles only
	500	Zero	Zero	Zero	$4.15\times10^{-7}\sin\omega_B t$	$1.0\times10^{-9}\sin\omega_B t$	$4.15\times10^{-7}\cos\omega_B t$	
	1000	Zero	Zero	Zero	$11.6\times10^{-7}\sin\omega_B t$	$2.0\times10^{-9}\sin\omega_B t$	$[1.6\times10^{-7}\cos\omega_B t$	
3-Axis Stabilized	100	2.0×10^{-8}	1.5×10^{-8}	5.0×10^{-8}	$1.0\times10^{-7}\sin 2\omega_e t$	$2.0\times10^{-7}\sin 2\omega_e t$	$[1.0\times10^{-7}\sin\omega_e t$	
	500	1.4×10^{-7}	1.0×10^{-7}	3.5×10^{-7}	$9.7\times10^{-7}\sin 2\omega_e t$	$1.65\times10^{-6}\sin 2\omega_e t$	$[7.5\times10^{-7}\sin\omega_e t$	
	1000	2.0×10^{-7}	1.5×10^{-7}	5.0×10^{-7}	$1.3\times10^{-6}\sin 2\omega_e t$	$2.2\times10^{-6}\sin 2\omega_e t$	$[1.0\times10^{-6}\sin\omega_e t$	
Gravity Gradient Stabilized	100	2.5×10^{-9}	Zero	Zero	Zero	$15\times10^{-7}\sin 2\omega_e t$	$10.5\times10^{-7}\sin\omega_e t$	
	500	1.2×10^{-8}	Zero	Zero	Zero	$25\times10^{-7}\sin 2\omega_e t$	$18\times10^{-7}\sin\omega_e t$	
	1000	2.5×10^{-8}	Zero	Zero	Zero	$35\times10^{-7}\sin 2\omega_e t$	$25\times10^{-7}\sin\omega_e t$	

* All torques expressed in ft-lb.

** From solar pressure curve, average daily DC component.

*** From equipment disturbances and solar paddle unwind.

It can be seen that accounting for shadowing effects is not simple, and would require an analytical digital computer study, possibly coupled with photographic techniques for problem simplification.

Data on the frequency and magnitude of solar flare is sparse. It is expected that the OSO experiments will yield the kind of information that will help in arriving at a reasonable model of the solar flare inputs. It is known that solar flares have occurred which produce short duration gust pressures 150 times that produced by totally absorbed solar radiation pressure. In preparing the torque model, the peak values used are 75 times totally absorbed solar radiation pressure. It is felt that this is a conservative assumption since the gust duration is probably small compared to the duration of one solar flare. The solar flare is taken to occur twice a year for a 20 hour period. More frequent gusts of lower magnitude occur at 27 day periods. The constant values of solar flare are approximately 22% of the solar radiation values; since the curves for solar radiation and solar flare have approximately the same shape, the solar radiation pressure values were increased by 25% to account for steady solar flares.

b. Magnetic Torque Disturbances

Magnetic torque disturbances will remain a secondary effect; however, the remaining areas, listed below, should be investigated for a final configuration.

(1) Torques due to eddy currents in the vehicle skin.

(2) Torques due to interaction with paramagnetically shielded magnets.

(3) Torque on an elongated vehicle made of paramagnetic materials.

(4) Effect of Sun's magnetic field.

c. Final Equipment Design

The final design may include horizon scanners, filter wheels, and moving mirrors, not included in the present torque model. The sensor protecting shutters may be of an unbalanced design, or, if balanced, they may operate with one element only, creating a force and torque pulse. Gyroscopic guidance equipment, or special thermodynamic control systems involving expelled or circulated fluids may cause drift. It is obvious that all of these possible torque sources must be thoroughly evaluated once the system design has been detailed.

D. SYSTEM DESCRIPTION

This section describes operation of the control systems for three axis stabilized, gravity gradient, and spin controlled spacecraft. Although several types of torque devices could be employed for each class of spacecraft, only one type will be discussed in each class, since the torquer does not influence the basic functions that must be performed.

Block diagrams of the control systems for the three basic spacecraft are presented, which include the following functions.

- Earth acquisition and reacquisition
- Earth tracking
- Initial orbital velocity correction
- Station keeping
- Failure modes

The overall control system descriptions presented herein are introduced primarily to give the reader a broad view of how the various system functions are interrelated prior to the presentation of the detailed discussions of each function in subsections E and F, following, and Sections 3 and 4.

1. 3-Axis Stabilized Spacecraft

Figure 2-17 is a block diagram showing the integrated control functions of a 3-axis stabilized system. This particular 3-axis system, identified as the gyro compass control system, is represented by the following equipments.

2 variable speed reaction wheels
1 fixed speed wheel
3-axis cold gas system
3 rate gyros
Horizon sensors
Control logic for various modes

The modes of operation provided by this system configuration are

- Automatic Earth acquisition and reacquisition
- Automatic Earth tracking
- Command control of initial velocity error correction
- Command control for station keeping
- Automatic or command control of gas system for reaction wheel momentum unloading
- Command control of pitch and roll angle biases
- Command rate control mode
- Automatic solar paddle drive control

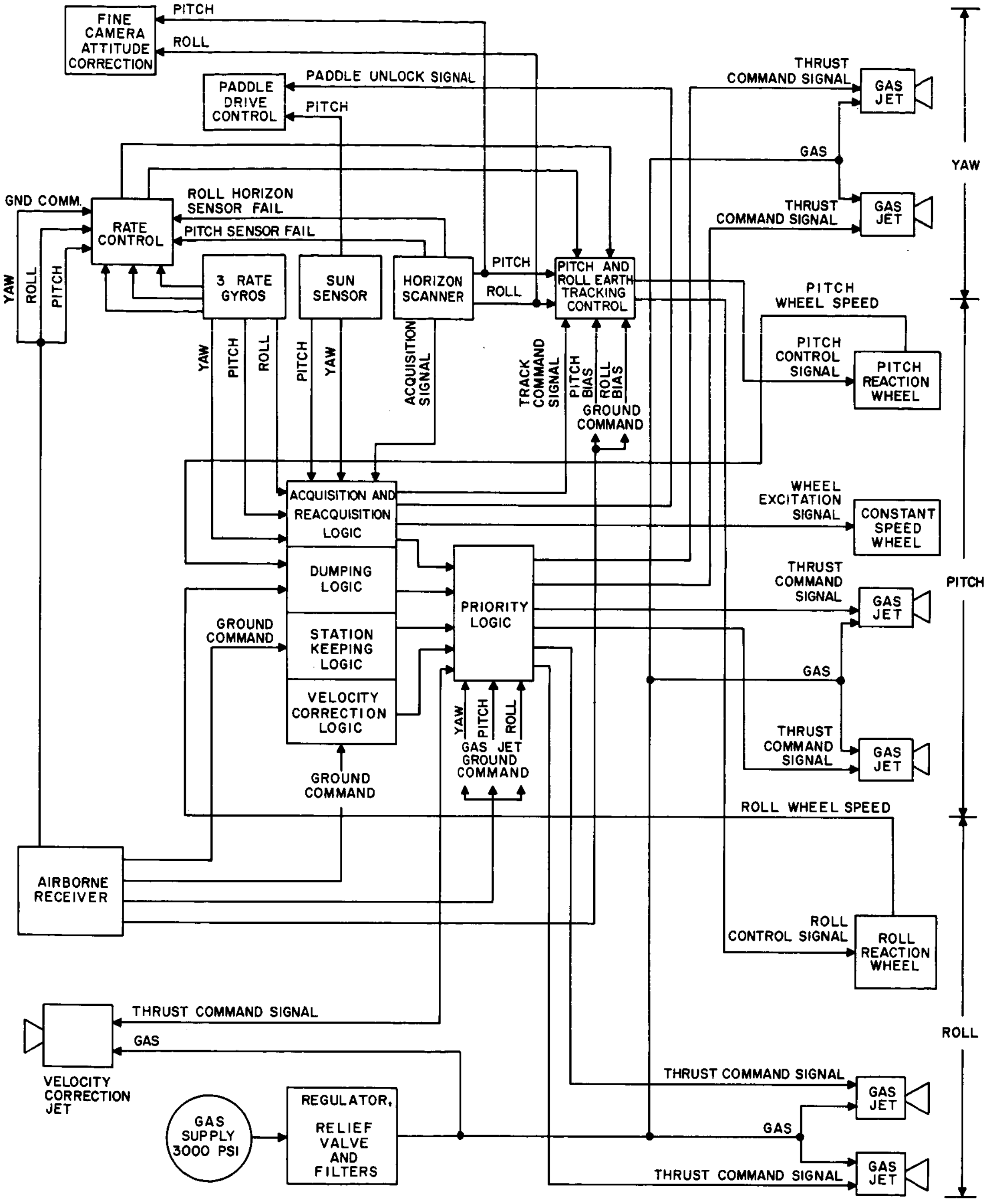
FINE CAMERA ATTITUDE CORRECTION
PITCH
ROLL
PADDLE DRIVE CONTROL
PADDLE UNLOCK SIGNAL
PITCH
THRUST COMMAND SIGNAL
GAS JET
YAW
GAS
THRUST COMMAND SIGNAL
GAS JET
GND COMM.
RATE CONTROL
ROLL HORIZON SENSOR FAIL
PITCH SENSOR FAIL
YAW
ROLL
PITCH
3 RATE GYROS
SUN SENSOR
HORIZON SCANNER
PITCH
ROLL
PITCH AND ROLL EARTH TRACKING CONTROL
PITCH WHEEL SPEED
PITCH CONTROL SIGNAL
PITCH REACTION WHEEL
YAW
PITCH
ROLL
PITCH
YAW
ACQUISITION SIGNAL
TRACK COMMAND SIGNAL
PITCH BIAS
ROLL BIAS
GROUND COMMAND
ACQUISITION AND REACQUISITION LOGIC
WHEEL EXCITATION SIGNAL
CONSTANT SPEED WHEEL
DUMPING LOGIC
PRIORITY LOGIC
THRUST COMMAND SIGNAL
GAS JET
PITCH
GROUND COMMAND
STATION KEEPING LOGIC
GAS
VELOCITY CORRECTION LOGIC
YAW
PITCH
ROLL
GAS JET GROUND COMMAND
THRUST COMMAND SIGNAL
GAS JET
GROUND COMMAND
ROLL WHEEL SPEED
AIRBORNE RECEIVER
ROLL CONTROL SIGNAL
ROLL REACTION WHEEL
THRUST COMMAND SIGNAL
ROLL
GAS
VELOCITY CORRECTION JET
THRUST COMMAND SIGNAL
GAS JET
GAS SUPPLY 3000 PSI
REGULATOR, RELIEF VALVE AND FILTERS
GAS
GAS JET
THRUST COMMAND SIGNAL

Figure 2-17. Block Diagram - 3-Axis Stabilized Control System

A brief description of each of the operational modes and control logic functions is given below.

a. Control Logic Functions

1) Priority Logic. The priority logic block indicated in Figure 2-17 performs the function of operating the cold gas system on a priority basis; i.e., the acquisition and reacquisition mode has priority over momentum dumping, velocity correction, and station keeping, and operates the cold gas system in a rate mode or Sun orientation mode. Momentum dumping has priority over the velocity correction and station keeping functions which are locked out if a dump signal exists. Velocity correction has priority over station keeping, but since both of these are ground commanded, the ground complex will know that initial velocity corrections must be performed prior to station keeping. Ground command signals are available to the priority logic block which provide the capability for command dumping.

2) Acquisition and Reacquisition. Acquisition and reacquisition logic provides for the control of the cold gas system for active despin, Sun orientation, and rotation about the Sun line which are fully described in subsection F. The acquisition logic requires yaw, pitch, and roll rate signals for active despin and for rotation about the Sun line. It also accepts Sun sensor pitch and yaw signals for the Sun orientation phase and an acquisition signal from the horizon scanner. This horizon scanner signal activates the pitch and roll Earth tracking control system, provides excitation to the constant speed wheel for initiating yaw alignment, and provides a solar paddle unlock signal.

3) Dumping Logic. This block provides signals to the cold gas valves for the removal of reaction wheel angular momentum. Inputs are reaction wheel tachometer signals which activate and deactivate the dumping logic on the basis of reaction wheel speed.

4) Injection Velocity Correction Logic. This logic selects the proper cold gas nozzles for injection velocity correction depending on the sense transmitted via ground command. The duration of velocity correction depends on the duration of the ground command signal which is based on a measured orbital velocity error or longitude drift rate.

5) Station Keeping Logic. This logic activates the cold gas nozzles for correction of velocity or mean motion errors due to orbital perturbations. Since the major perturbation is due to the Earth's equatorial ellipticity, this velocity error will always be one-sided, hence corrective thrust will always be applied in the same direction, opposed to the direction of motion. The ground command signal is therefore on-off in nature and does not require sign intelligence.

b. Operational Modes

1) Automatic Solar Paddle Drive Control. This mode provides for the alignment of the solar paddles with the Sun. The Sun sensor provides a continuous pitch error signal to the paddle drive servo. The drive servo thus maintains a paddle rate relative to the spacecraft body. This rate is equivalent

to the angular velocity of the spacecraft about the Earth and the angular velocity of the Earth about the Sun.

For purposes of storage within the launch vehicle, the paddles must be folded, and deployed after apogee kick. Following deployment, they must be locked so that the paddle surface is parallel to the body yaw-pitch plane. Thus, during acquisition where the body roll axis is directed toward the Sun, the solar paddles will be fully illuminated.

2) Command Rate Control. An external ground command rate mode is provided in the event horizon sensors fail, and also to provide stabilization at extremely low rates for high resolution pictures. Attitude feedback for this mode (in the event of horizon sensor failure) is by means of photographs of the Earth disc, and noting its displacement from frame center.

For the case where horizon sensors were operative, the system would revert to the normal tracking mode after completion of high resolution pictures.

3) Command Control of Pitch and Roll Bias. A ground command exists which can supply bias signals to compensate for horizon sensor bias errors. To ascertain that an error actually exists, it would be necessary to analyze Earth disc pictures and establish the magnitude of the pitch and roll errors.

Other modes of operation have been described under Control Logic. Acquisition and Earth tracking are fully discussed in subsections E and F.

c. Alternate 3-Axis Systems

Various 3-axis systems, which differ mainly in the type of torque device used, or in the implementation of control logic, are analyzed in subsection E. It is apparent that a major problem exists in the area of attitude control sensors for the Earth oriented satellite mission when a high degree of pointing accuracy is required in all axes.

An area for profitable future study would be the investigation and exploitation of high accuracy sensors such as Sun sensors and star trackers for the Earth oriented satellite mission. It is clear that existing Earth horizon sensors are undesirable for an Earth oriented mission requiring highly accurate pointing and/or rate stabilization. If high precision sensors, as used for inertially fixed spacecraft missions, could be used in a simple reliable manner for the SMS mission, an obvious weak link would be eliminated.

Many of the torquing devices investigated in this study would be applicable to the high performance mission. Indeed, the basic problem area is that of attitude sensing.

A likely possibility for the high accuracy mission would employ a Polaris star tracker for roll and yaw reference, and a single axis gimbaled

Sun tracker which tracks the Sun in a plane containing the vehicle pitch axis and the Sun. Horizon scanners would not be used during Earth tracking, but would be of use during the acquisition phase. Nonrotating torque devices would prove more suitable than those which produce inter-axis coupling.

2. Gravity Gradient Spacecraft

A block diagram for the gravity gradient control system is presented in Figure 2-18. Although the control for this type of satellite may be instrumented very easily for the Earth tracking mode, sufficient additional complexity is required for acquisition, so that actually, its basic advantages from a control viewpoint reduce to only two. These are the elimination of all attitude sensors for Earth tracking, and very low body rates while Earth tracking.

a. Earth Tracking Mode

The Earth tracking control system consists of three variable speed reaction wheels, one constant speed wheel, and three rate gyros. A gas system is not required for momentum dumping, but is provided to perform the station keeping and initial velocity correction functions.

Restoring control torques are provided by differential gravity in pitch and roll if the satellite long axis is misaligned with the vertical. Damping is provided by reaction wheel torquers which are excited by vehicle pitch and roll body rates. It is clear that no reaction wheel dumping is required if the vehicle momentum is essentially zero with respect to the orbital reference frame at the time the reaction wheel rate damping system is energized. The pitch rate gyro output signal must be biased at a rate equivalent to orbital angular velocity so that the pitch reaction wheel speed is unresponsive to this constant rate.

Ground commands are provided for station keeping and velocity correction functions. The logic blocks perform functions similar to those of the 3-axis stabilized system, as does the priority logic block. The rate mode logic selects one of two rate systems, depending on whether the system is in the acquisition or the Earth tracking phase. The Earth tracking rate system provides proportional control using reaction wheels, while an on-off gas system is used for acquisition rate control.

Selection of the Earth tracking rate control system energizes the constant speed wheel for gyro compass control of yaw attitude. While the wheel is accelerating to speed, a pitch reaction torque will exist. Since the pitch variable speed wheel cannot store momentum equivalent to that of the constant speed wheel, and because gravity gradient torque is too small to restrain vehicle motion, the pitch gas system must be employed during this wheel speedup period. When wheel momentum has reached its steady state value, rate damping is once again accomplished for the pitch axis by means of the pitch reaction wheel.

b. Earth Acquisition Mode

Acquisition and reacquisition are accomplished completely with the cold gas system torquers. Three reaction wheels and a constant speed wheel

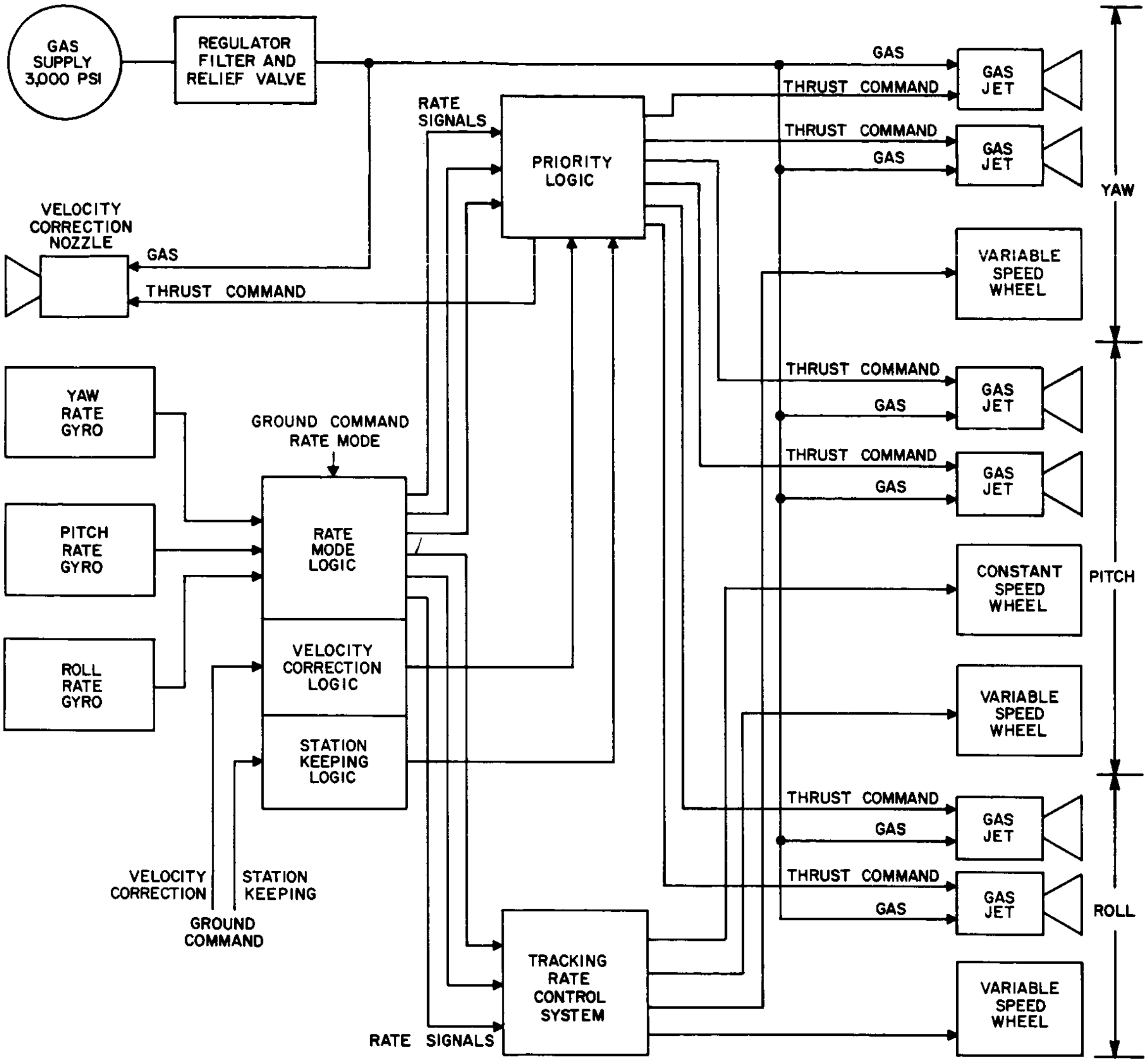

GAS SUPPLY 3,000 PSI
REGULATOR FILTER AND RELIEF VALVE
GAS
THRUST COMMAND
GAS JET
RATE SIGNALS
PRIORITY LOGIC
THRUST COMMAND
GAS
GAS JET
YAW
VELOCITY CORRECTION NOZZLE
GAS
THRUST COMMAND
VARIABLE SPEED WHEEL
YAW RATE GYRO
GROUND COMMAND RATE MODE
THRUST COMMAND
GAS
GAS JET
THRUST COMMAND
GAS
GAS JET
PITCH RATE GYRO
RATE MODE LOGIC
CONSTANT SPEED WHEEL
PITCH
ROLL RATE GYRO
VELOCITY CORRECTION LOGIC
VARIABLE SPEED WHEEL
STATION KEEPING LOGIC
THRUST COMMAND
GAS
GAS JET
VELOCITY CORRECTION
STATION KEEPING
THRUST COMMAND
GAS
GAS JET
ROLL
GROUND COMMAND
TRACKING RATE CONTROL SYSTEM
RATE SIGNALS
VARIABLE SPEED WHEEL

Figure 2-18. Block Diagram - Gravity Gradient Control System

remain at zero speed during this phase of operation. Since no attitude sensors are used during the Earth tracking phase, it is desirable to also accomplish acquisition without the aid of such sensors. As fully described in subsection F, the final phase of acquisition is accomplished on an open loop attitude basis by "steering" the spacecraft using rate control. Attitude intelligence is obtained during this steering process by means of a beacon signal or by observing pictures of the Earth disc with a wide angle camera.

Passive and active despin techniques, similar to those employed in the 3-axis acquisition system, are used for initial rate stabilization. Following the rate stabilization phase, the steering technique described above is used to obtain approximate alignment of the spacecraft long axis with the vertical. At this point, the gravity gradient vehicle is erected by separating the two equal masses which comprise the spacecraft.

After the two masses are separated, final alignment is obtained through differential gravity torques still using the cold gas rate system for damping. When ground monitoring discerns that rates are damped out, the damping system is switched into the reaction wheel rate control mode. Thereafter, the vehicle is considered to be in the Earth tracking mode.

3. Spin Stabilized Spacecraft

The spin stabilized spacecraft considered for the SMS mission is assumed to have its spin vector normal to the orbital plane. Other orientations offer no advantage, and would defeat the purpose of the SMS mission. Having the spin vector in the orbital plane and fixed in inertial space would provide even less Earth coverage than Tiros. If maintained in the orbital plane and precessed at orbital rate, extreme impulse requirements would result. The only sensible orientation is therefore normal to the orbit and inertially fixed. This, however, is not an optimum technique for obtaining high resolution pictures, unless image motion compensation is provided. Without compensation, only an Earth disc picture would be achieved. It is the latter mission to which the present discussion is directed.

a. Spin System Control Modes

The spin stabilized satellite control system is shown in Figure 2-19. The basic equipments are:

1 rate gyro

1 Sun sensor (fan beam)

1 Earth sensor (fan beam)

1 Polaris star tracker

Gas supply system with 2 nozzles for spin maintenance, 1 nozzle for initial velocity correction and station keeping, and 2 dual nozzle valves for attitude control

Various logic blocks

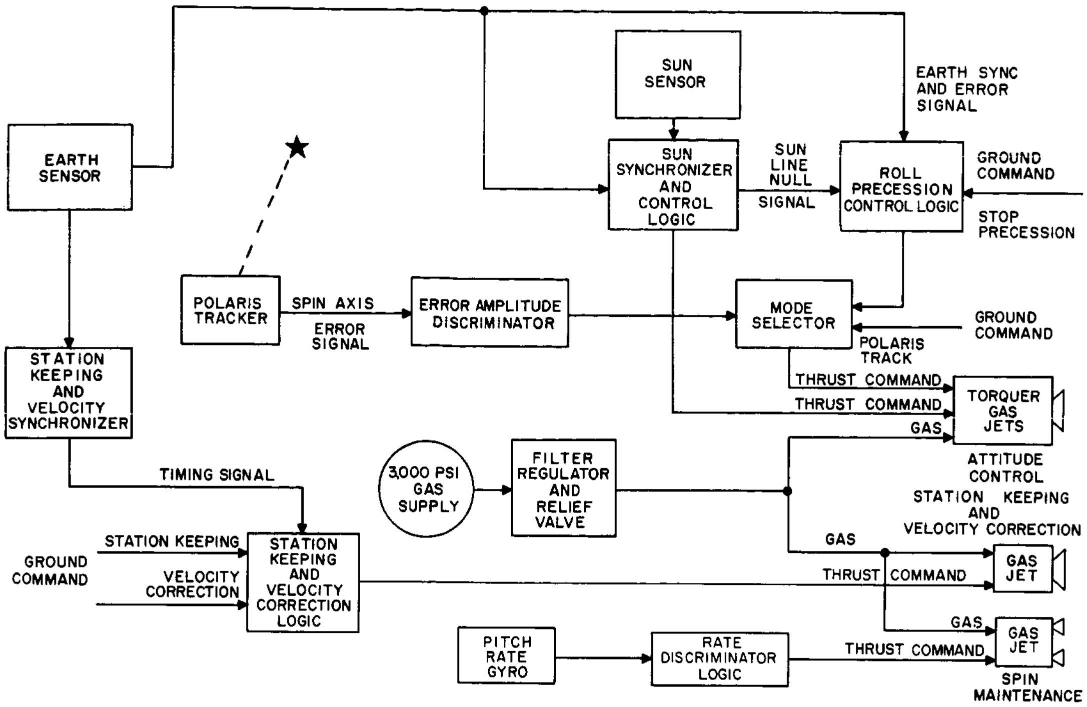
EARTH SENSOR
SUN SENSOR
EARTH SYNC AND ERROR SIGNAL
SUN SYNCHRONIZER AND CONTROL LOGIC
SUN LINE NULL SIGNAL
ROLL PRECESSION CONTROL LOGIC
GROUND COMMAND
STOP PRECESSION
POLARIS TRACKER
SPIN AXIS ERROR SIGNAL
ERROR AMPLITUDE DISCRIMINATOR
MODE SELECTOR
GROUND COMMAND
POLARIS TRACK
STATION KEEPING AND VELOCITY SYNCHRONIZER
THRUST COMMAND
THRUST COMMAND
GAS
TORQUER GAS JETS
ATTITUDE CONTROL
TIMING SIGNAL
3,000 PSI GAS SUPPLY
FILTER REGULATOR AND RELIEF VALVE
STATION KEEPING AND VELOCITY CORRECTION
GAS
STATION KEEPING
GROUND COMMAND
VELOCITY CORRECTION
STATION KEEPING AND VELOCITY CORRECTION LOGIC
THRUST COMMAND
GAS JET
GAS
PITCH RATE GYRO
RATE DISCRIMINATOR LOGIC
THRUST COMMAND
GAS JET
SPIN MAINTENANCE

Figure 2-19. Block Diagram - Spin Vehicle Control System

The fundamental control concept is an adaption of a scheme presented in Ref. 2-1. The basic scheme depends on regular precession (nutation) of a gyroscopic element when subjected to an impulsive torque. As the spin vehicle precesses in response to a control impulse, a second impulse is applied when the vehicle has precessed through an angle of 180°. At that point, regular precession stops and a net displacement of the spin axis has occurred as the result of this control action.

The first control impulse is triggered by either a Sun sensor or an Earth sensor, both with fan shaped fields of view, depending on whether the spacecraft is in a Sun or Earth orientation phase. The second impulsive torque is applied at a fixed time after the firing of the first.

1) Acquisition and Reacquisition Mode. These functions are accomplished by means of a passive despin device and an active impulsive torque device. Spin momentum is maintained at the desired level by an active rate control system consisting of a pitch rate gyro, rate discriminator, and cold gas impulsive torquer.

The Sun orientation system is provided to align the spin axis normal to the Sun line. A sun sensor with a fan shaped field of view, and control logic are used to activate impulsive torquers for control during this mode. When a null is achieved with the Sun line, the system is put in a roll precession, i.e., the spacecraft rolls about the Sun line. Eventually the fan shaped field of view Earth sensor indicates null, and roll precession is stopped on ground command. The boresight star tracker is then oriented so as to acquire Polaris and provide a yaw-roll attitude reference.

2) Earth Tracking Mode. This phase of the mission is accomplished by means of a Polaris boresight tracker, and an Earth sensor with a fan shaped field of view is used to provide a synchronization pulse signal. The pulse signal provides the trigger for firing the impulsive torquers.

An error amplitude discriminator is indicated in Figure 2-19 on the Polaris tracker error signal. The purpose of this is to provide a dead zone so that control action is initiated only when the error signal exceeds a specified magnitude. This level would be set at about 1° so that no corrective action is taken in response to sinusoidal external disturbance torques.

A rate discriminator is indicated in the block diagram; this provides for an allowable spin rate deviation range.

4. Control and Stabilization Performance Summary

Table 2-5 summarizes the estimated performance characteristics that could be expected from some of the types of control techniques considered.

TABLE 2-5

CONTROL AND STABILIZATION PERFORMANCE SUMMARY

Control System	Pointing Accuracy	Stabilization Rate	Acquisition Time	Comments
Discrete	0.5°	$3x10^{-3}$ deg/sec	13 hr (max)	Pointing accuracy and rate stabilization shown basically set by horizon sensor characteristics
Continuous			2 hr (min)	
Gyrocompass	0.5°	$3x10^{-3}$ deg/sec	13 hr (max) 2 hr (min)	
Spin	within 1° of Polaris	$5x10^{-5*}$deg/sec (spin vector control)	6.5 hr (max) 1 hr (min)	Pointing accuracy and rate stabilization determined by disturbance torques
Gravity Gradient	0.05°	$5x10^{-6}$ deg/sec	12 hr (max) 1.5 hr (min)	

* This figure applies to the control of the vehicle spin vector precession rate. Stabilization rates pertinent to the meteorological sensors are determined by the effectiveness of the image motion compensation techniques that must be employed for high resolution sensor data.

E. EARTH TRACKING -- DYNAMIC ANALYSIS AND SIMULATION

1. Discrete-Continuous Controller

a. Introduction

The use of a 3-axis, reaction-wheel, cold-gas system is one possible technique which may be utilized to control the SMS space vehicle during all modes of its operation. The initial spin-down and Earth acquisition modes would be accomplished by the gas system, where comparatively high-level, impulsive-type control torques are to be applied to the vehicle. The transition from acquisition to Earth track and the Earth tracking would be accommodated by the 3-axis reaction wheel system, where low-level, low-frequency control torques would have to be generated.

Figure 2-20 shows a simplified analytical representation of the closed control loop for any axis of a reaction wheel system. The basic loop operation is as follows. A disturbance T_D is applied to the vehicle, causing motion of the axis about the center of mass. This motion is sensed by an angle-sensing device (horizon scanner, yaw sensor, etc.) whose output compared to a reference yields the attitude error, ϵ_θ. The sensor output is shaped by a compensation network, and the output signals applied to a reaction wheel. The magnitude of the couple produced is dependent upon the error signal, and its direction is such that it tends to oppose the original disturbance and thus decrease the error. In order for a torque to be produced, the reaction wheel must accelerate, and if the reaction torque applied is to be a constant in one direction, the reaction wheel will, after some time, approach its saturation speed. The process of dumping the wheel angular momentum and thus reducing its speed is, effectively, to produce a controlled constant disturbance torque which is larger in magnitude and opposite in direction to the disturbance torque. This will create a deceleration of the wheel and reduce its speed to the desired level. The dump logic and torque magnitude required for dumping will be discussed subsequently.

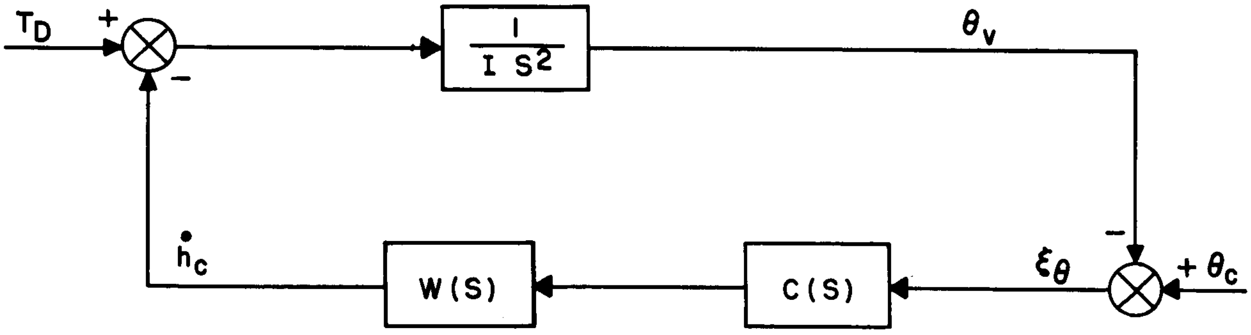

Figure 2-20. Block Diagram - Single Axis Reaction Wheel System

b. Analysis

1) Single Axis. As a preliminary approximation, each axis is treated independently, i.e., coupling terms are neglected. This simplified analysis allows a study of the effects of motor characteristics, loop gain, and compensation on system stability and performance. Control loops with parameter values obtained from these studies are then used as a starting point for more complex studies.

a) Motor Characteristics. The torque developed and the load torque of a two-phase servo motor, when a control phase voltage is applied, may be expressed by:

$$T_M \approx -K_M \dot{\delta} + K_E E_c \qquad (2\text{-}1)$$

$$T_L \approx J_M \ddot{\delta}$$

where T_M = torque developed

T_L = load torque

$\dot{\delta}$ = motor shaft angular velocity

$\ddot{\delta}$ = motor shaft acceleration

K_M = linearized slope of torque-angular velocity curve

K_E = linearized slope of torque-voltage curve

E_c = control voltage

J_M = equivalent polar moment of inertia of motor shaft and reaction wheel

Equation (2-1) for motor and load torque yields, in Laplace transform notation

$$\ddot{\delta}(S) = \frac{K_E}{J_M} \frac{S}{S + K_M/J_M} E_c(S) \qquad (2\text{-}2)$$

The control torque and momentum are given by

$$\dot{h}_c(S) = \frac{K_E S}{S + K_M/J_M} E_c(S) \qquad (2\text{-}3)$$

$$h(S) = \frac{K_E S}{S + K_M/J_M} E_c(S)$$

In preliminary studies of the SMS (Ref 2-1), motor characteristics were chosen such that

K_M = 9×10^{-4} in-lb/rad/sec

K_E = 9.5×10^{-3} in-lb/volt

J_M = 0.08 in-lb-sec^2

Typical servomotor curves are shown in Figure 2-21. However, it has been found that variation of the resistance of the rotor in the servomotor will effectively change the torque-angular velocity curves to the point where K_M is approximately zero over over a large portion of the curves. This change would effectively eliminate the differentiation and the lag in the servomotor transfer function and cause the motor to act as a pure-gain K_E with regard to torque to input voltage. Hence, design changes were made such that the motor curve would resemble those of Figure 2-22 with parameters:

$K_M = 0$

$K_E = 9.5 \times 10^{-3}$ in-lb/V

$J_M = 0.08$ in-lb-sec^2

The control torque and momentum are then expressed by

$$\dot{h}_c(S) = K_E \, E_c(S)$$
$$h_c(S) = \frac{K_E}{S} \, E_c(S) \qquad (2\text{-}4)$$

The advantages of the new design will be seen in the following sections.

b) Stability. Referring to Figure 2-20 for a pure motor gain, if no compensation is used, the system is seen to be oscillatory for all input disturbances; i.e., it is neutrally stable.

The use of the chosen form of loop compensation is a lead-lag network. This network will introduce a decaying exponential into the system for all inputs, but is quite adequate to produce a stable configuration. From Figure 2-20

$$\frac{\theta}{T_D}(S) = \frac{1/I\,S^2}{1 + \dfrac{K_A\,C(S)\,W(S)}{I\,S^2}} \qquad (2\text{-}5)$$

where $C(S) = (T_1 S + 1)/(T_2 S + 1)$

$W(S) = K_E$

then

$$\frac{\theta}{T_D}(S) = \frac{T_2 S + 1}{(I T_2)\,S^3 + (I)\,S^2 + (T_1 K_A K_E)S + K_A K_E} \qquad (2\text{-}6)$$

The disturbance torque model has been approximated as

$$T_D = 10^{-4} + 10^{-4} \sin \omega_o t \text{ (in.-lb)}$$

Application of the final value theorem to Eq. 2-6 with T_D conservatively taken as a step function of 2×10^{-4} in.-lb magnitude yields

$$\theta_F = \frac{2 \times 10^{-4}}{K_A K_E} \qquad (2-7)$$

Choosing a nominal gain of $K_A = 10^3$ volts/rad

$$\theta_F = 2.1 \times 10^{-5} \text{ rad}$$

which is felt to be an adequately small value.

It is seen that the angle error for the torque model will consist of a constant plus a sinusoid for the pure-gain motor; for the originally designed motor, the hangoff would have consisted of a sinusoid plus a linearly increasing angle with time.

Choice of lead-lag parameters was made through use of Bode-attenuation and phase-margin diagrams as shown in Figure 2-23. The lead and lag parameters were chosen to be

$$T_1 = 40 \text{ sec}$$

$$T_2 = 1 \text{ sec}$$

in order to ensure an adequate phase margin of about 35° at the open loop crossover point.

c) Dump Interval. For wheel sizing, the dump interval was chosen to be once per orbit. The total momentum stored in a wheel per orbit is

$$h_{max} = (10^{-4}) \text{ in.-lb } (8.6 \times 10^4) \qquad (2-8)$$

$$h_{max} = 8.64 \text{ in.-lb sec}$$

It is seen that the total momentum of the wheel is given by

$$h_{max} = J_M \omega_n = (0.08) \omega_n = 8.64 \qquad (2-9)$$

where ω_{ny} = wheel angular velocity in rad/sec

Thus, ω_n = 108 rad/sec as is shown in Figure 2-22.

The actual magnitude of the dump torque to produce a minimum expenditure will be treated in the following section where analog computer results are treated. However, when initial acquisition is treated, results show that a dump level of 0.25 in.-lb is advantageous.

d) Horizon Scanner Dead Zone. The Earth tracking mode will utilize horizon scanners which have dead zone characteristics as shown in Figure 2-24.

A describing function analysis is next conducted to ascertain the effect of horizon scanner dead zone on loop performance. From Figure 2-24(a), the characteristic of the horizon scanner dead zone may be described by a Fourier series

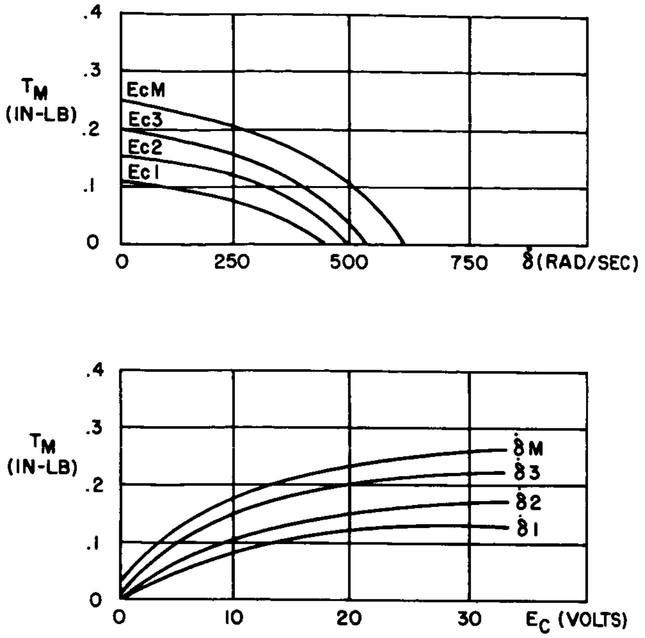

Figure 2-21. Typical Servo Type Reaction Wheel Characteristics

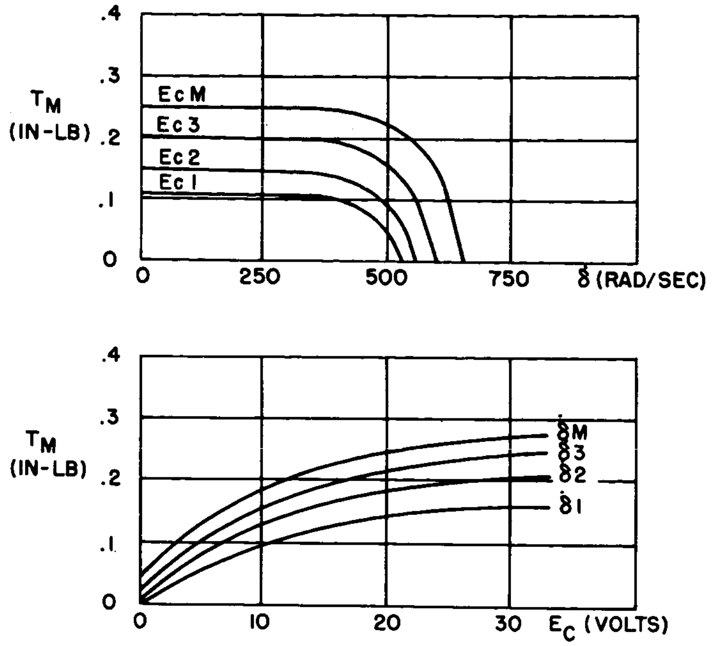

Figure 2-22. Typical "Flat" Reaction Wheel Characteristics

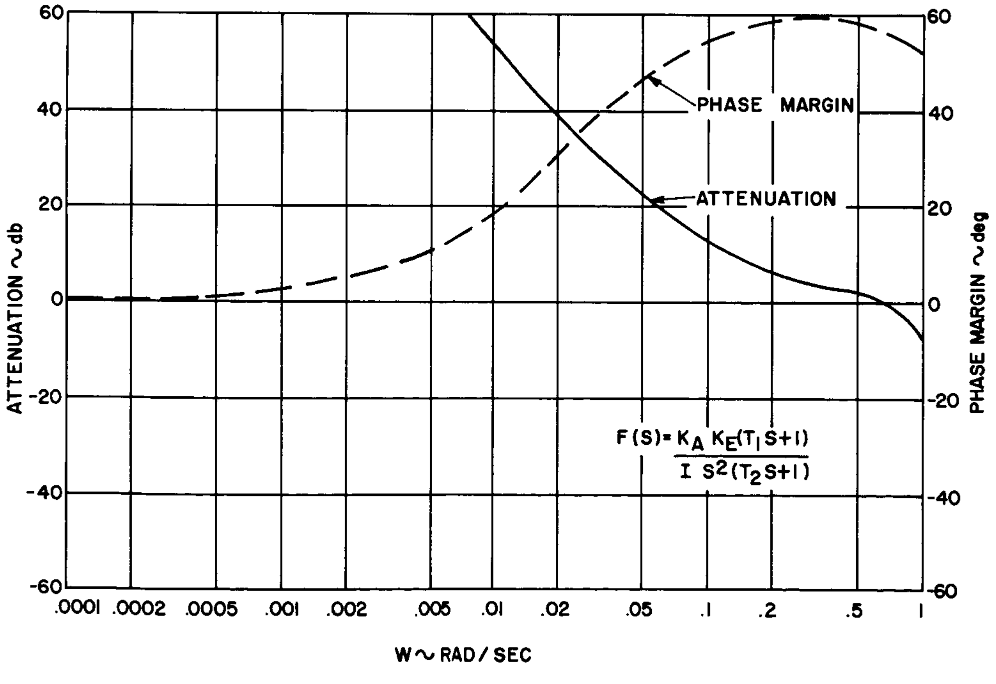

Figure 2-23. Attenuation and Phase Margin Diagram

$$\theta_{e_L} = \sum_{n=-\infty}^{\infty} C_n(\theta_e) e^{i\omega nt} \tag{2-10}$$

The describing function $N(\omega)$ is defined as the ratio of the amplitude of the output fundamental frequency to the amplitude of the input

$$N(\omega) = \frac{\theta_{o_L}}{\theta_o}(\omega) \tag{2-11}$$

Plots of various functions of $N(\omega)$ versus θ_o and ω are shown in Figure 2-25.

The characteristic equation of the system of Figure 2-24(a) is of the form

$$\frac{\theta}{T_D}(S) = \frac{1/IS^2}{1 + \left[\frac{K_A K_E (T_1 S+1)}{IS^2 (T_2 S+1)}\right]\left[N(S)\right]} \tag{2-12}$$

System stability is determined by

$$\frac{1}{N(S)} = -\frac{K_A K_E (T_1 S+1)}{IS^2 (T_2 S+1)}$$

A Nichols chart is presented in Figure 2-26 to illustrate the determination of the frequency and amplitude of possible limit cycles. It is seen that the output of the horizon scanner will be constant and of amplitude $(\Delta/2)$, and no limit cycle will exist. Analog computer runs were made to bear out these results, and are discussed in the following sections.

2) Coupled System. The total 3-axis moment equations have been derived and are shown in Appendix A, and have been simulated on an analog computer using small angle approximations. For a simplified theoretical analysis, it may be assumed that the pitch axis is essentially uncoupled from yaw and roll, since pitch coupling terms have a negligible effect except for the orbital angular velocity term (ω_o). The resulting moment equations may be expressed in linear form by

$$\begin{aligned} D_x &= I_{xx}\ddot{\phi} + \dot{h}_{c_x} - h_{c_y}\omega_o\phi - h_{c_x}\dot{\psi} - \omega_o h_{c_z} \\ D_y &= I_{yy}\ddot{\theta} + \dot{h}_{c_y} \\ D_z &= I_{zz}\ddot{\psi} + \dot{h}_{c_z} - h_{c_y}\omega_o\psi + h_{c_y}\dot{\phi} + \omega_o h_{c_x} \end{aligned} \tag{2-13}$$

It is seen that Eqs 2-13 represent a yaw-roll coupled system which may be expressed in terms of the system parameters as shown in Figure 2-27.

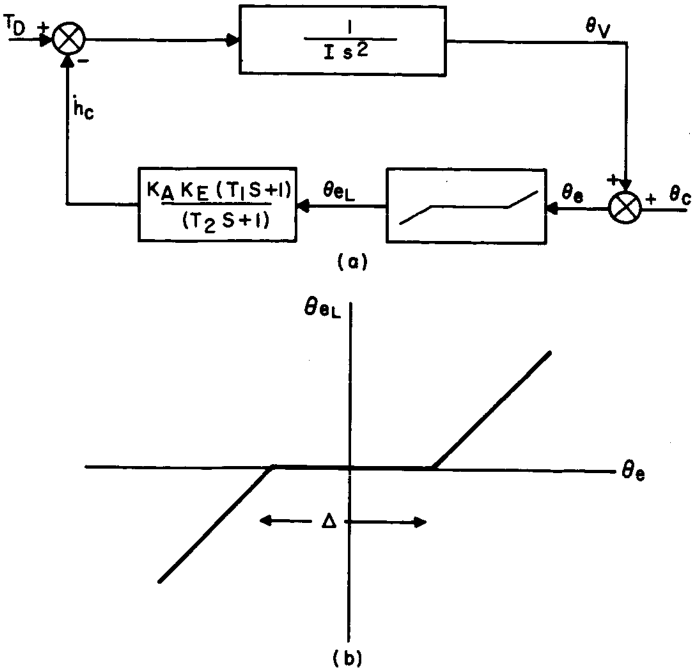
T_D
+
-
$\frac{1}{I s^2}$
θ_V
h_c
$\frac{K_A K_E (T_1 S+1)}{(T_2 S+1)}$
θ_{eL}
θ_e
+
+ θ_c
(a)
θ_{eL}
θ_e
Δ
(b)

Figure 2-24. Horizon Scanner Dead Zone Characteristic

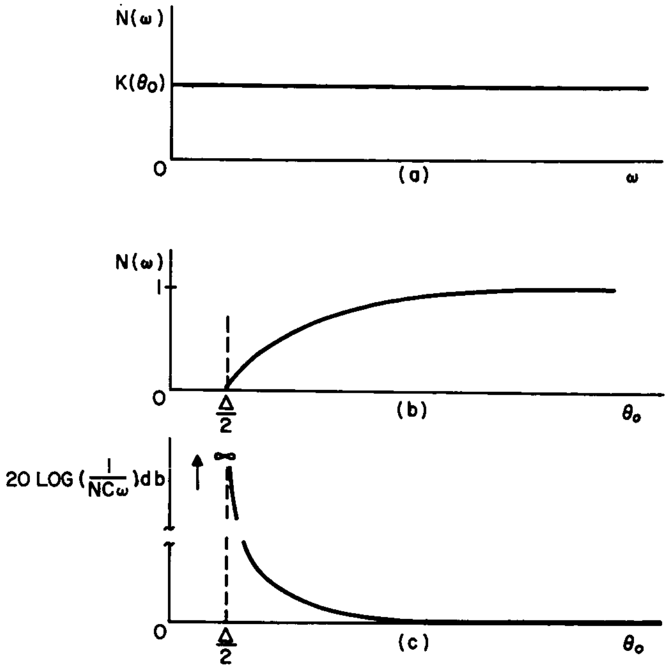

Figure 2-25. Describing Function for Horizon Scanner Dead Zone

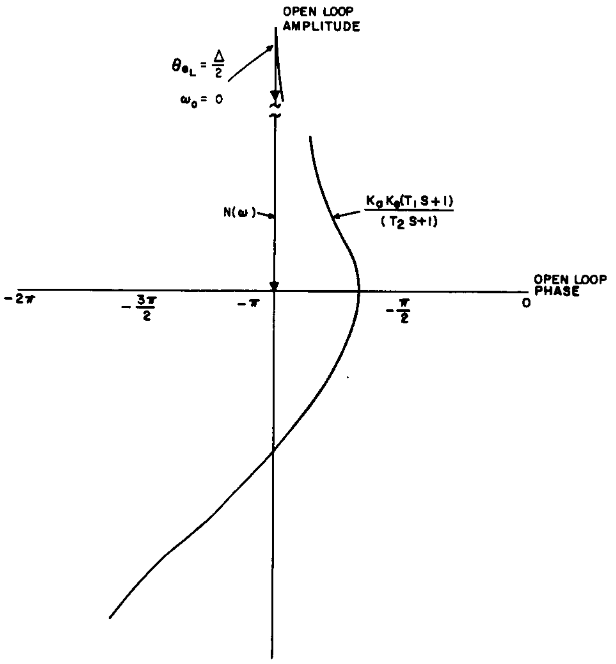

Figure 2-26. Nichols Plot of Horizon Scanner Describing Functions

The expressions relating attitude angle to disturbance torque are given by

$$\frac{\phi}{D_X}(S) = \frac{S^2\,(T_2 S + 1)}{(S^2 + \omega_o^2)\left[(I_{xx}\,T_2)\,S^3 + (I_{xx})\,S^2 + (K_A\,K_E\,T_1)\,S + K_A\,K_E\right]}$$

$$\frac{\theta}{D_Y}(S) = \frac{(T_2\,S + 1)}{(I_{yy}\,T_2)\,S^3 + (I_{yy})\,S^2 + (K_A\,K_E\,T_1)\,S + K_A\,K_E} \qquad (2\text{-}14)$$

$$\frac{\psi}{D_Z}(S) = \frac{S^2\,(T_2\,S + 1)}{(S^2 + \omega_o^2)\left[(I_{zz}\,T_2)\,S^3 + (I_{zz})\,S^2 + (K_A\,K_E\,T_1)\,S + K_A\,K_E\right]}$$

It is seen that the system is still essentially an uncoupled system and may be treated as the sum of three independent axes with a sinusoidal term present in yaw and roll. This system is neutrally stable in that an impulsive torque will produce a sustained oscillation in both the roll and yaw angles. When excited at orbital frequency, the roll and yaw angles will be of the form

$$\phi\,(t) = K \sin \omega_o t + K' \,t \cos \omega_o t$$

$$\psi\,(t) = K \sin \omega_o t + K' t \cos \omega_o t \qquad (2\text{-}15)$$

These angles tend to increase with time and therefore act as an unstable system when excited at orbital frequency. This effect had been noticed in Ref. 2-1.

A more detailed roll-yaw coupled analysis has been conducted to verify that this instability will be present when other cross coupling terms of large magnitude are included in the system dynamics. Plots of roll and yaw angles and reaction wheel angular momenta are shown in Figures 2-28 and 2-29 and will be correlated with the results of the three-axis analog computer study in the following section.

Inspection of Figure 2-27 and the dynamic equations shows that the oscillatory term in the system characteristic equations is the result of orbital rate feedback terms in yaw and roll. Since this problem arises because the vehicle has a constant angular velocity with respect to inertial space, a compensation may be effected by use of a computer which would negate the orbital coupling terms. Figure 2-30 illustrates a system of this form. However the orbital rate and the reaction wheel momenta must be exact for the system to be stable when excited at orbital frequency. However, if such a computer is used, vehicle attitude stability is achieved at the expense of divergent wheel momenta. The problem of errors in orbital rate and momenta causing instability are possible areas for future detailed study.

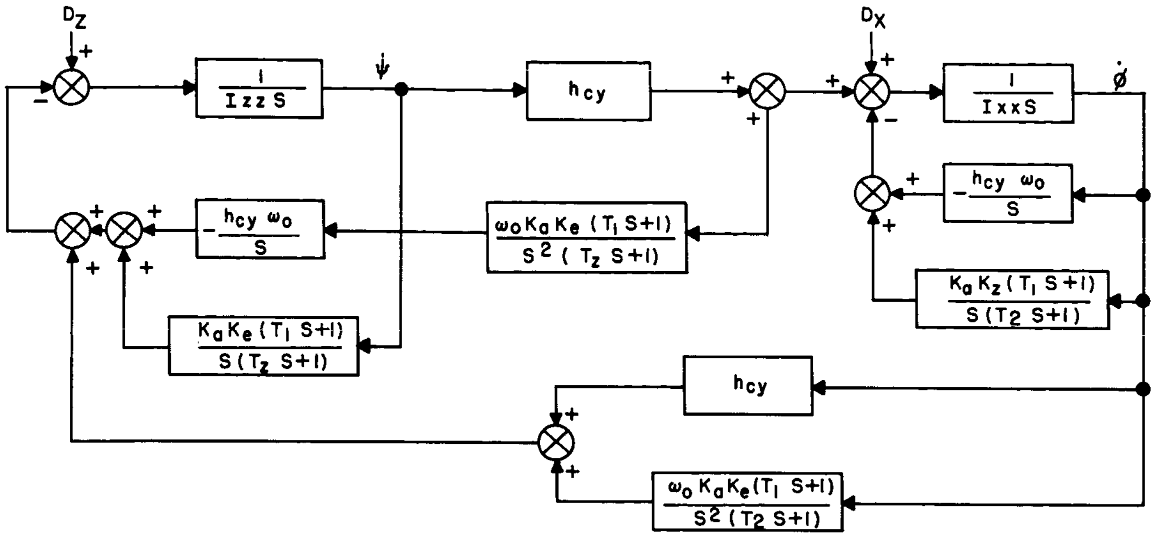
D_Z
$\dot{\psi}$
D_X
$\dot{\phi}$
$\frac{1}{I_{zz}S}$
h_{cy}
$\frac{1}{I_{xx}S}$
$-\frac{h_{cy}\,\omega_o}{S}$
$\frac{\omega_o K_a K_e (T_1 S+1)}{S^2 (T_z S+1)}$
$-\frac{h_{cy}\,\omega_o}{S}$
$\frac{K_a K_z (T_1 S+1)}{S (T_2 S+1)}$
$\frac{K_a K_e (T_1 S+1)}{S (T_z S+1)}$
h_{cy}
$\frac{\omega_o K_a K_e (T_1 S+1)}{S^2 (T_2 S+1)}$
+
−

Figure 2-27. Block Diagram-Coupled Yaw-Roll System

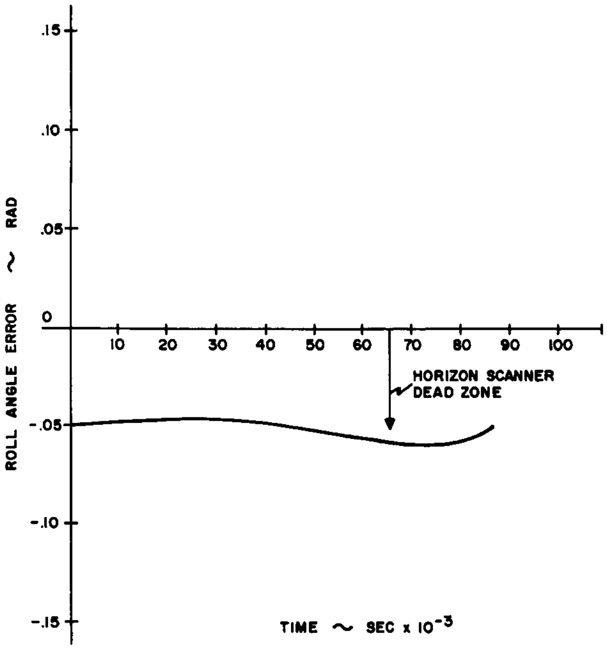

Figure 2-28. Roll Angle Time History

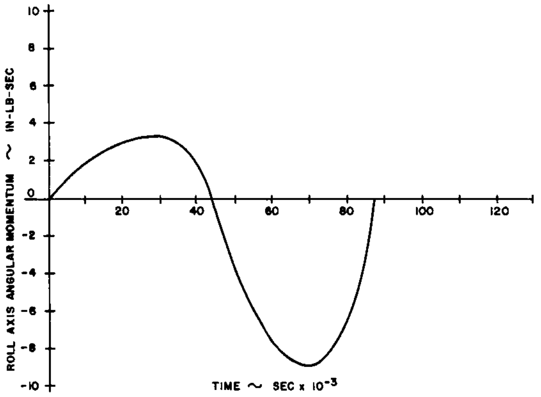

Figure 2-29. Calculated Roll Reaction Wheel Momentum Time History

c. Analog Computer Simulation

The 3-axis coupled dynamics system expressed by the equations of Appendix A were simulated on an analog computer. Preliminary runs were made of a simplified single-axis vehicle to determine system parameters with regard to stability and to note the effect of varying dumping levels and horizon scanner dead zones.

Figure 2-31 is a single axis run for various dumping levels. In Figures 2-32 to 2-35 are plotted various parameters versus dump level. It is seen that the optimum dump level is 0.175 in.-lb since reaction motor torque saturation occurs at all higher dumping levels.

Figures 2-36 and 2-37 are runs of the single-axis system showing dumping time and angle error for various values of horizon scanner dead zones. Figure 2-38 is a plot of vehicle angle hangoff versus horizon scanner dead zone. It is seen that the vehicle hangoff is linear with respect to dead zone. It is also evident from Figures 2-36 and 2-37 that the angle hangoff is always at one end of the dead zone. This result is in agreement with the results of the describing function analysis of the preceding section.

The 3-axis coupled runs presented in Figures 2-39 and 2-40 show system response to both constant and sinusoidal torques of orbital frequency.

From the simplified Eqs 2-14, the angular response for a constant unit disturbance is of the form

$$(S) = \frac{S^2 (T_2 S + 1)}{S (S^2 + \omega_o^2) (S + \gamma) ((S + \alpha)^2 + \beta^2)} \qquad (2\text{-}16)$$

where α, β, and γ are various combinations of the system parameters.

The system oscillation induced by the undamped term in the characteristic equation is of the form

$$\phi (t) = \frac{D_o T_2}{\omega_o I_{xx}} \sqrt{\frac{\omega_o^2 (1 + \omega_o^2)}{(\gamma^2 + \omega_o^2) (\alpha^2 + \beta^2 - \omega_o^2)^2}} \qquad (2\text{-}17)$$

For the system parameters used in this study

$$\phi (t) = 5.18 \times 10^{-5} \sin (\omega_o t + \phi_o) \text{ (rad.)} \qquad (2\text{-}18)$$

Similarly, the oscillation of the stored momentum may be calculated from

$$\frac{h_{c_x}}{D_x} (S) = \frac{1}{S} \left[\frac{K_A K_E (T_1 S + 1)}{(T_2 S + 1)} \right] \left[\frac{\phi}{D_x} (S) \right] \qquad (2\text{-}19)$$

then $h_{1_{c_x}} (t) = 4.92 \times 10^{-4} \sin (\omega_o t + \lambda_o)$ (in.-lb-sec.) (2-20)

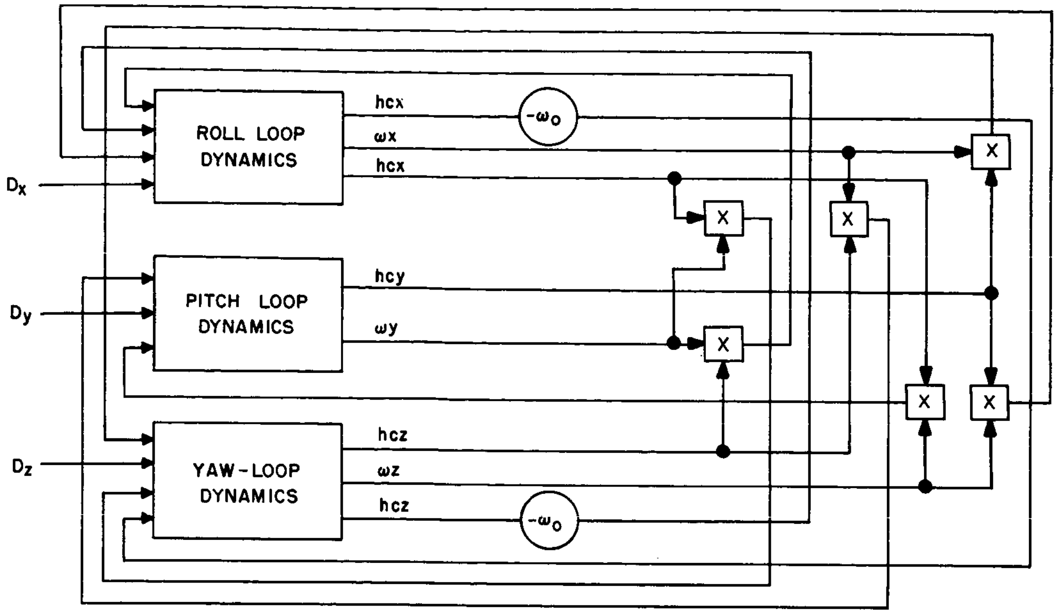

ROLL LOOP DYNAMICS
PITCH LOOP DYNAMICS
YAW-LOOP DYNAMICS
D_x
D_y
D_z
hcx
ωx
hcx
$-\omega_o$
hcy
ωy
hcz
ωz
hcz
$-\omega_o$
X
X
X
X
X
X

Figure 2-30. Block Diagram of Yaw-Roll Axes with Decoupling Computer

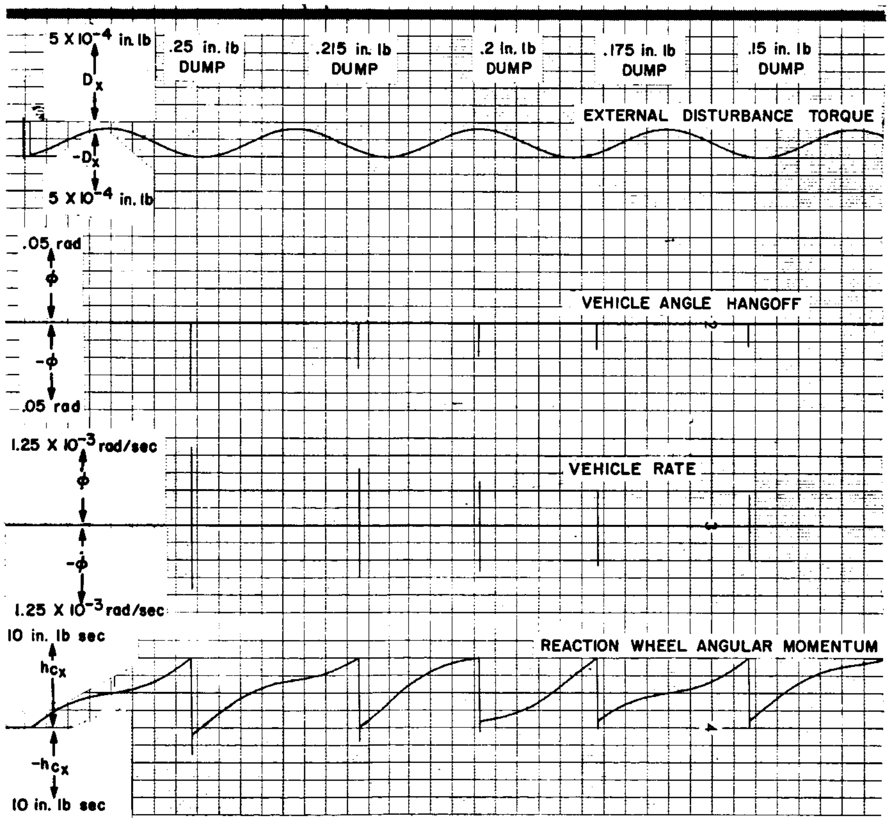

Figure 2-31. Computer Run of Vehicle Roll Attitude and Rate for Various Dumping Torque Levels

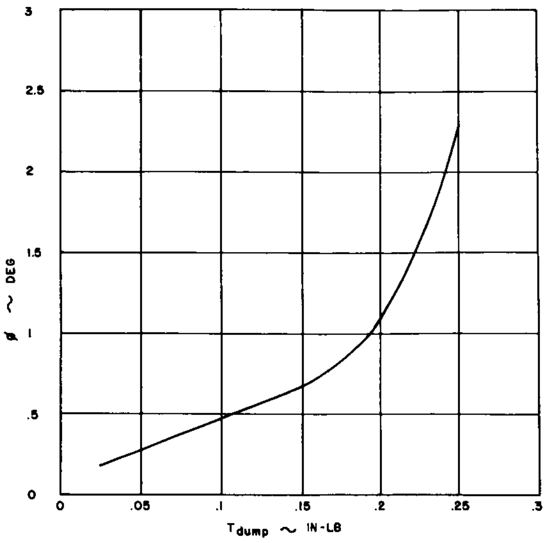

Figure 2-32. Peak Roll Attitude Excursion During Dump Interval as a Function of Dump Torque Magnitude

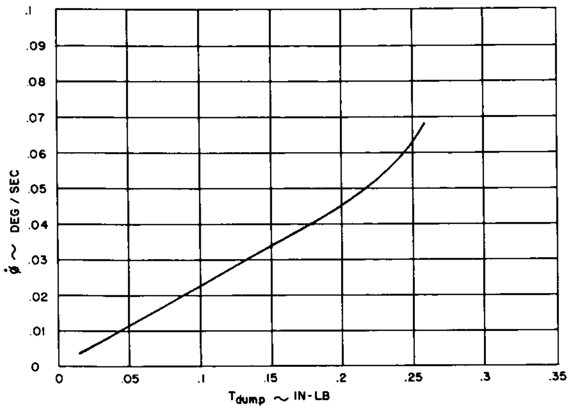

Figure 2-33. Peak Roll Rate During Dump Interval as a Function of Dump Torque Magnitude

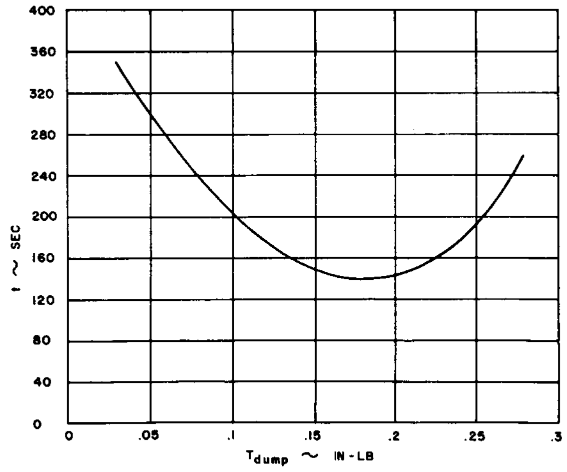

Figure 2-34. Plot of Dump Time for Various Dump Torque Levels

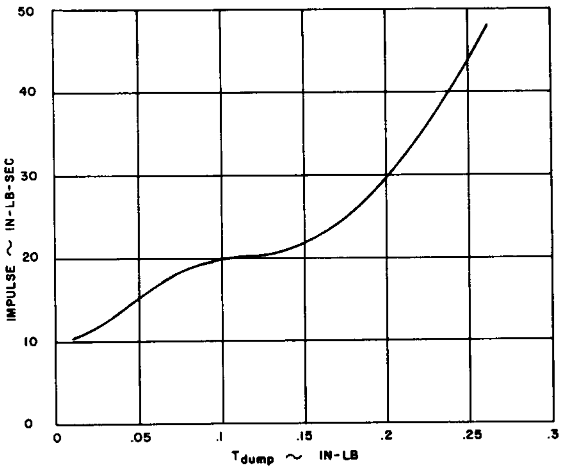

Figure 2-35. Impulse Necessary to Dump at Various Torque Levels

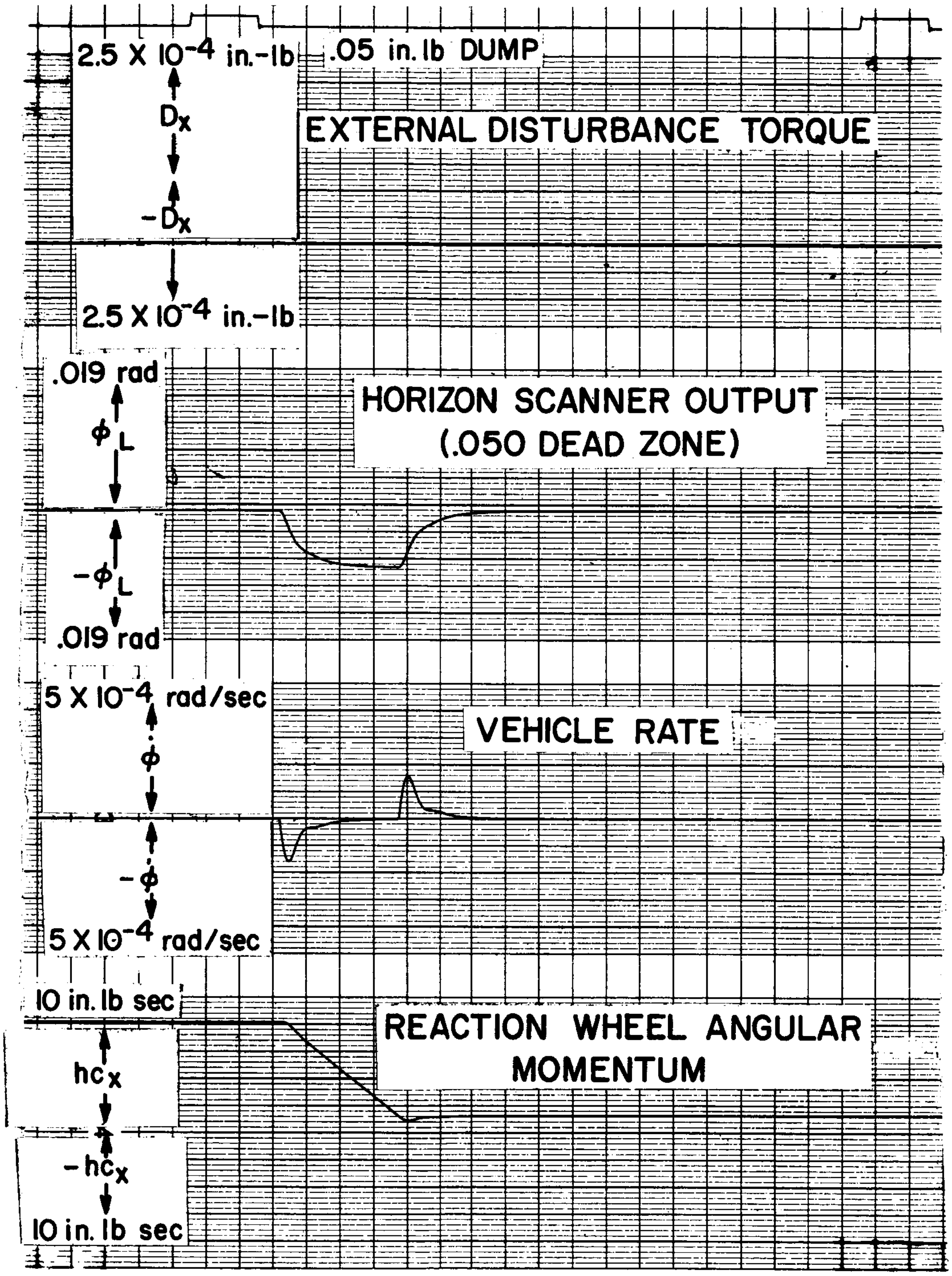

Figure 2-36. Computer Run of Vehicle Attitude and Dump Time for a Horizon Scanner Dead Zone of 0.05°

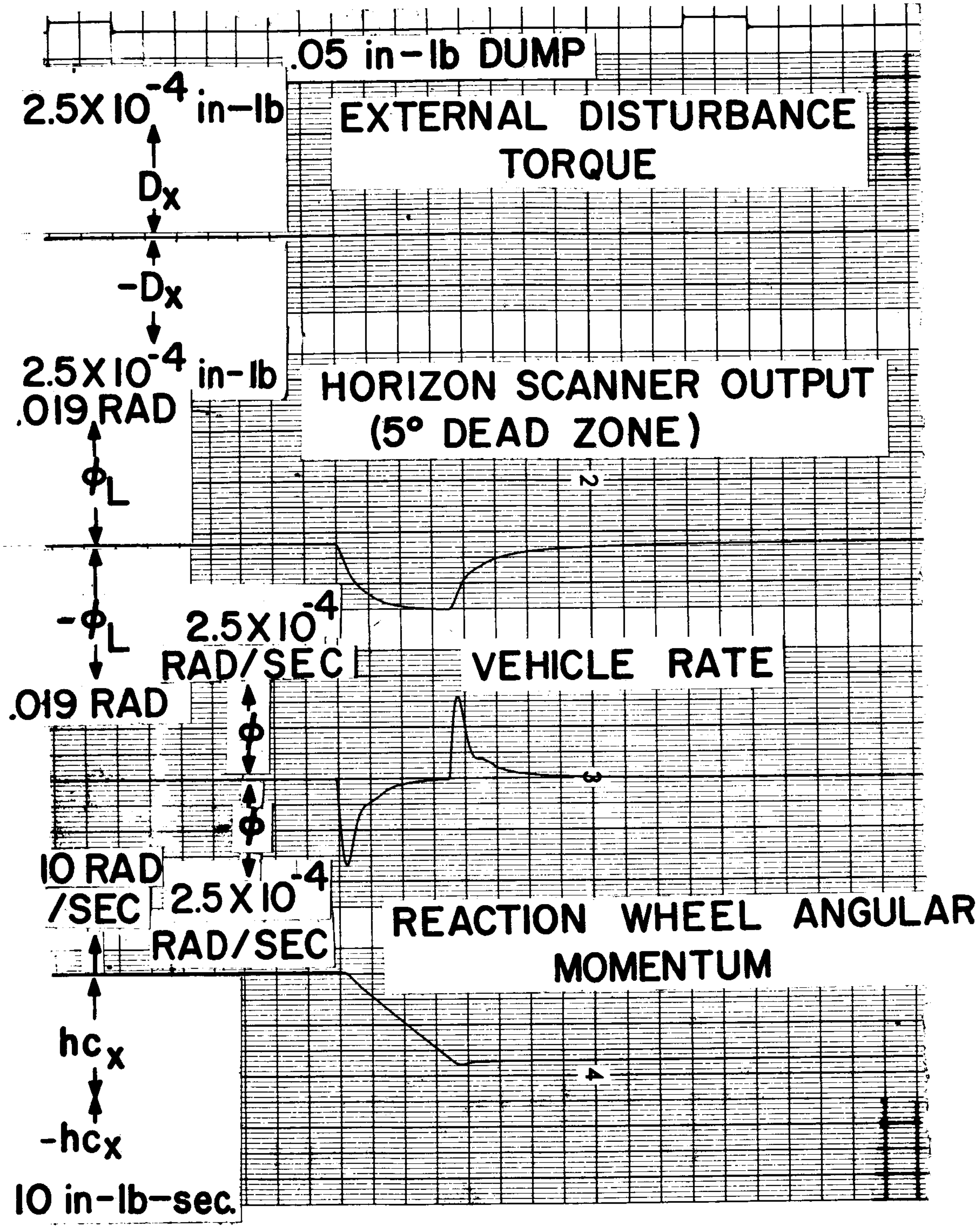

Figure 2-37. Computer Run of Vehicle Attitude and Dump Time for a Horizon Scanner Dead Zone of 0.5°

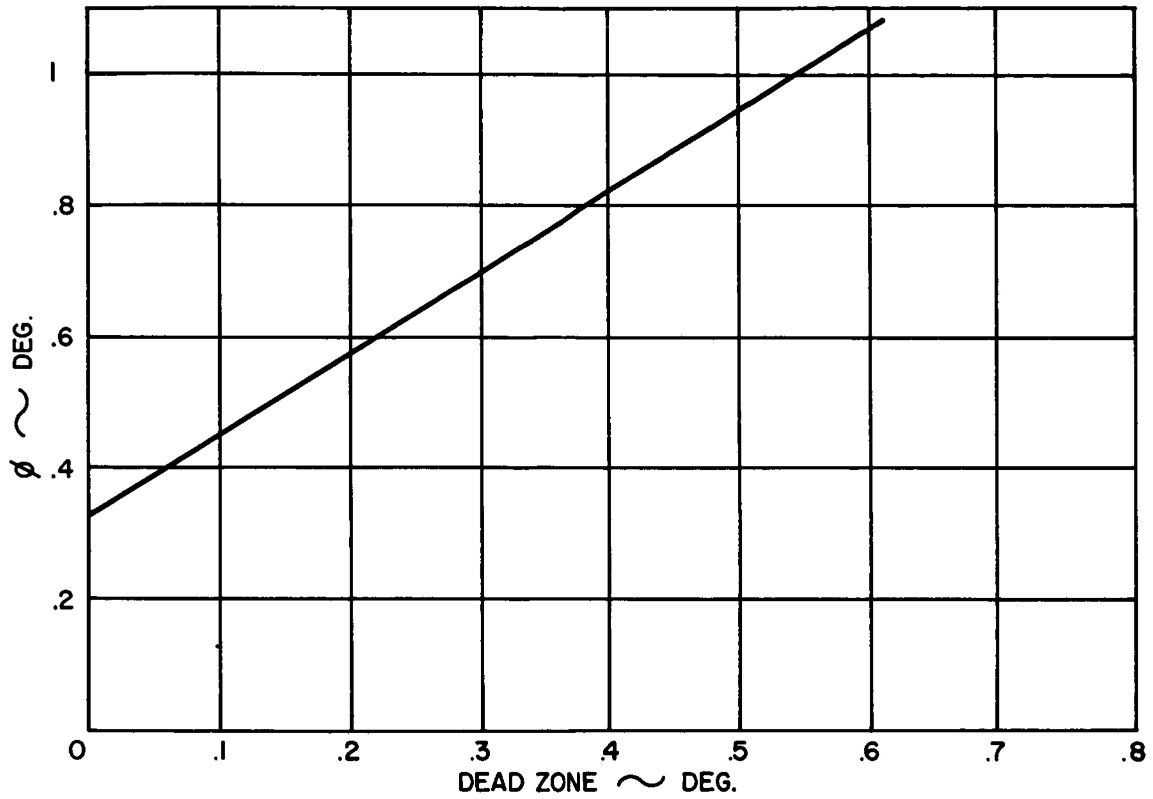

Figure 2-38. Plot of Vehicle Attitude Error Angle vs Horizon Scanner Dead Zone

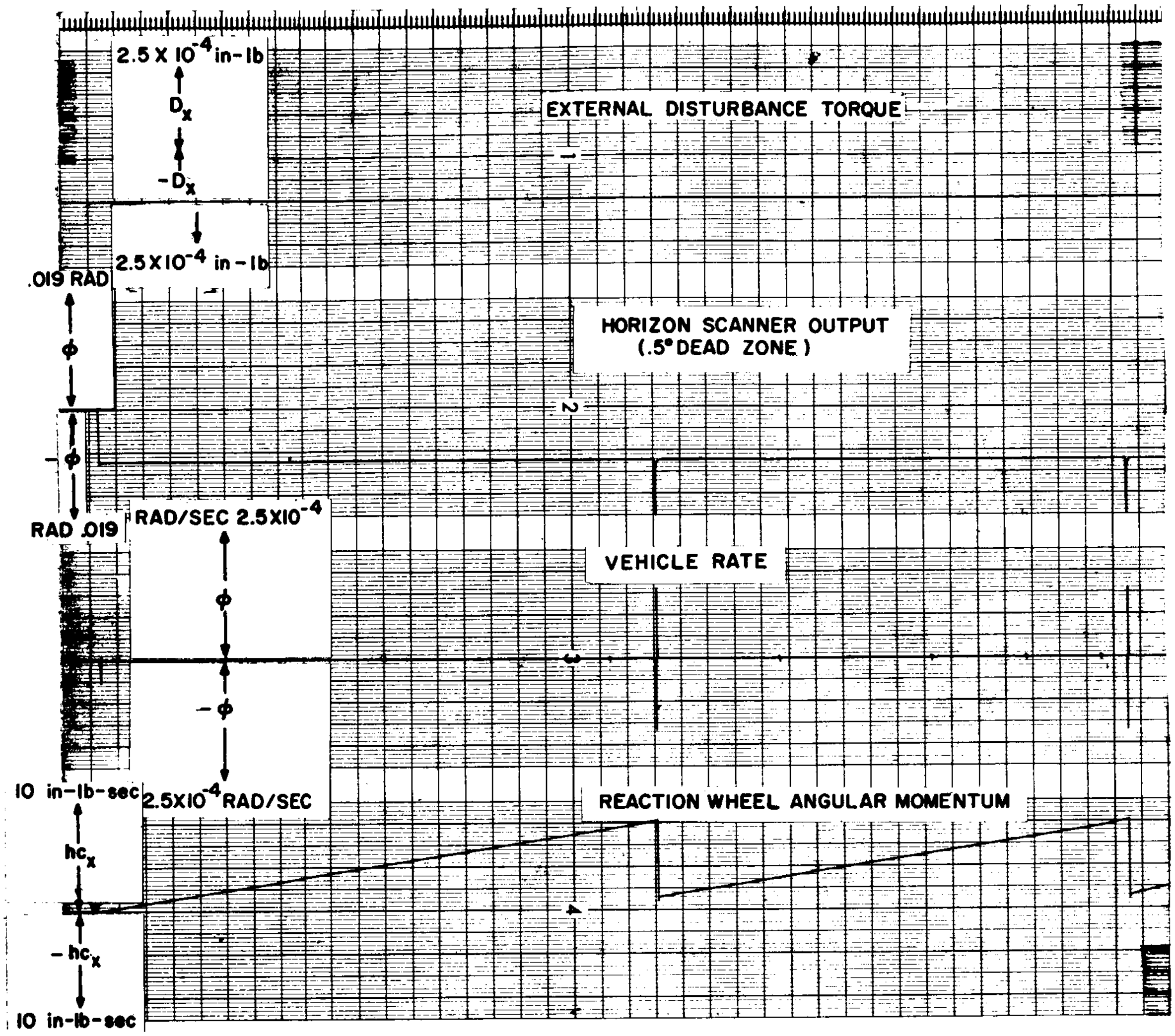

Figure 2-39. Computer Run of 3-axis Coupled System Response to a Steady Disturbance Torque

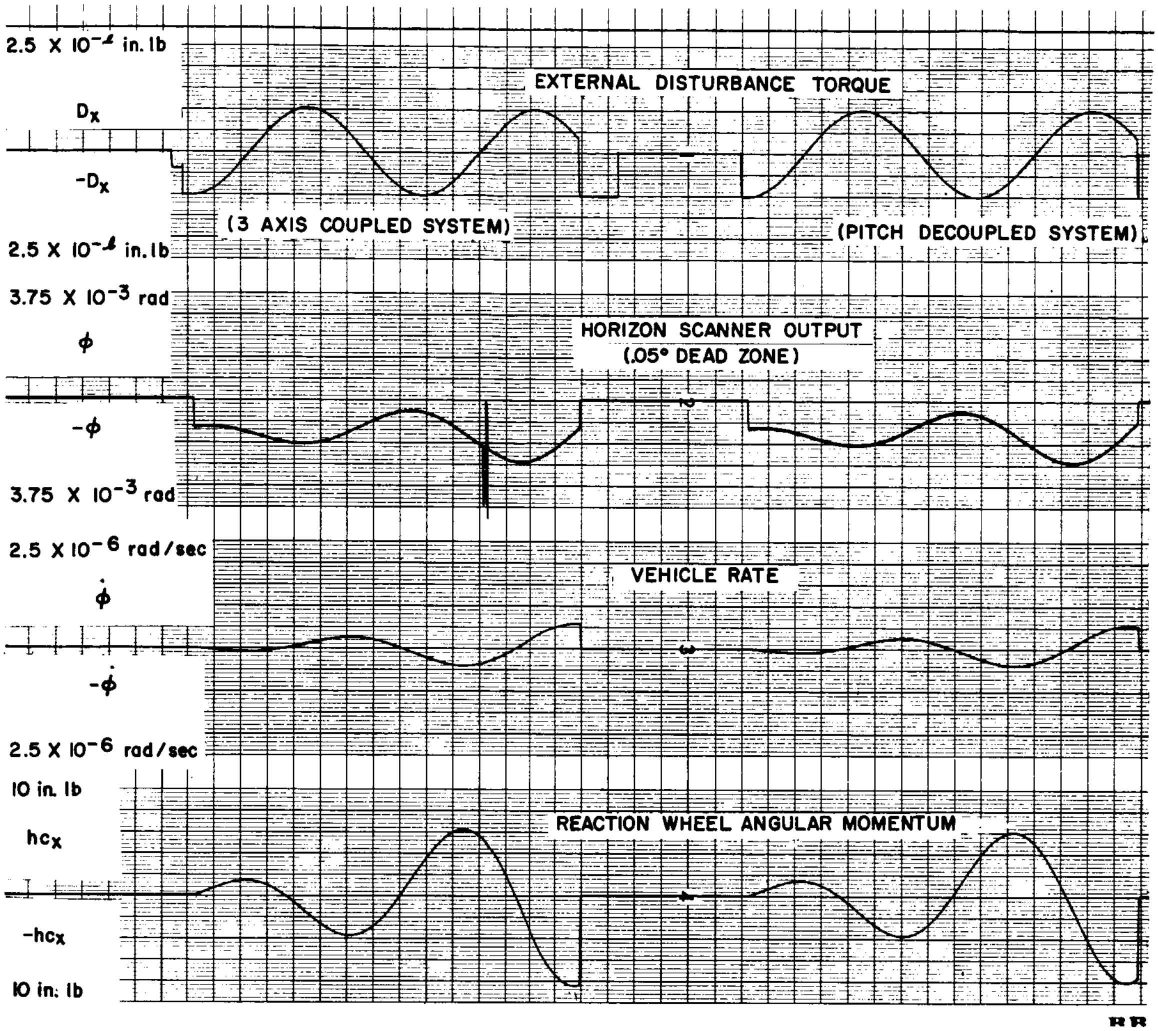

Figure 2-40. Computer Run of Yaw-Roll Coupled System Subjected to Sinusoidal Disturbance at Orbital Frequency

It is seen that these results indicate negligible magnitudes compared to the magnitude of the dead zone and the total wheel momentum and cannot be seen on the scales used for the run of Figure 2-39.

Figure 2-40 shows a run for which the system instability is induced by excitation of the system by a sinusoid of orbital frequency. The computer run is similar to Figures 2-28 and 2-29 except for the fact that it leads the calculated time histories by a particular phase angle. This is explained by the additional dynamic term which existed in the computer simulation. However, it is seen that the magnitudes of the calculated and the simulated system parameters are of the same order of magnitude.

Figure 2-41 is a run of the system with the orbital rate term removed. It is seen that the system acts as though it was composed of three independent loops. However, it may be again stated that a perfectly compensated system is physically unrealizable, and the 3-axis coupled system will eventually diverge up to the dump level.

2. Gyrocompass Yaw Control System

a. Introduction

This subsection presents the results of studies of an attitude control concept which uses a passive gyrocompass technique for yaw control. Active control is provided for the pitch and roll axes. This concept and its implementation requirements are discussed below.

Methods of linear analysis have been complemented with analog computer studies to both investigate and demonstrate the stability and performance of the gyrocompass system. The effects of various coupling terms between the three controlled axes have been explored for the yaw alignment and tracking mode. Two types of control torquers were considered for study, namely, reaction wheels and proportional control devices. Sensor effects such as noise and dead zone are discussed in terms of their influence on system performance.

Primary advantages of this type of control are elimination of the need for a yaw attitude sensor, and achieving yaw damping by putting otherwise undesired yaw-roll coupling effects to good use. A factor which must be considered, however, is that it provides a relatively small restoring torque (directly related to the momentum provided by a constant speed wheel). Considered in this study is a 10-lb wheel which develops steady angular momentum of 150 in.-lb-sec. The available control torque is $10^{-2} \sin \psi$ (in.-lb), where ψ is the yaw error angle. For the SMS application where disturbance torques are quite low, the concept is quite attractive.

b. Discussion

1) The Gyrocompass Principle. The gyrocompass method is based on the gyroscopic characteristics demonstrated by a rotating mass. It is well known that if a torque is applied perpendicular to the spin vector of a rotating mass, the mass will develop a precession vector perpendicular to both the spin vector and the applied-torque vector. The converse situation is true

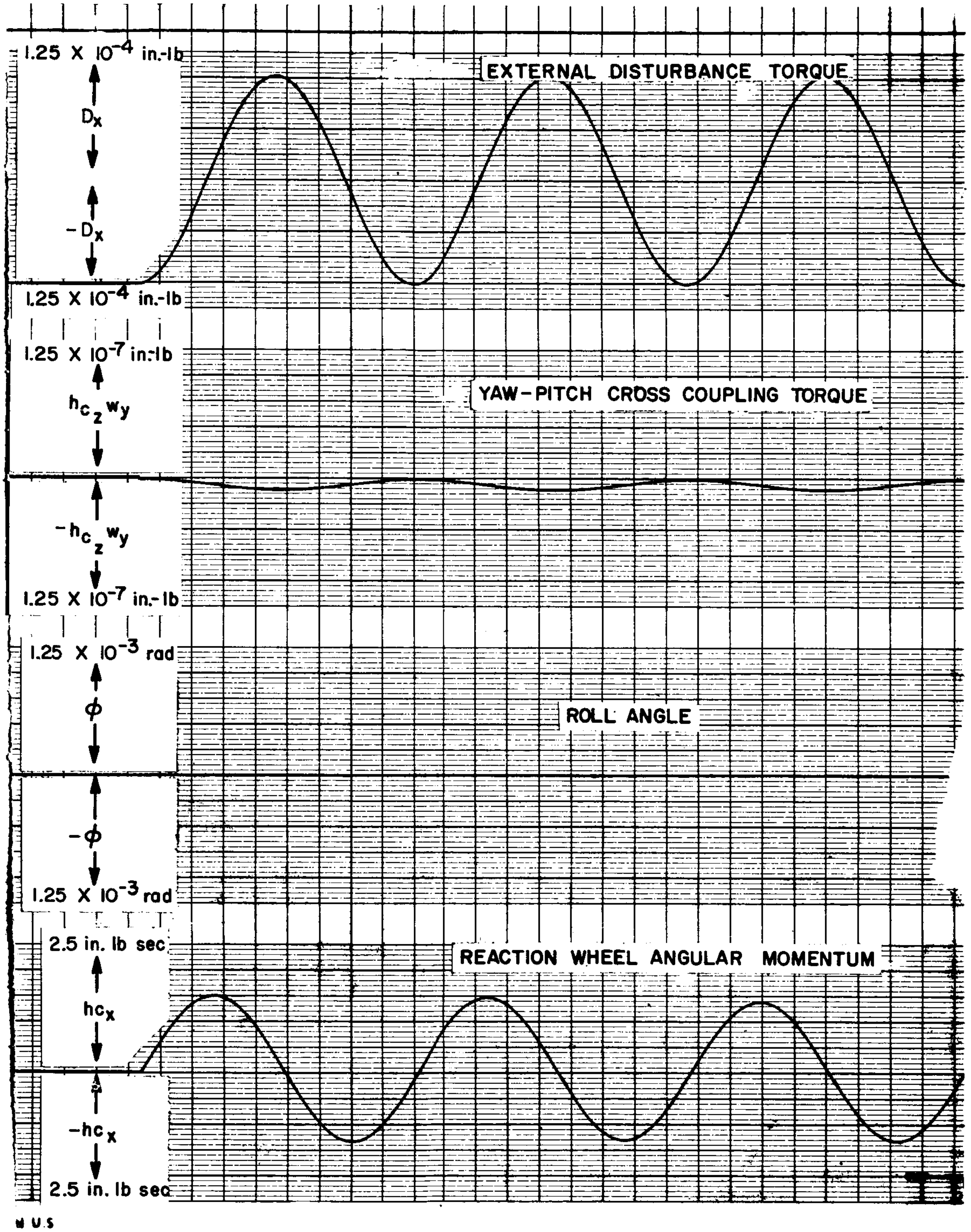

Figure 2-41. Computer Run of Yaw-Roll Coupled System Subjected to Sinusoidal Disturbance at Orbital Frequency (Orbital Rate Coupling Term (ω_0') Removed)

where the rotating element is rigidly supported by a constraining body; that is, the element is free to rotate about its spin axis but is permitted no other motion relative to the constraining body. If the constraining body has a rate of rotation with respect to inertial space, then the rotating element has a similar rate of rotation or precession. Because the rotating element is precessing, a torque is being applied to this element by the constraining body; and, hence, an equal and opposite reaction torque is applied to the constraining body by the rotating element.

A simple example of a gyrocompass is a single-axis, free gyro where the spin axis of the rotating element is mounted horizontally in a gimbal structure that is the constraining body. The gimbal is supported by frictionless pivot points so that it is free to move about a vertical axis. For clarity, the gyro is assumed to be placed on a horizontal table located at the Earth's equator.

The gimbal structure has a rotational rate, namely, the Earth's rotational rate. The interaction of the Earth's rotation and the angular momentum of the rotating element produces a reaction torque on the gyro gimbal. A sinusoidal motion of the gimbal structure will be noted. Because the gimbal bearings were assumed to be frictionless, the sinusoidal motion will be undamped, and the peak amplitude of the oscillation will be equal to the angle between the spin vector of the rotating element and true north at the time the gimbal is released. If the spin axis is initially aligned in a north-south direction, no motion will be observed. If it is initially in an east-west orientation, an undamped oscillation with a 90° peak amplitude will be observed.

To obtain an indication of north, the spin axis could be observed over one-half cycle and the angle of swing bisected. If damping were applied to the gimbal structure, the system would eventually stop oscillating, and the spin vector would point toward true north in the absence of external disturbing torques.

This, in essence, represents the gyrocompass concept that is under consideration for yaw control of the satellite.

2) Application of Gyrocompass to Yaw Control. The previous discussion of the gyrocompass principle will be adapted next to show how yaw control can be provided by this means. The attitude control system must align the body yaw axis (Z) along the geocentric vertical through the satellite mass center in the orbital plane. It also must align the roll axis (X) in the plane of the orbit. By maintaining vertical alignment of the Z axis by using active roll and pitch control systems, the satellite is given a rate of rotation about its pitch axis equal to the orbital rate. (That is, the satellite orientation in inertial space changes by 360° with each orbit.)

The satellite could be the constraining body, similar to the gyro gimbal in the simple illustration of the gyrocompass principle previously discussed. Thus, if a rotating element, such as a constant-speed wheel is rigidly mounted within the satellite, the situation is analogous to the single-axis free gyro. Because the satellite will orbit from west to east, the constant-speed wheel should be mounted so that its spin axis is directed along the negative pitch axis (in the same direction as the orbital angular velocity vector). Thus, when the vehicle is properly aligned in yaw, no gyroscopic torque is applied to the body yaw axis. If the vehicle is not aligned properly in yaw, a gyroscopic torque is applied to the vehicle in a direction to null the yaw error.

The vehicle, always rotating about its pitch axis (because the Z body axis is always directed toward the center of the Earth), contributes angular momentum about the negative pitch axis that would provide yaw restoring torque. However, the magnitude of this inherent vehicle angular momentum would not provide sufficient control torque to meet the stabilization requirements for the predicted disturbance torques.

Up to this point, the example of the satellite acting as a gyrocompass is still analogous to the single-axis, free gyro example, even to the extent that no damping exists about the yaw axis and that the amplitude of the resulting oscillation depends on the initial yaw error. Damping in yaw must be obtained to provide a stable platform for meteorological experiments and to properly orient thrust devices used for station keeping.

Addition of the constant speed pitch wheel strongly couples the yaw and roll modes through gyroscopic action. This yaw-roll coupling is desirable because damping in yaw is achieved if damping in roll is provided by using an active controller. Proper compensation must be provided in the roll system to achieve this damping.

With regard to the initial Earth acquisition and alignment mode, it is desirable to achieve yaw alignment as quickly as possible so that the solar paddles can be directed at the Sun for power generation. Hence, active yaw rate control is required for effective system damping during initial alignment. After the initial yaw alignment has been achieved, the auxiliary yaw rate control is not required.

The sequence of events to achieve yaw alignment, starting at the point where the roll and pitch systems have established a vertical alignment of the Z axis, is as follows:

(1) The pitch and roll systems have established a vertical alignment and the yaw rate has been nulled by spin-down control after injection into orbit by launch vehicle.

(2) The constant speed pitch wheel is accelerated to the desired speed; a maximum acceleration that does not disturb the pitch axis significantly is used.

(3) The vehicle is passively aligned in yaw; the estimated time requirement is approximately 1 hour for the worst possible initial misalignment (± 180°).

(4) The auxiliary yaw damper is deactivated when yaw alignment is completed.

c. Dynamic Analysis

1) General. For purposes of analysis, the basic equations, as developed in the Appendices, were simplified as shown below. The coupling between the yaw

and roll axis induced by the gyrocompass wheel was retained. The pitch axis was decoupled. An examination of the significance of various terms justified the validity of this approach (later supported by computer study).

$$T_{D_x} = I_x \ddot{\phi} + T_{C_\phi} + H_w \omega_o \phi \cos \psi + H_w \dot{\psi} \tag{2-21}$$

$$T_{D_z} = I_z \ddot{\psi} + H_w \omega_o \sin \psi - H_w \dot{\phi} + T_{C_\psi} \tag{2-22}$$

$$T_{D_y} = I_y \ddot{\theta} + T_{C_\theta} \tag{2-23}$$

where, for reaction wheel control the following control laws pertain

$$T_{C_\phi} = \dot{h}_{c_x} , \ \dot{h}_{c_x} = \left(\frac{K_{\phi_R} S}{\tau_m S+1} \right) \phi (S) \tag{2-24}$$

$$T_{C_\theta} = \dot{h}_{c_y} , \ \dot{h}_{c_y} = \left[\frac{K_m J_E S}{\tau_{m_2} S+1} \right] \left[\frac{K_{\theta_R} (\tau_m S+1)}{\tau_2 S+1} \right] \theta (S) \tag{2-25}$$

and for proportional control, the control laws are

$$T_{C_\phi} = K_\phi \left(\frac{\tau_1 S+1}{\tau_2 S+1} \right) \phi (S) \tag{2-26}$$

$$T_{C_\theta} = K_\theta \left(\frac{\tau_3 S+1}{\tau_4 S+1} \right) \theta (S) \tag{2-27}$$

$$T_{C_\psi} = K_\psi S \psi (S) \tag{2-28}$$

System transfer functions were developed from the preceding equations by linearizing via small angle assumptions. Note that the reaction wheel system was stabilized for small angle variations without using the yaw damper. Thus, the yaw damper term was deleted from the transfer functions when a roll reaction wheel torquer was used.

For proportional control devices, the yaw-roll transfer functions are

$$\frac{\psi}{T_{D_z}} = \frac{1}{D_1} \left[\tau_2 I_x S^3 + I_x S^2 + (K_\phi \tau_1 + H_w \omega_o \tau_2) S + K_\phi + H_w \omega_o \right] \tag{2-29}$$

$$\frac{\psi}{T_{D_x}} = \frac{1}{D_1} \left[S H_w (\tau_2 S + 1) \right] \tag{2-30}$$

$$\frac{\phi}{T_{D_x}} = \frac{1}{D_1} \left[\tau_2 I_z S^3 + (I_z + \tau_2 K_\psi) S^2 + (K_\psi + H_w \omega_o \tau_2) S + H_w \omega_o \right] \tag{2-31}$$

$$\frac{\phi}{T_{D_z}} = -\frac{1}{D_1}\left[SH_w\left(\tau_2 S+1\right)\right] \qquad (2\text{-}32)$$

The characteristic denominator D_1 is given by

$$\begin{aligned} & I_x I_z \tau_2 S^5 + I_x\left[I_2 + \tau_2 K_\psi\right]S^4 + \Big[I_x\left(K_\psi + H_w\omega_o\tau_2\right) + K_\phi\tau_1 I_z \\ & \quad + H_w\omega_o\tau_2 I_z + H_w{}^2\tau_2\Big]S^3 + \Big[H_w\omega_o I_x + K_\phi\left(I_z + \tau_1 K_\psi\right) \\ & \quad + H_w\omega_o\left(I_z + \tau_2 K_\psi\right) + H_w{}^2\Big]S^2 + \Big[K_\phi\left(K_\psi + \tau_1 H_w\omega_o\right) \\ & \quad + H_w\omega_o\left(K_\psi + H_w\omega_o\tau_2\right)\Big]S + H_w\omega_o\left[K_\phi + H_w\omega_o\right] \end{aligned} \qquad (2\text{-}33)$$

and the pitch transfer function is

$$\frac{\theta}{T_{D_y}} = \frac{1}{D_2}\left[\tau_4 S + 1\right] \qquad (2\text{-}34)$$

where

$$D_2 = \left[I_y\tau_4 S^3 + I_y S^2 + K_\theta\tau_3 S + K_{\hat{\vartheta}}\right] \qquad (2\text{-}35)$$

For the reaction wheel control of the roll axis (yaw damper deactivated) the system transfer functions are

$$\frac{\psi}{T_{D_z}} = \frac{1}{D_3}\left[\tau_m I_x S^3 + I_x S^2 + \left(\tau_m H_w\omega_o + K_\phi\right)S + H_w\omega_o\right] \qquad (2\text{-}36)$$

$$\frac{\psi}{T_{D_x}} = \frac{1}{D_3}\left[H_w S\left(\tau_m S+1\right)\right] \qquad (2\text{-}37)$$

$$\frac{\phi}{T_{D_x}} = \frac{1}{D_3}\left[\tau_m I_z S^3 + I_z S^2 + H_w\omega_o\tau_m S + H_w\omega_o\,)\right] \qquad (2\text{-}38)$$

$$\frac{\phi}{T_{D_z}} = -\frac{1}{D_3}\left[H_w S\left(\tau_m S + 1\right)\right] \qquad (2\text{-}39$$

where

$$\begin{aligned} D_3 = {} & \tau_m I_x I_z S^5 + I_x I_z S^4 + \left[\tau_m H_w\omega_o I_z + \tau_m H_w\omega_o I_x + \tau_m H_w{}^2 + K_\phi I_z\right]S^3 \\ & + \left[H_w\omega_o I_z + H_w\omega_o I_x + H_w{}^2\right]S^2 + \left[\tau_m H_w{}^2\omega_o{}^2 + K_\phi H_w\omega_o\right]S + H_w{}^2\omega_o{}^2 \end{aligned} \qquad (2\text{-}40)$$

It was found that an inherently well stabilized characteristic was present without using a yaw damper. This is demonstrated by a direct substitution of the evolved system constants, into the reaction wheel characteristic Eq 2-40. The numerically factored characteristic is shown below.

$$D_3 = (1.47S+1)\,(229\,S^2 + 26.03\,S+1)\,(1.9\text{x}10^8\,S^2 + 1.84\text{x}10^4\,S+1)$$

Thus, observe that the two oscillating components of the system response were well damped ($W_N = 0.066$ rad/sec, $\xi = 0.87$ and $W_N = 0.725 \times 10^{-4}$ $\xi = 0.67$). This was demonstrated by computer study.

The pitch and roll axes were stabilized by using reaction wheels with provision for momentum dumping by means of a cold gas system. A rate controlled on-off system using cold gas torquers was provided for the yaw axis for use in the initial yaw alignment mode. The gyroscopic coupling induced by the constant speed pitch wheel was used advantageously to stabilize the roll-yaw combination in the Earth tracking mode.

2) Yaw Alignment. The initial yaw angle at the time yaw alignment is started could have any value and, in the worst case, could be misoriented 180°. A prime consideration in the yaw control system design was minimizing the yaw alignment time. An auxiliary yaw rate control system was found to be beneficial in this respect.

When large initial yaw angles exist, the capability of the roll reaction wheel is exceeded in terms of total change of angular momentum. Thus, as the reaction wheel saturates under the influence of a yaw coupled torque ($H_W \dot{\psi}$), a roll axis dumping torque is required to restrain the roll angle as well as to reactivate the reaction wheel by unloading it. Preliminary studies indicated that a reaction wheel, provided on the yaw axis to supply yaw damping, would saturate under present sizing. Thus, auxiliary yaw control was provided by an on-off cold gas system for the yaw axis.

3) Tracking Mode. The roll-yaw combination was characterized by the presence of strong coupling terms. Using a roll-reaction wheel and constant speed pitch wheel to stabilize this combination was emphasized. Stabilization was achieved by reducing the time constant of the roll reaction wheel. The performance of the system proved to be a sensitive function of the control gain.

4) Pitch Wheel Spin-Up. For yaw alignment, the pitch wheel is accelerated in the negative pitch direction to a speed which will provide the desired angular momentum. The steady torque required is a function of the time allowed to bring the wheel up to speed.

$$T_p = \frac{H_W}{t}$$

In terms of yaw alignment time it is desirable to spin up the wheel as rapidly as is practical. Two effects tend to set the lower limit on this variable. The torque required to accelerate the pitch wheel induces a reaction torque on the vehicle about the positive pitch axis. Since this disturbance must be controlled by the pitch reaction wheel and its auxiliary dumping system, the maximum steady torque that may be applied is limited by the peak torque available in the cold gas system. Thus, the minimum time that may be assumed for this function can be related to this torque ($t_m = H_W/T_{c.g.} = 150$ in.-lb-sec/ 0.25 in.-lb = 600 sec = 10 min). For the proportional control system the predominant torques impressed upon the yaw axis in this mode are

$$T_z = - H_W \omega_o \sin \psi - H_W \dot{\phi} - \theta \dot{\psi} H_W$$

The steady state effect of the reaction torque on the pitch axis is to produce a positive pitch angle offset which may be represented by

$$\theta_{s.s.} = \frac{T_p}{K_\theta}$$

Since a positive yaw offset induces a negative yaw rate, the pitch coupling torque ($\theta\dot{\psi}H_w$) acts significantly to reduce the yaw alignment rate during pitch wheel spin-up. This effect may be observed directly by deleting roll axis coupling and equating the torques represented above

$$\dot{\psi}_{max} \leq \frac{-\omega_o \sin\psi}{\theta_{s.s.}}$$

By substitution from above

$$\dot{\psi}_{max} \leq \frac{-\omega_o \sin\psi K_\theta}{T_p}$$

The ≤ sign represents the fact that roll coupling also tends to oppose yaw alignment rate.

It was observed in the analog computer study that the transient involved in the pitch axis had negligible effect on the yaw axis. Thus, for initial alignment for large yaw angle offsets, as well as for cases of small yaw angle offsets, the dynamics involved could be represented by a set of linear equations. The following transfer function incorporates the steady state pitch angle induced by a steady torque impressed on the pitch axis.

$$\frac{\dot{\psi}}{T_{D_x}} = \frac{H_w S^2 (\tau_2 S + 1)}{D}$$

where

$$\begin{aligned}
D = {} & \bigl[I_z I_x \tau_2\bigr] S^5 + \Bigl[I_x I_z + \Bigl(K\psi + \frac{T_p H_w}{K\theta}\Bigr) I_x \tau_2 - \tau_2 H_w I_x T_p / K_\theta\Bigr] S^4 \\
& + \Bigl[I_z (K\phi \tau_1 + H_w \omega_o \tau_2) + \Bigl(K\psi + \frac{T_p H_w}{K_\theta}\Bigr) I_x + H_w \omega_o I_x \tau_2 + H_w^2 \tau_2 - \frac{H_w I_x T_p}{K_\theta}\Bigr] S^3 \\
& + \Bigl[I_z (K\phi + H_w \omega_o) + \Bigl(K\psi + \frac{T_p H_w}{K_\theta}\Bigr)(K\phi \tau_1 + H_w \omega_o \tau_2) + I_x H_w \omega_o \\
& - \frac{\tau_2 H_w^3 \omega_o T_p H_w}{K_\theta} + H_w^2\Bigr] S^2 + \Bigl[\Bigl(K\psi + \frac{T_p H_w}{K\theta}\Bigr)(K\phi + H_w \omega_o) \\
& + H_w \omega_o (K\phi + H_w \omega_o \tau_2) - \frac{H_w^2 \omega_o T_p}{K_\theta}\Bigr] S + H_w \omega_o (K\phi + H_w \omega_o)
\end{aligned}$$

d. Analog Simulation

1) General. The dynamic equations defining the gyrocompass yaw attitude control technique were simulated on an analog computer. The use of both proportional torquers and reaction wheels was studied. Figures 2-42 and 2-43 are schematics of the systems simulated. The equations were time scaled to run at a time ratio of 1000-1 to provide a rapid solution of the equations.

Equations 2-21, 2-22, and 2-23 for proportional control were simulated to examine the stability and performance of the gyrocompass system under the influence of full coupling. The significance of the roll-yaw coupling terms required building up the simulation in two steps. The strongly interdependent yaw-roll loops were stabilized and their performance examined under the influence of large yaw angle offsets. The pitch loop was then added and the fully coupled system was examined under a worst case yaw angle offset of just under 180°. This procedure allowed a qualitative comparison of the response of the fully coupled system to a yaw offset of just under 180°. This procedure allowed a qualitative comparison of the response of the system in terms of pitch coupling. Figure 2-44 presents the response of the fully coupled system to yaw offset of just under 180°. For this run, the pitch wheel was assumed initially at full speed. The response of the system was unaltered from an identical run with the pitch loop decoupled. Since the pitch loop remained essentially undisturbed during this mode, it illustrated the lack of significant coupling from the yaw-roll loop to the pitch loop. The condition explored represented a worst case in terms of perturbations impressed upon the pitch loop by disturbances in the roll and yaw loops.

The reaction wheel configuration was examined under a condition of small yaw angle offset. It was found that the system responded as had been predicted by linear analysis. The response time of the yaw loop was improved considerably by increasing the roll control gain. This improvement, however, was gained at the expense of roll angle response time. The system stability was unaffected by this variation. Figure 2-45 presents the response of the system at an increased control gain of 4400 in. -lb/rad.

2) Pitch Wheel Spin Up. The necessity of bringing the pitch wheel up to speed upon completion of Earth acquisition dictated the following run. A condition of yaw offset of just under 180° was again examined as a worst case of yaw misalignment, as well as for purposes of comparison. The pitch wheel was uniformly accelerated from $H_W = 0$ to $H_W = 150$ in. -lb-sec over a period of one hour. Figure 2-46 presents the time history of the response of the system. As expected, the rate of yaw alignment was reduced as compared to Figure 2-44 ($H_W = 150$ in. -lb-sec initially) during the first hour. This reduction stemmed from two effects not present when the wheel was assumed to be initially at full speed. The first and predominant effect came from a reduction of the average gyroscopic restoring torque ($H_W \omega o \sin \psi$) during the first hour. The second effect can be observed at the instant of time the wheel came up to full speed where the wheel accelerating torque was terminated. The reaction torque impressed upon the pitch axis had driven the pitch angle positive as a function of the wheel accelerating torque. Just prior to the wheel torque termination, the gyroscopic counter torque ($H_W \psi \theta$) impressed upon the yaw axis had reached its maximum. At torque termination the pitch angle was reduced to zero, thereby removing the torque coupled into the yaw axis from the pitch axis and causing a sudden increase in restoring yaw rate.

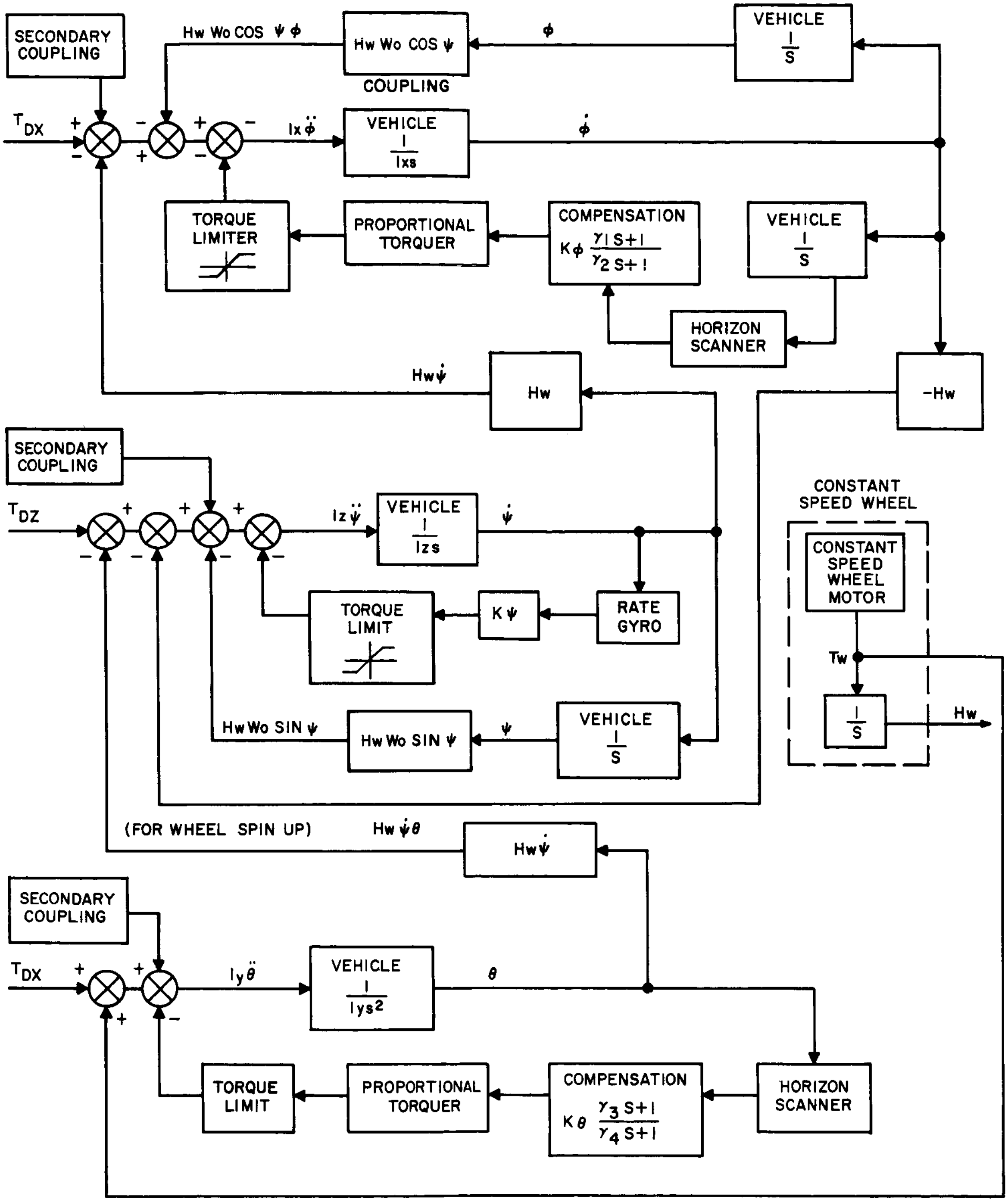
SECONDARY COUPLING
Hw Wo COS ψ φ
Hw Wo COS ψ
COUPLING
φ
VEHICLE 1/S
T_DX
Ix φ̈
VEHICLE 1/Ixs
φ̇
TORQUE LIMITER
PROPORTIONAL TORQUER
COMPENSATION Kφ (γ1 S+1)/(γ2 S+1)
VEHICLE 1/S
HORIZON SCANNER
Hwψ̇
Hw
-Hw
SECONDARY COUPLING
T_DZ
Iz ψ̈
VEHICLE 1/Izs
ψ̇
CONSTANT SPEED WHEEL
CONSTANT SPEED WHEEL MOTOR
Tw
1/S
Hw
TORQUE LIMIT
Kψ
RATE GYRO
HwWo SIN ψ
HwWo SIN ψ
ψ
VEHICLE 1/S
(FOR WHEEL SPIN UP)
Hw ψ̇ θ
Hwψ̇
SECONDARY COUPLING
T_DX
Iy θ̈
VEHICLE 1/Iys²
θ
TORQUE LIMIT
PROPORTIONAL TORQUER
COMPENSATION Kθ (γ3 S+1)/(γ4 S+1)
HORIZON SCANNER

Figure 2-42. Gyrocompass Yaw Attitude Control System - Proportional Control

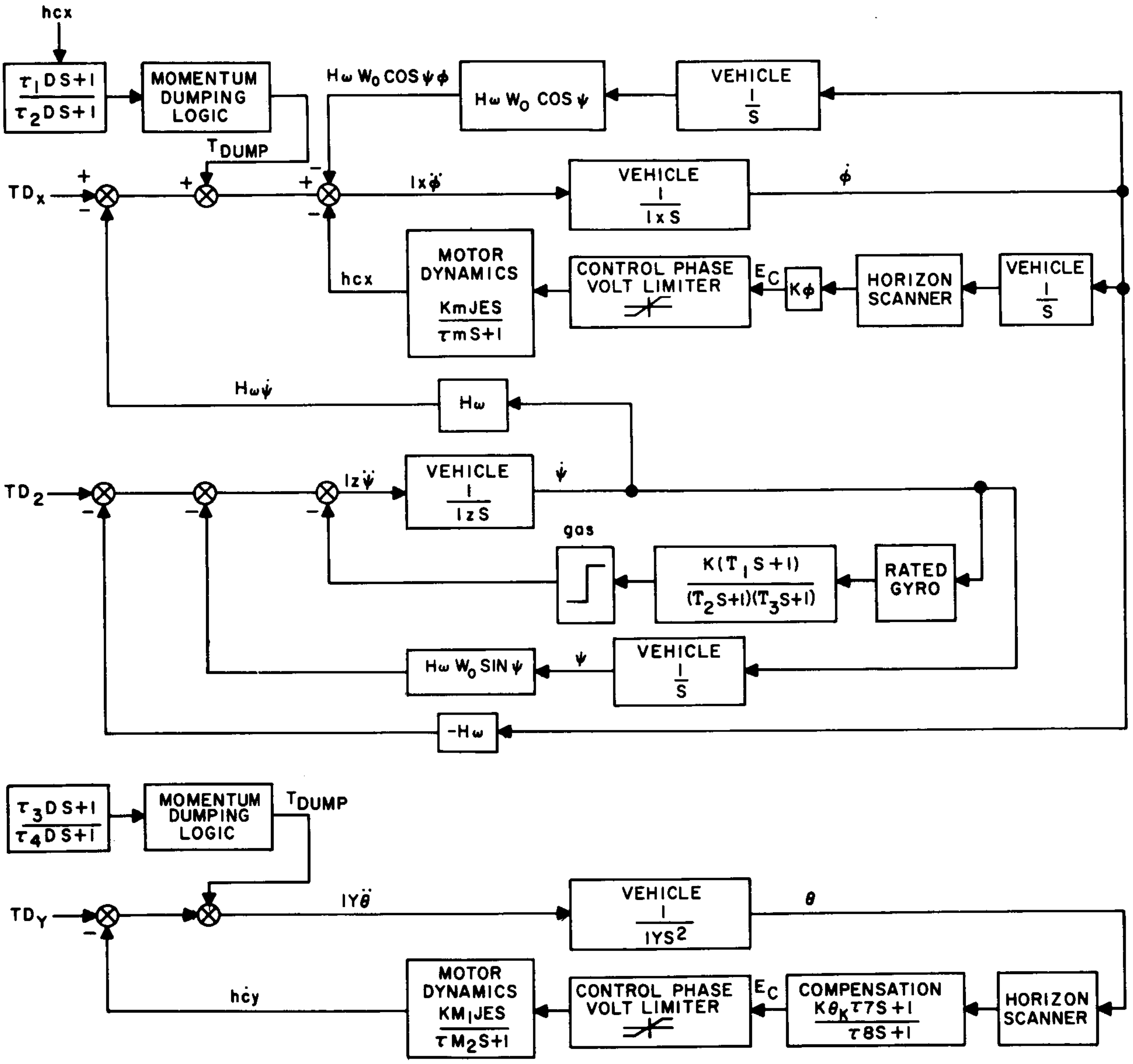
hcx
$\frac{\tau_1 DS+1}{\tau_2 DS+1}$
MOMENTUM DUMPING LOGIC
$H\omega W_0 \cos\psi\phi$
$H\omega W_0 \cos\psi$
VEHICLE $\frac{1}{S}$
T_{DUMP}
TD_X
+
−
+
+
−
+
−
$Ix\ddot{\phi}$
VEHICLE $\frac{1}{IxS}$
$\dot{\phi}$
hcx
MOTOR DYNAMICS $\frac{KmJES}{\tau mS+1}$
CONTROL PHASE VOLT LIMITER
E_C
$K\phi$
HORIZON SCANNER
VEHICLE $\frac{1}{S}$
$H\omega\dot{\psi}$
$H\omega$
TD_Z
−
−
−
$Iz\ddot{\psi}$
VEHICLE $\frac{1}{IzS}$
$\dot{\psi}$
gas
$\frac{K(T_1S+1)}{(T_2S+1)(T_3S+1)}$
RATED GYRO
$H\omega W_0 \sin\psi$
ψ
VEHICLE $\frac{1}{S}$
$-H\omega$
$\frac{\tau_3 DS+1}{\tau_4 DS+1}$
MOMENTUM DUMPING LOGIC
T_{DUMP}
TD_Y
−
$IY\ddot{\theta}$
VEHICLE $\frac{1}{IYS^2}$
θ
$h\dot{c}y$
MOTOR DYNAMICS $\frac{KM_1JES}{\tau M_2S+1}$
CONTROL PHASE VOLT LIMITER
E_C
COMPENSATION $K\theta_K\frac{\tau 7S+1}{\tau 8S+1}$
HORIZON SCANNER

Figure 2-43. Gyrocompass Yaw Attitude Control System - Reaction Wheel with Auxiliary Dumping

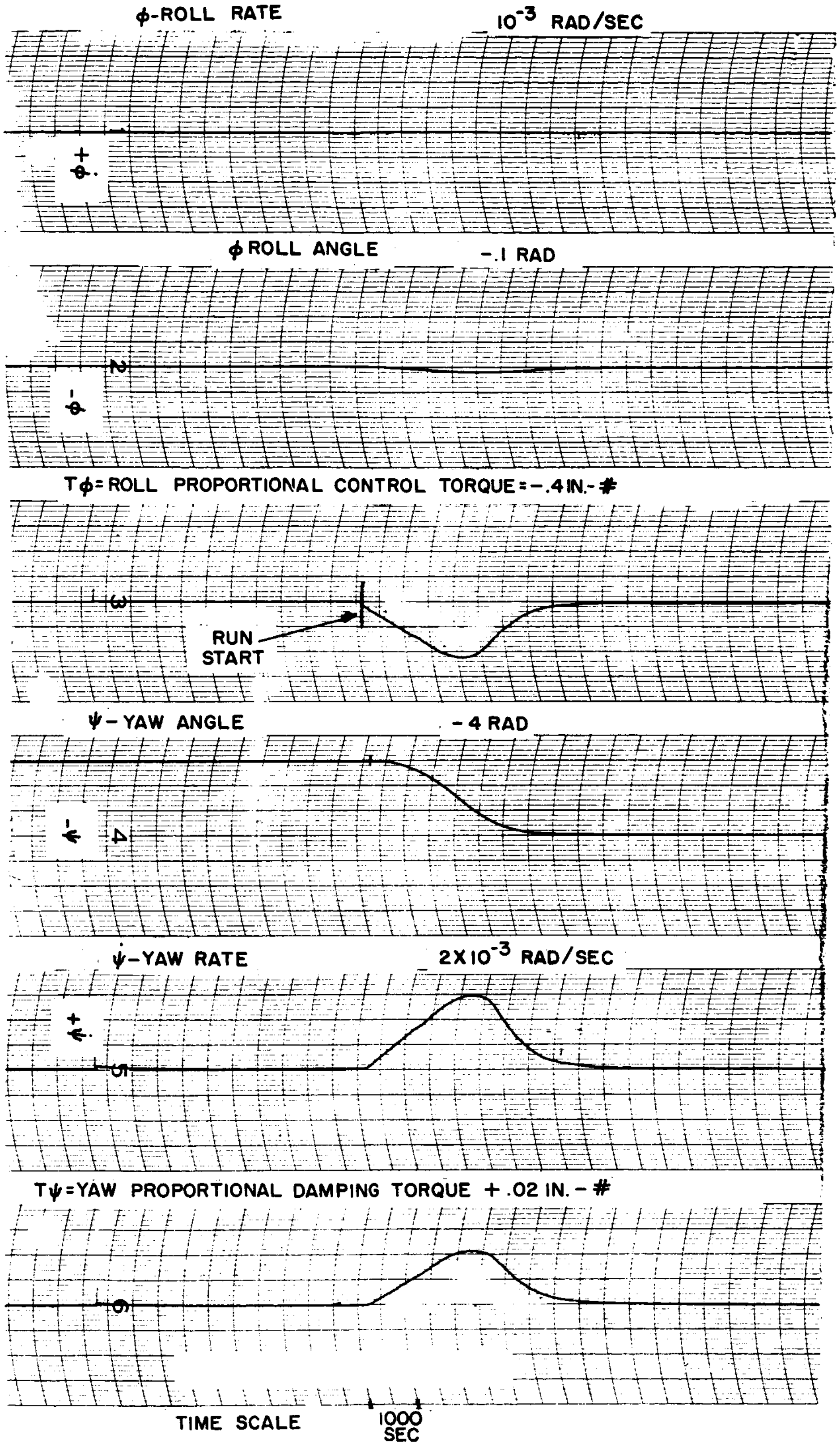

Figure 2-44. Initial Yaw Alignment with Proportional Noncoupling Control Torquers and Wheel Initially up to Speed

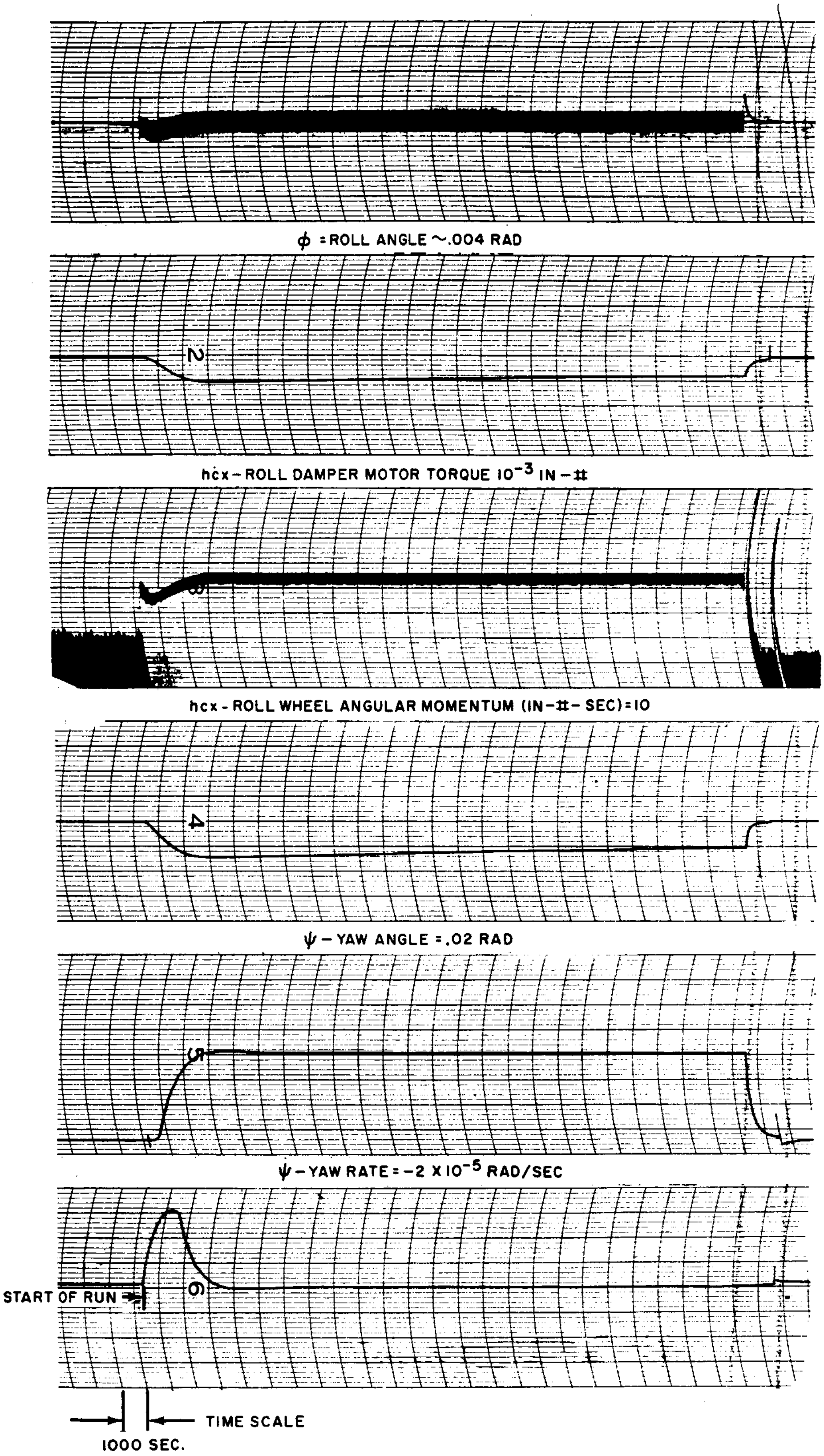

Figure 2-45. Transient Response of Yaw-Roll Gyrocompass System for Initial Small Yaw Misalignment - No Yaw Damper

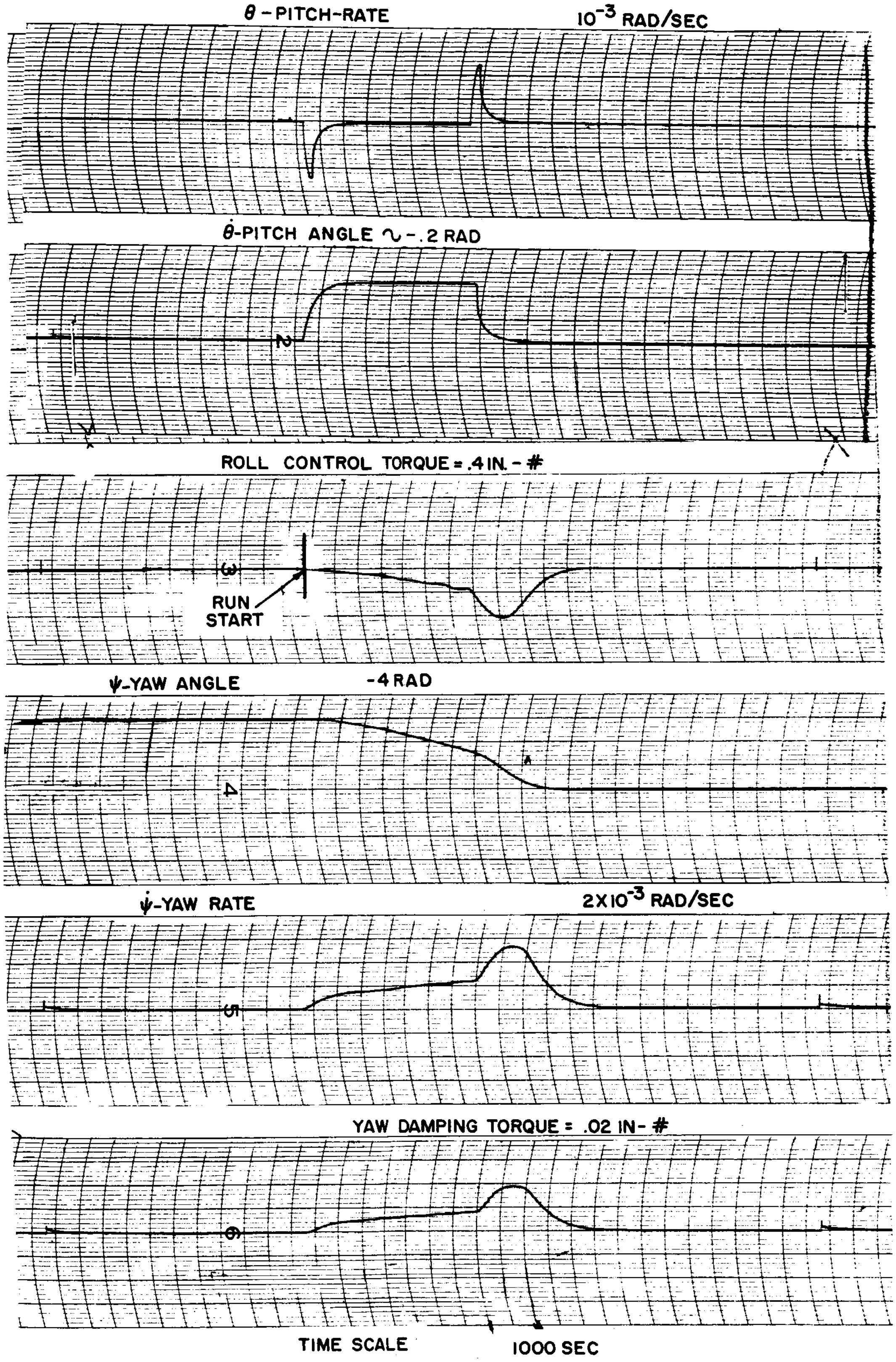

Figure 2-46. Initial Yaw Alignment While Accelerating Wheel up to Speed (Proportional Noncoupling Control Torquers)

The effect on total yaw alignment time of bringing the wheel up to speed over a full hour may be observed by a comparison with what can be considered the ideal situation of having the wheel initially at full speed. Table 2-6 presents this comparison as well as a listing of the total required change in control angular momentum.

TABLE 2-6

EFFECT OF WHEEL SPIN-UP ON YAW ALIGNMENT PERFORMANCE

	H_w=150 in.-lb-sec (initially)	H_w=0 to 150 in.-lb-sec (spin-up time=1 hour)
Total Yaw Acquisition Time	1.33 hr	1.70 hr
Yaw Axis Total change in Angular momentum	30 in.-lb-sec.	30 in.-lb-sec
Roll Axis Total change in Angular momentum	525 in.-lb-sec	500 in.-lb-sec
Pitch Axis total change in Angular momentum	0	150 in.-lb-sec

e. Summary of Parameters.

As a result of the dynamic analysis and analog studies previously discussed, the following parameters have been established.

SYSTEM PARAMETERS FOR GYROCOMPASS YAW CONTROL SYSTEM

I_x	-	Vehicle Roll Moment of Inertia	-	2460 in.-lb-sec^2
I_y	-	Vehicle Pitch Moment of Inertia	-	4152 in.-lb-sec^2
I_z	-	Vehicle Yaw Moment of Inertia	-	2460 in.-lb-sec^2
H_w	-	Constant Speed Pitch-Wheel Momentum	-	150 in.-lb-sec
ω_o	-	Orbital Angular Velocity	-	0.725×10^{-4} rad/sec
PROPORTIONAL CONTROL				
K_ϕ	-	Roll Control Loop Gain	-	34.9 in.-lb/rad
K_θ	-	Pitch Control Loop Gain	-	0.575 in.-lb/rad
K_ψ	-	Yaw Control Loop Gain	-	7.34 in.-lb/rad
τ_1	-	Roll Compensation Lead time Constant	-	183 sec
τ_2	-	Roll Compensation Lag time Constant	-	18.3 sec
T_1	-	Torque Limit, Pitch, Roll, and Yaw	-	0.25 in.-lb
τ_3	-	Pitch Compensation Lead Time Constant	-	180 sec
τ_4	-	Pitch Compensation Lag Time Constant	-	18 sec
REACTION WHEEL				
$h_{c_{x\max}}$		Motor Maximum Angular Momentum	-	10 in.-lb-sec
$h_{c_{z\max}}$		Motor Maximum Angular Momentum	-	10 in.-lb-sec
J_e		Motor Inertia (Yaw and Roll)	-	0.05 in.-lb-sec
τ_m		Motor Time Constant - Yaw	-	1.26 sec

f. Effects of Actual Horizon Scanner Characteristics

1) Effect of Horizon Scanner Noise. The effect of horizon scanner noise ($\Phi_i(\omega)$) on the tracking accuracy of the gyrocompass system with reaction wheel control was examined. The output mean squared error is

$$\sigma_{\dot{\theta}}^{2} = \frac{1}{2\pi} \int_{-\infty}^{\infty} \Phi_i(\omega) \left|G(j\omega)\right|^2 d\omega$$

where $G(j\omega)$ = system transfer function $(\dot{\theta}/\epsilon_\theta)$

$\Phi_i(\omega)$ = power spectral density function of noise

A white noise source of amplitude R ($\text{deg}^2/\text{cps}^2$) was assumed in the output of the roll axis horizon scanner. Thus

$$\sigma_{\dot{\theta}}^{2} = \frac{R}{2\pi} \int_{-\infty}^{\infty} \left|G(j\omega)\right|^2 d\omega$$

The mean error in roll angle, roll rate, yaw angle, and yaw rate was evaluated by graphically performing the above integration.

$$\frac{\Phi_o}{\Phi_i} = G(s)_1 = \frac{K_\phi S(I_z S^2 + H_w \omega_o)}{D_3}$$

$$\frac{\Phi_o}{\Phi_i} = G(s)_2 = \frac{K_\phi S^2 (I_z S^2 + H_w \omega_o)}{D_3}$$

$$\frac{\Psi_o}{\Phi_i} = G(s)_3 = \frac{H_w{}^2 \omega_o S}{D_3}$$

$$\frac{\Psi_o}{\Phi_i} = G(s)_4 = \frac{H_w{}^2 \omega_o S^2}{D_3}$$

where = D_3 = the characteristic denominator of the gyrocompass system with reaction wheel control given in Eq 2-40.

Figure 2-47 presents the results of this analysis, where it is seen that a horizon sensor white noise level of 0.02° results in an RMS roll rate of 0.003°/sec. Yaw rate is seen to be relatively uneffected by the roll horizon scanner noise content. It should be noted that noise suppression studies were not performed during this study. Optimum filtering techniques could markedly reduce the indicated RMS rate error.

2) Effect of Horizon Sensor Dead Zone. In the gyrocompass control system, the effect of dead zone takes on a different form than for a standard reaction wheel system. As pointed out in subsection E.1, dead zone results in a hangoff attitude error for the standard reaction wheel system. With gyrocompassing, however, the system is oscillatory when within the dead band and would oscillate at two distinct frequencies if disturbed. These are orbital frequencies, ω_o, and $H_w/\sqrt{I_x I_z}$.

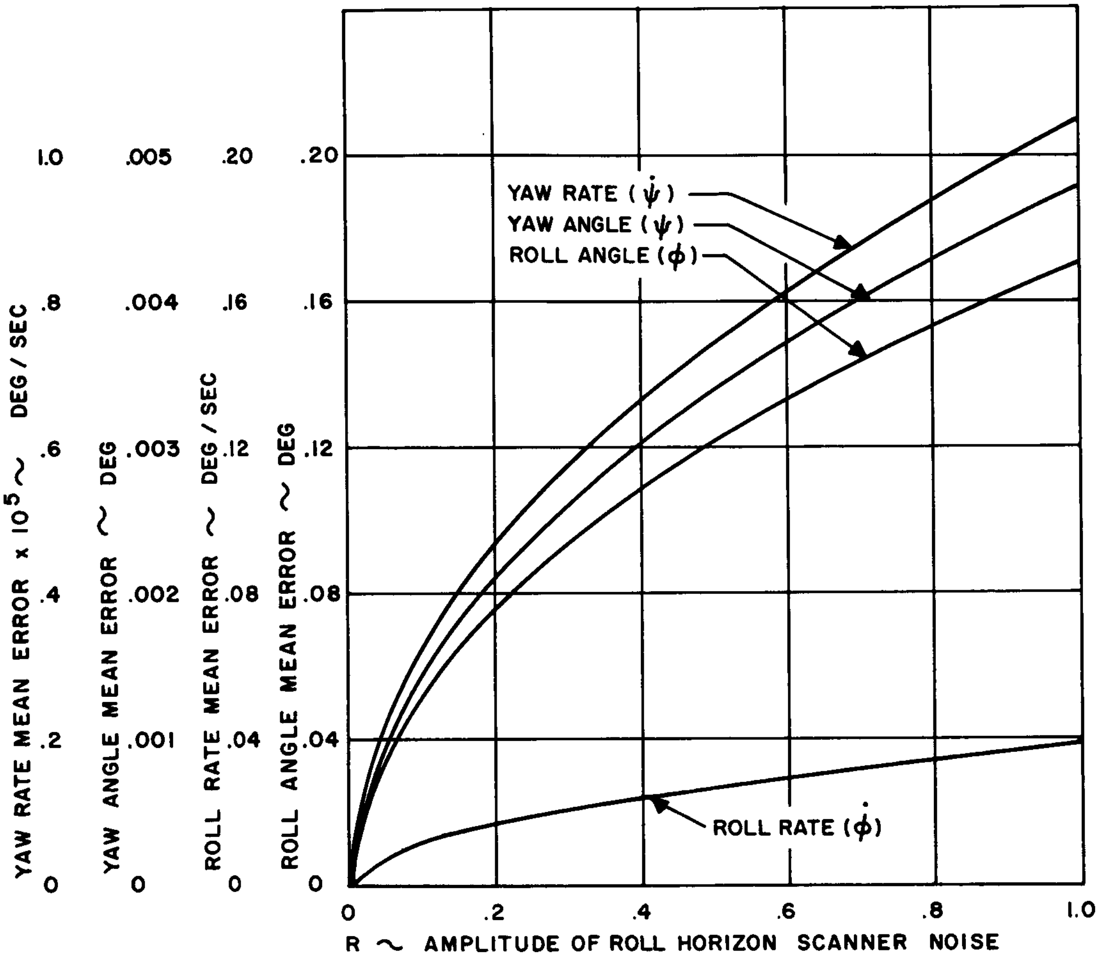

Figure 2-47. Gyrocompass System - Horizon Scanner Noise Effect on Tracking Accuracy

The amplitude of the roll oscillation would be bounded at an amplitude equal to the dead zone amplitude. Therefore, if

$$\phi = A \left[\sin \omega_o t + \sin \left(H_W / \sqrt{I_x I_z} \right) t \right]$$

where A is the dead zone magnitude, then the rate amplitude would be

$$\dot{\phi} = A \left[\omega_o \cos \omega_o t + \frac{H_W}{\sqrt{I_x I_z}} \cos \left(H_W / \sqrt{I_x I_z} \right) t \right]$$

3. Discrete Controller

a. Ion Engine Control System

A parametric study of an ion engine, 3-axis attitude control system which covers the range of pointing accuracy from ±0.05° to ±1.0° is shown in Figures 2-48 and 2-49. These curves show the average power requirement and solar cell weight, respectively, for 3-axis attitude control as a function of disturbance-torque to moment-of-inertia ratio for various attitude accuracy values. The vertical dotted lines represent maximum torque (122 dyne-cm) to moment-of-inertia ratios for the three vehicles under consideration.

These data do not include any station keeping function, but do take into consideration power conditioning efficiencies.

The total power source weight (solar cells and batteries) required for the station keeping system is shown in Figure 2-50 as a function of satellite weight. These weights are also broken down into the N-S and E-W contributions. In addition, the dotted line on Figure 2-50 represents the solar-cell weight when the system is operated in a continuous thrust mode. This thrusting mode is planned for the Mark II control system and will eliminate essentially all battery requirements, thereby providing a substantial weight savings.

Table 2-7 shows all of the pertinent operating characteristics and requirements of an ion propulsion, station-keeping system for satellite weights of 100 lb, 500 lb, and 1000 lb. Again, the power system characteristics are given for complete orbit control, as well as for the individual N-S and E-W corrections.

b. Hardware

The ion propulsion attitude control, and station keeping system is presently under development at the Hughes Research Laboratories under NASA Contract NAS3-2510. This system is capable of holding a satellite's orientation to ± 0.5° and its angular rate to about 1°/hr. (This latter capability can probably be extended, if necessary.) The system will also maintain the position of the satellite relative to a point on Earth to less than ± 0.1° in both longitude and latitude.

Table 2-8 lists the weights of the basic control system components. This system, which has complete redundancy, is designed to control a 550 lb synchronous satellite for 3 years. (Lesser mission times or satellite weights will reduce feed system weights.) It should be noted that these weights represent "first effort" accomplishments and, therefore, can be expected to be reduced as component designs become more refined. (See list in Table 2-8 under heading - Target.)

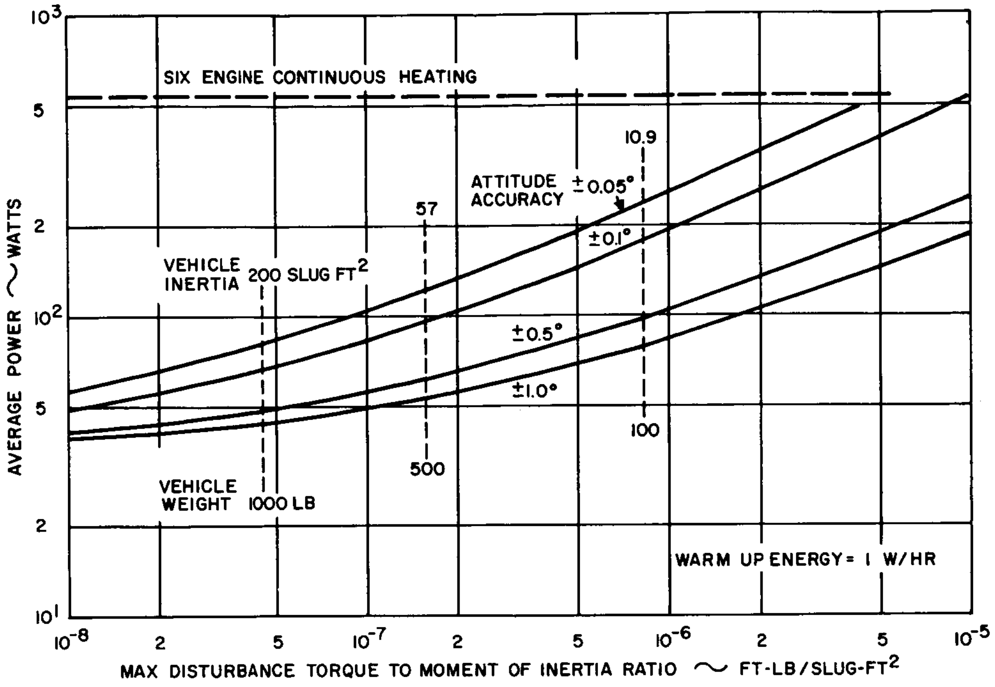

Figure 2-48. Power Required for Ion Engine 3-Axis Control System

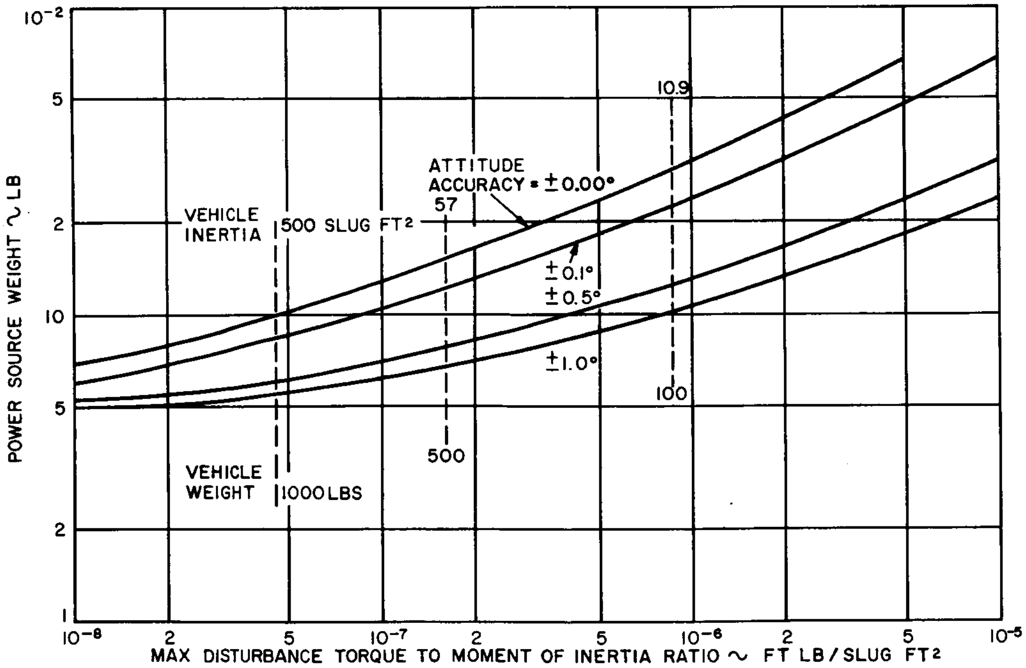

Figure 2-49. Weight of Power Supply for Ion Engine 3-Axis Control System

TABLE 2-7
STATION KEEPING SYSTEM CHARACTERISTICS

Satellite Mass (lb)	Correction	Duty Cycle (%)	Thrust Interval (min)	Average Power Requirement (W)	Solar Cell Weight (lb)	Energy Storage Requirement (W-hr)		Battery Weight (lb)		Total Power Supply Weight (lb)	
100	EW	0.05	0.66 (one per day)	0.22	0.03	5.2	Total	1.9	Total	1.9	Total
	NS	1.4	3.3 (six per day)	6.6	0.84	26	31	3.8	5.7	4.6	6.6
500	EW	0.23	3.3 (one per day)	1.1	0.14	26	Total	3.8	Total	3.9	Total
	NS	6.9	16.5 (six per day)	33	4.2	130	156	19	21	23	25
1000	EW	0.46	6.6 (one per day)	2.2	0.28	52	Total	7.6	Total	7.9	Total
	NS	14	33 (six per day)	66	8.4	260	312	36	44	44	53

P/T = 267 kW/lb

η P. C = 85%

P = 470 W (including power conditioning)

T = 1.5 mlb

TABLE 2-8
SYSTEM WEIGHTS

System Components	Present	Target
Engine Stations (4)	52	45
Engines (3 per station) - 3		
Feed System (loaded with 3-yr cesium supply) - 8		
Rotator - 2 lb		
Power Conditioning Equipment	26	20
Power Control System	5	2.5
Overall System Controls	5	2.5
Cabling	5	5
Sensors	5	5
Signal Conditioning	2	2
Totals	100 lb	82 lb

(Includes power supply for EW station keeping)

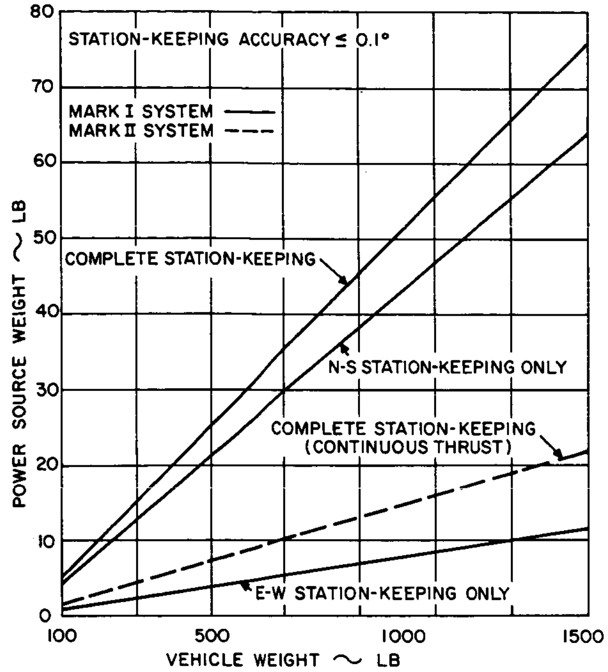

Figure 2-50. Parametric Plot of Station Keeping System Characteristics - Ion Engine

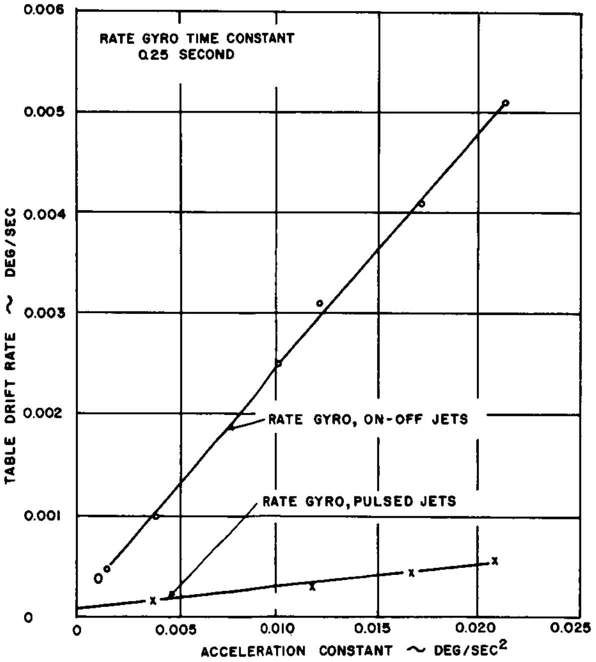

Figure 2-51. Experimental Systems for Low Rate Limit Cycle Attitude Control

Table 2-8 refers to a dual function control system (i.e., attitude control and station keeping) for a three-year mission. Most component weights would be significantly reduced if only attitude control were required.

The weight of the power system for a 500-lb satellite with a moment of inertia of 57 slug ft^2 in the presence of a maximum disturbance torque of 122 dyne-cm is 8 lb for attitude control (Figure 2-49), and 25.5 lb for station keeping (Figure 2-50); 21.1 lb of the latter is for the N-S correction.

The average power demand is 62W (Figure 2-48) for the attitude control function and 34W for the station keeping function (Table 2-7). Of the 34W required for station keeping, 33W are used for the N-S correction.

c. Sensors

Since the evaluation of sensors for the ion engine attitude control system has been only recently investigated, the information available is preliminary in nature. It appears that, for one of the axes, a star tracker is capable of accuracies sufficient to provide the ±0.5° accuracy requirement imposed on the system.

d. Plasma Engine Control System

This system is described in Volume 7.

4. Continuous Noncoupling Systems

a. Summary

This subsection edited by Republic, presents the bulk of a study conducted by Minneapolis-Honeywell on the usefulness of this type of attitude controller for the SMS mission.

This subsection describes some Minneapolis-Honeywell developments applicable to satisfying the mission and vehicle constraints for the SMS as outlined in Table 2-9. In particular, this subsection examines the problems associated with 3-axis active control for this satellite to meet these constraints.

The main concern in supplying 3-axis attitude control for the SMS is to establish an extremely low-rate, limit cycle with a control system having the inherent reliability to continue functioning satisfactorily for at least one year. Part of this study effort consisted of tests using actual hardware on the Minneapolis-Honeywell Air Bearing Table Spacecraft Simulator. These tests have achieved limit cycle rates less than the 0.0001°/sec desired for SMS using cold gas reaction jets with acceleration levels as low as $0.003°/sec^2$.

The discussion portion of this document covers work which has been done on various alternate solutions applicable to the SMS control problem. The most reasonable approach to mechanization of the control system is discussed along with some of the considerations involved in its application. The concept of attitude control using derived rate, dubbed "Pseudo rate," is recommended as

TABLE 2-9
SMS MISSION AND VEHICLE REQUIREMENTS

Mission Time	1 year
Stabilization Rate	0.0001°/sec
Pointing Accuracy	0.05 to 1.0°
Torque Level	0.05 to 0.25 in.-lb (0.0042 to 0.021 ft-lb)
Torque/Inertia Ratio	0.003 to $0.022°/\text{sec}^2$

Vehicle Characteristics:

	Inertia (slug-ft2)	Nozzle to Nozzle Distance (in.)
100 lb configuration	$I_x = 10.9$	38
	$I_y = 17.4$	42
	$I_z = 10.9$	38
500 lb configuration	$I_x = 57$	92
	$I_y = 68$	50
	$I_z = 57$	92
1000 lb configuration	$I_x = 205$	82
	$I_y = 346$	90
	$I_z = 205$	82

the most reliable and as offering the least fuel consumption in limit cycle with reasonable fuel requirements during acquisition

b. Discussion

1) Limit Cycle Criteria. a. Introduction. Limit cycle rate can be shown to be related to on-off control system parameters by the following equation (assuming a symmetrical limit cycle)

$$\dot{\theta}_{LC} = \frac{2K\,\Delta\theta_A + 2\Delta\dot{\theta}_h + \Delta\dot{\theta}_{lag} + \Delta\dot{\theta}_I\left[1 - \dfrac{\Delta\dot{\theta}_I K}{2\ddot{\theta}}\right]}{2 - Kt_D - \dfrac{K\Delta\dot{\theta}_I}{\ddot{\theta}}}$$

with the system parameters defined as below

$\Delta\theta_A$ = Switching hysteresis of on-off switch
$\Delta\dot{\theta}_h$ = Threshold of rate sensor
$\Delta\dot{\theta}_{lag}$ = Rate sensor lag due to filter or other system time constants
$\Delta\dot{\theta}_I$ = Reaction jet velocity impulse after switchoff
t_D = Transport delay time in turning reaction jet on
K = Ratio of attitude to rate gain (switching line slope)
$\ddot{\theta}$ = Angular acceleration

The sum of the contributions of the individual parameters, as defined in the equation, must be made less than the limit cycle rate desired. Also, the rate contribution of the reaction jet minimum impulse bit, $\Delta\theta_I$, obviously, must be less than the desired limit cycle rate. To meet the limit cycle objective, therefore, it is necessary to make the other system parameters negligible with respect to $\Delta\dot{\theta}_I$. As a starting point, then, the expected contributions of these individual parameters should be investigated prior to examining the means available for minimizing their contributions to the limit cycle rate. These individual terms are discussed below.

b.) Rate Sensor Threshold or Hysteresis ($\Delta\dot{\theta}_h$). Assuming rate information is necessary, the method of obtaining this rate information would be by rate gyros. The concern is the value of the limit cycle rate at which rate information becomes available with respect to the low (0.001°/sec) limit cycle rate desired for SMS. If this threshold exists above the limit cycle rate desired, this constrains the limit cycle rate attainable unless a control scheme, which is stable without rate information, is available.

Hardware investigations have been performed at Minneapolis-Honeywell to ascertain this threshold. Various rate gyros were mounted on the Minneapolis-Honeywell Air Bearing Table and used to supply the rate information necessary to control the ABT in a stable limit cycle through operation of reaction jets. All of the rate sources were able to achieve limit cycle rates of 0.00025°/sec or below. Extrapolation of data obtained predicts a minimum threshold for all sources of 0.0001°/sec with the results actually achieved for some sources being below this value. Figure 2-51 shows some typical data obtained using both pulsed and non-pulsed operation of reaction jets. Here pulsed operation is defined as impulse control; i.e., the jets are turned on as a function of attitude and rate error but turned off as a function of time. Non-pulsed operation means that the jets are turned on and off strictly as a function of attitude rate error. The pulsing operation eliminates the effects of some system time constants and permits lower rates to be achieved.

The tests portrayed in Figure 2-51 were not aimed at achieving a 0.0001°/sec limit cycle but only at proving that rate source thresholds are well below 0.001°/sec. Therefore, it is felt that some of the residual limit cycle rate existing when results are extrapolated to zero acceleration is due to incomplete minimization of the contributions of some of the parameters involved. Note that,at an acceleration level of $0.003°/sec^2$, limit cycling slightly above 0.0001°/sec was achieved.

c) Switching Hysteresis ($K \Delta\theta_A$). With a deadband of 1° assumed during the SMS limit cycle and a switching line slope equal to one, the electronic switch must have a hysteresis of 0.01% or less to achieve the 0.001°/sec limit cycle desired. There are several methods of either achieving or reducing the effective hysteresis to this level or of avoiding the need for it.

(1) Since the $K\Delta\theta_A$ term is of concern rather than the $\Delta\theta_A$ term alone, a large rate gain can be used to decrease the switching line slope and, thus, decrease the effect of the hysteresis level. However, the gain increase emphasizes noise from the rate sensor which also raises its effective threshold level.

(2) Another approach to decreasing the effect of hysteresis is by proper scaling. By generating the limit cycle deadband separately from the switch, its gain can be made large in relation to that of the switch, decreasing its effective hysteresis.

(3) A last, and possibly best approach, is to attack the switch hysteresis directly. A conventional approach to electronic switch design yields a hysteresis of about 1%. However by placing a small sine wave dither on the switch to switch it on and off at a high frequency, its effective hysteresis can be greatly lowered. This approach is used in the Gemini Attitude Control System to achieve a hysteresis of less than 0.01%.

(4) A somewhat similar approach is to generate reaction jet pulses of a fixed on-time to avoid having the switch hysteresis determine the turn-off time. Various pulsing techniques experimented with at Minneapolis-Honeywell are discussed in later sections.

d) Rate Sensor Lag ($\Delta\dot{\theta}_{lag}$). The increment of rate added to the limit cycle velocity by a lag in the source of rate information is equal to the product of the vehicle acceleration and the lag time constant ($\frac{T}{J}\tau$). The acceleration levels considered for SMS range from 0.003 to 0.022°/sec^2. The allowable system time lags to obtain a 0.0001°/sec limit cycle are then 0.03 second and 0.004 second, respectively. Various component time lags can far exceed these values. In Minneapolis-Honeywell tests performed on an air bearing table, noise filters as large as 0.25 second were required at the output of rate gyros to reduce low frequency noise to an acceptable level. Deriving rate information from a horizon scanner requires larger time constants. Gemini experience indicates that the lag of a horizon scanner can be represented by 2 or 3 one-second time constants in series. Several practical means exist for eliminating the effect of system time constants. First, two levels of reaction jet thrust can be used--one level to damp out high separation rates and achieve necessary acquisition, and a second, lower level to maintain the limit cycle. However, to achieve the low limit cycle rate desired, the low level reaction jet would have to supply thrust one or two orders of magnitude below the thrusts presently being considered (or as low as 0.006 to 0.06 t grams). This appears unreasonable both from thrust magnitude considerations and from the requirement of carrying two sets of jets of different thrusts. Reaction jet thrust levels below one gram are not felt to be practical because of the likelihood of clogging of the orifice.

A second and more useful method is to operate the reaction jets in pulses rather than in a simple on-off manner. The aims and method of approach to the mechanization of various pulse logics are considered in the following paragraphs.

c. Pulse Logic Mechanizations

1) Introduction. The development of pulsed reaction jet control is necessary to eliminate the effect of system time lags and/or to eliminate the need for rate information. Included is the possibility of attempting to obtain a limit cycle below a particular rate sensor's threshold.

Pulsing concepts can be separated into two types--those requiring rate information and those stable without rate information. The first type eliminates the effect of time lag by timed interruption of switch operation. This is done by making the pulse rate function such that the slowest pulse rate has an off-time interval (lockout) sufficiently long for the rate sensing lag to disappear. This allows each pulse to be based on a true measurement of rate and eliminates the effect of rate lag. Pulsing concepts stable without rate information automatically eliminate the effects of $\Delta\theta_{lag}$. Various pulsing concepts investigated by Minneapolis-Honeywell are discussed below.

2) Rate Stable Pulsing. This system must be mechanized to provide both pulse rate and pulse width modulation. The system also requires rate information for stability. The reaction jets must be turned off after each on-period for approximately 3 times the system time constant. This is equivalent to turning the system off and waiting to observe the effect of the reaction jet pulse. This constrains the system to a low pulsing frequency for large time constants (> 1 second). With this condition, analytical studies and analog computer runs show that rapid convergence with reasonable fuel economy are difficult to achieve. Assuming smaller time lags (< 0.1 sec), good response is possible although not to the extent possible with other concepts. This type of pulsing in its most elementary form is simple clock pulsing where the reaction jet is turned on and off at regular intervals by a timer as long as the error signal is exceeded.

3) Pseudo-Rate Pulsing. Rather than use a logic to establish a particular pattern of switching in relation to an error signal, this concept provides a lead signal for reaction jet turnoff. A lagged feedback around the reaction jet switch acts as an integration for short periods of time providing a pseudo-rate signal. Because this signal does not pass through any sensors or actuators but is fed directly around the switch, it can compensate for lags and delays in those components. Because the sum of the attitude and pseudo-rate signal forms an exponential switching line, the interception of this switching line by the vehicle acceleration parabola on the phase plane produces pulsed operation of the reaction jets. This pulsing yields a pulse width and frequency modulation which provides sufficient damping to make this concept stable without rate information.

The theory and operation of this stabilization concept are derived from Figure 2-52. Consider the feedback around the jet relay controller. Assuming the vehicle acceleration constant is known, the output of the gain adjustment is $\ddot{\theta}'$. The compensation H should be ideally an integration to give a pseudo-signal. This mechanization would tend to drift to a saturated condition.

Thus, the preferred form for the compensation is

$$H = \frac{\tau}{\tau S + 1}$$

The use of a time constant rather than an integration tends to degrade the effectiveness of the pseudo-rate signal. Analysis so far shows that acceptable stability is achieved with time constants less than five seconds. Performance is also satisfactory with long time constants. The system tolerates variations in this time constant from 5 to 60 seconds. The longer time constants are better for control in the limit cycle but, generally, poorer during acquisition.

Figure 2-53 illustrates some of the system characteristics. The vehicle starts with an initial value $\dot{\theta}_o$. At point 1 the jets are turned on. The switching line is as shown asymptotically approaching its maximum value. At the switch-off point, the vehicle returns at the rate $\dot{\theta}_r$; and the pseudo-rate signal decays toward zero. The jets will turn on again at point 3, for example, if the pseudo-rate signal has decayed such that the sum of attitude and pseudo-rate is greater than the deadband. Thus, the rate decay establishes the minimum overshoot velocity $\dot{\theta}_r$. The more rapid the decay, the higher the return velocity. Note that, if a pure integration compensation could be used, very small drift velocities could be obtained.

The basic mechanization of this concept is illustrated in Figure 2-54. A DC error signal is fed through a network which establishes the deadband, and is then summed with the pseudo-rate signal. The total signal is chopped, amplified, and fed into a phase detector to excite the proper ON-OFF jet switch. The output from each switch is fed through a filter which generates the pseudo-rate signal. A DC bias sets the operating point of the switch while an AC dither minimizes the switching hysteresis.

This concept provides a very satisfactory method of lag compensation with high reliability because of its simplicity of mechanization. It provides excellent flexibility through ease of varying parameters to satisfy a wide range of operating conditions.

4) Error Pulsing Without Rate Information. This method of control logic is based on the principles used in the "orbit mode" on Mercury shown in Figure 2-55. The mechanization provides improvement in performance and flexibility over the present Mercury system. For example, it will handle the problem of erratic (intermittent) jet operation by supplying a great number of pulse commands with increasing time durations. As many as 4000 pulses can be supplied over a 40-volt error signal variation.

This concept, shown in Figure 2-55, uses a series of switching lines to command different pulse widths on crossing, up to a final line at which the jets are full-on. The switching lines are actuated only for an increasing error signal. This forces the switching lines to be present in only the first and third quadrants of the phase plane. A further restriction on the attitude error pulsing scheme is that the impulse bit on any switching line must not be greater than the sum of the previous pulses. Gaylord and Keller of STL analyzed this control logic in an ARS paper, 1921-61.

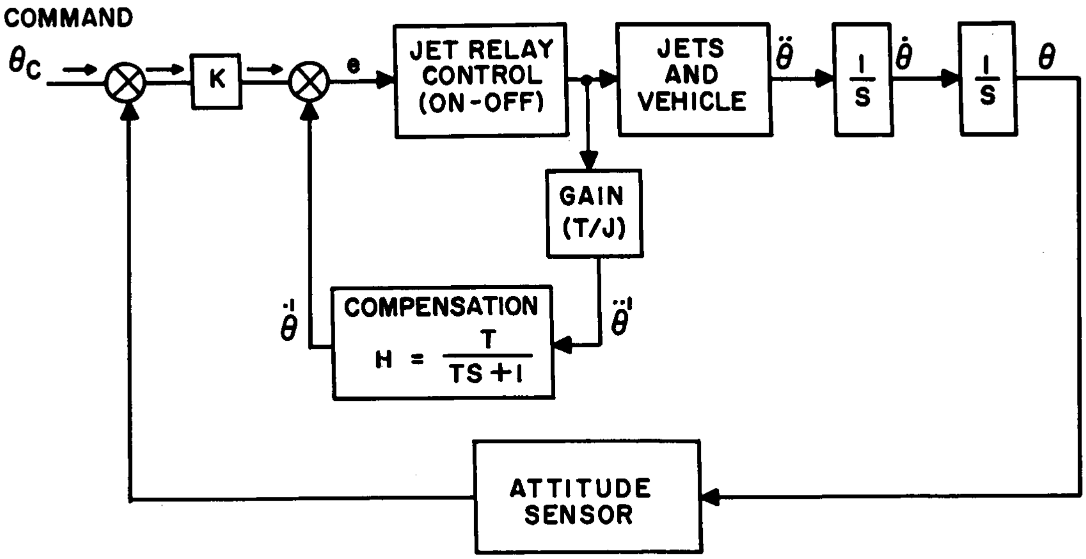
COMMAND
θ_C
K
e
JET RELAY CONTROL (ON-OFF)
JETS AND VEHICLE
$\ddot{\theta}$
$\frac{1}{S}$
$\dot{\theta}$
$\frac{1}{S}$
θ
GAIN (T/J)
COMPENSATION
$H = \frac{T}{TS+1}$
$\dot{\theta}'$
$\ddot{\theta}'$
ATTITUDE SENSOR

Figure 2-52. Block Diagram-Attitude Control System with Pseudo-Rate Compensation

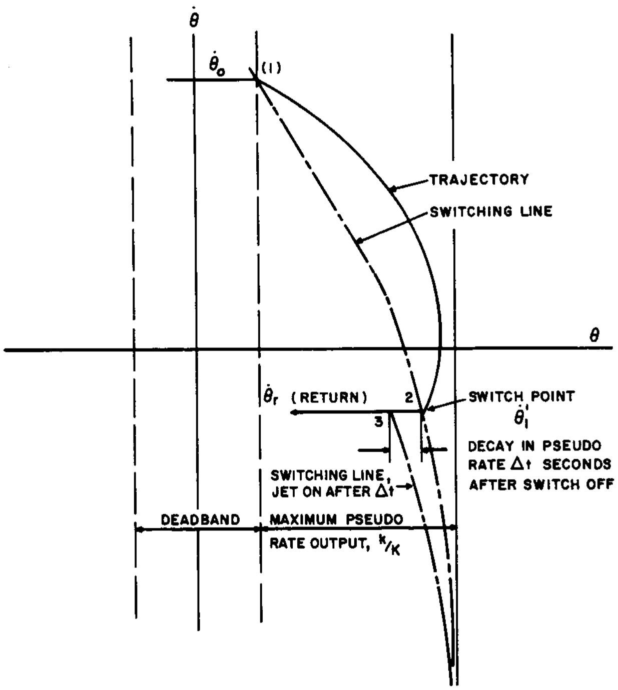
$\dot{\theta}$
$\dot{\theta}_o$
(1)
TRAJECTORY
SWITCHING LINE
θ
$\dot{\theta}_r$ (RETURN)
2
3
SWITCH POINT
$\dot{\theta}_1'$
DECAY IN PSEUDO RATE Δt SECONDS AFTER SWITCH OFF
SWITCHING LINE, JET ON AFTER Δt
DEADBAND
MAXIMUM PSEUDO RATE OUTPUT, $^k/_K$

Figure 2-53. Characteristic Switching Line Established by the Sum of Attitude and Pseudo-Rate

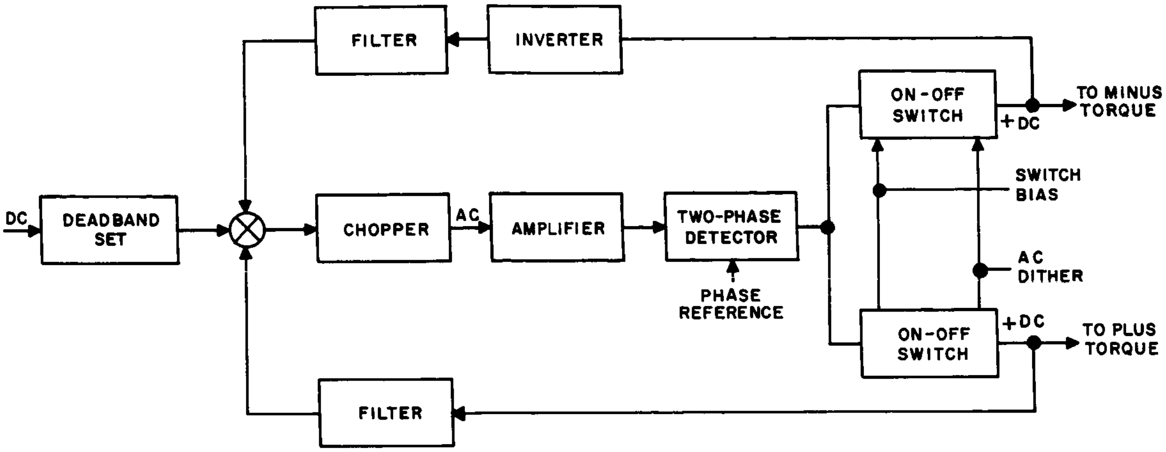
FILTER
INVERTER
ON-OFF SWITCH
+DC
TO MINUS TORQUE
SWITCH BIAS
DC
DEADBAND SET
CHOPPER
AC
AMPLIFIER
TWO-PHASE DETECTOR
PHASE REFERENCE
AC DITHER
ON-OFF SWITCH
+DC
TO PLUS TORQUE
FILTER

Figure 2-54. Clock Diagram for Pseudo-Rate Mechanization

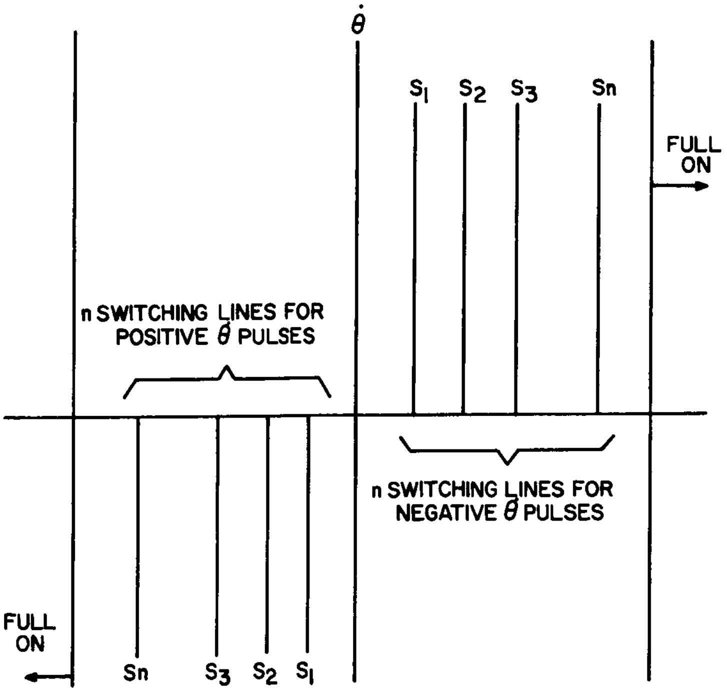
$\dot{\theta}$
S_1
S_2
S_3
Sn
FULL ON
n SWITCHING LINES FOR POSITIVE θ PULSES
n SWITCHING LINES FOR NEGATIVE θ PULSES
FULL ON
Sn
S_3
S_2
S_1

Figure 2-55. Phase Plane Diagram of Mercury System Switching Lines

Figure 2-56 is a typical phase plane trajectory obtained from an analog computer simulation. The vehicle starts with an initial rate of 5°/sec. The trajectory extends into the full-on region, the jets finally shutting off upon entering the "no pulse" region in the fourth quadrant. This is the primary performance difference between this stabilization logic and the pseudo-rate logic because the pseudo-rate logic permits pulsing in any quadrant. This, however, does not result in any particular advantage of the pseudo rate over the error pulsing scheme.

The Mercury mechanization contemplated can provide a large number of pulses in the pulsing region. This has been found to give better performance than that of a logic having only a few pulses. However, the pseudo-rate system can be mechanized with about half as many parts as the Mercury system; thus, it has a reliability advantage.

Minneapolis-Honeywell research has found that both the advanced Mercury and pseudo-rate compensation techniques provide very satisfactory convergence and limit cycle control. Both are also stable without rate information. However, the pseudo-rate concept is suggested because its inherent reliability is better since reliability will be a prime consideration in the SMS mission.

d. Application of Pseudo Rate to SMS

1) Introduction. While extensive study has been accomplished by Minneapolis-Honeywell on use of pseudo-rate techniques, each application must be considered separately insofar as optimization is concerned. This section describes the factors to be considered in optimizing this technique for the acquisition and limit cycling of the SMS.

2) Acquisition Mode. Figures 2-57 through 2-60 were obtained from an analog computer simulation of a pseudo-rate control system with rate information available. Figure 2-61 shows a simple on-off control for comparison. The SMS is characterized by a lower torque/inertia ratio (acceleration level) than any vehicle to which pseudo-rate has as yet been applied. Figure 2-57 illustrates the effect of vehicle control acceleration. The highest acceleration (Figure 2-57) results in less fuel converging to the limit cycle but, of course, the limit cycle fuel consumption will be higher. The lowest acceleration level (Figure 2-57) takes more time to converge and results in more pulsing (note difference in scale of graph). The limit cycle shown could be reduced by reducing switching hysteresis.

The system shown in Figure 2-57 had not been optimized for any particular operating mode. Figures 2-58 and 2-59 show what can be done in the way of parameter variation for system optimization. Figure 2-58 indicates the effect of varying the pseudo-rate time constant. Increasing the time constant provides a closer approximation to a pure integration and, in doing so, increases the rate of convergence. The Apollo and Gemini control systems use time constants in the vicinity of 1 and 15 seconds, respectively, while Jet Propulsion Labs, in the Mariner Program, is considering time constants of 5 to 60 seconds. However, increasing the pseudo-rate time constant, while desirable for damping, increases the lag in response to the attitude sensor output. This is undesirable when attempting to achieve acquisition. The attitude bias produced during the steady state limit cycle by disturbance torques, as discussed later, is also increased.

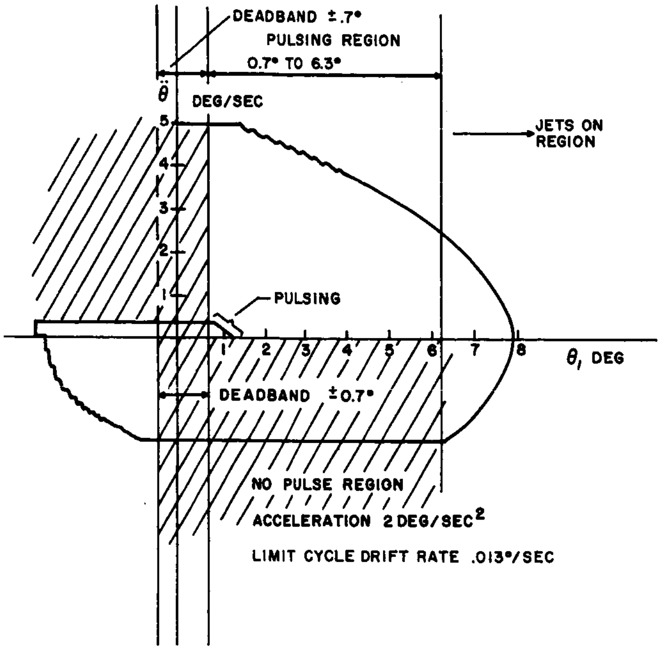

Figure 2-56. Typical Trajectory - Mercury Type Switching Logic

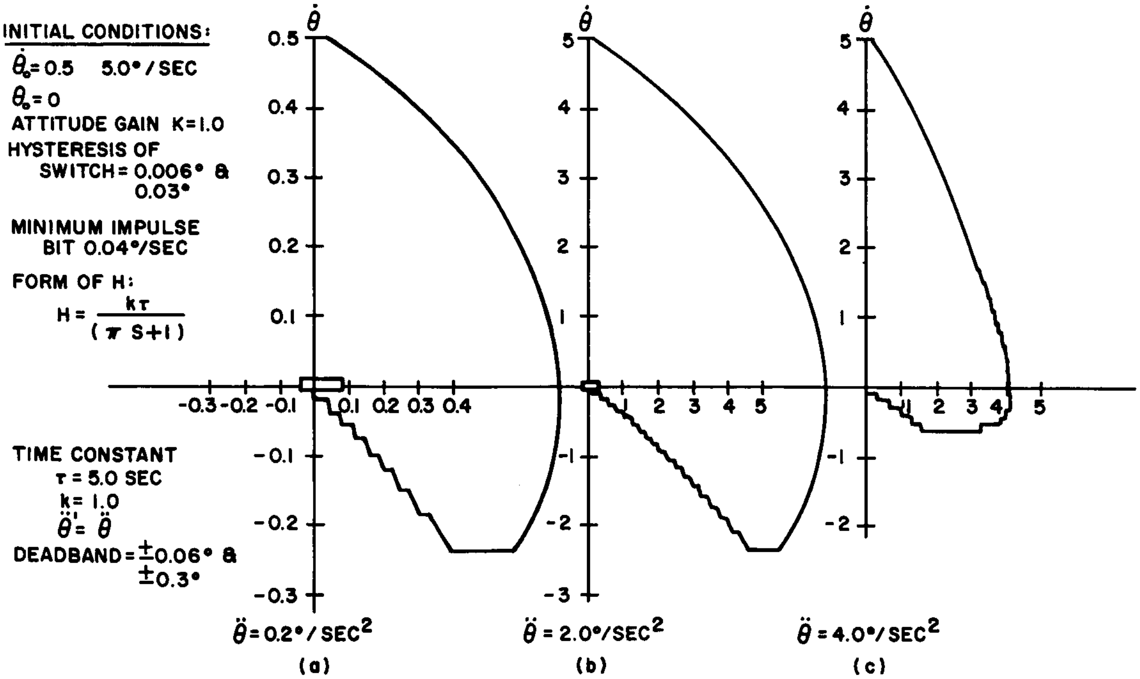

Figure 2-57. Phase Plane Diagram of Pseudo-Rate Control System for Different Values of Acceleration

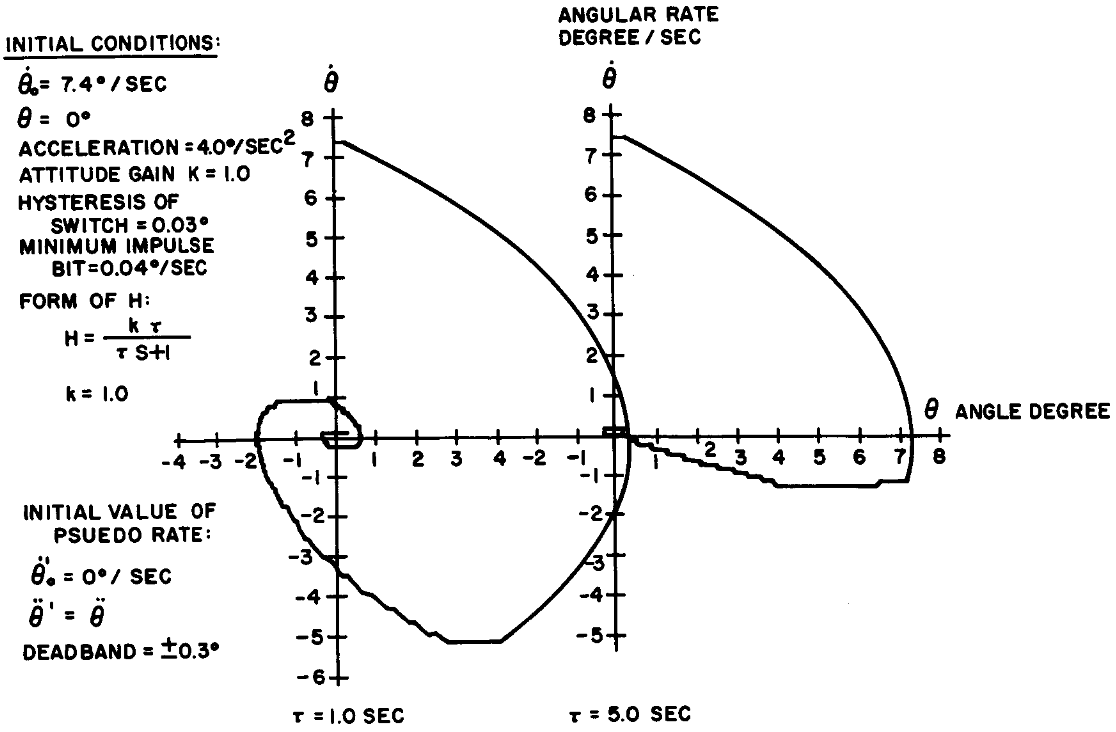

Figure 2-58. Phase Plane Diagram of Pseudo-Rate Control System for Different Values of Time Constant

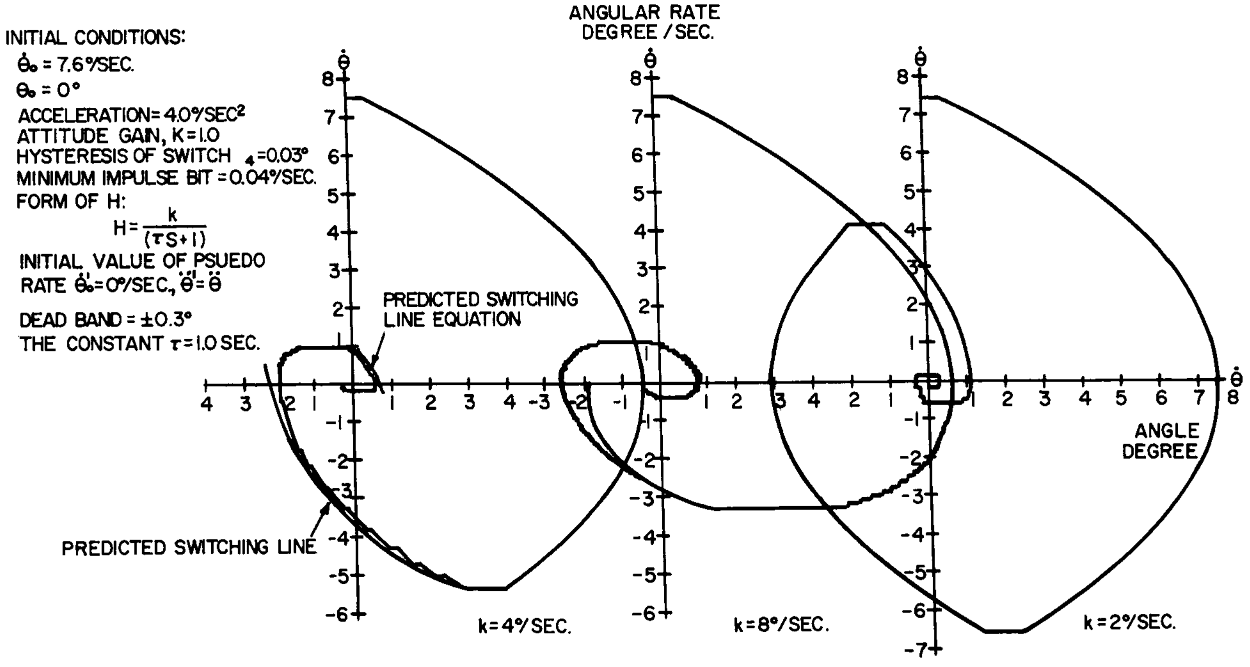

Figure 2-59. Phase Plane Diagrams of Pseudo-Rate Control System for Different Values of Gain (K)

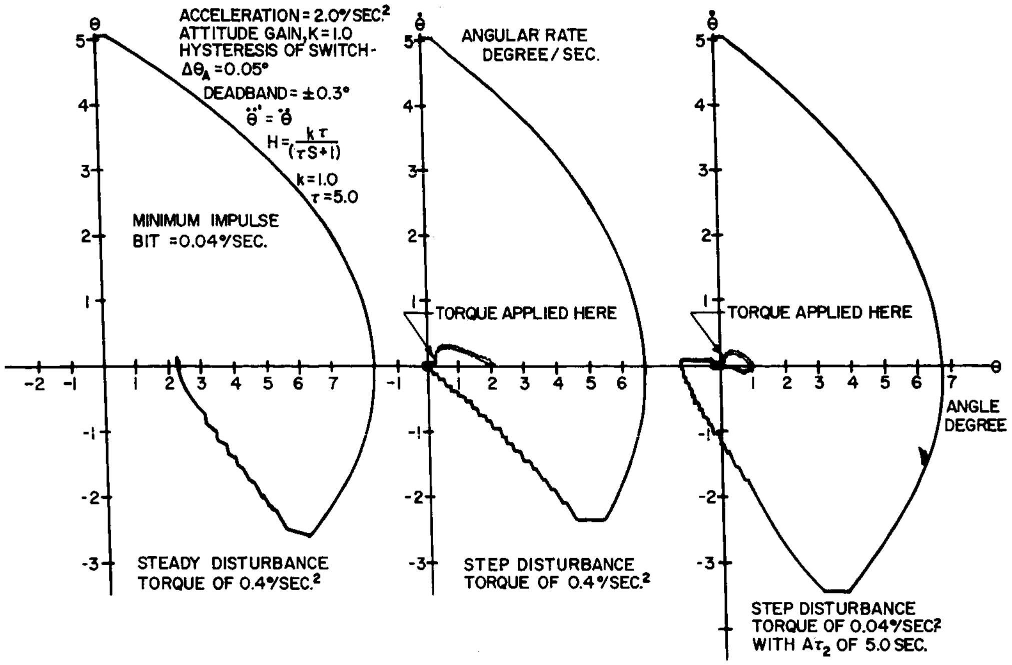

Figure 2-60. Phase Plane Diagram of Pseudo-Rate Control System with Disturbance Torques

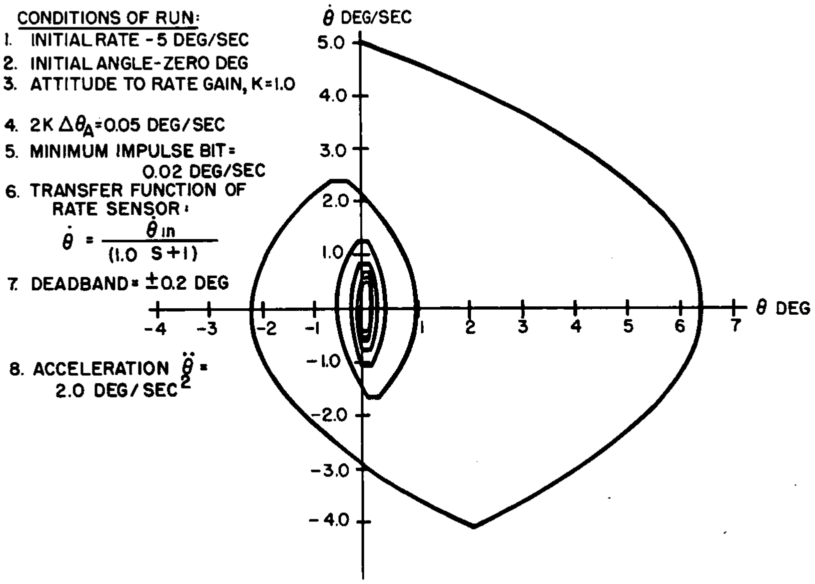

Figure 2-61. Phase Plane Diagram of Simple ON-OFF Control System

The above discussions have assumed the use of rate information during convergence. However, the pseudo-rate compensation method is stable without rate information and, therefore, the use of rate gyros may be eliminated during acquisition and/or reacquisition. Limit cycle operation is essentially unchanged. Acquisition of the limit cycle from large rate or attitude errors, however, becomes very lightly damped. In the SMS, this would mean that acquisition may take in excess of one hour (depending upon the initial rate of attitude error assumed). Also, fuel consumption will increase considerably--possibly by a factor of five. Variation of the pseudo-rate time constant from acquisition to limit cycle is a possibility. This method of acquisition, including the design of sensor output, is presently under consideration by Jet Propulsion Labs and is discussed in Ref. 2-2.

Figure 2-59 shows the effect of varying the pseudo-rate gain which is the inverse of switching line slope. For every system, an optimum value of pseudo-rate gain exists--this is shown by Figure 2-60(a). This demonstrates better convergence (and less fuel consumption) than the slightly lower and higher values of acceleration shown in Figures 2-60(b) and 2-60(c). If the pseudo-rate gain is too low, the system stays full-on too long before beginning to pulse and, consequently, requires an excess number of cycles in converging. If gain is too low, convergence is likewise slow. Because the pseudo-rate gain is in the feedback of the switch, its effect is to lower overall system loop gain and thereby the acceleration capability of the system for a given attitude error. Too high a value of pseudo-rate gain causes the system to pulse excessively and go through large attitude excursions with damping from some initial attitude or rate error.

3) Limit Cycle Operation. As discussed previously, an optimum pseudo-rate system for acquisition may not be optimum for limit cycle operation. The constraints in the limit cycle mode are minimum impulse bit, attitude sensor lag, and disturbance torque level. The minimum impulse bit decreases with increased pseudo-rate gain. Large attitude sensors (such as associated with horizon scanners) require larger pseudo-rate lag time constants for stability and, likewise, higher pseudo-rate gain. The bias effect of a disturbance torque is increased by having a large pseudo-rate time constant. This bias effect is shown in Figure 2-60 for steady-state and step-disturbance torques. The effect is somewhat exaggerated here because the magnitude of the disturbance torque in relation to the control torque is much greater than would be expected for the SMS. However, the system builds up an attitude bias proportional to any steady torque, as shown. Bias due to gravity gradient is estimated for the control parameters given in Figure 2-60 and an Earth orbit (400 miles) to be equal to

(1) Bias ~ 0.7 arc second per degree of angle with respect to local vertical.

(2) Maximum bias ~ 40 arc seconds for a 45-degree angle.

The same values computed for 4,000 miles are

(1) Bias ~ 0.01 arc second per degree.

(2) Maximum bias ~ 7 arc seconds for a 45-degree angle.

For greater distances the value becomes too small to consider.

A transition disturbance will have no effect in the deadband region. It will only effect the system at or near the regions where the jets fire as follows. If the disturbance moves the vehicle such that a dwell time beyond the deadband is longer than the pulsing rate, more than one pulse will occur while the vehicle is turning around.

e. Reaction Jet Characteristics in Pulsed Mode Operation

1) Introduction. When used in a pulsed mode of operation, reaction jet characteristics change from those expected in the usual on-off application where they function in relatively long bursts. In the pulsed mode, the effect of jet delays on the limit cycle must be considered as well as variation in I_{sp} produced by operation under transient rather than steady state conditions. Details on some common reaction jet types are given below.

2) Cold Gas. The present state of the art for the solenoids used with cold gas jets gives a transport delay, on opening and closing, as low as 3 milliseconds for low thrusts. The rise and decay time to be expected following solenoid opening or closing are about 1.5 ms. At Minneapolis-Honeywell the lowest thrust used in tests to date has been 0.001 lbs with a minimum impulse bit of 10^{-5} lb-sec. No information is available on loss of I_{sp} during operation but it is ex pected to be low due to the sharp response times and lack of a combustion process.

3) Liquid Hypergolics. It does not presently appear practical to attempt to obtain thrusts below approximately 0.1 lb using hypergolic liquids. This limit can be extended, however, by using hypergolic gases. Figure 2-62 illustrates the loss of I_{sp} that occurs when using hypergolics in the pulse mode. The case shown is for 100-lb thrust jets and may not be quite as dramatic for low thrust levels, but it does serve to indicate that this loss is to be considered in any type of reaction jet.

4) Hydrogen Peroxide. With the hydrogen peroxide reaction jets used in the Mercury Program, it was found that not only did I_{sp} decrease drastically with a decrease in pulse on-times (due to the transient nature of the reaction) but it also dropped off with increasing time between pulses. This was due to drop off in catalyst bed temperature. For pulse off times in the order of several hundred ms long, as much as a 50% drop in I_{sp} can be expected. This effect is also obviously related to the on-time; because on-time builds up the catalyst bed temperature. I_{sp} also can be expected to drop off as pulse length is decreased.

Transient times are exceptionally large also for hydrogen peroxide jets. Time to achieve full thrust may vary from approximately 50 ms to in excess of 100 ms again depending on catalyst bed temperature.

5, Gravity Gradient Controller

a. Introduction

The problem of using the gravitational attraction of the Earth to control a space vehicle has previously been studied by many investigators where the small angle expression for gravity gradient restoring torque has been expressed in the orbital coordinate system as

$$\vec{T}_{R_o} = \begin{bmatrix} -3\omega_o^2 (I_{yy} - I_{zz})\phi \\ -3\omega_o^2 (I_{xx} - I_{zz})\theta \\ 0 \end{bmatrix} \tag{2-41}$$

where $\vec{T}_{R_o}$ is the vehicle restoring torque.

Transformation of Eq 2-41 into vehicle body coordinates yields

$$\vec{T}_{R_B} = \begin{bmatrix} -3\omega_o^2 (I_{yy} - I_{zz})\phi \\ -3\omega_o^2 (I_{xx} - I_{zz})\theta \\ -3\omega_o^2 (I_{yy} - I_{xx})\phi\theta \end{bmatrix} \tag{2-42}$$

The vehicle configuration is shown in Figure 2-63. If the system is assumed to be a pair of point masses M, the system inertia is seen to be

$$I_v = M \begin{bmatrix} z^2 + y^2 & 0 & 0 \\ 0 & z^2 + x^2 & 0 \\ 0 & 0 & x^2 + y^2 \end{bmatrix} \approx M \begin{bmatrix} 4r^2 & 0 & 0 \\ 0 & 4r^2 & 0 \\ 0 & 0 & 0 \end{bmatrix} = \begin{bmatrix} I & 0 & 0 \\ 0 & I & 0 \\ 0 & 0 & 0 \end{bmatrix}$$

The simplified dynamic equations which define three single-axis undamped systems are of the form

$$\begin{aligned} I\ddot{\phi} &= -3\omega_o^2 I\phi \\ I\ddot{\theta} &= -3\omega_o^2 I\theta \\ I\ddot{\psi} &= 0 \end{aligned} \tag{2-43}$$

which are seen to be undamped in ϕ and θ.

b. Vehicle Control System Analysis

The control loop of Figure 2-64 can be used to provide pitch and roll damping where the vehicle rate is sensed by a rate gyro. The rate signal drives a reaction wheel system to damp vehicle oscillations induced by external disturbances. In this simplified analysis, the gyro and reaction wheel dynamics are neglected since basic performance capability is the objective.

The transfer function of attitude angle to disturbance torque is given by

$$\frac{\theta}{D}(s) = \left(\frac{1}{I}\right)\left[\frac{1}{S^2 + 2L\omega_n S + \omega_n^2}\right] \tag{2-44}$$

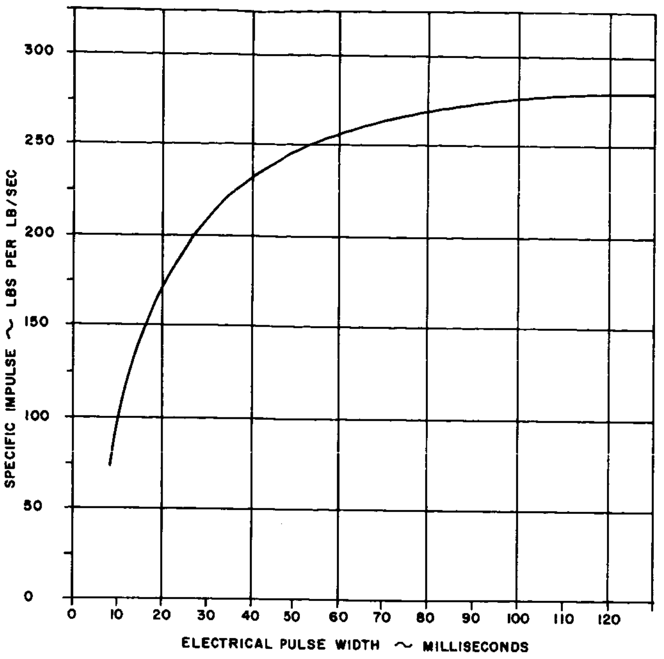

Figure 2-62. Loss of Specific Impulse vs Pulse Size

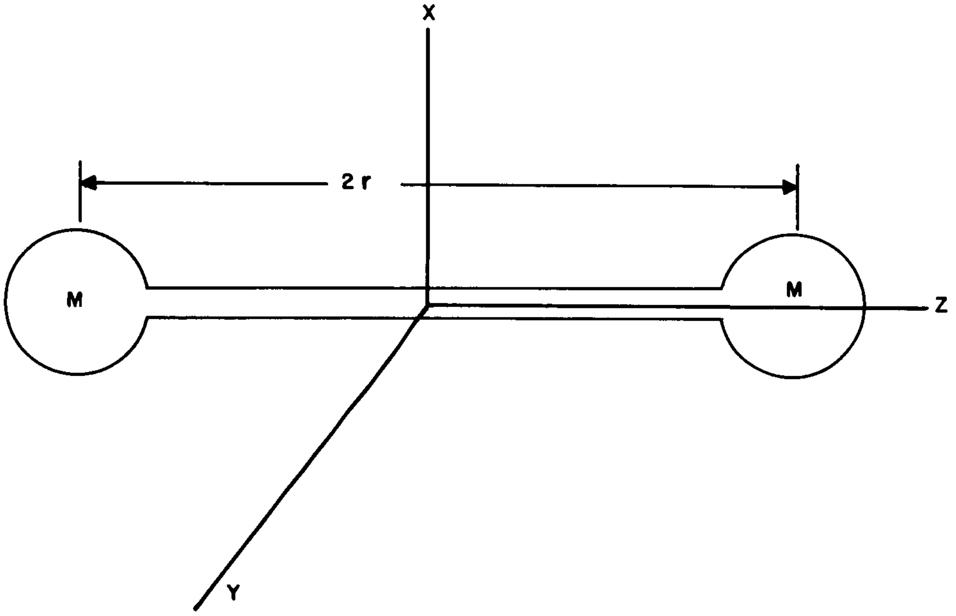

Figure 2-63. Typical System Configuration for a Gravity Gradient Controlled Space Vehicle

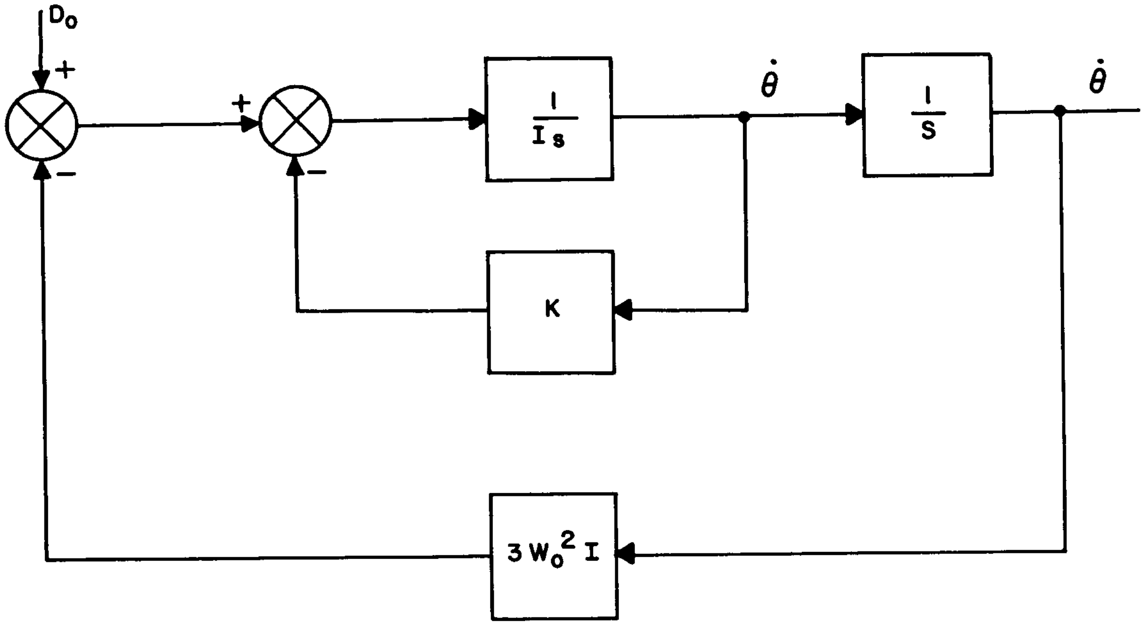
D_o
+
+
−
−
$\frac{1}{Is}$
$\dot{\theta}$
$\frac{1}{s}$
θ
K
$3W_o^2I$

I = VEHICLE INERTIA (IN-LB-SEC^2)
θ = VEHICLE HANGOFF (RAD)
$\dot{\theta}$ = VEHICLE RATE (RAD/SEC)
K = RATE LOOP GAIN (IN-LB-SEC/RAD)
W_o = ORBITAL ANGULAR VELOCITY (7.27×10^{-5} RAD/SEC)
D_o = EXTERNAL DISTURBANCE TORQUE (IN-LB)

Figure 2-64. Single Axis Pitch, Roll, Gravity Gradient Control Loop

where

$$\omega_n = \sqrt{3}\,\omega_o$$

$$= K/2\sqrt{3}\,\omega_o I \qquad (2\text{-}45)$$

For a damping ratio L = 0.65, the time response of Eq 2-44 for a constant disturbance D_o/s is

$$\theta(t) - \frac{D_o}{3\omega_o^2 I}\left[1 - 1.32\, e^{-0.65\omega_o t} \sin(1.32\,\omega_o t + 0.274\pi)\right] \qquad (2\text{-}46)$$

The steady state response of Eq 2-46 is given by

$$\theta_{ss} = \frac{D_o}{3\omega_o^2 I}$$

$$\dot{\theta}_{ss} = 0 \qquad (2\text{-}47)$$

Similarly, for a sinusoidal input

$$\theta_{ss} = \frac{D_o}{3\omega_o^2 I}$$

$$\theta_{ss} = \frac{D_o}{3\omega_o I} \qquad (2\text{-}48)$$

Three vehicles of masses M_1 = 3.11 slugs, M_2 = 15.55 slugs, and M_3 = 31.10 slugs have been considered. Figures 2-65a through 2-65f, 2-66a through 2-66f, and 2-67a through 2-67f, represent the parameters of Eqs 2-45, 2-46, 2-47, and 2-48 for each of the three vehicles, respectively.

On the basis of the simplified single axis equations of motion, with provision for auxiliary damping, the gravity gradient control concept for SMS appears feasible to the extent of meeting stabilization requirements. Advantages would be the apparent simplicity of control during Earth tracking (damping in pitch and roll with gyrocompassing for yaw control).

A detailed analysis of 3-axis coupling effects would be required to verify actual system performance. A recent contribution to gravity gradient satellite theory is presented in Ref 2-3. The result of that brief study indicates that an infinity of equilibrium orientations are possible with a dumbbell configuration. Reference 2-3 does not indicate the nature of these equilibrium states (i.e., stable or unstable). Additional investigations would be required to assess the implications of this infinity of equilibrium states and to explore the feasibility of using passive damping techniques that would be much more attractive than using active damping.

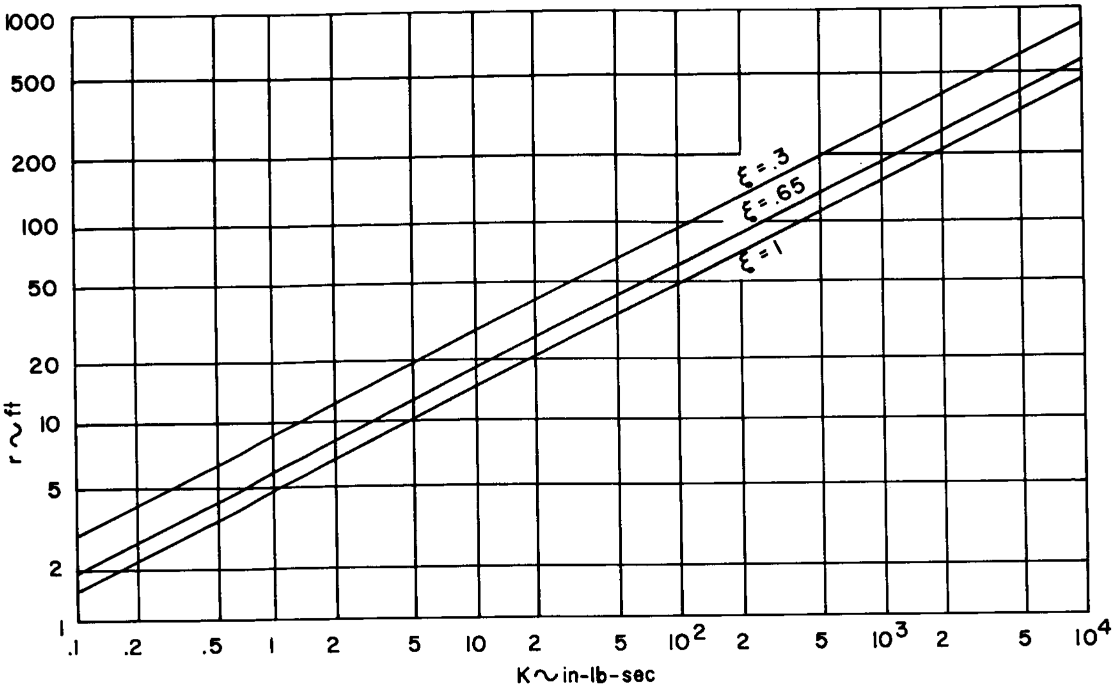

Figure 2-65a. Plot of Vehicle Length (r) vs Rate Loop Gain (K) for Various Values of Rate Loop Damping for Vehicle of Mass M_1 = 3.11 Slug

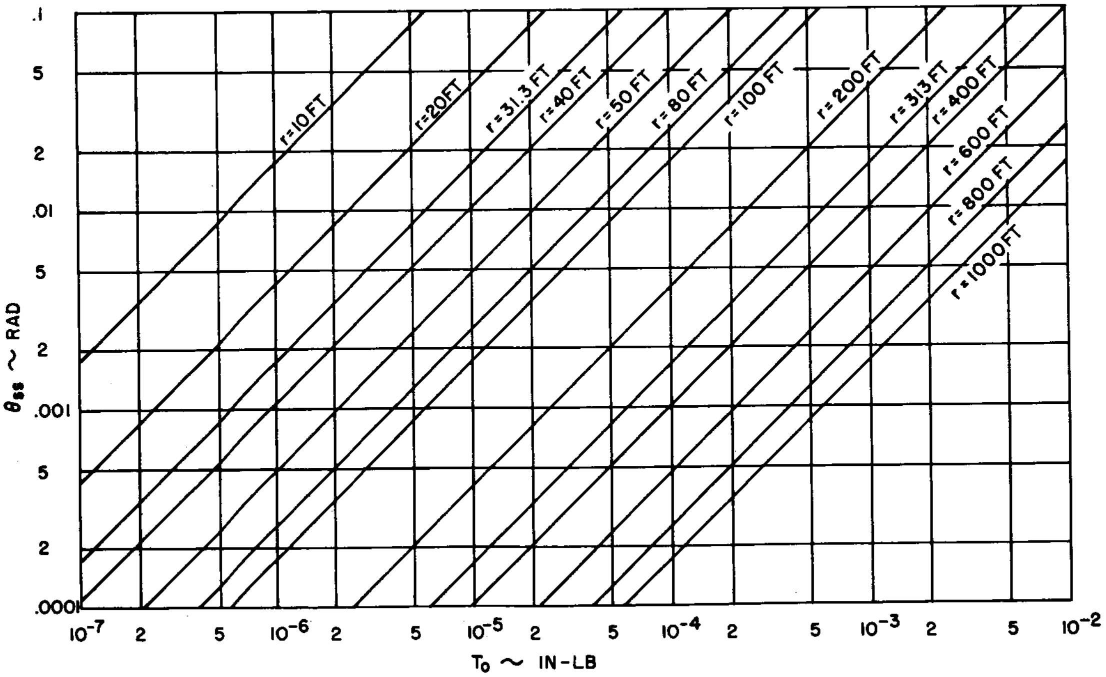

Figure 2-65b. Plot of Steady State Vehicle Attitude Error vs Constant Disturbance for Various Lengths of Vehicle of Mass M_1 = 3.11 Slug

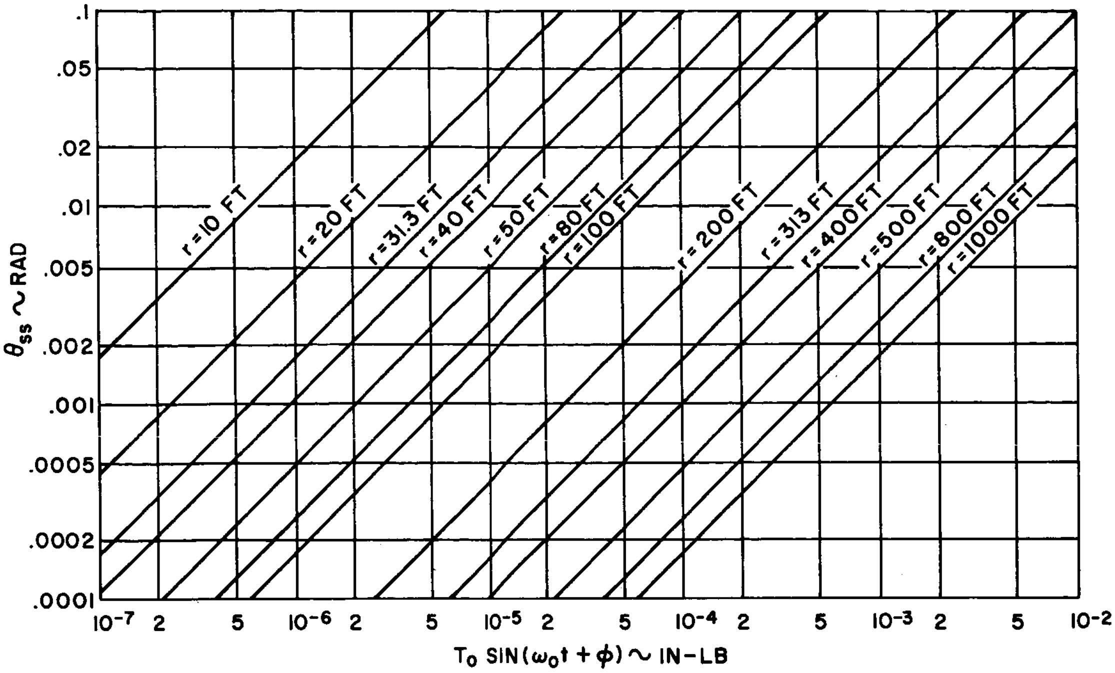

Figure 2-65c. Plot of Peak Vehicle Attitude Error vs Sinusoidal Disturbance Torque for Various Lengths of Vehicle of Mass M_1 = 3.11 Slug and Damping Coefficient $\xi = 0.65$

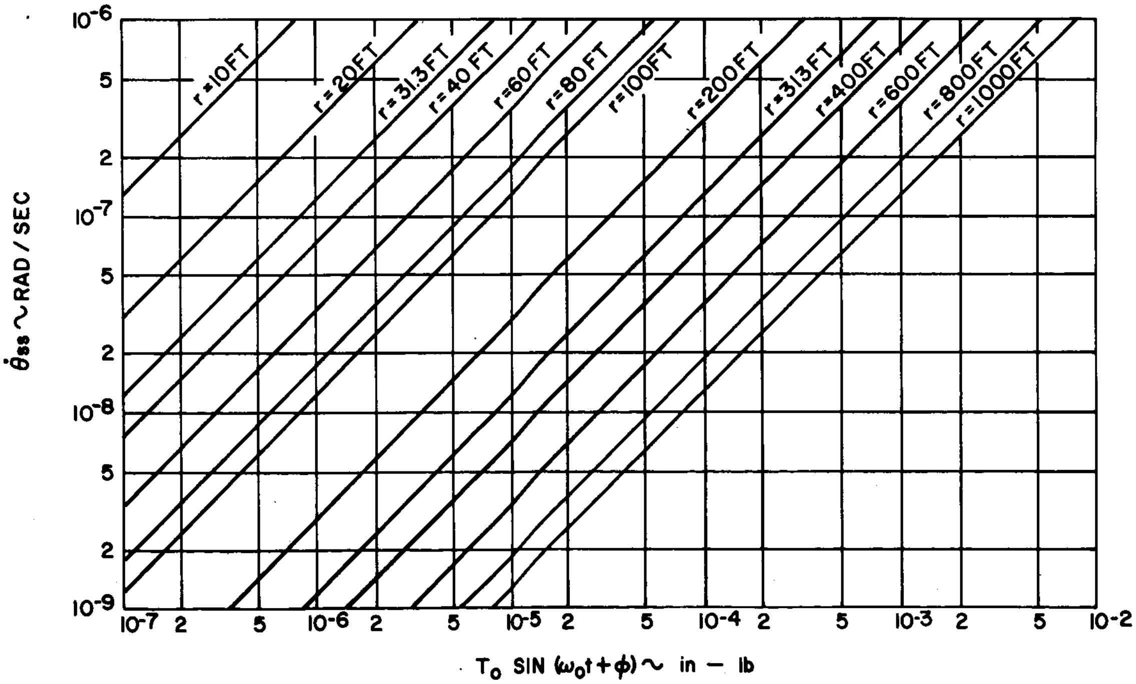

Figure 2-65d. Plot of Peak Vehicle Rate vs Sinusoidal Disturbance Torques for Various Lengths of Vehicle of Mass M_1 = 3.11 Slug and Damping Coefficient ξ=0.65

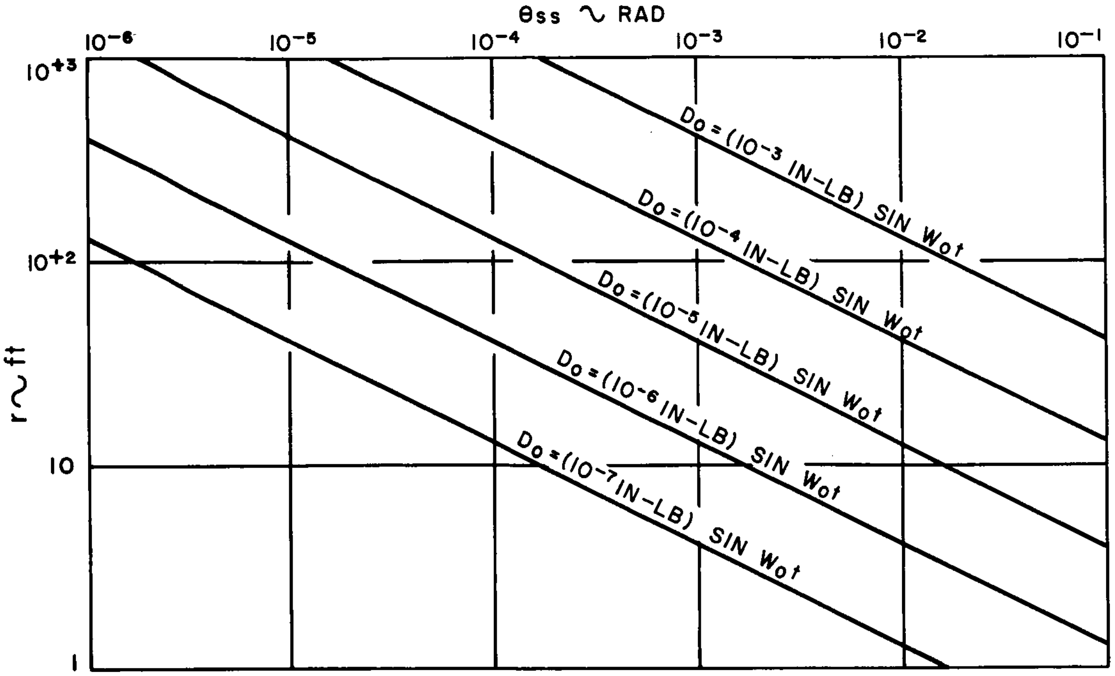

Figure 2-65e. Plot of Peak Vehicle Attitude Error vs Radius of Vehicle of Mass M_1 = 3.11 Slug and Damping Coefficient ξ = 0.65 for Various Sinisoidal Disturbance Torques

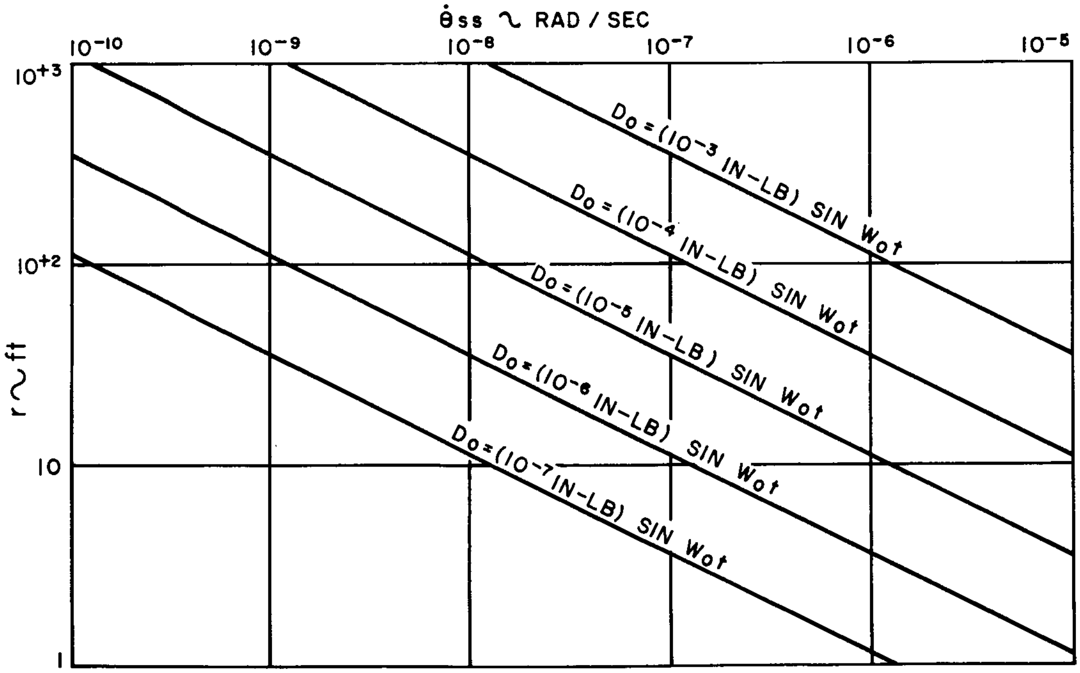

Figure 2-65f. Plot of Peak Vehicle Rate vs Radius of Vehicle of Mass M_1 = 3.11 Slug and Damping Coefficient ξ = 0.65 for Various Sinusoidal Disturbance Torques

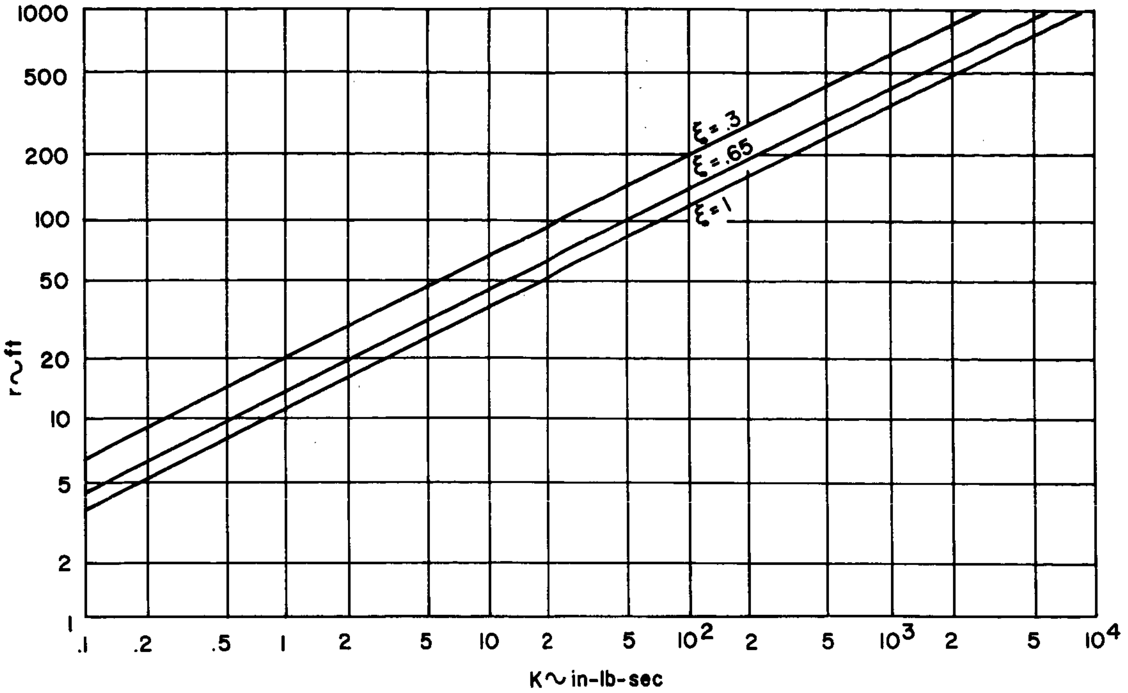

Figure 2-66a. Plot of Vehicle Length (r) vs Rate Loop Gain (K) for Various Values of Rate Loop Damping for Vehicle of Mass M_2 = 15.55 Slug

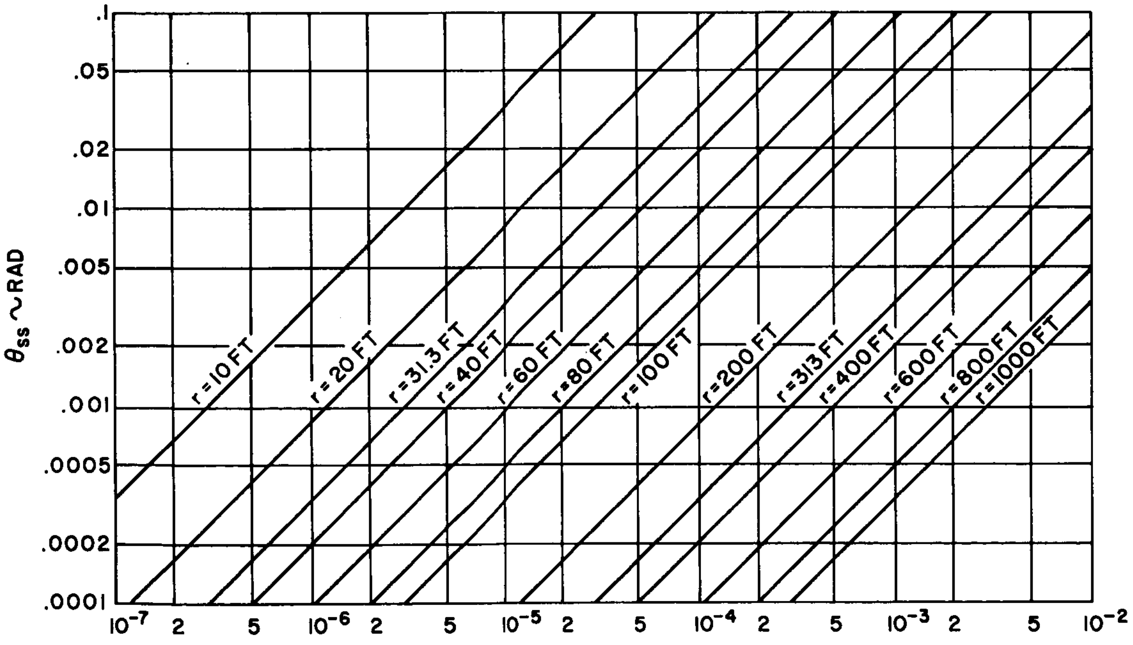

Figure 2-66b. Plot of Peak Vehicle Attitude Error vs Constant Disturbance for Various Lengths of Vehicle of Mass M_2 = 15.55 Slug

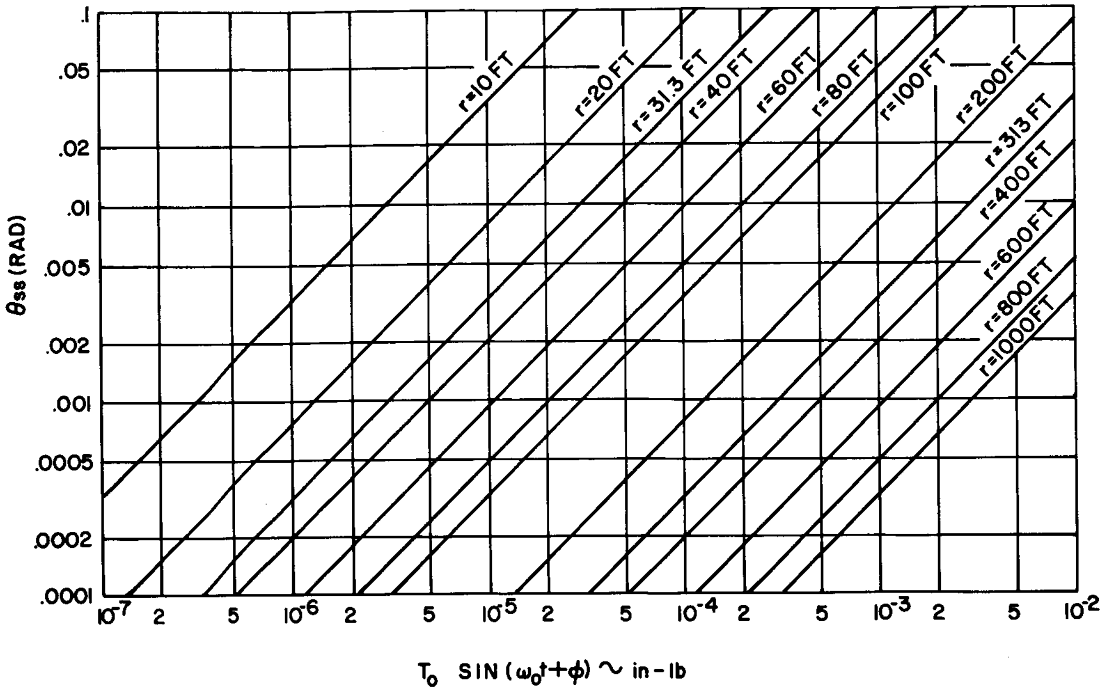

Figure 2-66c. Plot of Peak Vehicle Attitude Error vs Sinusoidal Disturbance Torque for Various Lengths of Vehicle of Mass M_2 = 15.55 Slug and Damping Coefficient of $\xi = 0.65$

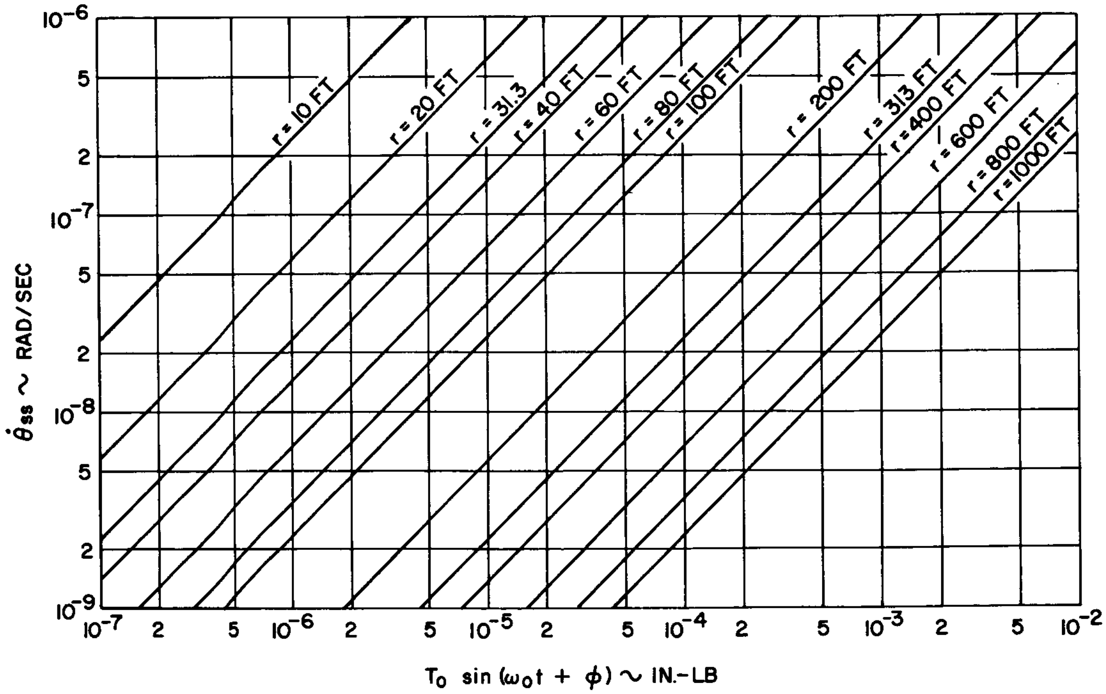

Figure 2-66d. Plot of Peak Vehicle Rate vs Sinusoidal Disturbance Torque for Various Lengths of Vehicle of Mass M_2 = 15.55 Slug and Damping Coefficient $\xi = 0.65$

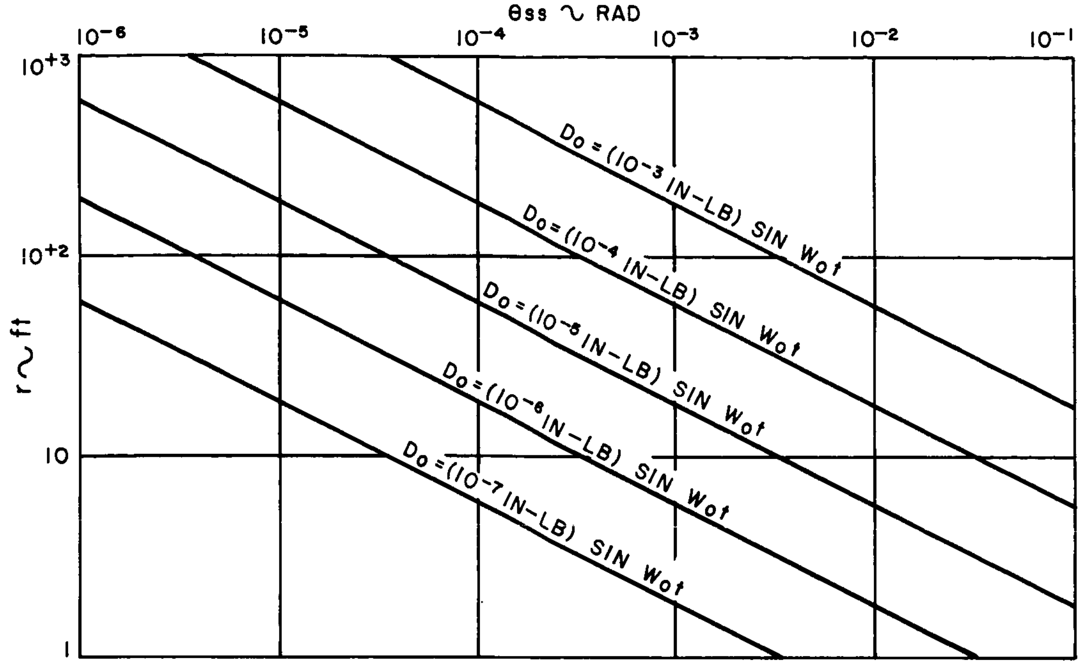

Figure 2-66e. Plot of Peak Vehicle Attitude Error vs Radius of Vehicle of Mass M_2 = 15.55 Slug and Damping Coefficient $\xi = 0.65$ for Various Sinusoidal Disturbance Torques

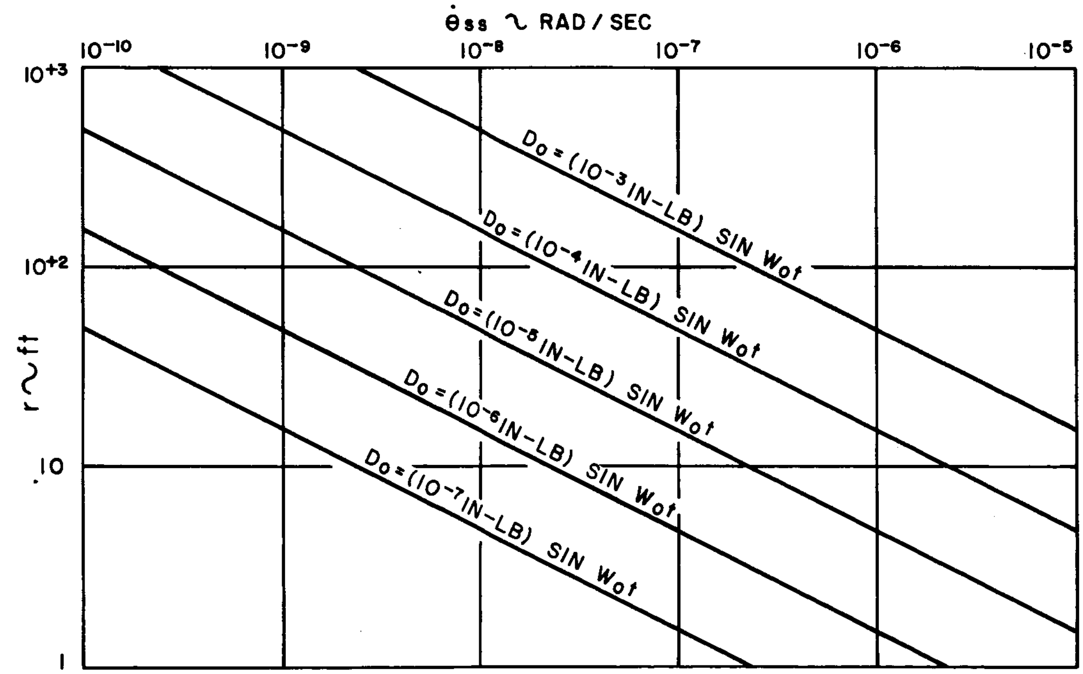

Figure 2-66f. Plot of Peak Vehicle Rate vs Radius of Vehicle of Mass M_2 = 15.55 Slug and Damping Coefficient $\xi = 0.65$ for Various Sinusoidal Disturbance Torques

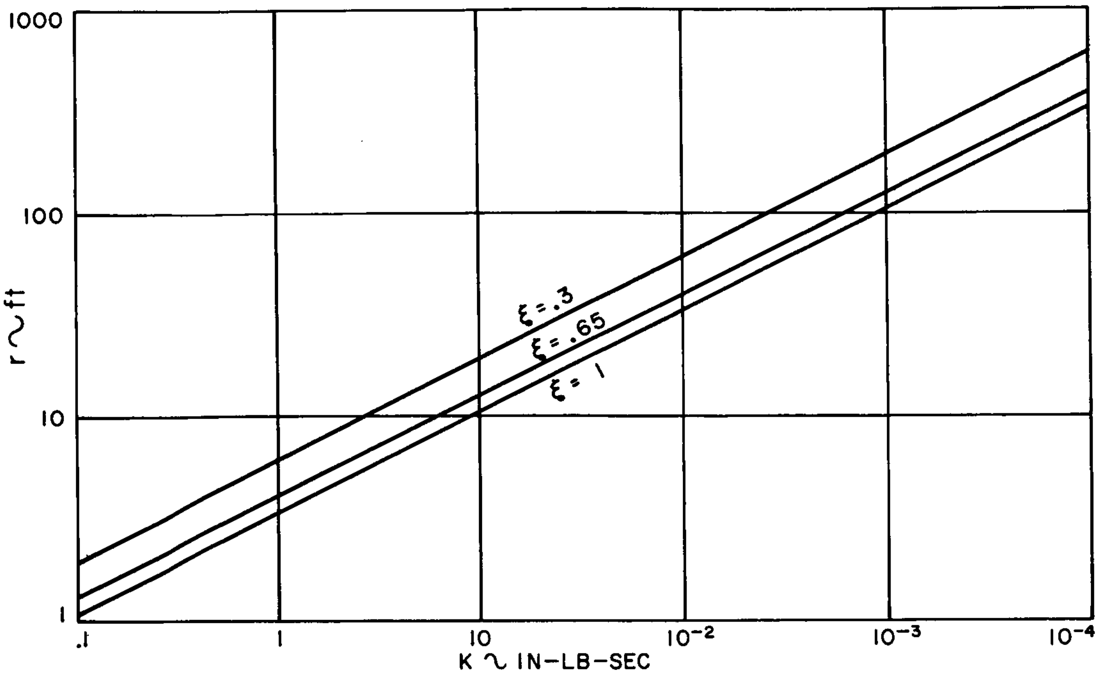

Figure 2-67a. Plot of Vehicle Length (r) vs Rate Loop Gain (K) for Various Values of Rate Loop Damping for Vehicle of Mass $M_3 = 31.10$ Slug

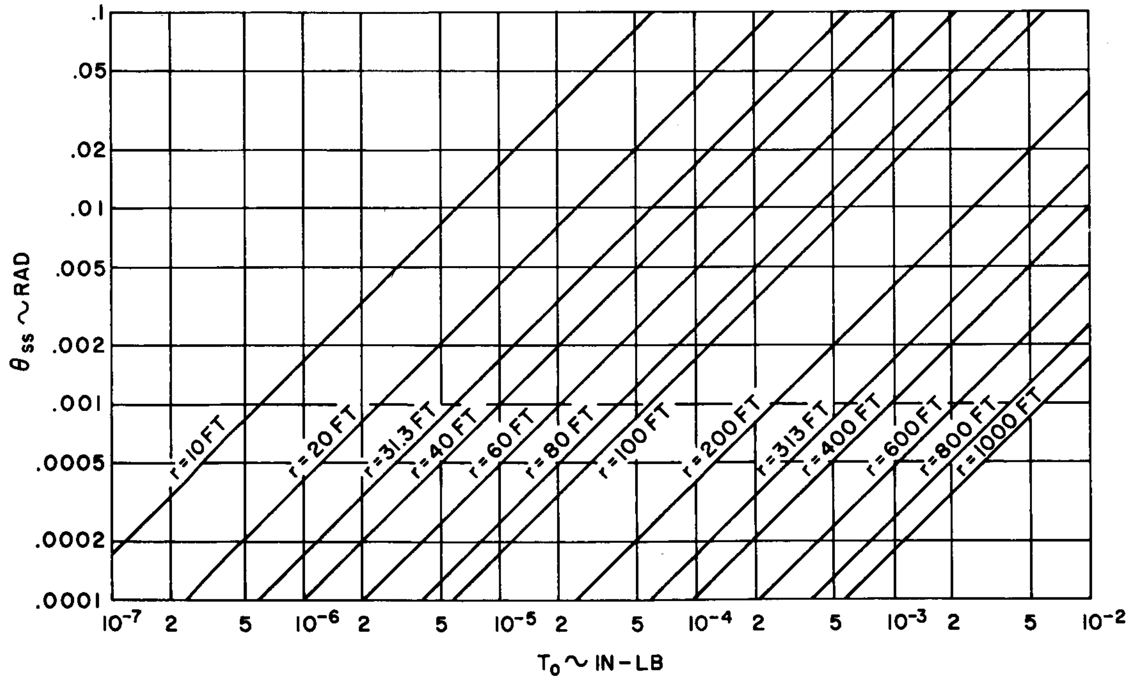

Figure 2-67b. Plot of Steady State Vehicle Attitude Error vs Constant Disturbances for Various Lengths of Vehicle of Mass $M_3 = 31.10$ Slug

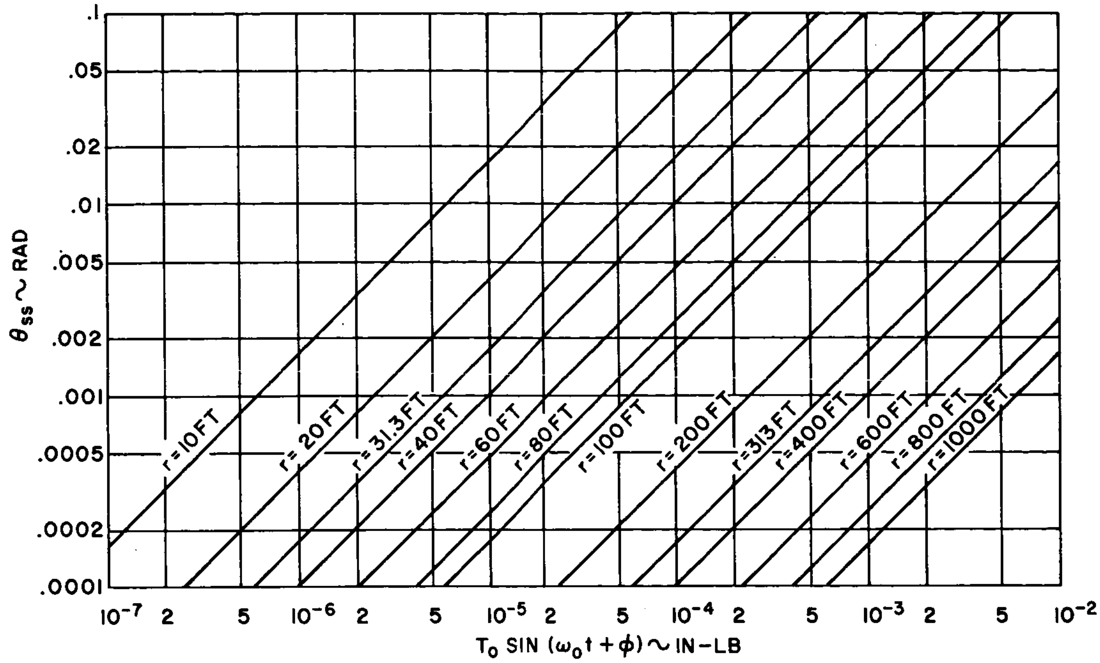

Figure 2-67c. Plot of Peak Vehicle Attitude vs Sinusoidal Disturbance Torques for Various Lengths of Vehicle of Mass M_3 = 31.10 Slug and Damping Coefficient ξ = 0.65

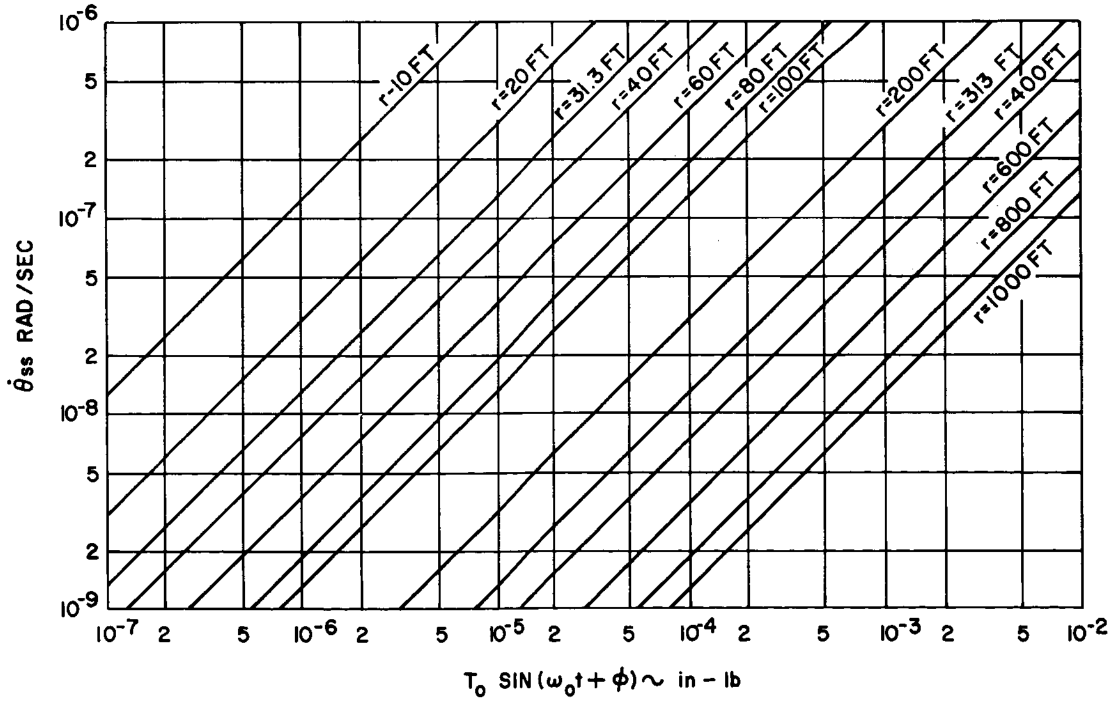

Figure 2-67d. Plot of Peak Vehicle Rate vs Sinusoidal Disturbance Torques for Various Lengths of Vehicle of Mass M_3 = 31.10 Slug and Damping Coefficient ξ = 0.65

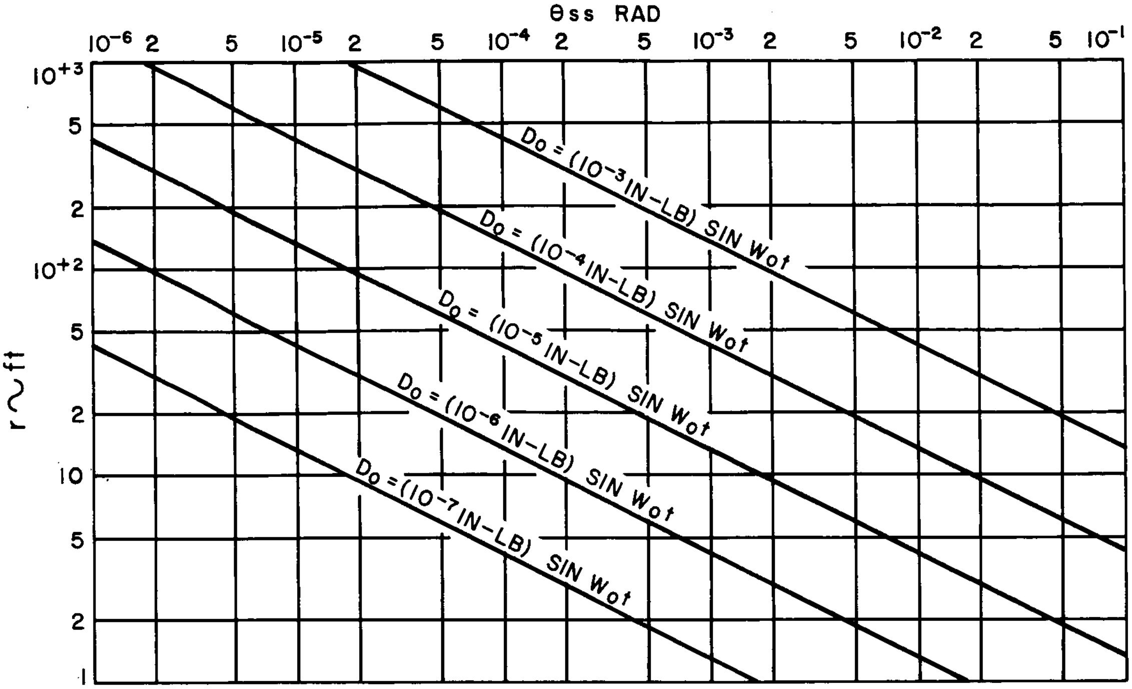

Figure 2-67e. Plot of Peak Vehicle Attitude Error vs Radius of Vehicle of Mass M_3 = 31.10 Slug and Damping Coefficient ξ = 0.65 for Various Sinusoidal Disturbance Torques

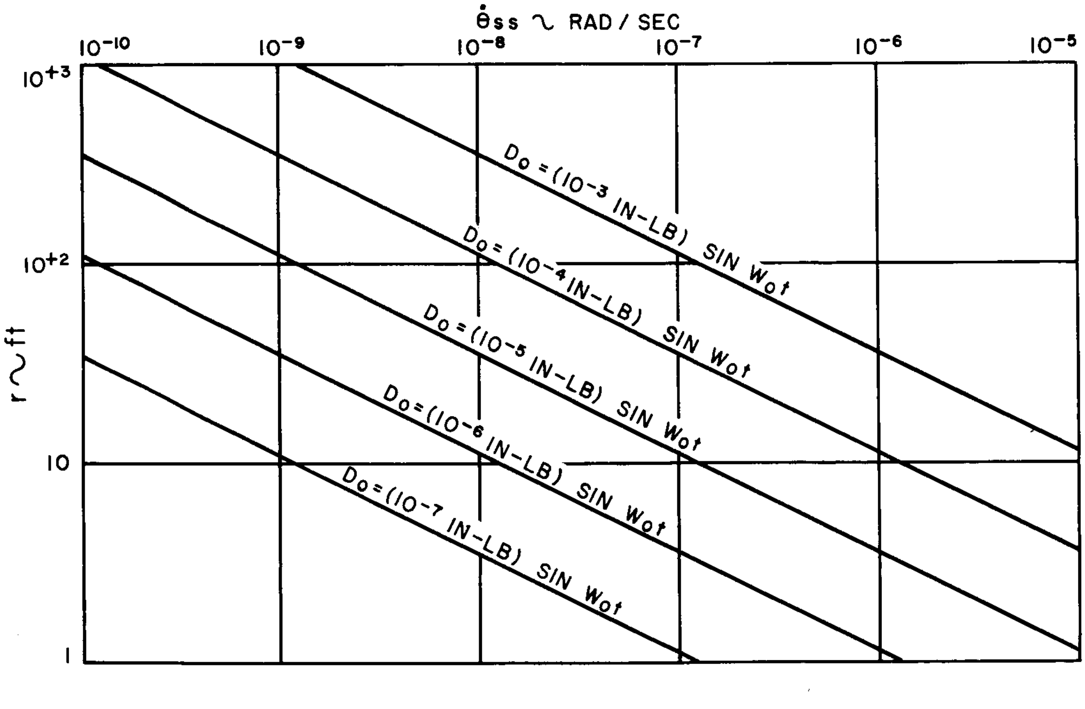

Figure 2-67f. Plot of Peak Vehicle Rate vs Radius of Vehicle of Mass M_3 = 31.10 Slug and Damping Coefficient ξ= 0.65 for Various Sinusoidal Disturbance Torques

6. Spin Controller

a. Introduction

Fundamentally, the control concept depends on the principle of nutation of a gyroscopic element when subjected to an impulsive torque. Figure 2-68 is a vector diagram showing the geometry of a complete control cycle. Initially, the spacecraft is spinning with angular momentum $\vec{H}_S$ and with its spin axis directed toward p_1; an impulse of momentum $\vec{\delta H}$ is applied at this time.

The impulse of momentum $\vec{\delta H}$ is directed normal to the spacecraft spin axis and is contained in the plane defined by the central body, the cg, and the initial spin axis. Following the application of $\vec{\delta H}$, the total momentum is $\vec{H}_T$, and the spacecraft spin axis precesses about this total momentum vector at an inertial rate of $\vec{\omega}_T$, where

$$\vec{\omega}_S = \vec{\omega}_S \left(\frac{I_S}{I_o}\right) \qquad (2\text{-}49)$$

where $\vec{\omega}_S$ = spin angular velocity

I_S = spin inertia

I_o = inertia about other two body axes, taken to be equal when the spin axis again lies in the plane of $\vec{H}_S$ and $\vec{\delta H}$ directed toward point p_2, a second impulse is applied which causes nutation to stop. Thus, a net angular displacement of 2Δ of the vehicle spin axis in this plane has been achieved.

The time to precess the spin axis about $\vec{H}_T$ by π radians from p_1 to p_2 is π/ω_T sec. During this time the body has rotated through an angle equal to $\left(\frac{\omega_T}{\omega_S}\right)\pi$ radians, which is equivalent to $\left(\frac{I_S}{I_o}\right)\pi$ radians when Eq 2-49 is substituted. This implies that the two torque producing devices are to be separated on the body by an angle equal to $\left(\frac{I_S}{I_o}\right)\pi$ radians in order to effect a 2Δ angular rotation of the spin axis in the desired direction without any residual precession error.

The control system thus operates in the following manner. A trigger pulse is obtained from the fan shaped sensor as it sweeps by the edge of the central body. This pulse fires the first torque device. When the body has precessed through an angle of 180°, the second torquer is fired on the basis of a computed time interval equal to π/ω_T sec.

Figure 2-69 depicts the geometrical arrangement of the two torque devices and the triggering sensor device.

An alternate technique for spin control using a pinch plasma engine as a torque device has been presented in Ref 2-4. This technique results in essentially the same performance characteristics and the same total impulse requirement.

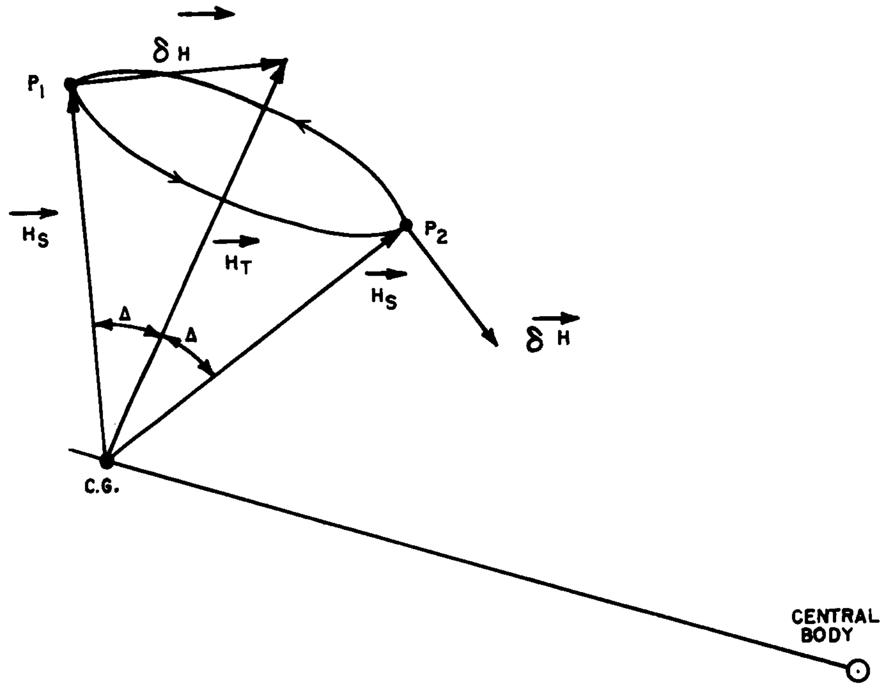
$\vec{\delta H}$
P_1
$\vec{H_S}$
$\vec{H_T}$
P_2
$\vec{H_S}$
$\vec{\delta H}$
Δ
Δ
C.G.
CENTRAL BODY

Figure 2-68. Spin Vehicle Momentum Vector Diagram

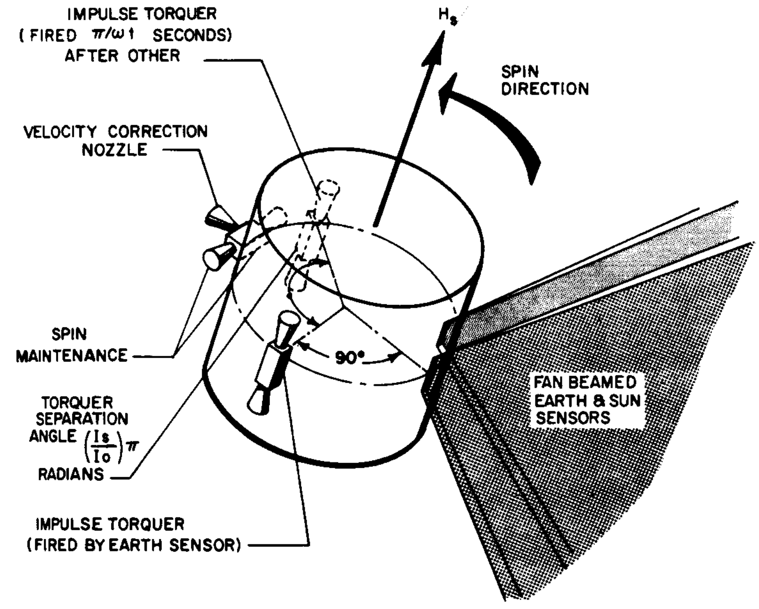
IMPULSE TORQUER (FIRED π/ω_t SECONDS) AFTER OTHER
H_s
SPIN DIRECTION
VELOCITY CORRECTION NOZZLE
SPIN MAINTENANCE
90°
TORQUER SEPARATION ANGLE $\left(\frac{I_s}{I_o}\right)\pi$ RADIANS
FAN BEAMED EARTH & SUN SENSORS
IMPULSE TORQUER (FIRED BY EARTH SENSOR)

I_s - SPIN INERTIA
I_o - CROSS INERTIA
H_s - SPIN MOMENTUM
ω_t - PRECESSION ANGULAR VELOCITY

Figure 2-69. Geometrical Arrangement of Basic Spin Control Components

b. Impulse Torquer Requirements

The 100-lb spacecraft has moments of inertia for $I_S = 14$ slug ft^2 and $I_o = 9$ slug ft^2. For a half cone angle Δ of 0.1°, $\delta\vec{H} \approx 0.2$ in.-lb-sec for $\delta H = \Delta H_S$, where $H_S = I_S \omega_S$ and $\omega_s = 10$ rpm.

The impulse torque magnitude for a 50 ms pulse width, would be 3.96 in.-lb. For a control lever arm of 19 in., a thrust level of about 0.2 lb is required.

F. EARTH ACQUISITION AND REACQUISITION

1. Introduction

The purpose of this subsection is to describe the control functions for vehicle attitude stabilization during the transfer ellipse, initial Earth acquisition, and Earth reacquisition for the various vehicle configurations and control techniques considered.

Stabilization during the transfer ellipse is defined for the period from separation of the satellite from the launch vehicle to the time that apogee motor burn has been completed. Initial Earth acquisition begins with the completion of apogee motor burn, and is completed when the satellite is properly oriented for Earth surveillance. Reacquisition begins at any time that Earth tracking is lost, and is completed when Earth tracking is resumed. A final velocity error correction will occur at different times in the above sequencing, depending on the particular vehicle and control system configuration. A detailed acquisition sequence is described in the section applicable to each configuration.

It is recognized that design of control systems for space vehicles that require large angular maneuvers (as during the Earth acquisition phase of the SMS mission) necessitates investigations of vehicle stability at attitudes grossly misoriented from the reference coordinate axes. Republic Aviation Corporation sponsored studies in this area are currently being pursued. Two reports are to be published on this program, which will define the overall attitude problem, demonstrate techniques used for solution, and present results for a synchronous satellite mission.

2. Attitude Stabilization During Transfer Ellipse

While traversing the transfer ellipse which brings the spacecraft to synchronous altitude, it is necessary to provide attitude stabilization to ensure that the vehicle is properly oriented for the apogee kick maneuver. Several techniques could be used to perform this function; however, spin stabilization will be shown to represent the simplest and most reliable technique.

a. Spin Stabilization

This technique requires that the boost vehicle (i.e. Agena stage) provide sufficient impulse to put itself and the spacecraft payload into the transfer orbit. After supplying this impulse, the vehicle must change its attitude with respect to the plane of the transfer ellipse by a predetermined angle. The spacecraft is then accelerated on the Agena spin table to a desired rate of 100 RPM, (minimum rate of 25 to 50 RPM) and separated from the boost vehicle.

During the approximately 5 hours that the spacecraft takes to arrive at the transfer ellipse apogee, its attitude must be maintained to an accuracy compatible with the synchronous orbit eccentricity and inclination requirements.

Study of the circular orbit injection phase has indicated that an out of plane (roll) angle misalignment of the apogee motor of 1.0° will produce a 0.5° orbital inclination error and an in plane angle error (pitch) of about 1° and will result in an eccentricity of 0.01. To minimize the inclination and eccentricity errors for this one factor of apogee thrust vector misalignment, it has been decided to provide spacecraft spin stabilization to 0.1° in both pitch and roll spacecraft axes. (Spacecraft Earth tracking axes are rotated through a +90° pitch angle to obtain orientation for apogee boost.)

The predominant factor in determining attitude accuracy for spin stabilization is the set of external disturbance torques acting during the transfer ellipse. Upon examining these disturbance torques, it has been found that solar flare disturbances are dominant. An expression for the required vehicle spin angular velocity (W_S) is given by Eq 2-50.

$$W_s = \frac{Dt}{I_s \epsilon} \qquad (2\text{-}50)$$

where W_S = rad/sec
D = external disturbance torque, in.-lb
t = time in transfer ellipse, sec
I_S = spin axis inertia, in.-lb-sec^2
ϵ = Attitude error at apogee in radians

Equation (2-50) has been plotted in Figure 2-70, parametrically, for the 500 lb spacecraft. It is seen that for the solar flare disturbance torque level

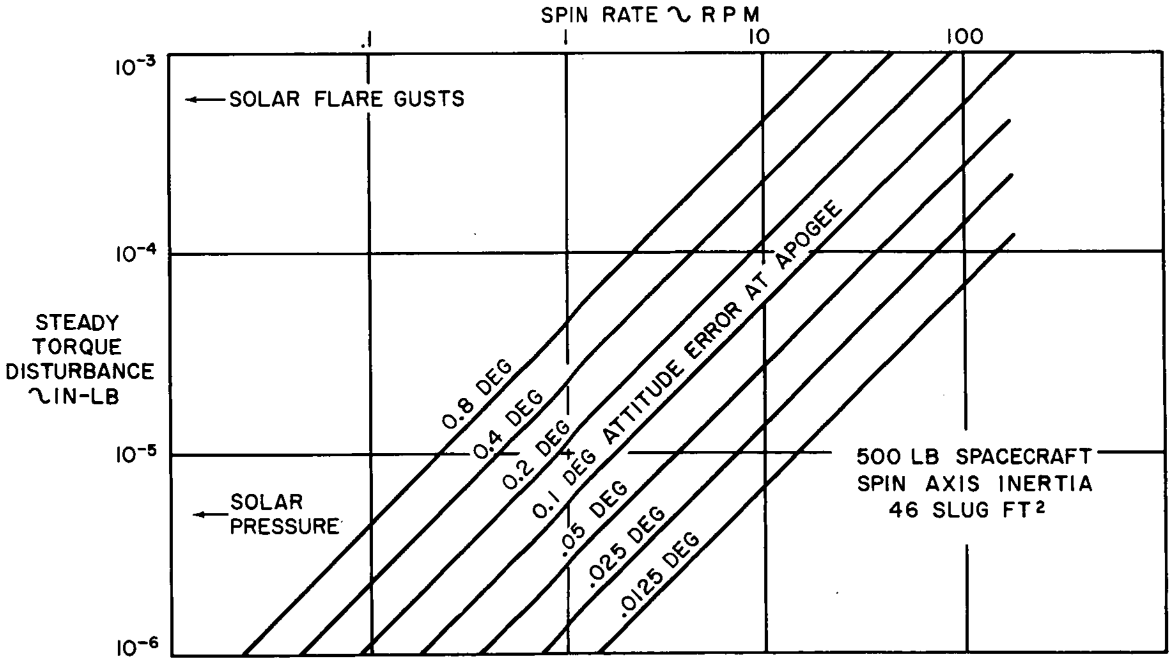

Figure 2-70. Spacecraft Spin Rate Requirement During Transfer Orbit

described in subsection C, a spin velocity of about 100 RPM is conservatively taken as adequate to provide the desired attitude accuracy. Future, more detailed studies would be required for a more exact determination of the required spin rate; a reduction of the required spin rate to 25 to 50 RPM may be possible.

During the firing of the apogee motor, misalignment of the thrust vector with the spacecraft center of mass will produce disturbing torques. The major attribute of spin stabilization is that of minimizing the effect of misalignment by rotation of the apogee motor in space about its thrust axis.

b. 3-Axis Spacecraft Stabilization

An alternate technique would require 3-axis stabilization of the spacecraft during the transfer ellipse. To accomplish this, the Agena vehicle must provide an impulse to put itself and the spacecraft in the transfer orbit. The Agena must then reorient itself with respect to the plane of the transfer orbit through a predetermined angle, and then separated from the spacecraft. Prior to separation, the spacecraft attitude sensors (i.e., pitch, roll, and yaw sensors) would have to be operating and hence, providing their respective output signals. A sensor for yaw attitude is as yet undefined for this type of stabilization mission. Horizon sensors could be used for pitch and roll if their accuracy were better than the 0.1° requirement at apogee.

Over and above the sensor problem, other significant drawbacks exist with this technique. The most serious occurs during the firing of the apogee motor. This results in thrust vector misalignment with the spacecraft center of mass. The best alignment that can be achieved is 0.02 in. between throat and nozzle exit, by means of boresighting techniques.

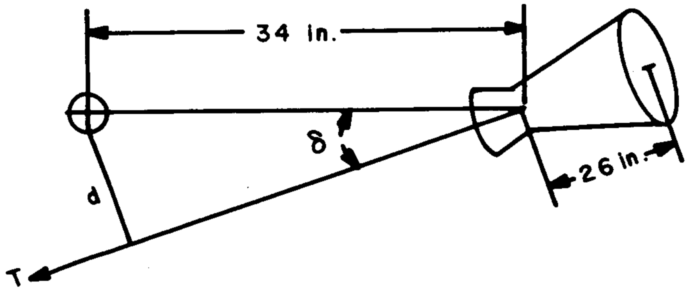

Figure 2-71. Apogee Motor Thrust Vector Misalignment

From Figure 2-71 it can be seen that the resultant misalignment angle δ, is 7.7×10^{-4} radians. If the motor pivots at the nozzle throat point, it is seen that the moment arm, d, is 0.0262 in. The apogee rocket for the 500 lb vehicle is characterized by a 4200 lb thrust level and a 47 sec burning time. The resulting torque acting on the vehicle due to motor misalignment is 110 in.-lb.

Over the 47 sec burning period, the spacecraft would accumulate an angular momentum of 5170 in.-lb-sec due to thrust vector misalignment. Based on these considerations, it is evident that none of the torque producing devices being considered for control of the satellite during Earth tracking and Earth acquisition have the torque capability or momentum storage required to maintain vehicle attitude while firing the apogee rocket.

c. Conclusions

The foregoing discussion of spin stabilization, as opposed to 3-axis stabilization, during the transfer ellipse and apogee motor firing, indicates that spin stabilization is far superior to 3-axis stabilization.

The only significant disadvantage to spin stabilization is that spin-down is required following the completion of apogee boost. Disadvantages associated with 3-axis stabilization are:

(1) Spacecraft torque devices normally used for Earth tracking would be inadequate for stabilization during apogee burn; either additional torque devices would be required or the capacity of those existing would have to be increased.

(2) Horizon sensors would have to have an accuracy of better than 0.1°.

(3) Yaw sensing would be extremely difficult and would require an auxiliary mechanism. No device being considered for yaw sensing during Earth tracking has the capability of performing this function while the vehicle is in the transfer ellipse.

3. Acquisition and Reacquisition for Various Vehicle and Control System Configurations

As stated earlier, initial Earth acquisition begins at the completion of the apogee kick maneuver. The spacecraft state at this time would be represented by a maximum spin rate of 100 RPM about the body yaw axis (Z_b), and maximum rates of 1°/sec about the body pitch and roll axes (Y_b, X_b).

The first phase of acquisition for all spacecraft configurations considered will be that of passive despin. This will consist of the unfurling of weights on extensible wires to reduce the spin rate to 10°/sec. From the law of conservation of momentum

$$I_2 = \left(\frac{\omega_1}{\omega_2}\right) I_1$$

where the subscript 1 denotes vehicle conditions prior to extending weights, and subscript 2 the conditions after extension.
I = Spin axis inertia
ω = Spin angular velocity

For the 500 lb, 3-axis stabilized spacecraft, $I_1 = 552$ in.-lb-sec^2, and $\omega_1 = 100$ RPM $(10.5 \frac{\text{rad}}{\text{sec}})$. Therefore, to obtain ω_2 of 10°/sec$(\frac{10}{57.3} \frac{\text{rad}}{\text{sec}})$, it is seen that I_2 must be 33,000 in.-lb-sec^2. It is clear that the major contribution to this required inertia must come from the extensible weights. Two 5 lb weights will be considered to perform this despin function. The required cable length for each weight would be 94 ft for the above spacecraft and conditions considered. The passive despin phase is completed by separation of the weights and wires from the spacecraft.

The remaining phases of acquisition depend on the particular spacecraft configuration and control system being considered. There are three basic configurations for which the remaining acquisition sequences will be discussed. These are; 3-axis stabilized, spin, and gravity gradient vehicles.

a. Earth Acquisition of the 3-Axis Stabilized Spacecraft

The 3-axis stabilized spacecraft could consist of the following types of control elements. The acquisition sequence to be described is applicable to all.

(1) Gyrocompass - gas
(2) Reaction wheels - gas
(3) Electric propulsion
(4) Twin gyros - gas
(5) Glopac - gas
(6) Pure gas (modulated, adaptive, pseudo-rate, etc)

Initial spacecraft state for this portion or acquisition is represented by a tumbling motion with maximum body rates of 1°/sec existing about the pitch and roll axes and 10°/sec in yaw. The procedure to be followed is to actively despin the vehicle about all three axes to the threshold level of the rate control systems, 0.01°/sec, as indicated in Figure 2-17.

It should be noted here that alternate approaches for the active spin-down phase are currently being investigated in Republic's All Attitude Control Program. These alternate approaches are:

(1) Active despin of pitch and yaw rates to threshold level and despin of roll rate to a nominal desired level (0.1°/sec prior to initiating the Sun orientation mode which is subsequently discussed.

(2) Active despin of roll rate to nominal desired level. The Sun orientation phase is initiated with existing rates in the pitch and yaw body axes.

Following active despin, a Sun orientation phase is initiated. Sun orientation serves a dual purpose. It provides the proper vehicle orientation for the generation of electrical power by solar cells; and it provides a quasi-inertial reference line from which a search for the Earth disk may be initiated.

Having oriented the spacecraft negative roll axis toward the Sun, a roll rate of 0.1°/sec is commanded. The rate magnitude is based on a minimum of two possible intersections of the Earth by the horizon scanners as the spacecraft moves in its orbit. An increase in the slewing rate would require that the control element torque capability be increased to ensure continued Earth lock-on while the roll rate is being nulled.

Having established the vertical alignment, the next phase consists of establishing yaw alignment about the vertical axis. For the gyro compass 3-axis control system this consists of bringing the constant speed wheel up to its operating speed. For other 3-axis systems, the yaw alignment procedure consists of establishing the yaw reference and controlling the Spacecraft to null out any existing yaw error.

Procedures for reacquisition are similar to those of initial acquisition; however, the initial conditions (i.e., body rates) will differ. Initial rates for the start of a reacquisition phase would depend on the factors which resulted in the loss of Earth tracking. Possible causes are impulsive torques due to micrometeorites, loss of electrical power, failure of sensory equipment, etc. A realistic possibility is an intermittent loss of electrical power, which has been the case for several existing satellites.

Control systems which use reaction wheels as torquing devices would eventually impart an angular momentum to the vehicle equivalent to that stored in the wheels at the time of power failure. Wheel speed decay would depend only on windage and bearing friction. Thus, the torque levels acting on the spacecraft would be relatively small. If the power failure persisted long enough, however, all the reaction wheel momentum would be transferred to the spacecraft.

Reaction wheels have been sized to 10 in.-lb-sec maximum momentum. For an assumed power failure, spacecraft body rates would be based on the corresponding vehicle momenta about all axes for the study of reacquisition. For 3-axis control systems which do not use momentum storage devices, the reacquisition body rates would depend on the duration of power failure and the magnitude of external disturbance torques acting in that interval.

Table 2-10 depicts the acquisition sequence for 3-axis stabilized spacecraft and approximate duration of each phase for the 500 lb spacecraft.

TABLE 2-10
MISSION SEQUENCE - 3-AXIS STABILIZED SPACECRAFT

Phase	Duration	Remarks
Passive Despin	10 sec	1/32 g deceleration at 1 ft radius based on 10°/sec initial body rate.
Active Despin	400 sec	
Sun Orientation	2000 sec	
Earth Search	12 hr (max)	
Earth Track	1 year	
Reacquisition	12 hr (max)	Repeats initial acquisition sequence

b. Earth Acquisition for Gravity Gradient Spacecraft.

As discussed in the section Earth Tracking - Dynamic Analysis and Simulation (subsection E) the gravity gradient spacecraft would consist of a simple control system for Earth tracking which would provide effective rate control to very low rates. However, the Earth acquisition requirement adds additional complexity to the overall gravity gradient system. The addition of a gas system is required to perform the acquisition function, in particular for active despin and during initial alignment. Thereafter, only the reaction wheels and rate gyros are used for damping, while restoring torques are provided by gravity gradient and gyrocompassing.

The major portion of the acquisition phase of the gravity gradient spacecraft is accomplished prior to separation of the two masses which constitute the dumbell configuration. By completing the major portion of acquisition prior to erection, the acquisition time is considerably reduced. This is due to the much larger spacecraft moments of inertia when fully erected.

The first phase of acquisition would be passive despin of the spacecraft yaw rate to about 10°/sec. Rates about pitch and roll are considered to be 1°/sec. Following passive despin, active despin is accomplised by means of rate control systems using rate gyros and a cold gas system. The spacecraft body rates about all axes are reduced to about 0.01°/sec.

At this point in the acquisition sequence, it must be determined whether the section of the spacecraft containing the meteorological sensors is below the local horizontal. To ensure that the sensory section is oriented in the direction of the Earth during Earth tracking, this section of the spacecraft must be below the local horizontal prior to erection of the two-mass spacecraft configuration. This aspect has not been investigated in detail; however, the following possibilities exist for establishing the desired gross orientation.

(1) Wide angle photo taken from sensory package and transmitted to ground. If Earth disc is viewed, orientation is grossly correct.

(2) Application of RF beacon techniques to determine coarse attitude information.

(3) Use of a hemispherical Earth sensor at high noon to obtain Earth direction information.

Ideally, the gravity gradient spacecraft should have its "long" axis aligned with the local vertical prior to separation of the two masses. By doing this, acquisition time is significantly reduced. This is because the spacecraft damped natural frequency, when erected is $\sqrt{3}\ \omega_0$. This implies that considerable time would be required to align to the local vertical from an arbitrary initial attitude. Using one of the above attitude sensing techniques in conjunction with the on-board rate control system would prove beneficial in reducing acquisition time. The rate control system would be commanded from the ground to provide approximate alignment of the local vertical and the spacecraft "long" axis.

After vertical alignment has been completed, the constant speed pitch wheel would be brought up to speed to provide yaw alignment. Thereafter, the spacecraft is considered to be in the Earth tracking mode. At this time the velocity correction and station keeping functions may be initiated.

Table 2-11 indicates the estimated time period for each phase of the gravity gradient spacecraft acquisition.

TABLE 2-11
GRAVITY GRADIENT SPACECRAFT
Acquisition Time Profile

Phase	Duration (min)	Remarks
Passive Despin	0.17	100 RPM to 10°/sec
Active Despin	7	10°sec to threshold
180° Rotation	3	Required if sensor package upside down
Vertical (Alignment Prior to Erection of Spacecraft)	1.5	Rate controlled
Erection Time	5	
Final Vertical Alignment	15	
Yaw Alignment	60	Gyrocompass wheel speed-up
Total	91.67	

c. Earth Acquisition for Spin Controlled Spacecraft

Acquisition for the spin controlled spacecraft consists, sequentially, of passive despin, active despin, Sun orientation, Earth orientation, and alignment with Polaris.

Passive despin is accomplished by weights on extensible wires, and is used to reduce the transfer ellipse spin rate to the magnitude required for final stabilization. Following passive despin, active rate control is used on the spin axis to maintain the desired angular momentum.

The next phase is that of orientation of the spacecraft spin axis normal to the Sun line. This is accomplished by using a Sun sensor with a narrow fan shaped beam covering ± 90° as indicated in Figure 2-18. After establishing this Sun line orientation, the spacecraft is precessed about the Sun line until a null is indicated from an Earth sensor having a fan shaped beam. This situation is illustrated by Figure 2-72.

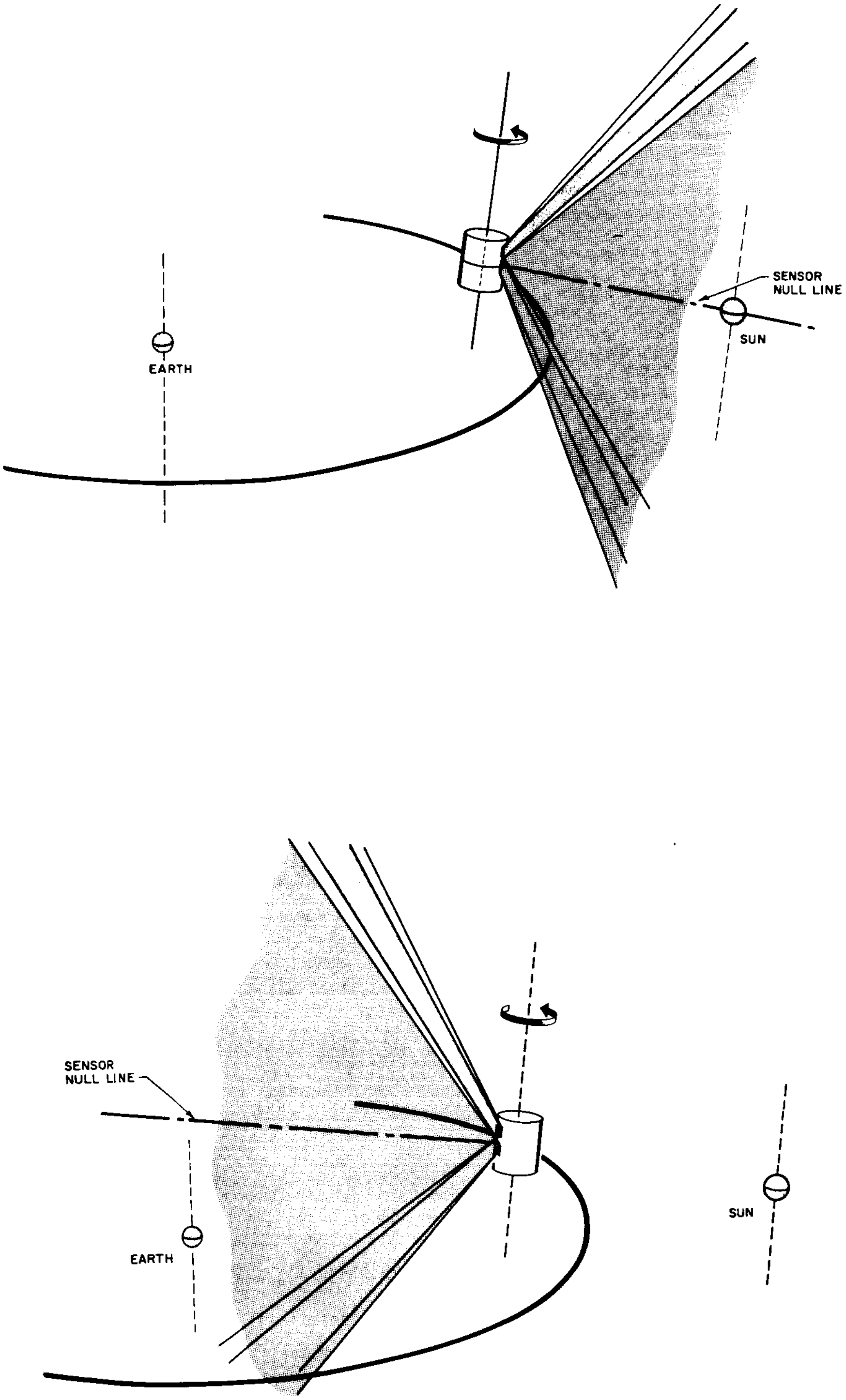
SENSOR NULL LINE
SUN
EARTH
SENSOR NULL LINE
EARTH
SUN

Figure 2-72. Spin Vehicle Sensor Geometry

At this point in the acquisition sequence, the Sun line control is removed and precession about the Sun line is stopped. The spacecraft spin axis at this point can be a maximum of 23.5° ± 55 min out of alignment with Polaris if at autumnal or vernal equinox. However, a quarter of an orbit later, the maximum misalignment with Polaris would then be only 55 min of arc. Because the field of view of the Polaris boresight tracker is approximately ±8°, Polaris can be captured quite easily. Once Polaris tracking starts, the fan shaped Earth sensor is used merely for synchronization of control torque pulses.

An obvious deficiency exists in the initial acquisition procedure described. That is the inability of the system to discern north from south. Indeed, the spacecraft spin vector could end up in either direction. A technique to overcome this would use an RF beacon mounted on one end of the cylindrical spacecraft. During that portion of acquisition where the spacecraft is precessed about the Sun line, precession would continue until the beacon swung past the Earth. Control logic would then allow the spacecraft to switch over to Earth tracking the first time the Earth sensor indicated a null output. This would ensure that the Polaris boresight tracker was oriented in a northerly direction for the final acquisition of Polaris.

Table 2-12 summarized the times to complete the various phases of Earth acquisition.

TABLE 2-12
SPIN CONTROLLED SPACE CRAFT - ACQUISITION TIME PROFILE

Phase	Duration	Remarks
Passive Despin	1/6 min	Spin-down to 10 RPM
Active Despin	negilgible	Maintain spin at 10 RPM
Sun Orientation	15 min	Based on initial 90° misalignment
Sun line Precession	15 min	Based on initial 90° misalignment
Polaris Search and Lock-on	6 hr (max)	
Total (Max)	6.5 hr (max)	

G. LIST OF SYMBOLS

A = area, square feet

c = speed of light in vacuum, 186,000 miles/sec.

F_D = F_{Drag} = net force extended on body along direction of incident radiation

F_L = F_{Lift} = net force extended on body, perpendicular to direction of radiation

I = emitted radiation pressure from diffuse surface

m = $\frac{E}{c^2} = \frac{S}{c^2}$ = mass associated with matterwave of light radiated by Sun

N = force normal to surface at a point

R = surface reflectivity expressed as a fraction: $\frac{\text{incident energy - absorbed energy}}{\text{incident energy}}$

$\vec{r}$ = position vector from center gravitational attraction to centroid of cylindrical body of 3-axis stabilized vehicle. (Distance along pitch, roll and yaw body axes are Δp, Δr, Δy, respectively.)

S = solar constant (ft lb/sq ft sec) at one astronomical unit = $(C)10^{-7}$

$\frac{S}{c}$ = pressure exerted by totally absorbed solar radiation (zero reflection, omnidirectional reradiation)

$\left[\frac{S_f}{c}\right]$ = pressure exerted by inelastic collision of solar flare emitted particle with a flat plate surface (a value of $75 \times 10^{-7} \text{lb/ft}^2$, which is half the probable peak listed in Ref 2-1 is used for computation)

T = force tangential to surface at a point (shear)

t = elapsed time, seconds

α = angle between Earth's spin axis and the ecliptic plane (66.5°)

γ = fraction of absorbed radiation converted to electrical power

ω_B = spin rate of satellite

ω_E = angular rate of satellite center about Earth

ω_{SE} = angular orbital rate of Earth center about Sun

All rates are with respect to inertial reference

H. REFERENCES

2-1 'Proposal for Studies of Synchronous Meteorological Satellite System Problems," Republic Aviation Corporation Report No. RAC 826, 23 July 1962

2-2 JPL Space Programs Summary, No. 37-20, Vol. II, pp 39-50 (Confidential)

2-3 Michelson, I., "Equilibrium Orientations of Gravity Gradient Satellites," AIAA Journal, February 1963

2-4 Rifkin, A., and Vogel, E., 'Attitude Control of Spin Stabilized Spacecraft." Paper presented at the 1963 IEEE International Convention

SECTION 3 - ORBIT GETTING AND STATION KEEPING

A. ASCENT, ORBIT INJECTION, AND CORRECTION

1. Summary

Ascent phasing and injection correction techniques suitable for injecting a payload into a synchronous orbit centered over the equator at 90°W longitude were investigated. It was found that the Atlas-Agena and Atlas-Centaur boost vehicles can perform this mission within 6.43 hours based on a 1.5° off-east launch azimuth and a short low altitude wait period. At synchronous altitude, a solid rocket engine can be used to supply the required apogee kick impulse ($\Delta V_k = 6030$ ft/sec) to inject 500 and 1000 pound spacecraft into nominally synchronous, equatorial orbits for the Atlas-Agena and Atlas-Centaur boost vehicles, respectively.

For the nominal injection errors specified in Ref 3-13, only the period and eccentricity errors require correction. Corrective action is initiated subsequent to the apogee kick maneuver by the application of tangential thrust. A cold gas propulsion system (Section II) can be used to correct the small, given injection errors.

For larger injection errors, representative of the Atlas-Agena-spacecraft system, again only mean motion and eccentricity errors require correction. These corrections culd more efficiently be accomplished by a hot gas propulsion system (H_2O_2 or equivalent), rather than a cold gas propulsion system.

Thor-Delta or Thor-Ad boost vehicles can inject a 50 to 100 pound payload into a 28.3° inclined orbit whose central longitude is 90°W. A maximum time of two weeks may be required for this maneuver. The apogee kick velocity (applied 5.41 hours after launch) corresponds to 4653 ft/sec. Two additional impulses totaling 199 ± 39 ft/sec are deemed necessary for correction of the given injection errors and final circularization. Due to the specified ± 1000 second random period error, a residual propellant equivalent to 78 ft/sec may remain unused. Injection velocity errors greater than 39 ft/sec ($\Delta P = 1000$ sec) would alter the above requirements, but the total required increase in characteristic velocity for the injection and circularization maneuvers would still be equal to the random injection velocity error.

2. Introduction

Two classes of ascent trajectories capable of establishing a synchronous 24-hour satellite at a central station position defined by 90°W longitude have been studied. One ascent path is characterized by a low altitude waiting orbit, the other by a high altitude waiting orbit. A low altitude waiting orbit can be provided by a launch vehicle whose upper stage has a restart capability (e.g., Atlas-Agena or Atlas-Centaur). A high altitude waiting orbit must be used for those vehicles with nonrestartable upper stages (e.g., Thor-Delta or Thor-Ad).

The purpose of this section is to define the phasing requirements, the apogee kick requirements, and the procedure for correcting random injection errors for both low and high altitude waiting orbit maneuvers. Ascent phasing characteristics in the absence of injection errors are discussed in subsections C and D. The influence of guidance injection errors on the subsatellite drift pattern and the recommended correction process for establishing a 90°W longitude station are discussed in subsection E. Spacecraft engine requirements are given in subsection F.

3. Low Altitude Waiting Trajectory

a. General

Payload optimization considerations dictate an essentially fixed space trajectory into a low altitude waiting orbit. This phase is based on an Atlas-partial Agena or Atlas-Centaur powered ascent trajectory launched eastward from Cape Canaveral. At the second (ascending) nodal crossing, a Hohmann transfer, (coplanar with the near circular waiting orbit) is initiated by the Agena or Centaur booster. Hohmann apogee corresponds to the 24-hour orbit altitude. The application of an impulse at apogee reorients the orbit plane and ideally establishes the desired synchronous orbit centered above 90°W longitude. Subsequent impulses are required for injection error correction. The use of an inclined 24-hour orbit, rather than an equatorial orbit for the Synchronous Meteorological Satellite (SMS) results in certain mission advantages, and can be achieved most efficiently by constraining the apogee kick impulse to lie in the transfer orbit plane. The advantages of an inclined orbit are an increase in useful payload, an increase in viewing capability, and a slight decrease in drift rate due to the Earth's equational ellipticity. Useful payload can be increased approximately 14%* if the launch orbit inclination of 28.3 degrees (due east launch from Cape Canaveral) is maintained. Also, an additional Earth coverage capability equivalent to ±28.3° in latitude and ±3.7° in longitude is available during any given circuit of the synchronous satellite. Other mission factors, however, mitigate against an inclined orbit with its pronounced figure-8 ground trace.

b. Phasing Requirements

The powered ascent phase terminates in a low altitude waiting orbit (h = 100 nm)(Ref 3-1) inclined to the equator. A transfer ellipse can be initiated at any equatorial nodal crossing, thereby permitting final injection at an equatorial station. Initiation time is given by

$$t_1 = t_o + (j - 1) \frac{P_w}{2}$$

Integer j describes each successive nodal occurrence. Odd integers denote descending node, while even integers denote ascending node transfer positions. To achieve the desired 90°W longitude station, a transfer maneuver at the first ascending node (j = 2) is employed (see Figure 3-1).

---

*Based on a velocity penalty of 1178 ft/sec: ΔV_k (i = 0) = 6030 ft/sec; ΔV_k (i = 28.3°) = 4852 ft/sec.

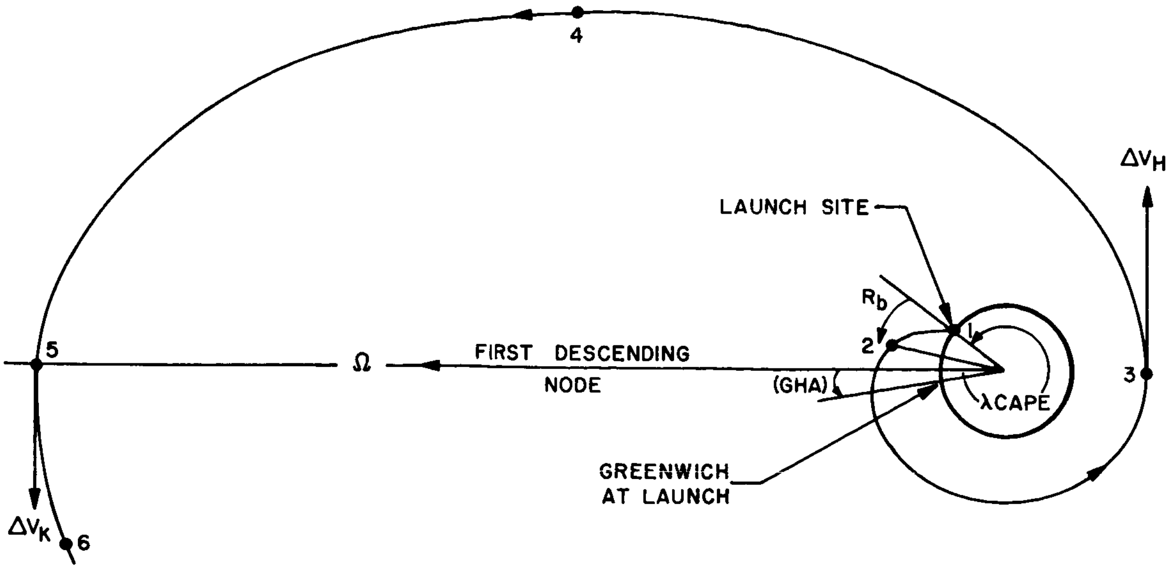

NOTE: (a) PAPER REPRESENTS THE PROJECTION ON EQUATORIAL PLANE
(b) ALL ANGLES SHOWN IN A POSITIVE SENSE

1. LAUNCH
2. SECOND-STAGE PARTIAL BURNOUT AT 100-NM WAITING ORBIT (INCLINED 28.5°)
3. SECOND-STAGE IMPULSE APPLICATION FOR DEPARTURE FROM 100-NM PARKING ORBIT INTO HOHMANN TRANSFER ORBIT
4. VEHICLE IN HOHMANN ELLIPTICAL TRANSFER ORBIT (INCLINED 28.5°)
5. APOGEE KICK FOR REORIENTATION AND CIRCULARIZATION
6. VEHICLE IN 24-HOUR ORBIT

Figure 3-1. Ascent Schematic

The parameter t_o is the time of the first nodal crossing. This includes the powered trajectory as well as a partial orbit coast. Both burning time and range angle achieved during the powered phase are dependent on the booster characteristics. As will be shown, these parameters have a small influence on the phasing requirements necessary to establish a given station longitude.

When the first ascending node of the low altitude waiting orbit is reached, the second burn of either the Agena or Centaur commences, and the vehicle is transferred to a Hohmann path whose apogee altitude is coincident with the synchronous altitude. The characteristic velocity required to perform this maneuver is 8069 ft/sec.

A high altitude node is attained at time t_2, where

$$t_2 = t_1 + \frac{P_H}{2}$$

where P_H = period of the Hohmann ellipse

At this instant, the satellite longitude (λ) is given by

$$\lambda = 2\pi - (GHA_o + \omega_e t_2)$$

where ω_E = rotational velocity of the Earth

GHA_o = Greenwich hour angle of Cape Canaveral at launch measured from the first descending node (℧)

The right ascension between the descending node and Cape Canaveral at launch is independent of booster characteristics. This angle is dependent on launch azimuth only. For a due east launch, the right ascension is essentailly -90°; hence

$$GHA_o = -90 - \lambda_{\substack{\text{Cape} \\ \text{Canaveral}}} = -9.54°$$

Booster burnout conditions (t_b, R_b) have a small influence on the ability to establish a desired equatorial station position when a low altitude waiting orbit is employed. The final station position is shifted by the time difference between given boosters in transversing a given powered ascent range angle. To illustrate, consider an Atlas-Centaur powered ascent to orbit specified by a boost time (t_b) of 0.15 hour and an inertial range angle (R_b) of 17.94° (Ref 3-1). Let the Hohmann transfer be initiated at the first ascending node. Then

$$t_1 = 0.15 + \frac{P_W (72.06)}{360} + \frac{P_W}{2} = 1.18 \text{ hour}$$

and $\lambda_{24} = 2\pi = \left[-9.54 + 15.03 \, (6.44)\right] = 87.2°W$

where λ_{24} = satellite longitude at injection into a synchronous orbit.

If burnout were assumed to occur directly over Cape Canaveral, at time zero, then t_1 would equal 1.10 hour and $\lambda_{24} = 86.0°W$. Thus, the phasing requirements also apply to an Atlas-Agena powered ascent ($t_b = 0.14$ hour, $R_b \approx 15°$).

A desired equatorial station located at 90°W longitude can readily be established by an off-east launch. This effectively shifts the inertial position of the descending node westward with respect to Greenwich at launch. The desired 2.8° westward shift is accomplished by a launch azimuth of 91.5° (Figure 3-2) and an associated 10 ft/sec characteristic velocity penalty charged to the booster (see Ref 3-1).

In the absence of injection errors, both circularization and orbit plane reorientation, as desired, are accomplished by the apogee kick motor at Hohmann apogee altitude. A 6030 ft/sec velocity impulse is required to perform this maneuver for the case of a final equatorial orbit. This impulse is applied

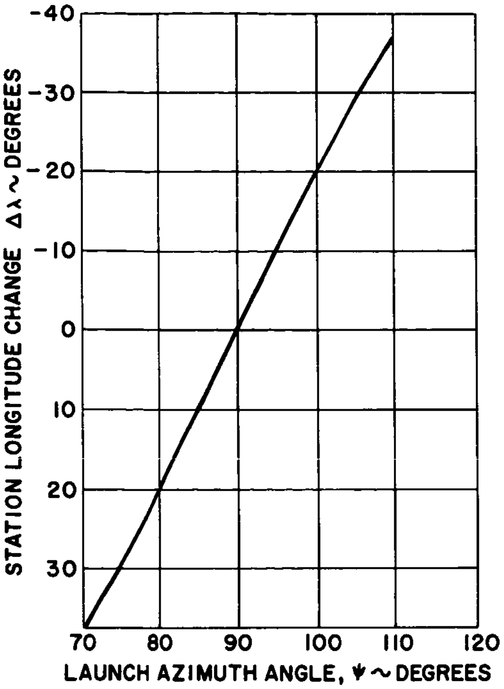

Figure 3-2. Ability to Alter Station Longitude based on Off-East Launch Azimuth

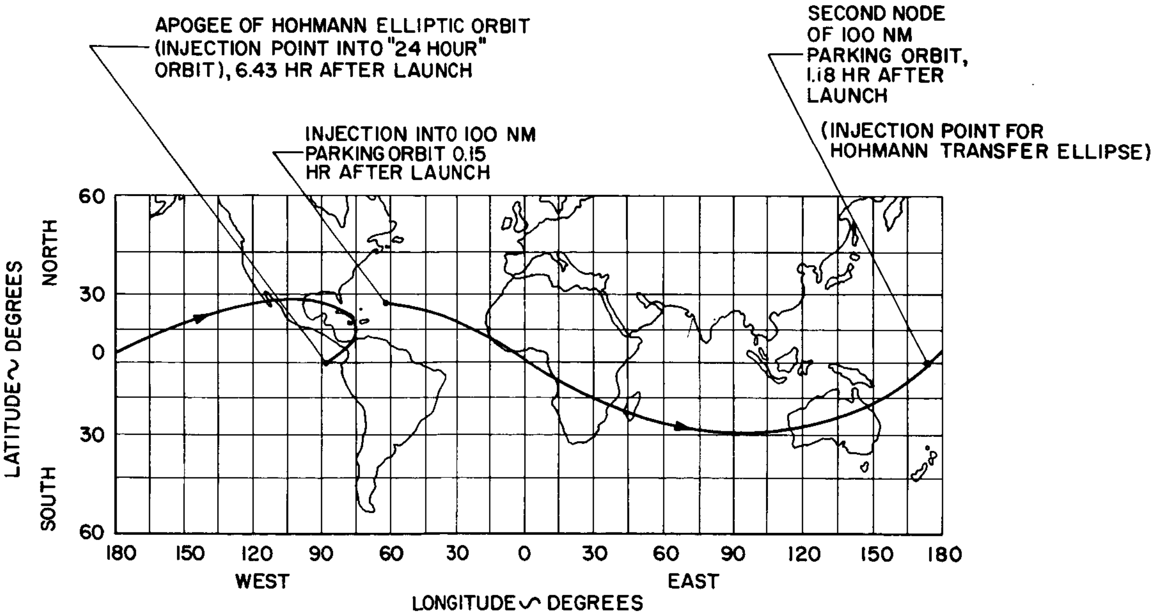
APOGEE OF HOHMANN ELLIPTIC ORBIT (INJECTION POINT INTO "24 HOUR" ORBIT), 6.43 HR AFTER LAUNCH
INJECTION INTO 100 NM PARKING ORBIT 0.15 HR AFTER LAUNCH
SECOND NODE OF 100 NM PARKING ORBIT, 1.18 HR AFTER LAUNCH
(INJECTION POINT FOR HOHMANN TRANSFER ELLIPSE)
LATITUDE ~ DEGREES
NORTH
SOUTH
60
30
0
30
60
180
150
120
90
60
30
0
30
60
90
120
150
180
WEST
EAST
LONGITUDE ~ DEGREES

Figure 3-3. Earth Track of Low Altitude Wait Ascent Mode

in the plane of the horizon at an azimuth angle of 52.7° measured from the local direction of motion. Figure 3-3 presents the ground track associated with the low altitude wait ascent maneuver.

4. High Altitude Waiting Trajectory

Powered ascent trajectories, associated with high altitude waiting orbits, must be employed by those booster vehicle systems which do not have restart capability. Both the Thor-Delta and Thor-Ad launch vehicles fall into this category. These boosters can inject payloads ranging from approximately 50 to 100 pounds into an inclined synchronous orbit. The powered ascent terminates at perigee of a Hohmann transfer trajectory whose apogee corresponds to synchronous altitude. Unlike the low altitude waiting trajectory, the Hohmann perigee is not located at a node.

A circularizing impulse ($\Delta V_K = 4852$ ft/sec) applied at Hohmann apogee ($\phi = -26.8°$) results in a synchronous 24-hour orbit inclined 28.3° to the equator at a nominal longitude station of 38.5°E. This station longitude is based on the ascent path considered earlier ($t_b = 0.15$ hour, $R_b = 17.94°$, $h_b = 100$ nm).

The powered ascent burnout condition has a more pronounced effect on injection station position for high rather than low altitude waiting ascent paths, since the equatorial station position is shifted by the time required for a synchronous satellite to traverse the burnout range angle. For example, if $t_b = R_b = 0$, then the nominal injection station longitude would be 20.5°E. As mentioned earlier, it is appreciated that the powered Thor-Delta ascent trajectory is fixed based on payload considerations. However, regardless of where the direct ascent subsatellite longitude is situated ($20.5° < \lambda_{24} < 38.5°$), the phasing requirement to obtain a 90°W longitude station is essentially unaffected. For this reason, it is arbitrarily assumed that $t_b = 0.15$ hour and $R_b = 17.46°$.

A high altitude waiting orbit must be established at Hohmann apogee to achieve the desired nominal 90°W station position. There are two alternatives: either the period of this waiting orbit $P_W < 23.94$ hours and the vehicle drifts east, or $P_W > 23.94$ hours and the vehicle drifts west. If the vehicle is caused to drift east (by not fully accelerating it to synchronous velocity at Hohmann apogee) then the total impulse velocity requirement including the injection manuever at Hohmann apogee, ΔV_K, and the circularization manuever, ΔV_c remains constant ($\Delta V_K + \Delta V_c = 4852$ ft/sec). This results because of the colinear positive addition of velocity impulses ΔV_K and ΔV_c. A velocity impulse in excess of 4852 ft/sec ($\Delta V_K > 4852$) is always required to sustain a westward drift. Moreover, at the appropriate time, all excess velocity must be removed for circularization. Hence, in the absence of injection errors, it is always more economical to drift east rather than west ($\Delta V_{Tot} \begin{smallmatrix}\text{West}\\ \text{Drift}\end{smallmatrix} - \Delta V_{Tot} \begin{smallmatrix}\text{East}\\ \text{Drift}\end{smallmatrix} = 2\,\Delta V_c$). The relationship between waiting orbit period and various velocity additions of interest are shown in Figure 3-4.

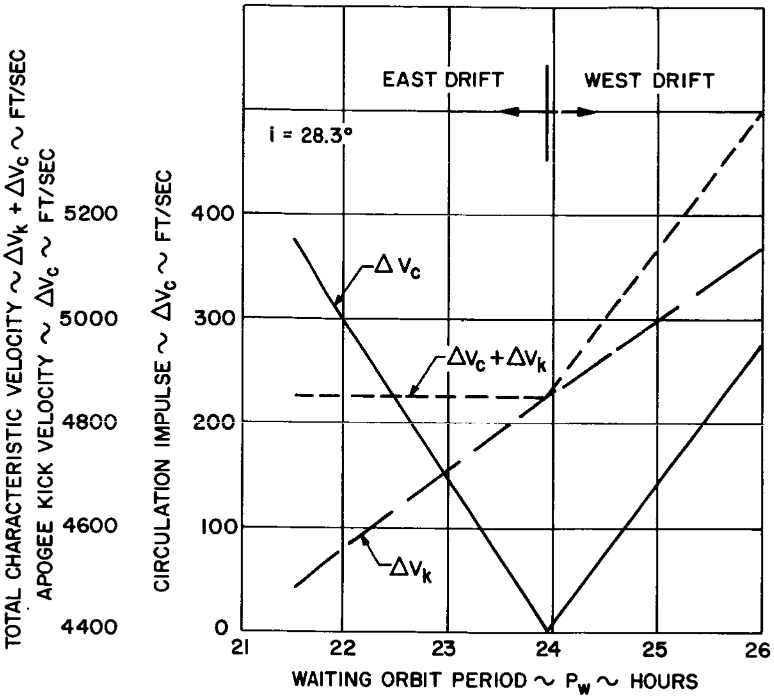

Figure 3-4. High Altitude Waiting Orbit - Circularization Characteristics

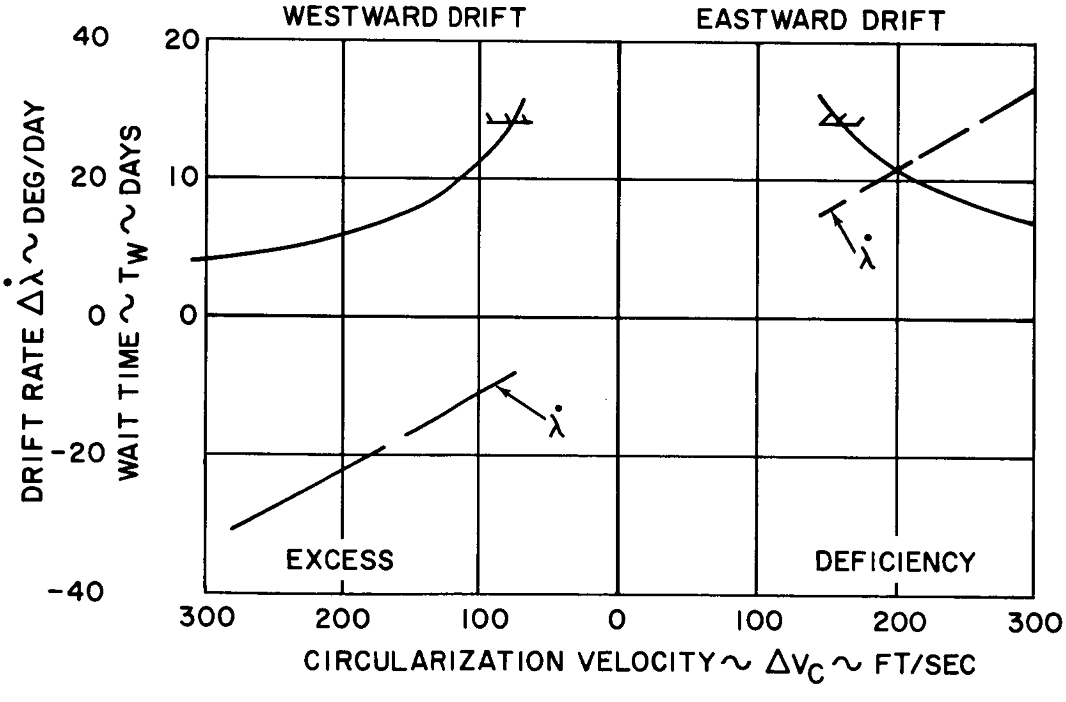

Figure 3-5. High Altitude Waiting Orbit - Drift Characteristics

Vehicle drift rate and waiting orbit period are related through the following expression

$$\Delta\dot{\lambda} = \frac{P_{24} - P_W}{P_W} \; 360°/\mathrm{day} = \frac{\Delta\lambda}{T_w} \; °/\mathrm{day}$$

Parameter T_W represents the allowable waiting time to drift the required Δ $\Delta\lambda = 128°W$ or $\Delta\lambda = 232°E$.

Figure 3-5 depicts the required velocity deficiency or excess, with respect to synchronous speed at Hohmann apogee, as a function of allowable waiting time T_W. Velocity ΔV_c must be added or subtracted to achieve final synchronous station conditions. Naturally, as allowable waiting time T_W increases, ΔV_c decreases. Injection errors must be considered prior to the selection of a preferred waiting time and phase mode.

5. Injection Errors

a. The Effect of Orbit Element Errors on the Subsatellite Pattern

Velocity magnitude, pitch angle, and yaw angle errors exist after each thrusting interval (burnout into waiting orbit, Hohmann transfer initiation, synchronous orbit injection). As stated in Ref 3-2, the effects of these guidance errors are taken to result in the following synchronous orbit element errors after final orbit injection:

Inclination error, $\Delta i = 0.8°$

Longitude error, $\Delta\lambda = 0.3°$

Eccentricity, $\Delta e = 0.013$

Period error, $\Delta P = 1000$ sec

If the orbit plane has an inclination error of Δi, then the satellite will exhibit a daily latitude error oscillation of $\pm \Delta i$. An 0.8° inclination disparity would thus cause a ± 0.8° daily latitude oscillation and a ± 0.003° daily longitude oscillation. This inclination error could be eliminated by the application of a 141 ft/sec impulse ($\Delta V \simeq 10,088i$) applied at a node normal to the orbit plane. Since the inclination perturbation resulting from terrestrial and extra-terrestrial sources, in addition to the expected 0.8° injection error, is significantly less than the maximum allowable latitude drift (±5°) considered tolerable for mission success, it is therefore recommended that this error remain uncorrected.

A longitude position error of ±0.3° at station injection need not be immediately corrected. This error will be negligible compared to the longitude excursion produced by the mean motion injection error. If an orbit eccentricity e should exist, then a daily longitude error oscillation $\Delta\lambda$ (in degrees) of from 115e to 230e will be experienced, depending on the injection position with respect to the line of apsides. Thus an orbit eccentricity of 0.013 would result in daily longitude excursions from the desired station position of between 1.5 and 3.0°. Orbit eccentricity corrections are discussed below in combination with the semimajor axis correction.

The most significant orbit element error is the mean motion error. A period error of 1000 seconds (Δa = 0.051 Earth radii) produces a steady longitude drift of 4.2°/day. This error must be corrected before significant off-station drift occurs. Guidance corrections could be started within 4 to 6 hours after injection. Correction of the semimajor axis, or equivalently, the initial mean motion error, is of prime concern because of the associated longitude drift. A simple differential correction guidance scheme has therefore been considered wherein all velocity additions are applied in the orbit plane normal to the radius vector.

b. Correction of the Given Injection Errors (Impulsive)

The differential change in the orbital elements of interest (semimajor axis a and eccentricity e) caused by small circumferential impulsive velocity corrections, are

$$\frac{\Delta a}{a} = \frac{2V^2 a}{\mu} \cos \gamma \, \frac{\Delta V}{V}$$

$$\Delta e = \frac{1}{\cos \gamma} \left[2 \cos \theta + e \left(1 + \cos^2 \theta\right) \right] \frac{\Delta V}{V}$$

where γ = flight path angle

θ = true anomaly

These equations apply to the orbit achieved after the apogee kick. The maximum flight path angle (γ) occurs at a true anomaly given by $\theta = \cos^{-1} (-e)$; hence, $\cos \gamma \cong 1$, since $\cos \gamma_{max} = \sqrt{1 - e^2} \sim 1 = \frac{e^2}{2} \sim 0.999925$. Therefore, for the nearly circular orbit under consideration, Δa may be further approximated as

$$\frac{\Delta a}{a} = \frac{2}{3} \frac{\Delta P}{P} \sim \frac{2 \Delta V}{V}$$

Nominally, 39 ft/sec will be required to correct for the indicated mean motion drift (ΔP = 1000 sec; Δa = 0.051 Earth radii; $\Delta n = \dot{\lambda} = 4.2$°/day). This correction alters the eccentricity as follows:

$$\Delta e \sim \frac{\Delta a}{2a} \left[2 \cos \theta + e \left(1 + \cos^2 \theta\right) \right]$$

If the satellite drifts eastward ($\Delta a < 0$) after injection with an initial e = 0.013, then the appropriate corrective velocity impulse should be imparted at apogee. A westward drift ($\Delta a < 0$) requires a braking correction at perigee. In either case, assuming a maximum period error of ± 1000 seconds, the eccentricity will be diminished from 0.013 to 0.005. Further reductions in eccentricity can be accomplished during the station keeping mode. (If Δa or Δe should prove to be zero following injection, then the use of two tangential impulses 12 hours apart will permit correction of one element without affecting the other.)

c. Correction of the Given Injection Errors (Nonimpulsive)

Since the specified mean motion error is small, it is desirable to correct the in-plane guidance injection errors (Δa and Δe) utilizing the cold gas, low thrust, attitude control propulsion engine. The semimajor axis perturbation equation is independent of the thrust level, provided tangential thrust is always applied and the initial orbit is nearly circular. Eccentricity perturbations, however, must be modified for the extênted, low-level thrust case. For tangential thrust

$$\dot{e} = \frac{\sqrt{1 - e^2}}{na} (\cos E + \cos \theta) \frac{T}{m}$$

Eccentricity errors are diminished by thrusting in the direction of motion, (when $\Delta a < 0$), in a bounded region of true anomaly defined by $90 \leq \theta \leq 180°$, or by thrusting opposite to the direction of motion (when $\Delta a > 0$) in a region bounded by $-90 \leq \theta \leq 90°$.

d. Correction Technique for Low Altitude Waiting Ascent

With regard to the Agena or Centaur ascent mode, it is assumed that sufficiently accurate tracking data can be obtained approximately 5 hours after apogee firing to determine the errors in the orbital elements a and e.

A mean motion correction can be applied between 5 and 24 hours after injection and always compensate the eccentricity error. When the correction is effected, the station longitude error will thus be less than 5° for the worst case. This initial longitude error is considered as an initial condition for the station keeping mode.

e. Correction Technique for High Altitude Waiting Ascent

The high altitude phasing technique recommended below is predicated on the 1000 sec/period error stipulated in the work statement. Any significant increase in this error would alter the phasing technique.

1) Eastward Drift. The selection of a maximum allowable wait time, coupled with the given period error of ±1000 sec * subsequent to the apogee kick, specifies the propellant necessary for final orbit circularization. For purposes of discussion, let the maximum wait time be two weeks. On this basis, the nominal velocity deficiency to ensure this eastward drift is $\Delta V_c = 199$ $\Delta V_c = 199$ ft/sec, since the required $\dot{\lambda} = 232°/14$ days and from Figure 3-5, $\Delta V_c = 160 + 39$ ft/sec to cover a possible opposing injection error. This corresponds to an apogee kick velocity of $\Delta V_K - 4653$ ft/sec. The maximum and minimum waiting times are 14 and 9 days, respectively, depending on the actual

---

* It is assumed that the period error is approximately equivalent to a ± 39 ft/velocity error for the range of waiting orbit periods considered.

value of the injection velocity error (opposing or aiding $\dot{\lambda}$). It is thus seen that a 238 ft/sec (199 + 39 ft/sec) velocity reserve must be made available for final circularization. Should an equivalent excess velocity error of +39 ft/sec remain after injection, then approximately 78 ft/sec of unused propellant would remain after circularization. An increase in period error $|\Delta P|$ increases this propellant contingency.

2) Westward Drift. To obtain a westward drift of the satellite, an injection velocity in excess of the nominal injection velocity of 4852 ft/sec must be provided, with due allowance for the random injection velocity error. Thus, an apogee velocity increment of $\Delta V_K = 4971$ ft/sec nominal results in a maximum two-week westward drift maneuver to the desired longitude station. The nominal excess velocity at injection is 119 ft/sec to guarantee the required minimum $\dot{\lambda}$ of 128°/14 days, and the reserve velocity required to ensure circularization is 158 ft/sec. Approximately 238 ft/sec more characteristic velocity is required for the westward, as opposed to the eastward, drift maneuver. Accordingly, an eastward drift maneuver is recommended. It is assumed that ground track stations (South Africa, Australia) will be available during the eastward drift maneuver to provide required orbital data.

It is noted that for higher injection velocity errors, the total increase in characteristic velocity for the injection and circularization manuevers would still be equal to the random injection velocity error. The off-nominal bias for the injection velocity would be correspondingly smaller, however.

3) Intermediate Drift Correction. The number of discrete waiting revolutions and the drift rate in the eastward waiting orbit are related as follows:

$$N = \frac{\Delta\lambda}{\Delta\dot{\lambda}} \, \frac{P_{24}}{P_W} = \frac{\Delta\lambda}{360} \, \frac{360 + \Delta\dot{\lambda}}{\Delta_{\dot{\lambda}}}$$

Since $16.6°/\text{day} < \Delta\dot{\lambda} < 26.8°/\text{day}$, (based on $\Delta V_c = 199$ ft/sec and $\Delta V = \pm 39$ ft/sec), N is bounded by $9.3 < N < 14.6$. In general, therefore, the exact station longitude will not be accessible when the vehicle is at the waiting orbit apogee. Circularization must be accomplished near apogee. A horizontal impulse ($\Delta V_c \sim 199$ ft/sec) applied at a position removed from $\theta = 180°$, for the range of waiting orbit eccentricity chosen ($0.03 < e_W < 0.05$), would yield unacceptable eccentricity errors in the final orbit.

Two alternatives for circularizing near apogee exist:

(1) Apply ΔV_c during that revolution which results in a minimum station longitude miss.

(2) Apply a small period correction a few days prior to station attainment. At the subsequent appropriate time (when vehicle and station are at desired positions) apply circularizing impulse.

Technique (1) is predicated on a single restart capability subsequent to the apogee kick maneuver. In this instance, the maximum longitude miss distance may reach 14°. Rather than applying an exact circularizing impulse, therefore, a velocity defined by $\Delta V_c \pm \epsilon$ must be applied at the nearest apogee. The velocity increment ϵ initiates a drift toward the desired station position. When on-station tolerance is realized, the station keeping mode is activated. This technique has two drawbacks. First, eccentricity corrections are charged to the station keeping mode and second, a total drift time in excess of 2 weeks can result.

Technique (2) is favored. During the extended drift time the orbital elements can accurately be determined. Accordingly, a few days prior to station attainment, a small corrective impulse is applied. This impulse both corrects eccentricity and adjusts the semimajor axis to yield an integral number of revolutions before the desired longitude station is reached and before circularization can be effected. Three firing intervals, including ΔV_K, are required. A typical longitude-latitude trace of the high altitude waiting maneuver, to station injection, is shown in Figure 3-6.

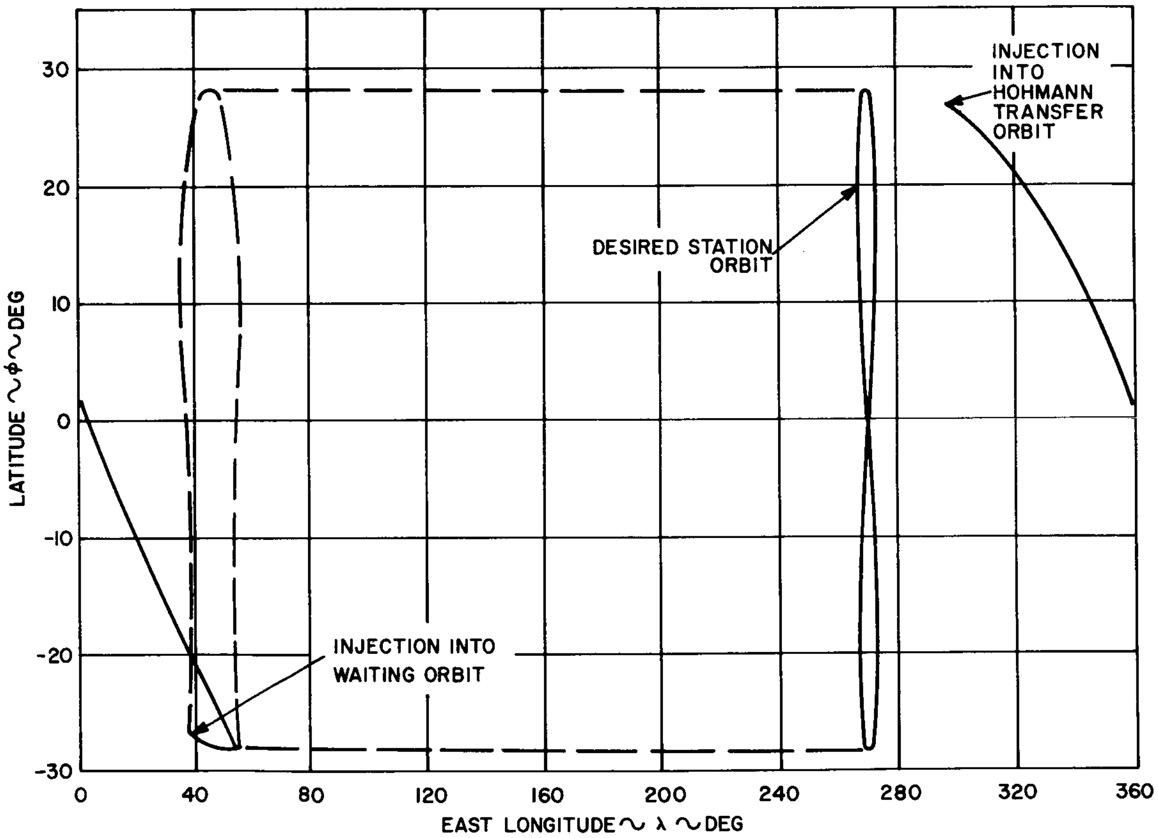

Figure 3-6. High Altitude Waiting Trajectory-Latitude-Longitude Trace

6. Propulsion Requirements

a. Apogee Kick Maneuver

Liquid rocket engines were compared to solid engines and a low thrust gas system in an attempt to define suitable spacecraft engines for the apogee kick, injection error correction, and station keeping modes. Factors such as spacecraft adaptability, reliability, payload weight, and error correction magnitudes formed the basis for the study. Maximum payload and adaptability constraints were satisfied (see Volume 2) by utilizing a solid engine to supply the apogee kick impulse (4653 to 6030 ft/sec).

b. Injection Error Correction

The given injection velocity error (39 ft/sec) and eccentricity error (0.013) can be corrected by using the cold gas altitude thrust system considered in Section II. Four attitude jets will supply a combined rearward corrective thrust of 0.044 lb (see Section 4). A single nozzle engine is used to provide a 0.044 lb forward thrust if needed. Semimajor axis correction for the given injection errors requires a nominal burn time of $t_b \approx 39 \left[\frac{1200}{0.044(32.2)}\right] \approx 33 \times 10^3$ sec or about 0.4 day. If thrust is initiated when $90° < \theta < 126°$ $(\Delta a < 0)$, then the eccentricity can be reduced to an acceptable value of 0.008.

The injection error for the Atlas-Agena-spacecraft system can be larger than the given injection errors. A 3σ estimate of these errors is given below (Ref 3-3):

ΔV (inclination) = 106 ft/sec
ΔV (mean motion) = 132 ft/sec
e = 0.025

The inclination error corresponds to 0.6°. This is within tolerable excursion limits; consequently, nonplanar corrections are unnecessary. The corrective propulsion system must therefore be sized to provide a velocity increment equivalent to 132 ft/sec, which can also compensate the indicated eccentricity.

7. Conclusions

The following conclusions are drawn

(1) Boosters which have restart capability can inject a satellite into a synchronous equatorial orbit stationed at 90°W longitude within 6.43 hours. A small (1.5°) off-east launch azimuth is required. The apogee kick (ΔV_K = 6030 ft/sec) is supplied by a solid rocket engine.

(2) The given injection velocity error (39 ft/sec) and eccentricity error (0.013) can be corrected within 5 to 24 hours by the horizontal application of a 0.044 pound

thrust generated by the cold gas attitude propulsion system. The given inclination error ($\Delta i = 0.8°$) need not be corrected, since the resultant subsatellite latitude oscillations will be within the ±2° desired.

(3) A waiting time between 9 and 14 days in a high altitude waiting orbit is required to establish a 28.3° inclined synchronous orbit centered at 90°W longitude utilizing a nonrestartable booster (Thor-Ad). Waiting time is predicted on a nominal period error of 1000 sec and an apogee kick equivalent to 4653 ft/sec which is biased low by 199 ft/sec from the nominal injection velocity of 4852 ft/sec. This causes the satellite to drift east from its injection longitude of 38.5°E to its desired longitude of 90°W within 14 days.

During the high altitude wait period, where the orbit elements become known, a corrective impulse which properly adjusts the vehicle-station phasing and partially corrects eccentricity errors is applied. A subsequent velocity impulse during the on-station pass circularizes the orbit. The sum of both velocity impulses is bounded by 199 ± 39 ft/sec. Thus, the total increase in characteristic velocity required for the apogee kick and circularization maneuvers is 39 ft/sec, the given random injection velocity error. The same result would hold for higher injection velocity errors, but the initial bias on injection velocity would be correspondingly smaller.

B. PERTURBATIONS

1. Summary

Terrestrial and extra-terrestrial perturbations on 24-hour satellites in equatorial and inclined orbits have been computed. A satellite initially located at 90° W longitude in a synchronous, equatorial orbit will drift west 75° in 1.1 years. This longitude excursion results primarily from the second sectorial harmonic of the Earth's gravitational field. A longitude station keeping requirement is therefore established. Lunar-solar perturbations cause a maximum latitude excursion of ± 0.75 degree after one year which does not require correction. The foregoing results are not substantially altered for an orbit with moderate inclination ($i \leq 30°$), although the longitude drift will be somewhat reduced.

2. General

The SMS is to be launched into a "stationary", geocentric orbit that is fixed (or centered for an inclined orbit) at a 90° W longitude station. This concept of a "stationary position" relative to the Earth (apart from the figure-8 ground trace pattern associated with an inclined orbit) is limited to two-body mechanics. Inclusion of noncentral and/or non-Newtonian forces cause the satellite to drift from its "ideal position." Knowledge of satellite deviations becomes essential for defining station keeping propellant and guidance requirements.

The more important perturbation influences relative to the SMS mission are treated herein. Earth oblateness and extra-terrestrial perturbations are included in subsection B.3, while perturbations resulting from the Earth's equatorial ellipticity are discussed in subsection B.4. Subsection B.5 pertains to the approximate changes in the ideal two-body injection altitude due to the inclusion of multi-body effects.

3. Earth Oblateness and Extra-Terrestrial Perturbations

a. General

The perturbative influences due to Earth oblateness, lunar-solar gravitational forces, and solar radiation pressure forces have been developed in Ref. 3-1. These results were based on general perturbation theory (Refs. 3-4 to 3-11) and verified by special perturbation techniques (Refs. 3-2, and 3-12 to 3-15). Orbital perturbation forces ascribed to solar winds, interplanetary dust, solar reradiation from the Earth, and electrostatic and magnetic drag were neglected, since these forces are many orders of magnitude less than the perturbations mentioned above.

Guidance system limitations preclude the achievement of an exact cir cular orbit. Hence, for the initial perturbation studies reported herein, an initial orbit eccentricity of 0.005 was assumed.* (The ascent and injection studies of Section III-A consider the nominal eccentricity error of 0.013 given in Ref. 3-1.) This initial location of the argument of perigee (ω) has a moderate influence on the maximum osculation of the elements. This effect, as well as the results of Ref. 3-1, are next summarized for the case of an equatorial orbit.

---

* An increase in initial eccentricity to 0.013 would have no significant effect on the subsequent perturbations.

b. Semimajor Axis

The semimajor axis a is the most crucial element with regard to longitude drift. Solar, lunar, or Earth oblateness gravitational perturbations cannot produce a secular change in a semimajor axis. Also, to the extent of the subject analysis, Δa experiences no long period motion from the aforementioned gravitation sources. Solar radiation pressure forces, however, induce a semimajor axis change each time the satellite enters the shadow. This change, based on 78 hours of shadow time for the most critical perigee orientation of an assumed 0.005 eccentric orbit, amounts to an 8 ft/year Δa reduction.* Accordingly, secular Δa perturbations can be safely neglected.

Short period perturbations due to lunar-solar gravitational effects are shown in Figure 3-7 for two Moon-Sun-satellite initial configurations. A 12°/yr steady easterly subsatellite drift occurs when the Sun, Moon, and satellite are all initially aligned along a common radius. Altering the initial configuration (Sun and Moon located along a common radius and positioned 90° from the satellite; $\theta = -90°$; $g_{s_0} = g_{m_0} = 0$; $\Omega_m = \Omega_s = 0$) alters the osculation level.

It is emphasized that relative drift, ascribed to Δa, can be nullified completely by injecting the satellite at the "correct altitude" regardless of Sun-Moon-satellite orientation or the Earth's polar shape. Specifically, once the correct mean motion is established, there will be no secular drift. The problems associated with establishment of the correct mean motion are discussed in subsection B.5.

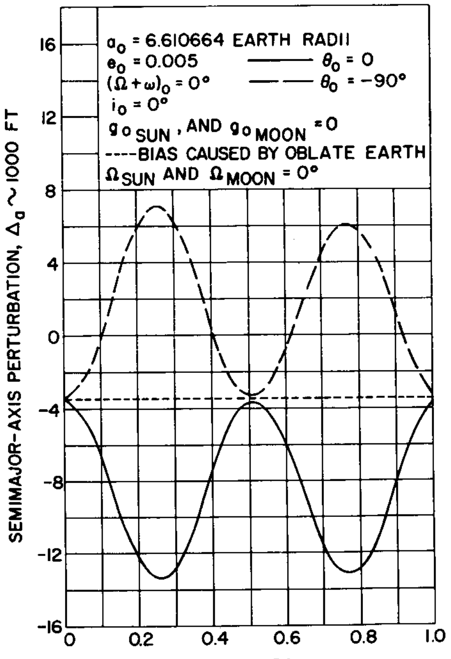

Figure 3-7. Satellite Semimajor Axis - Perturbation vs Time

---

* Based on disturbing acceleration $k = \frac{L_\odot}{4\pi C r_\odot} \frac{A}{m} = 1.8 \times 10^7 \text{ ft}^2/\text{sec}^2$.

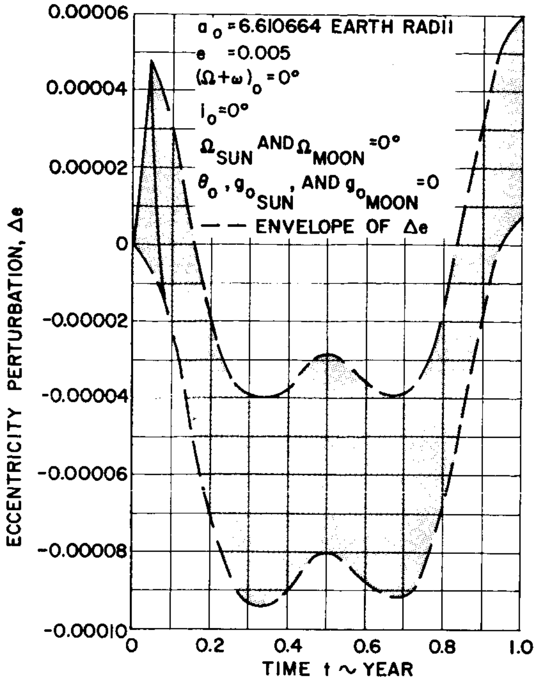

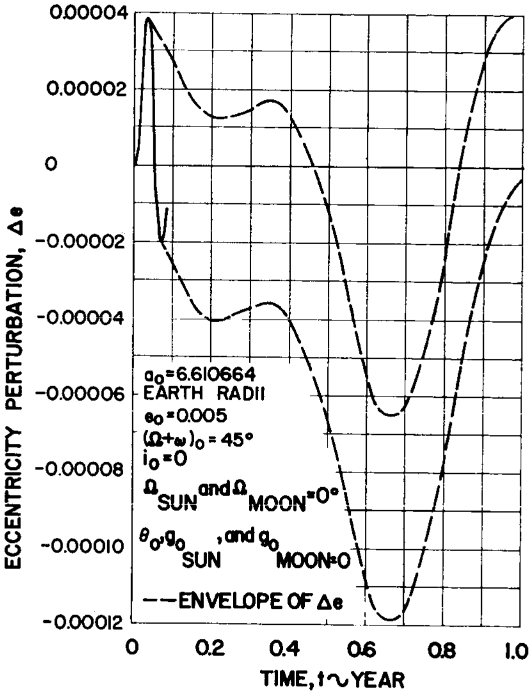

Figure 3-8a. Satellite Eccentricity Perturbations $(\Omega+\omega)_0 = 0$

Figure 3-8b. Satellite Eccentricity Perturbations $(\Omega+\omega)_0 = 45°$

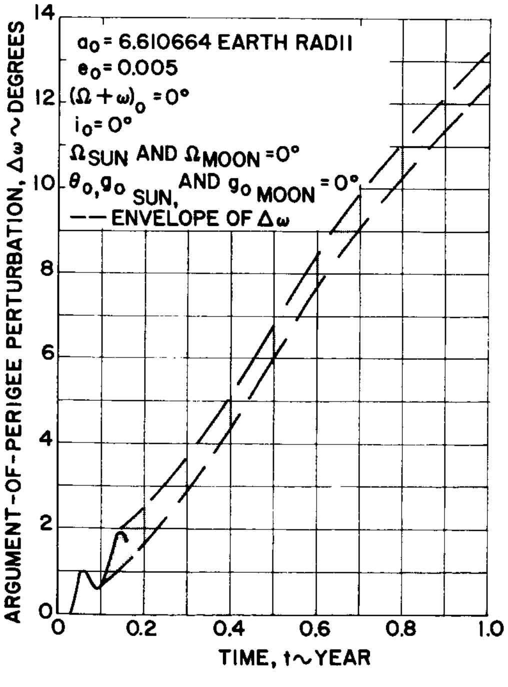

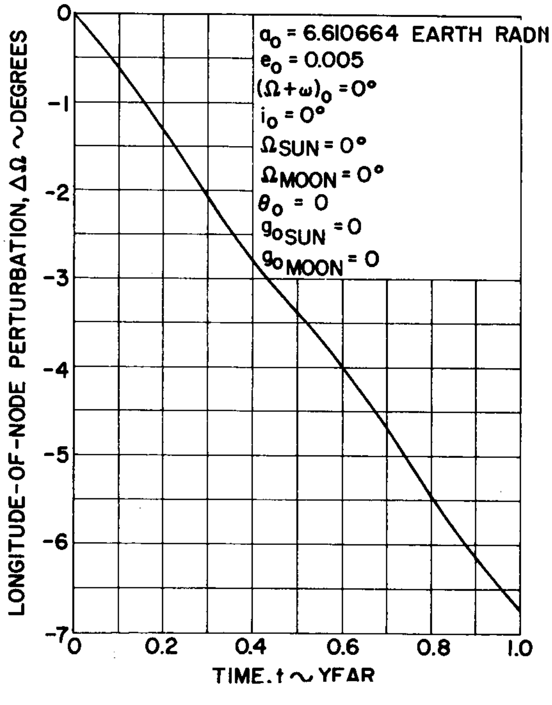

Figure 3-9. Satellite Argument of Perigee Perturbation

Figure 3-10. Satellite Longitude of Node-Perturbation vs Time

c. Eccentricity

The Earth's oblateness contribution to long period eccentricity (c) perturbations is approximately two orders of magnitude less than perturbations arising from other sources. Solar pressure forces exert a dominant influence on eccentricity. For example, when the SMS perigee is directed toward the Sun ($\Omega_s = g_s = \omega = 0$) $\Delta e_{max} = 0.82 \times 10^{-4}$ compared to lunar and solar gravitational increments of 0.55×10^{-4} and -0.47×10^{-4}, respectively. The latter values also assume that the satellite and Moon are in conjunction with the Sun. Excluded from the above increments is an additional long period change in eccentricity attributed to the secular variation in $\Delta\omega$ and $\Delta\Omega$. This term has a 26.7 year period and a maximum amplitude corresponding to $\Delta e = 2.6 \times 10^{-4}$.

A summary of the total Δe perturbations is given in Figures 3-8a and 3-8b for $\omega = 0$ and $\omega = 45°$. It is seen that perigee location influences the perturbation time history. The maximum amplitude of each preceeding perturbation can be either positive or negative depending on the perigee location or Sun-Moon orientation at maneuver outset. It is conceivable, therefore, that during a year $e_o \pm \Delta e_{max} \Big|_{LP} = 0.005 \pm 0.0002$.

d. Argument of Perigee

Figure 3-9 presents argument-of-perigee (ω) perturbations. After one year, secular terms outweigh all long period perturbations. Apsidal rotation causes a distortion rather than a growth in the longitude-latitude pattern of the subsatellite point.

e. Right Ascension of the Ascending Node

Secular longitude of the node perturbations overshadow all long period terms as shown in Figure 3-10. Nodal regression directly alters the satellite's position within the basic subsatellite pattern established by the remaining orbital elements for the assumed case of an equatorial orbit. Indirectly, the secular variation in this element induces a growth in the subsatellite pattern by virtue of its effect on other elements, notably Δi.

f. Inclinations

Inclination excursions result primarily from lunar-solar gravitational accelerations. These excursions were computed from the planetary equations (Ref. 3-7) using Musen's disturbing function (Ref. 3-4) and subsequently corroborated by special perturbation techniques (Refs. 3-12 and 3-15).

The accumulation of inclination perturbations after one year is small, about 0.75°, as shown in Figure 3-11. Nevertheless, they impart a gradual expansion in the latitude deviations from the ideal subsatellite position. The "apparent secular growth" in inclination is attributed to long period perturbations dependent on $\dot{\Omega}$ and $\dot{\omega}$. This long period contribution produces a maximum inclination change of 6.5° (0.26° caused by the Sun,and 0.49° by the Moon) and has an associated period of approximately 54 years.

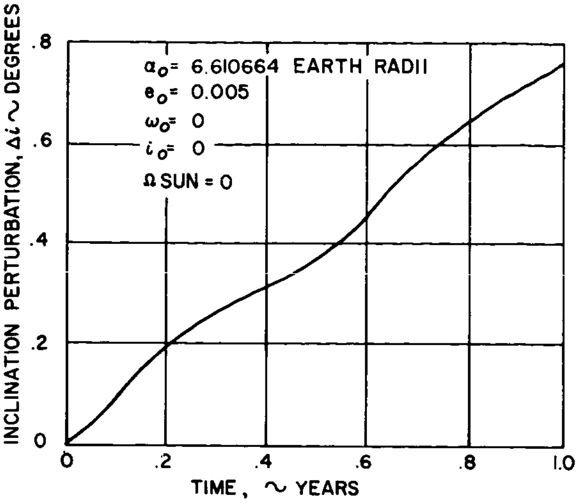

Figure 3-11. Satellite Inclination Perturbation

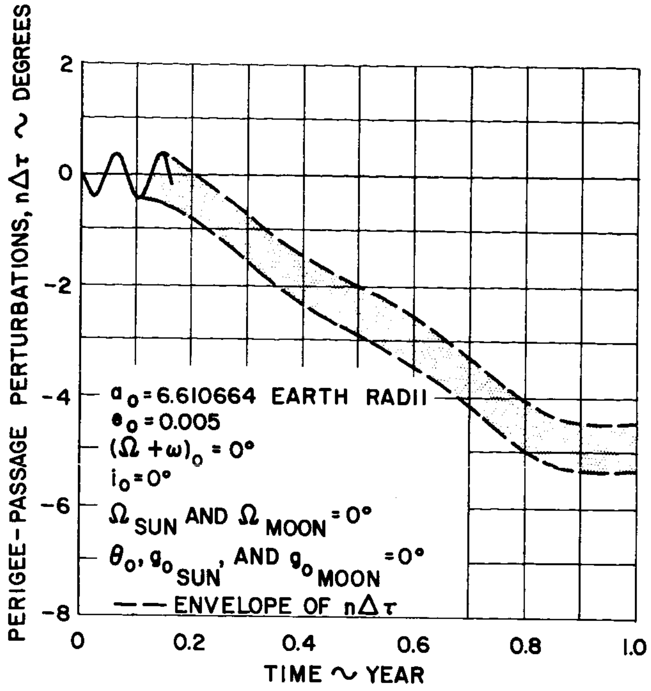

Figure 3-12. Satellite Perigee Passage-Perturbation vs Time

g. Perigee Passage

Time of perigee passage (τ) fixes the position of the vehicle in its orbit relative to an absolute time scale. Time of perigee passage perturbations, given in Figure 3-12, are unaffected by solar radiation forces. Variations in this element do not contribute to the growth or shape of the basic longitude-latitude subsatellite figure. Instead, it locates the satellite timewise within the normal pattern dictated by the proceeding elements.

h. Summary of Drift Perturbations for an Equatorial Orbit

Secular longitude drift, due to Earth oblateness and extra-terrestrial perturbations is nonexistent once a perturbed average mean motion of 2π radians per sidereal day is established. Neglecting initial eccentricity and inclination injection errors, the longitude and lattitude excursions caused by these perturbative effects after a one year mission are ± 0.25° and ± 0.75°, respectively. These excursions can safely be neglected with regard to SMS mission requirements which specify longitude-latitude excursions of ± 2° desired, ± 5° maximum.

i. Inclined Orbit

The foregoing conclusion also applies to an orbit with modest inclination ($i \leq 30°$). An obvious reduction to the secular advance of perigee and nodal regression rate for an inclined orbit is noted (Ref. 3-5).

$$\Delta\dot{\Omega}_{i\neq 0} = \Delta\dot{\Omega}_{i-0}\cos i$$

$$\Delta\dot{\omega}_{i\neq 0} = \Delta\dot{\omega}_{i=0}\left(\frac{2-5/2\,\sin^2 i}{2}\right)$$

The long period solar-lunar perturbations on orbit inclination appear to increase slightly with orbit inclination (Ref. 3-4). Also, short period semimajor axis perturbations become more pronounced, as does the eccentricity perturbation due to solar radiation pressure. Kept in the proper perspective, however, these perturbative effects are negligible compared to the Earth's equatorial ellipticity perturbation and the expected injection errors.

4. Terrestrial Perturbations - Tesseral and Sectorial Harmonics

a. General

Station keeping requirements for a 24-hour equatorial satellite stem from the dominant perturbations induced by the Earth's sectorial shape. Excursion time histories were developed in Ref. 3-1. These data are conservative, since they were based on a fundamental constant ($J^{(2)}_{(2)}$) for the second sectorial harmonic* which is 2.3 times greater than the most recent accepted value (Ref. 3-11). Accordingly station keeping correction frequencies and propellant requirements given in Ref. 3-1 are reduced as discussed herein and in subsection 3.c.

An analysis has been conducted on the effect of orbit inclination ($i \leq 30°$) on this longitude drift. Prior to discussing the results of this study, however, it is appropriate to review the large angle longitude drift excursions experienced by an equatorial satellite in the absence of station keeping.

b. Large Angle Longitude Excursions

Considering only the Earth's second sectorial gravitational harmonic, a satellite in an equatorial, circular orbit at synchronous altitude will oscillate about the nearest end of the Earth's minor axis (longitude, $\lambda m = -127.5°$). Both the magnitude and period of this oscillation depend on the initial relative position λ_{R_o} between the minor axis and satellite $\lambda_{R_o} = \lambda - \lambda m$. An approximate relationship between radial excursion (Δr, in Earth radius) and longitudinal excursions measured from the minor axis ($\Delta\lambda_m$) is (Ref. 3-14).

$$\Delta r = 4\sqrt{J^{(2)}_{(2)}}\,\sin\lambda_{R_o}\left[1 - \frac{\sin^2\Delta\lambda_m}{\sin^2\lambda_{R_o}}\right]^{1/2}$$

$$J^{(2)}_{(2)} = 2.32 \times 10^{-6}$$

---

* The graviational disturbance forces associated with this harmonic are larger by nearly an order of magnitude than those for the other harmonics at the desired longitude station of 90° W.

Figure 3-13 presents the expected radial and longitudinal excursions for a satellite injected at 90°W longitude ($\lambda_{R_0} = 37.5°$). In the absence of injection errors, the satellite initially moves toward the minor axis at longitude 127.5°W and experiences an increase in radial displacement. The period of this oscillation is 2.22 years. After 1.11 years, the satellite is displaced 75°W from the desired subsatellite station. Obviously, this motion must be restrained, since the maximum tolerable longitude oscillation is ± 5°.

c. Nodal and Inclination Perturbations

Inclination changes due to the second sectorial harmonic are nonexistent for an equatorial orbit. As the orbit inclination increases, however, both nodal and inclination perturbations are introduced.

Incremental inclination and nodal excursions were developed from the force function (see Appendix C) which includes the second harmonic $J_2(2)$ as well as $J_3^{(1)}$, $J_3^{(3)}$, and $J_4^{(1)}$. These harmonics were chosen, since their coefficients are of the same relative magnitude (Ref. 3-13). From the development given in Appendix C, it was found that the long period motions can be represented by the following expressions (i = 28.3°)

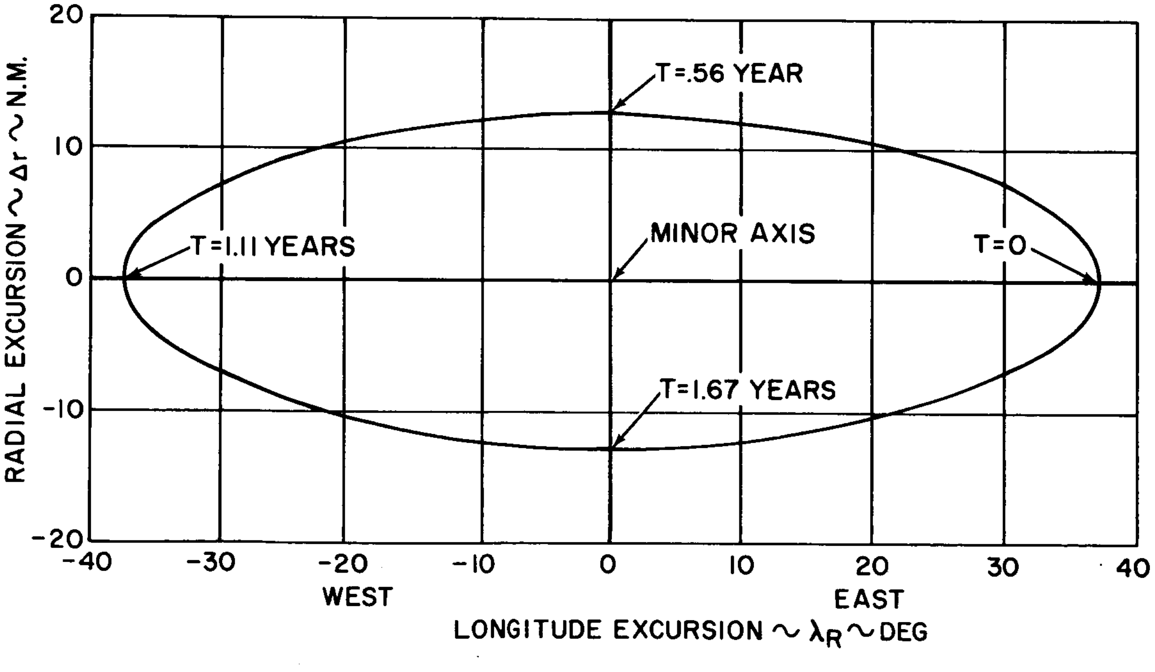

Figure 3-13. Long Period Oscillation for a Satellite Injected into a Synchronous Equatorial Orbit at 90°W Longitude

$$\Delta\dot{\Omega} = -0.088\,[-4.36 \sin(2\Omega+74) - 0.569 \sin(\Omega-22) + 0.310 \sin(3\Omega-154)]$$

$$\Delta i = 0.186\,[8.20 \cos(2\Omega+74) - 0.098 \cos(\Omega-22) + 1.23 \cos(3\Omega-154)]$$

A maximum nodal change of 0.12° is noted after one year, whereas, in the same time period, the inclination changes by 0.19°.

d. Small Angle Excursions for an Indirect Orbit

Based on the foregoing, the orbit plane can be assumed to remain essentially space fixed for the desired mission time under consideration. As a result, the determination of longitude drift for an inclined 24-hour orbit is resolved to a planar problem, where the orbit plane is treated as the fundamental reference and only those perturbative forces which act in the plane need be considered. Hence, planar equations of motion are taken as follows

$$\ddot{r} - r\dot{\theta}^2 = -\frac{\mu}{r^2} - \frac{\partial v}{\partial r}$$

$$r\ddot{\theta} + 2\dot{r}\,\dot{\theta} = -\frac{\partial v}{r\partial\theta}$$

where v represents the perturbing potential function. The radial and normal acceleration perturbations due to the fundamental harmonic ($J_2^{(2)}$) are of prime concern, since the other harmonics, when appropriately included in the equation, are nearly an order of magnitude smaller. These accelerations are (see Appendix C and Figure 3-14):

$$F_r = -\frac{\partial V}{\partial r} = -\frac{9}{4}\frac{\mu J_2^{(2)}}{r^4}\Big[(1+\cos i)^2 \cos 2(\theta - h_{M_o} - n_s t) + 2 \sin^2 i \cos 2(h_{M_o} + n_s t)$$
$$+ (1-\cos i)^2 \cos 2(\theta + h_{M_o} + n_s t)\Big]$$

$$F_\theta = -\frac{\partial V}{r\partial\theta} = -\frac{3}{4}\frac{\mu J_2^{(2)}}{r^4}\Big[2(1+\cos i)^2 \sin 2(\theta - h_{M_o} - n_s t) + 2(1-\cos i)^2 \sin 2(\theta + h_{M_o} + n_s t)\Big]$$

where h_{M_o} is the major axis hour angle at problem start. True anomaly deviations* ($\Delta\theta$) from the idealized two-body problem are sought. In the absence of perturbative forces $r = r_s$; $\theta = \theta_o = n_s t$; $\dot{r} = \theta$; $\dot{\theta} = n_s$. Small deviations from this motion are found by perturbing the above set ($r = r_s + \Delta r$, $\theta = \theta_s + \Delta\theta$). This yields

$$\Delta\ddot{r} - 2r_s n_s \Delta\dot{\theta} - 3n_s^2 \Delta r = -\frac{9}{4}\frac{\mu J_3^{(2)}}{r_s^4}\Big[(1+\cos i)^2 \cos 2h_{M_o} + 2 \sin^2 i \cos 2(h_{M_o} + n_s t)$$
$$+ (1-\cos i)^2 \cos 2(h_{M_o} + 2n_s t)\Big]$$

$$r_s \Delta\ddot{\theta} + 2n_s \Delta\dot{r} = -\frac{3}{2}\frac{\mu J_2^{(2)}}{r_s^4}\Big[-(1+\cos i)^2 \sin 2h_{M_o} + (1-\cos i)^2 \sin 2(h_{M_o} + 2n_s t)\Big]$$

---

* This deviation is equivalent to longitude excursion ($\Delta\lambda$) when i = 0.

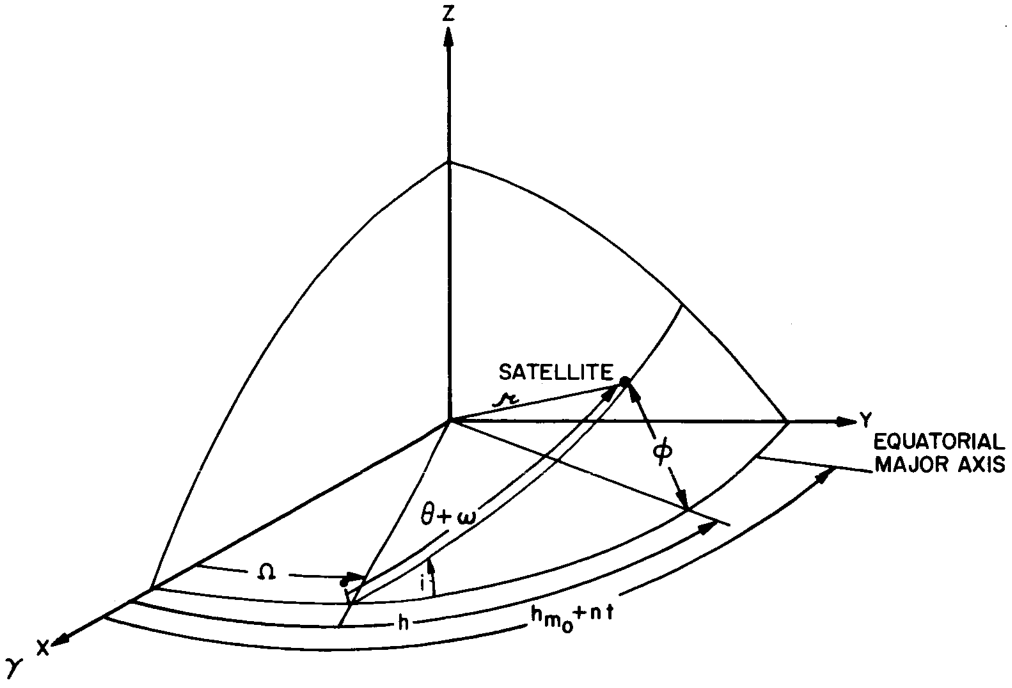

Figure 3-14. Geometry Schematic

It has been assumed that

(1) Products of differentials are negligible

(2) The reference axis coincides with the node at the desired equatorial station ($\Omega = 0$); hence, for a satellite at 90°W longitude $h_{M_o} = 90-37.5 = 52.5°$

(3) The products formed by $J_2^{(2)}$ and the differentials are small and can be neglected in the presence of $J_2^{(2)}$. This assumption leads to erroneous periodic motion; however, the character of the more important, apparent secular contributions will not be altered.

The change in radius and angle is thus given by

$$\Delta r = a \sin n_s t + b \cos n_s t + \frac{\alpha}{n_s^2} t + \frac{\beta}{n_s^2} - \frac{\gamma}{3n_s^2} \cos 2(h_{M_o} + n_s t) - \frac{\delta}{15 n_s^2} = \cos 2(h_{M_o} + 2n_s t)$$

$$\Delta\theta = d + ct + \frac{\alpha^* t^2}{2} - \frac{2}{r_s}(b \sin n_s t - a \cos n_s t) - \frac{\gamma^*}{4n_s^2} \sin 2(h_{M_o} + n_s t) - \frac{\delta^*}{16n^2} \sin 2(h_{M_o} + 2n_s t)$$

where the arbitrary constants are

$$a = \Delta r_o - \frac{\beta}{n_s^2} + \frac{\cos 2h_{M_o}}{2n_s^2}\left(\delta + \frac{\delta}{5}\right)$$

$$b = an_s + \frac{\alpha}{n_s^2} + \frac{2\gamma}{3n_s}\sin 2\, h_{M_o} + \frac{4\delta}{15n_s}\sin 2\, h_{M_o}$$

$$c = \Delta\dot{\theta}_o + \frac{2ns}{r_s} + \frac{\cos 2h_{M_o}}{2n_s}\left(\gamma^* + \frac{\delta^*}{2}\right)$$

$$d = \Delta\theta_o - \frac{2a}{r_s} + \frac{\cos 2h_{M_o}}{2n_s}\left(\gamma^* + \frac{\delta^*}{2}\right)$$

and

$$\alpha = \frac{3(1+\cos i)^2}{r_s^4} n\mu J_2^{(2)} \sin 2\, h_{M_o};\ \alpha^* = -\frac{3}{2}\frac{\alpha}{r_s n_s}$$

$$\beta = -\frac{9}{4}\frac{(1+\cos i)^2}{r_s^4}\mu J_2^{(2)} \cos 2\, h_{M_o}$$

$$\gamma = -\frac{9}{2}\frac{\sin^2 i}{r_s^4}\mu J_2^{(2)} \qquad ;\ \gamma^* = -\frac{4}{3}\frac{\gamma}{r_s}$$

$$\delta = -\frac{3}{2}\frac{(1-\cos i)^2}{r_s^4}\mu J_2^{(2)} \qquad ;\ \delta^* = \frac{7}{15}\frac{\delta}{r_s}$$

Only those terms which exhibit an apparent secular drift are of interest; hence, for $\Delta r_o = \Delta r_o = \Delta\dot{\theta}_o = \Delta\theta_o = 0$

$$\Delta r = \frac{3t(1+\cos i)^2}{r_s + n_s}\mu J_2^{(2)} \sin 2\, h_{M_o}$$

$$\Delta\theta = -\frac{9}{4}t^2\frac{(1+\cos i)^2}{r_s^5}\mu J_2^{(2)}\sin 2h_{M_o} + \frac{3}{2}t\frac{\left(\frac{5}{2}+7\cos i+\frac{5}{2}\cos^2 i\right)}{r_s^5 n_s}\mu J_2^{(2)}\cos 2h_{M_o}$$

It is thus seen that the effect of the equatorial ellipticity on drift rate diminishes with orbital inclination.

A satellite positioned at the desired station 90°W of Greenwich would exhibit the drift tendency shown in Figure 3-15. These data are based on the constant $J_2^{(2)} = 2.32 \times 10^{-6}$ with the semimajor axis located at 37.5°W longitude (Ref 3-13). The satellite whose orbit is inclined 28.3° drifts 5° in 74 rather than 70 days.

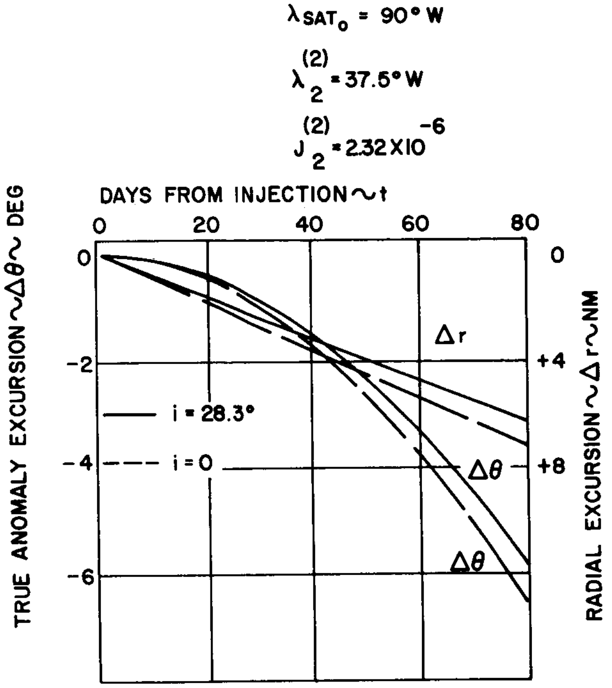

Figure 3-15. SMS Station Drift

e. Ideal Station Keeping Requirements

The nominal circular velocity is given by

$$V = r_s n_s$$

The velocity increment necessary to correct small orbital perturbations is

$$\Delta V = r_s \Delta n + n_s \Delta r$$

where the average change in mean motion can be represented by

$$\Delta n = \Delta\dot{\bar{\theta}} = -\frac{9}{2}t\frac{(1+\cos i)^2}{r_s^5}\mu J_2^{(2)}\sin 2h_{M_o}$$

Hence, the corrective velocity becomes

$$\Delta V = -\frac{3}{2} t \frac{(1+\cos i)^2}{r_s^4} \mu J_2^{(2)} \sin 2\, h_{M_o}$$

This expression could have been obtained by determining the velocity requirement necessary to suppress the circumferential acceleration perturbation

$$\left(\Delta V = -\frac{3}{2} \frac{\mu J_2^{(2)}}{r_s^4} \left[(1+\cos i)^2 \sin 2 h_{M_o} \int_0^t dt + (1-\cos i)^2 \int_0^t \sin(h_{M_o} + 2 n_s t)\, dt\right]\right).$$

It is computed that the velocity impulse necessary to maintain a station position at 90°W longitude is approximately 7 ft/sec/yr. This velocity requirement is independent of the number of discrete station keeping corrections made during a year's operation. Accordingly, two horizontal impulses are sufficient to maintain a ± 5° station longitude tolerance during the first 370 days from injection. This subject is further discussed in Section 3.c.

5. Injection Altitude Correction

a. General

The ideal or two-body orbit injection conditions (h_o, V_o) must be modified slightly to ensure a sidereal period in the presence of multibody forces. Estimates of the appropriate change in Keplerian semimajor axis due to Earth oblateness and lunar-solar effects are next given for comparison with the expected period error of 1000 sec (Ref 3-2) caused by the injection guidance system.

b. Polar Flattening

The difference in mean motion from two-body considerations $(n\phi)_S$ due to the introduction of the second zonal harmonic* for the Earth's gravitational field is (Ref 3-10)

$$\Delta n = n - n_s = n_s \frac{J_i}{a_o^2} (1 - 1.5 \sin^2 i)$$

For a synchronous satellite orbit inclined 28.3°, the mean motion increase is equivalent to a daily reduction of 2.14 sec. This effect is compensated by increasing the semimajor axis by 2270 ft ($\Delta a = \frac{2}{3} \frac{\Delta P}{P} a$). The altitude change required for an equatorial orbit is shown in Figure 3-7.

c. Lunar-Solar Gravitation

First order, short period, semimajor axis excursions resulting from lunar-solar perturbations (for circular orbits) can be approximated as

---

* Higher order harmonics have a negligible effect on semimajor axis.

$$\Delta a = \frac{3}{4}\left(\frac{\mu}{R^3}\right)\frac{a}{n_s}\left[\frac{\cos 2(\theta+\Omega)\sin^2\iota'}{n_s+\dot{\Omega}} + \frac{\cos 2(\theta+\Omega-g')}{n_s+\dot{\Omega}-\dot{g}'}\left(\frac{1}{2}+\frac{\cos^2\iota'}{2}+\cos\iota'\right) + \frac{\cos 2(\theta+\Omega+g')}{n_s+\dot{\Omega}+\dot{g}'}\left(\frac{1}{2}+\frac{\cos^2\iota'}{2}-\cos\iota'\right)\right]$$

Parameter ι' is the relative orbital inclination with respect to either the lunar or solar plane. Parameter g' represents the true anomaly of the Moon or Sun.

Satellite drift due to injection at the "incorrect altitude" ($a_o = \left(\frac{\mu P^2}{4\pi^2}\right)^{1/3}$) depends on the initial relative position between the Sun, Moon, and satellite. Let the satellite, Moon, and Sun be aligned at injection ($\theta = g_m = g_S = 0$), and assume $i = 28.3°$, $i_m = 19°$, $i_S = 23.4°$. On this basis, the semimajor axis must be increased by 5090 ft (3500 ft Moon, 1550 ft Sun) to compensate for the effective change in central mass. The change in semimajor axis required for an equatorial orbit is given in Figure 3-7.

d. Nodal Regression

The nodal regression rate for an inclined circular orbit is

$$\Sigma\dot{\Omega} = -\cos i\left[\frac{J_2 n_s}{a^2} + \frac{3}{4n_s}\left\{\frac{\mu_m}{R_m^3}\left(1-\frac{3}{2}\sin^2\iota_m\right)\bigg|_{\text{Moon}} + \frac{\mu_s}{R_s^3}\left(1-\frac{3}{2}\sin^2\iota_s\right)\bigg|_{\text{Sun}}\right\}\right]$$

Hence, using the previous inclination values, where $\Sigma\dot{\Omega} = -4.30 - 1.17_m - 0.48_S = -5.95°/\text{year} = 0.0164°/\text{day}$.

It is desired that the satellite coincide with a given longitude (90°W) at each equator crossing (see sketch). At injection let the satellite and desired longitude be at position A. After 3.92 seconds less than a sidereal day, ($\Delta P = \Delta\dot{\Omega}/\omega_{\text{Earth}} = 0.0164/\omega_E$), the desired longitude will again coincide

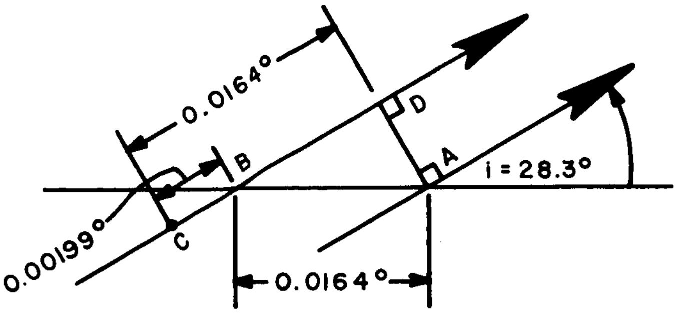

ANGLE AD REPRESENTS THE SATELLITE'S INERTIAL PERIOD with the orbit's ascending mode. However, the satellite will be at position C ($\overline{CD} = \Delta\Omega$). Unless corrected, this "drift" will build up with time. A correction implies a period "speed up" such that the satellite travels along the arc $\overline{CB}$ in the time it takes the Earth to rotate through the angle AB (360° - 0.0164°). This is accomplished by a 0.475 sec period reduction or equivalently a 507 ft semimajor axis reduction.

e. Summary of Altitude Errors

The foregoing semimajor axis changes represent known perturbations to the two-body ideal injection altitude. Even if the injection altitude were based on an ideal model, the subsequent drift would be extremely small compared to injection guidance errors which correspond to a semimajor axis error of 0.051 E. R. (ΔP = 1000 sec). As a result, the foregoing altitude errors can be neglected with respect to the injection errors.

6. Conclusions

The following general conclusions are drawn concerning Earth oblateness and extra terrestrial perturbations.

(1) The secular changes in semimajor axis due to radiation pressure is negligible during the useful SMS lifetime. Hence, secular longitude drift due to those perturbations is nonexistent once a "24-hour" perturbed mean motion (n) is established.

(2) Orbital corrections to compensate for these perturbations are unnecessary for the planned one year SMS lifetime, since longitude-latitude deviations are well within maximum tolerable values (± 5°).

(3) More stringent longitude-latitude tolerances, coupled with an extended lifetime capability, would dictate thrust connections requirements due to the buildup of orbital inclination and eccentricity.

The following conclusions pertain to perturbations associated with the terrestrial and sectorial harmonics of the Earth's gravitational field.

(1) The Earth's equatorial ellipticity associated with the dominant second sectorial harmonic causes a 24-hour equatorial satellite, located at 90° west longitude, to drift west by 75° in approximately one year. Hence, a station keeping requirement is established.

(2) A slight reduction in longitude drift can be expected for an inclined SMS orbit. The SMS takes 4 days longer to drift 5° (74 days instead of 70) when the orbit inclination is increased from 0 to 28.3°.

(3) The tesseral harmonics cause small nodal and inclination excursions on a SMS inclined orbit. These perturbations can be safely neglected.

Finally, the two-body synchronous injection conditions must theoretically be modified slightly to compensate for noncentral gravitational forces; however, such effects will be completely overshadowed by the expected period error caused by injection guidance inaccuracies.

C. STATION KEEPING

1. Introduction and Summary

This section describes briefly the results of general studies conducted on the station keeping problem for the Synchronous Meteorological Satellite (SMS). The major portion of these studies was devoted to the case of an equatorial orbit, although consideration was also given to inclined orbits. For these studies, in order to satisfy the meteorological mission of this satellite, the station keeping requirements were based largely on ensuring effective coverage of the area of interest by the sensors under consideration.

For the studies described first in this section, it was assumed that it is desired to put the satellite into a circular, equatorial, synchronous orbit above a 90° W longitude station. The satellite station keeping requirements were specifically taken to be the following:

(1) The latitude of the satellite subpoint shall be held within ± 5° maximum, ± 2° desired.

(2) The longitude excursions of the satellite subpoint about the desired 90° W longitude shall also be held within ± 5° maximum, ± 2° desired.

The mission duration was assumed to be one year. A major design objective was to use the same thrust devices for station keeping as are used for attitude control (see Section 2). It was further assumed that the ground radar angular tracking accuracies are of the order of 10 milliradian, as dictated by communication system requirements.

The primary guidance function considered in the studies was that of keeping the satellite above the desired longitude on the Earth's equator. A further limited study was conducted on the required compensation of possible injection errors so as to put the satellite into the desired orbit within the allowable tolerances set by the primary quantities of interest; namely, the longitude and latitude excursions of the satellite subpoint.

Perturbative influences on the assumed synchronous orbit include the gravitational attraction of the Sun and Moon, solar radiation pressure, and the gravitational disturbances caused by the nonspherical shape of the Earth. The most significant perturbing influence on the synchronous satellite has been established to be that caused by the nonsphericity of the Earth, in particular its equatorial variations. (Earth oblateness was also examined, and its primary effect is shown to affect only the mean motion of the satellite, this effect being largely obscured by the realizable initial mean motion errors caused by injection errors.)

In subsection 3.B.4, the major orbit perturbing influence caused by the Earth's nonspherical shape is discussed in detail. More specifically, attention is focused on the perturbations of the longitude of the satellite subpoint caused by the second sectorial harmonic associated with the Earth's equatorial ellipticity, which is the predominant perturbing influence on the SMS. The latitude and longitude excursions of the satellite subpoint caused by the other existing orbital perturbing influences will not exceed the assumed station keeping tolerances. Therefore, guidance corrections will not be needed to compensate for them.

Various methods of longitudinal station keeping against the second sectorial harmonic are subsequently discussed, and it is indicated that a simple mean motion correction technique based solely on observations of the satellite subpoint longitudinal excursions is satisfactory. The impulse requirement for the associated transverse velocity corrections to compensate for terrestrial gravititional disturbances was determined. A value of 7.4 ft/sec is required for keeping a satellite positioned on station at 90° W longitude for one year. This station is about 53° west of the major axis of the Earth's equatorial ellipse represented by the second sectorial harmonic.

The orbit injection studies described in Section 3.A indicate that two elements of the initial satellite orbit will deviate from their desired values because of injection errors, as given in Ref 3-2, to an extent requiring compensation if the longitude deviation requirements are to be met. The most critical element is the semimajor axis, which is related to the period or the mean angular motion of the satellite; the other important element is orbit eccentricity.

The typical period error given in Ref 3-2 would cause a completely unacceptable steady longitudinal drift of the satellite subpoint of about 4.2°/day. A study was conducted to establish how well this major injection error could be compensated using effectively the same guidance technique considered for accomplishing the station keeping function. For initial mean motion errors in magnitude less than or equal to 5°/day, it appears that the orbit eccentricity (in particular, the associated daily longitudinal excursions) remaining after the transverse velocity correction would be acceptable, based on the assumed station keeping tolerances. However, the thrust level required for this initial velocity correction would be relatively high. (This higher thrust level is needed to prevent an intolerable excursion of the satellite subpoint from its desired injection longitude while the satellite mean error is being corrected.) Reaction jets with thrust levels of 0.007 to 0.015 pound have been considered for attitude control (see Section 2). Using four of these jets symmetrically exhausted for translation control, a suitable thrust level is provided for both correction of the mean motion injection error given in Ref 3-2 and for station keeping.

Thus, with the assumed tolerances on latitude and longitude of the satellite subpoint, it appears that longitude control is the only significant station keeping problem for the SMS in a circular, synchronous, equatorial orbit. The requirements for the longitude guidance system are effectively set by the expected initial mean motion (or period) error and eccentricity and by the perturbing effects of the Earth's equatorial ellipticity. Even on an open loop uncontrolled basis, the satellite subpoint latitude errors caused by expected injection errors and the existing orbit perturbation influences should be within the assumed tolerances (± 2° desired, ± 5° maximum) for a one year mission. If the SMS were injected into an inclined synchronous orbit, then the velocity impulse for one year of station keeping would be somewhat reduced as shown in Section 3.B. However, account must then be taken of the figure-8 satellite ground track in determining the time for initiating the drift corrections.

2. Station Keeping Against Terrestrial Gravitational Disturbances

a. Equations of Motion

For the purposes of this study, linearized perturbation equations of motion for the satellite were employed, based on deviations from a synchronous, circular, equatorial orbit. The perturbing forces associated with the gravitational potential field for a triaxial Earth (including only the fundamental and second harmonic associated with Earth oblateness and equatorial ellipticity) were introduced. The corresponding perturbation equations of motion were derived in Section 3.B for the case of an inclined orbit. Simplifying these equations to represent an equatorial orbit and adding explicit thrust terms gives

$$\begin{aligned} &\ddot{\rho} - 2r_s M_s \dot{\lambda} - 3M_s^2 \rho = \delta \frac{F}{m} \operatorname{Sin} \alpha \\ &r_o \ddot{\lambda} + 2M_s \dot{\rho} = \frac{2K_2 \sin 2\Lambda_o}{r_o^4} + \delta \frac{F}{m} \operatorname{Cos} \alpha \end{aligned} \qquad (3\text{-}1)$$

where
Λ_o = initial longitude relative to Earth's major axis, $\Lambda_o = \lambda_o - \lambda_M$
K_2 = $3J_2^{(2)} a_e^2 \mu$
ρ = radius pertubation, $r = r_x + \Delta r \equiv r_s + \rho$
λ^1 = longitude pertubation, $\lambda = \lambda_o + \Delta\lambda \equiv \lambda_o + \lambda^1$

The synchronous radius (r_s) is chosen so as to account for the constant radial force terms caused by the gravitational field of Earth, including the fundamental component, as well as the second harmonics caused by oblateness and equatorial ellipticity and to yield to synchronous mean motion, M_s. (Because only equatorial motions are considered here, the effect of oblateness is taken into account by this choice of the basic synchronous radius, r_s.) The constant $J_2^{(2)}$ relates to the second sectorial harmonic associated with the equatorial ellipticity of Earth. The term F/M corresponds to the force per unit mass (acceleration) generated by the thrust engine in the operation of the guidance system. The term α is the orientation of this force vector measured in the orbit plane; thus, $\alpha = 0$ for a forward transverse thrust and 90° for an outward radial thrust. The variable δ has three values (+1, -1, and 0), which denote accelerating, decelerating, and zero guidance thrusts for $\alpha = 0$. As discussed later, some of the initial studies were devoted to establishing the superiority of transverse thrusting over radial thrusting for mean motion changes. All of the closed loop guidance studies of the station keeping problem were then based on the use of transverse thrusts.

b. Guidance Approach

In choosing a guidance technique for keeping the satellite above a desired point on the equator, strong emphasis was placed on the following criteria. The technique should be highly reliable, simple to implement, and require only a minimum of ground track data. For these reasons, a differential mean motion correction system has been evolved. Preset, horizontal transverse thrust forces are used which are compatible with the desired vehicle orientation and the attitude control thrust requirements (see Section 2). The thrust forces are applied for prescribed times to yield prescribed velocity impulses. Only nominal accuracies are required of the ground tracking radar (well within the communication system needs) for such a guidance approach.

This mean motion correction technique operates basically as follows. It is assumed that a synchronous, circular, equatorial orbit has been attained for the desired satellite position (90° W longitude).

(1) The disturbing force associated with the equatorial ellipticity of Earth causes the satellite to drift westward relative to Earth.

(2) When this drift is observed to exceed a preselected value ($\lambda^1{}_{LIM}$), the same thrust devices that are used asymmetrically to provide attitude control torques will be exhausted symmetrically to provide a translation force for a prescribed time. (If $\lambda^1{}_{LIM}$ is 2° and $\lambda^1{}_o = \dot{\lambda}_o = 0$, this condition would be reached in about 39 days, as shown later in this section.)

(3) This corrective velocity impulse, which is actually a westward braking impulse, will increase the mean motion of the satellite and cause it to drift eastward relative to the Earth.

(4) If the magnitude of this impulse is properly chosen, the satellite can be caused to drift eastward again a maximum of 2° from the desired longitude before the gravitational perturbing forces stop its relative motion and again cause it to drift westward.

(5) When the satellite again drifts past $\lambda^1{}_{LIM}$ boundary (92° W longitude), another corrective velocity impulse is applied, and the sequence is repeated. The pattern of satellite motion is shown in Figure 3-16.

From a consideration of Figure 3-16 it can be reasoned that the desired magnitude of the periodic ΔV corrective impulses must effectively be chosen to accomplish the following:

(1) Cancel the $\dot{\lambda}$ existing at the time when $\lambda^1 = -\lambda^1{}_{LIM}$, this $\dot{\lambda}$ being caused by the gravitational disturbing forces.

(2) Introduce a counter $\dot{\lambda}$ so that λ^1 reaches a value of $+\lambda^1{}_{LIM}$ before the disturbing forces again reduce the relative longitude rate to zero.

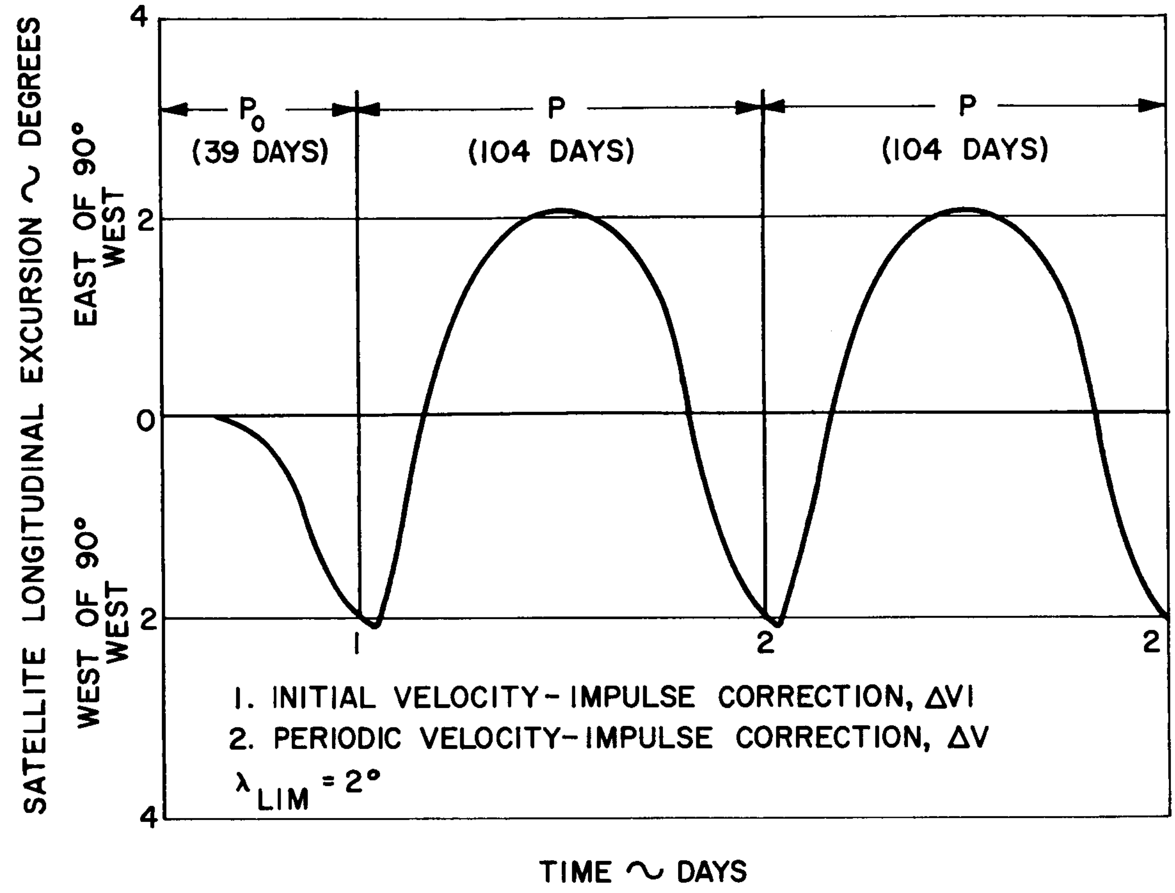

Figure 3-16. Approximate Station Keeping Pattern

Thus, the required periodic velocity impulse is given by

$$\Delta V = \frac{2\,\dot{\lambda}}{0.107}\ \Bigg|\ \lambda^1 = \lambda^1_{LIM} \qquad (3\text{-}2)$$

where ΔV is in feet per second and $\dot{\lambda}$ is in degrees per day.

Because the disturbing force is nearly constant, the $\dot{\lambda}$ produced by it is proportional to its time of action. Therefore, even for the low-level thrust cases considered (Figure 3-16)

$$\Delta V_i \cong k(P_0 + P/2)$$
$$\Delta V = k(P/2 + P/2) = P$$

and, therefore

$$\Delta V \cong \left[\frac{P_0 + P/2}{P}\right] \Delta V \qquad (3\text{-}3)$$

It can be seen from Figure 3-16 that each ΔV must compensate the $\dot{\lambda}$ produced by the constant disturbing force from the time $\lambda^1 = -\lambda^1_{LIM}$ previous to the application of that ΔV to the next time $\lambda^1 = -\lambda^1_{LIM}$.

The magnitudes of the ΔV's (these being all equal) can be established in advance if sufficiently accurate knowledge of the Earth's equatorial ellipticity is available; alternatively, they can be computed and executed on command, as must ΔV, based on the observed $\dot{\lambda}$ value when $\lambda^1 = -\lambda^1_{LIM}$.

Only one longitude boundary is used to trigger a corrective thrust during the final station keeping mode; this is the boundary toward which the terrestrial gravitational disturbing forces caused the vehicle to drift. Because there is a steady disturbing acceleration field caused by the terrestrial gravitational disturbing force (the second sectorial harmonic), a station keeping guidance method based on dual control boundaries on each side of the desired longitude station (with possible attendant stability problems) is not required. (A modification of this guidance logic could be required if the satellite were located near an extension of the equatorial major axis.)

c. System Simulation on the Analog Computer

An analog computer simulation was used for a parametric study of this guidance concept, which was originally evolved by analytical consideration of closed form solutions to equations equivalent to Eqs 3-1. During the computer study, an investigation was made of the effects of varying such system parameters as

(1) The disturbing gravitational force levels.

(2) Corrective thrust levels, duration time, and orientation in the orbit plane.

(3) Level of longitude excursions required to trigger a corrective thrust.

(4) Bias errors in the measurements of such excursions.

The general results of this study are described in the following paragraphs.

d. Analog Computer Analysis

1) Effects of Thrust Forces on the Orbit. In the first computer runs, a study was made of the effects that various thrust forces have on the orbit elements. For this study, the gravitational perturbations were ignored; that is the terms in Eqs 3-1 involving K2 were removed. An acceleration of 0.84×10^{-5} ft/sec^2 (a level representative of an electric engine thrust indicated to be promising for attitude control, as discussed in Volume 7) for 500 to 1000 lb vehicles was applied to an assumed vehicle for various lengths of time. The result was the application of a velocity impulse to the vehicle of the value

$$\Delta V = (F/m)t_I$$

where F/m = the acceleration of the vehicle caused by the thrust, F (0.84×10^{-5} ft/sec^2)

t_I = The time over which the thrust is applied

Typical computer runs are shown in Figures 3-17 through 3-20. In Figure 3-17 a positive transverse acceleration of 0.84×10^{-5} ft/sec^2 is applied for 1.3×10^5 seconds, yielding an input velocity impulse ΔV of 1.09 ft/sec. This figure illustrates that a steady negative longitude drift rate ($\dot{\lambda}$) of 0.12°/day is realized with an average increase in the orbit radius ($\bar{\rho}$) of 31,000 feet would be predicted. An eccentricity is introduced into the new orbit as evidenced by the daily oscillations in ρ.

Figure 3-18 presents the results of applying the same impulse in an outward radial direction. It is observed that, during the time of thrusting, an average apparent increase in orbit radius of about 2000 feet is realized with an associated longitude drift rate of only about 0.01°/day. When the thrust is removed, ρ oscillates about zero (because of the new orbit eccentricity), and there is no residual longitude drift.

In Figure 3-19 a positive transverse acceleration of 0.84×10^{-5} ft/sec^2 is applied for 0.065×10^5 seconds or approximately 1 day. No orbit eccentricity is introduced for this case.

Figure 3-20 shows a case where the vehicle is initially displaced from its desired longitude by 5°. This error is corrected by a series of two transverse thrusts; one thrust develops a drift rate, and another stops this drift by the time the desired station is reached.

Considering the transverse ($\alpha = 0°$) versus radial ($\alpha = 90°$) thrusting, it can be seen that only the transverse method is effective in producing a mean motion correction for the satellite. The steady state longitudinal drift ($-\dot{\lambda}_{SS}$) following a fixed velocity impulse varies as the cosine of the angle, indicating that the vertical component of the guidance force contributes nothing significant to this parameter. Because control of the satellite longitude must be provided in the presence of steady transverse disturbing forces caused by the equatorial ellipticity of Earth, only transverse thrust forces in the plane of the orbit are truly effective for this purpose and will be further considered.

2) Effects of the Equatorial Ellipticity of Earth. As shown by the second sectorial harmonic terms associated with the equatorial ellipicity of Earth (those involving K_2 in Eqs 3-1), the disturbing effect varies, depending on the longitude of the vehicle with respect to the longitude of the principal axis of the equatorial ellipse. Reference 3-10 indicates the latter to be at 37.5° W longitude. The longitude drift of the satellite (λ) as a function of time (if it is assumed that there are no guidance corrections) for various longitude locations relative to this major axis (Λ_0) is shown in Figure 3-21. The satellite is observed to drift eastward away from the major axis. The related westward longitude drift from the desired 90° W longitude position would closely correspond in magnitude to that shown for a Λ_0 of 45°.

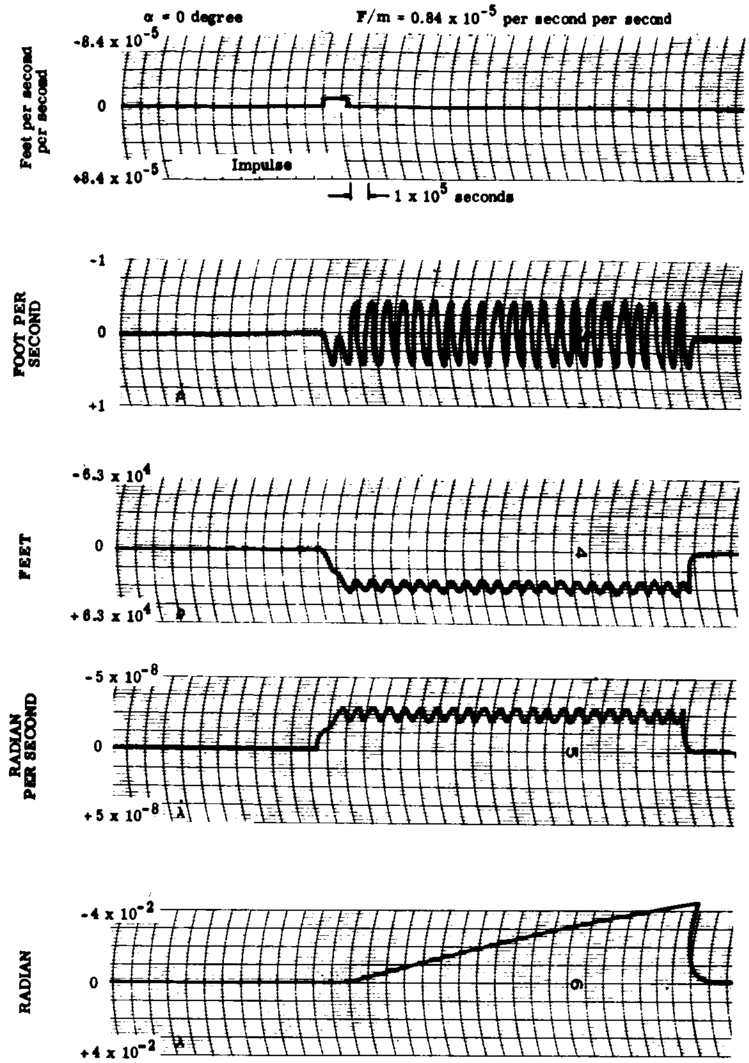

Figure 3-17. Horizontal Thrust Case - Typical Computer Run

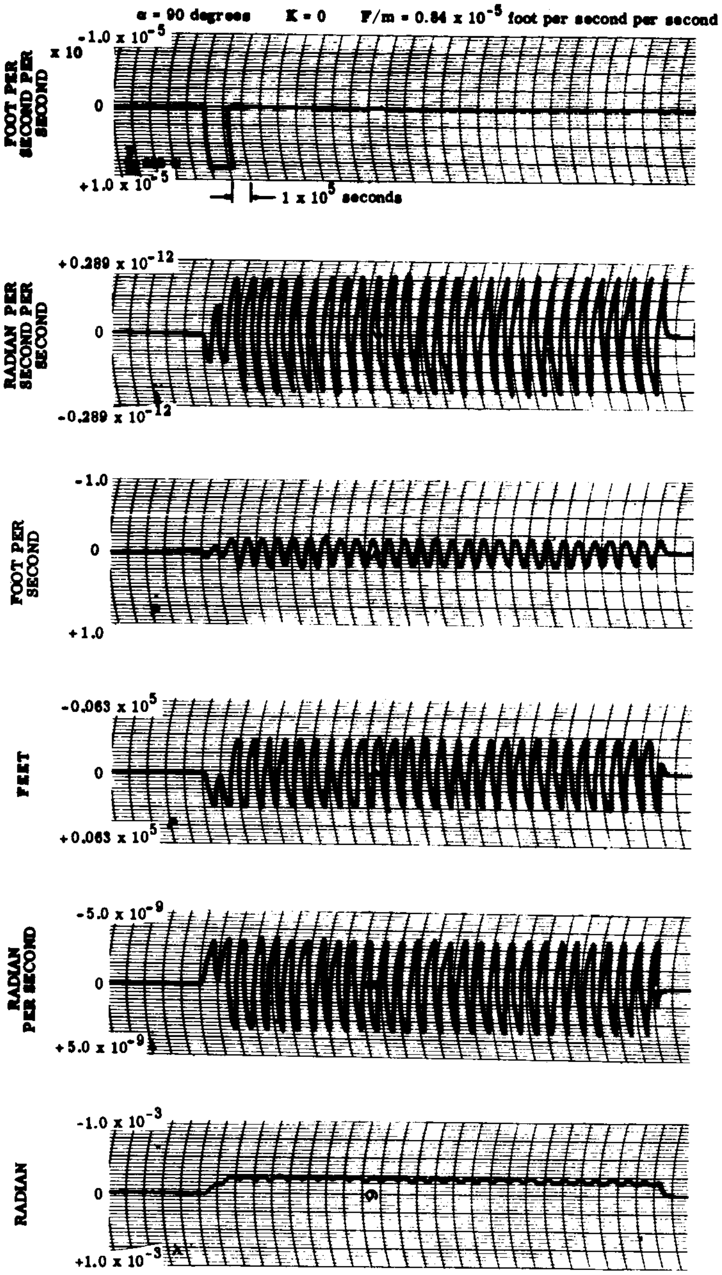

Figure 3-18. Vertical Thrust Case- Typical Computer Run

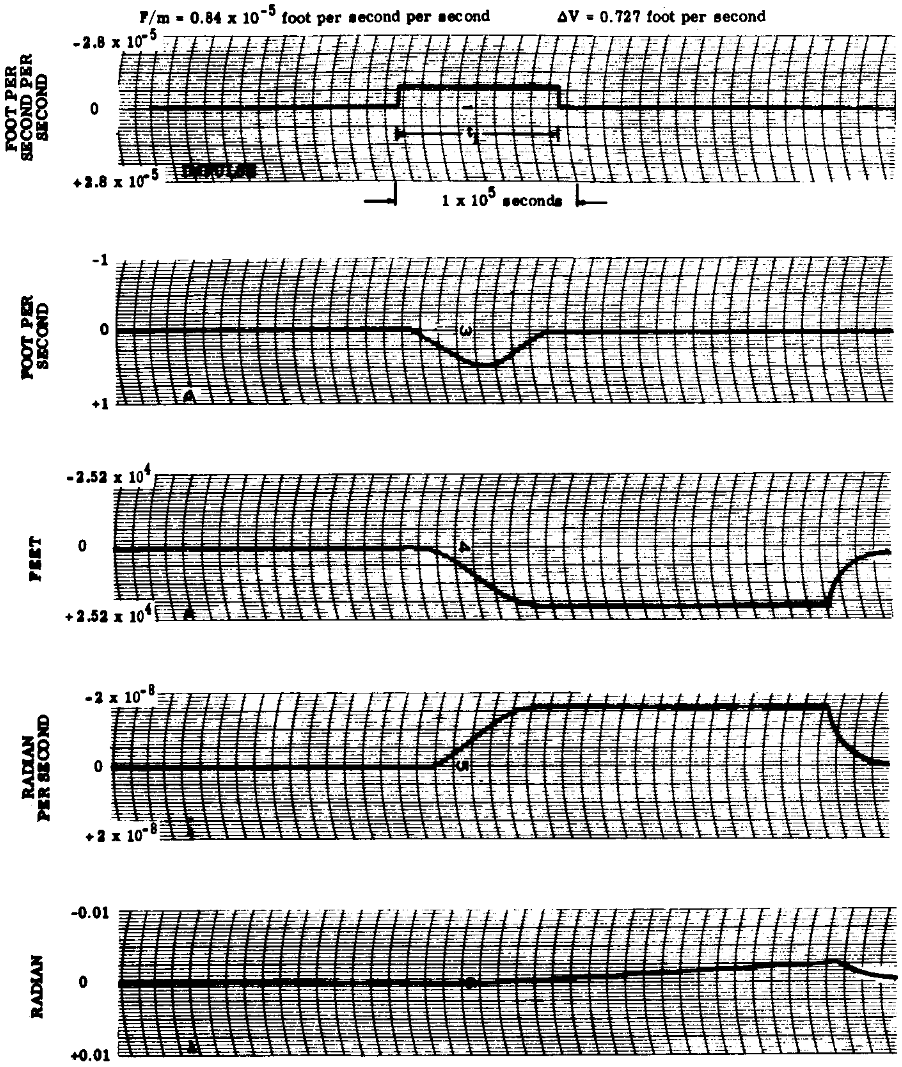

Figure 3-19. Horizontal Thrust for One Day - Typical Computer Run

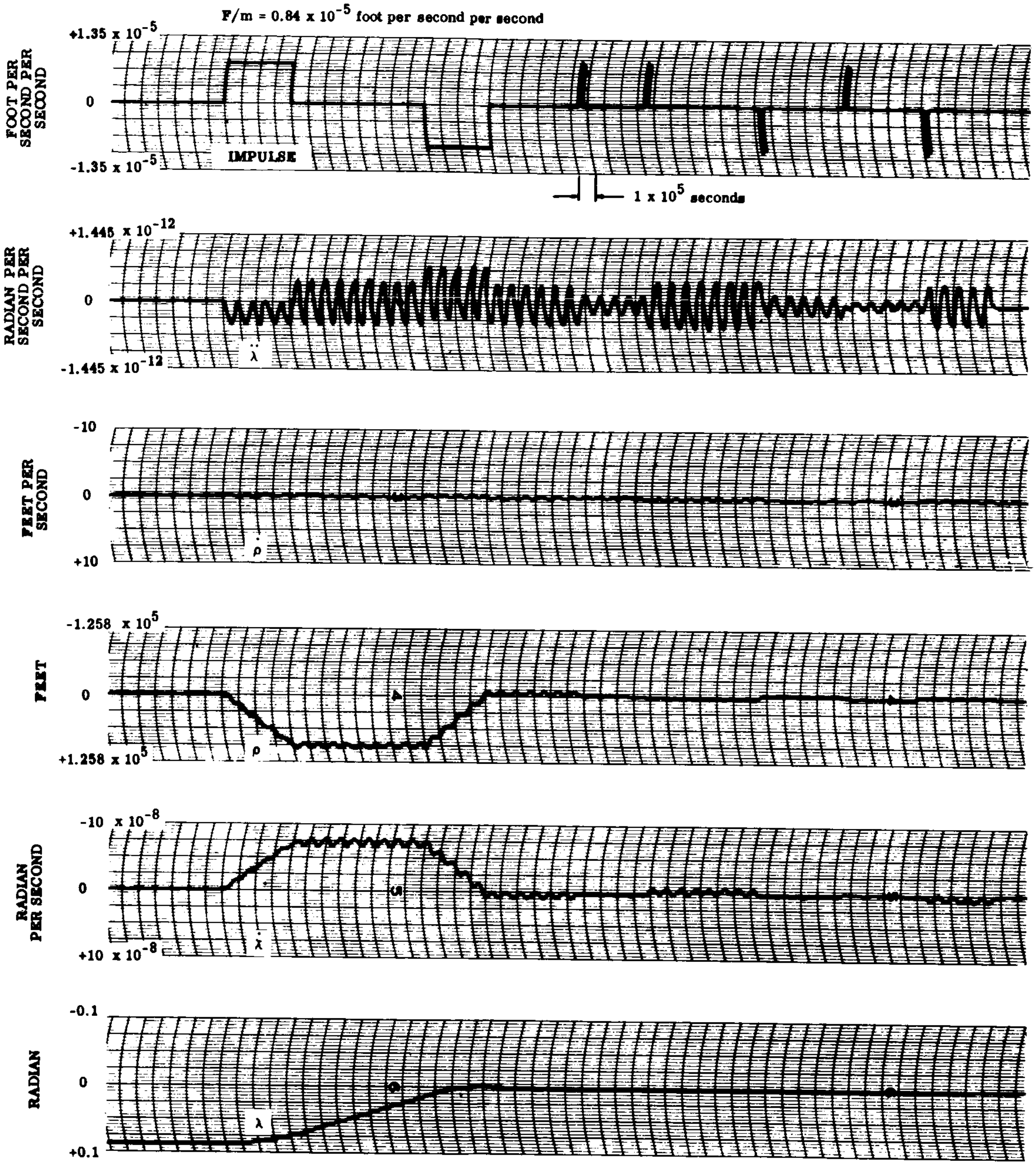

Figure 3-20. Removal of 5° Station Error - Typical Computer Run

The computer results given in Figure 3-21 agreed very closely with the analytical solutions obtained to Eqs 3-1. The analog computer equations used for this study are those given in Eqs 3-1, plus the additional terms due to perturbing the terrestrial acceleration terms. These terms are $\frac{-6\,K_2 \operatorname{Sin}\hat{2}\,\Lambda_o}{r_o^4}\,\lambda^1$ in the radial direction, and $+\frac{4\,K_2 \operatorname{Cos}\hat{2}\,\Lambda_o}{r_o^4}$ in the transverse direction. A separate examination of the radial and transverse disturbing forces indicated that only the transverse terms in the $\ddot{\lambda}$ equations are effectively responsible for the observed longitude drift.

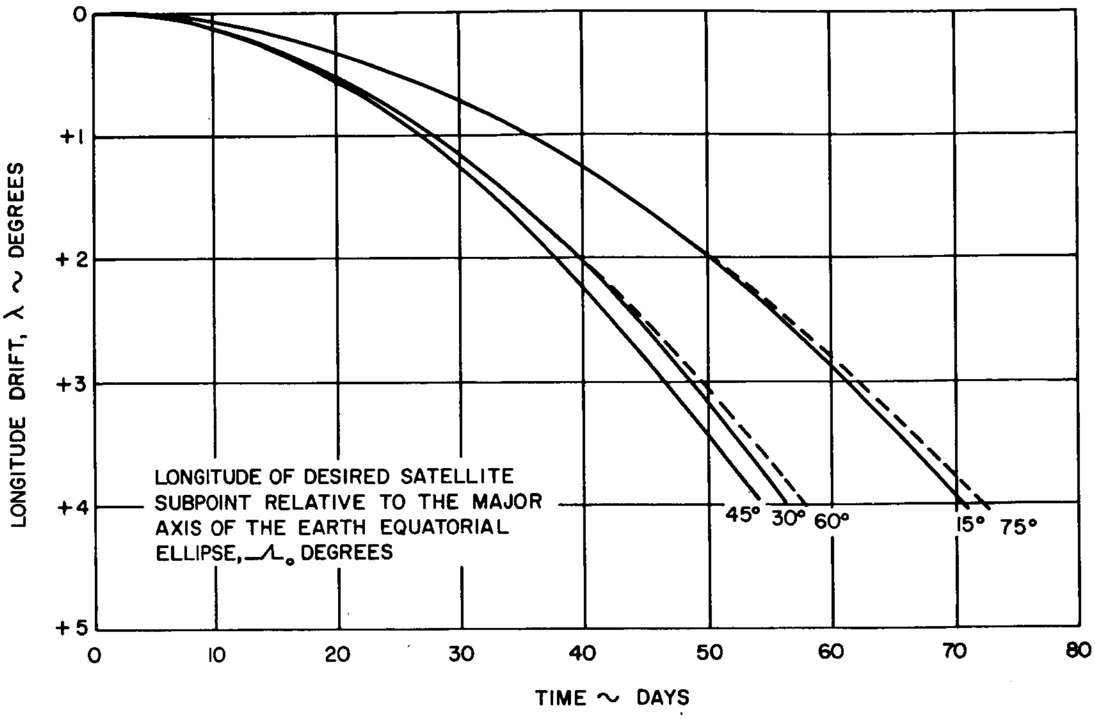

Figure 3-21. Longitude Drift Rate Caused by Second Sectional Harmonic vs. time for various Relative Longitudes

It would appear that there are two stable longitude positions over which a truly synchronous orbit can be realized without the requirement for subsequent guidance corrections. These are the longitude stations corresponding to either end of the minor axis of the equatorial ellipse (52.5°E longitude and 127.5°W longitude according to Ref 3-10. (The longitude stations corresponding to the ends of the equatorial major axis are unstable equilibrium points.) However, when account is taken of the higher harmonics in the Earth gravitational potential function, drifts would be experienced at these longitudes also. For the desired longitude station of 90°W, the perturbing effects of the second sectorial harmonic being considered are larger by nearly an order of magnitude that those of the other harmonic terms.

3) Initial Guidance Study.

a) General Results. As previously noted, a guidance technique is considered that uses a differential mean motion correction based on reasonably accurate knowledge of the satellite longitude angle and an initial measurement of longitude drift rate. This technique commands a preset, transverse thrust for a prescribed time whenever the longitude angle deviation from the desired longitude station exceeds a specified limit value ($\lambda^1{}_{LIM}$). At the end of the prescribed thrusting time, the thrust level is automatically reduced to zero. Thus, a fixed velocity impulse, $\Delta V = (F/m) t_I$, is applied at required intervals so that the vehicle stays within given bounds about the desired longitude.

This method depends on reasonably accurate knowledge of the initial vehicle longitude and longitude rate at the start of the guidance sequence, the sectorial harmonics producing the disturbing acceleration field, the guidance thrust magnitude, and choice of the drift angle limit. If this knowledge is inaccurate, then a nonuniform oscillation about the desired longitude station will exist. This could be remedied by calculating a better ΔV value based on the observed λ time histories over one period or on the $\dot{\lambda}$ existing at the time of correction and controlling the magnitude of the correction impulse. This guidance method has been tested by simulation, using the analog computer setup described, and was found to be stable and operationally satisfactory.

A typical computer run is shown in Figure 3-22 for a longitude limit value ($\lambda^1{}_{LIM}$) of 2°. This figure shows that the thrust device, giving an acceleration level of 0.85×10^{-5} ft/sec, is used for approximately 3.6 days every 104 days for the desired 90°W longitude station longitude relative to the Earth major axis, Λ_0, of -52.3°. This typical computer run also shows the daily oscillations characteristic for thrust duration times that are not integral mutliples of days. Although there is a change of amplitude of oscillation (caused by a change in orbit eccentricity), this is not serious enough to be noticeable on the trace of longitude, which is the prime variable of interest. Using a larger thrust, a noticeable eccentricity is produced, as is later shown.

The computer simulation was next used to determine the required impulse for each individual correction based on a tolerance of ± 2° from various longitude stations (Λ_0) relative to the major axis of the equatorial ellipse. Figure 3-23 shows a plot of the individual steady state velocity impulses as a function of Δ_0. The required impulses are essentially zero at the major and minor axes (Λ_0 of zero and 90°) and will be similar for the other three quadrants.

Figure 2-23 also gives the required duty cycle (ratio of engine on-time to total time for the steady station keeping pattern) with an $(F/m)_0$ of 0.84×10^{-5} ft/sec^2. This is fairly close to the value calculated as the theoretical minimum for overcoming the forces associated

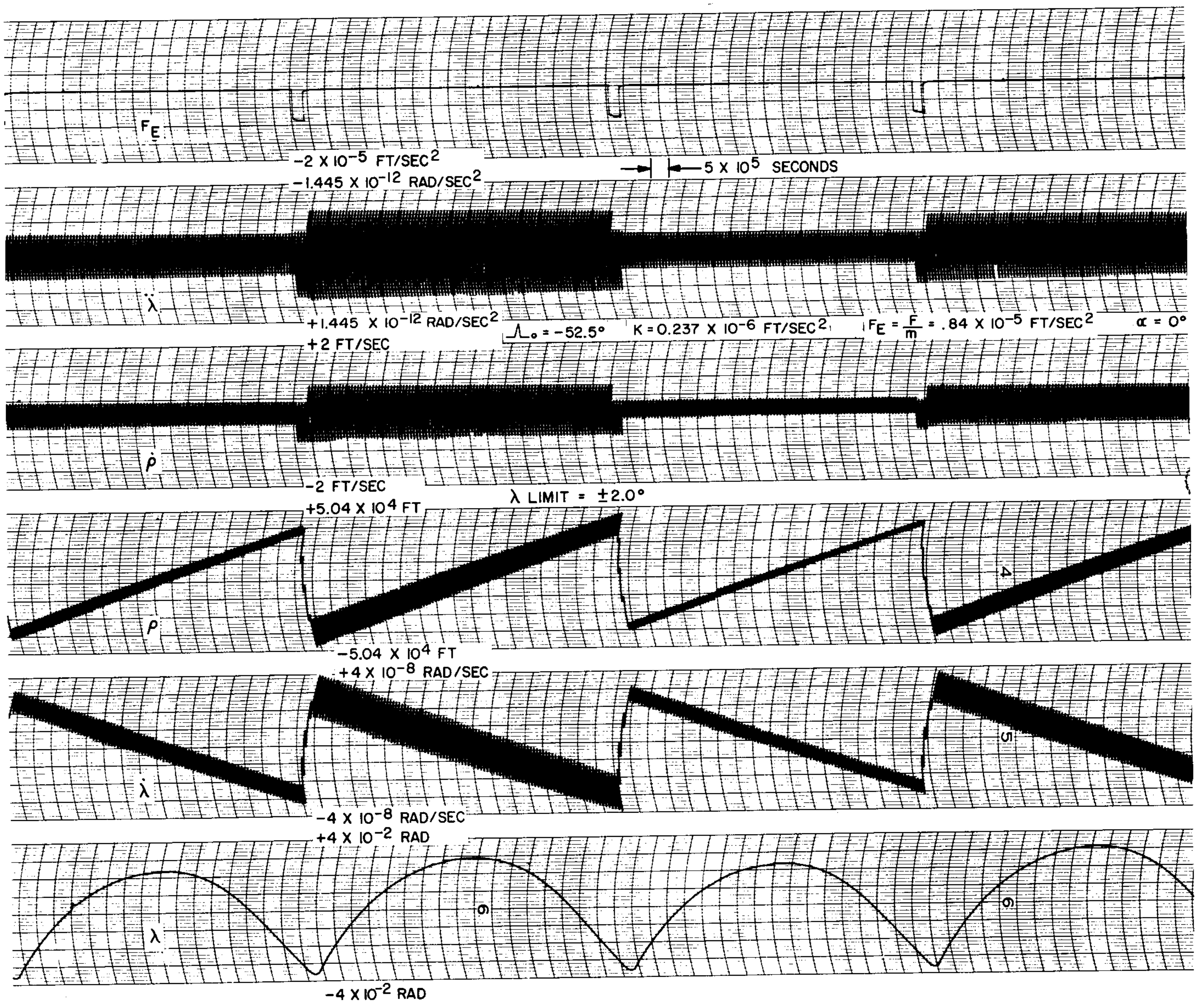

Figure 3-22. Longitude Limit Value of 2° - Typical Computer Run

with the second sectorial harmonic based on a ratio of engine acceleration to perturbing acceleration. The period (P) associated with the required ΔV corrections during the steady station keeping mode is given by $P = (\Delta V). (F/m)_o$ (duty cycle).

The curves of Figure 3-23 can be used as working curves to determine the required impulse for holding a desired longitude station. The total impulse (ΔV_T) required for a specified mission duration time (t_M) in seconds is approximately given by ΔV_T (foot per second) = t_M $(F/m)_o$ (duty cycle) = $(0.84 \times 10^{-5}) t_M$ (duty cycle). The duty cycle, of course, ratios inversely with F/m.

A plot of ΔV_T as a function of time during the steady station keeping mode (with $\lambda_o = 0$ but $\lambda_o + 0$) is given by Figure 3-24. The total impulse ΔV_T increases by discrete steps with each required correction. Curves are given for peak to peak longitude excursions of 4° and 0.33°.

The data of Figures 3-16, 3-21, and 3-23 are next used to establish the basic period and velocity impulse requirements for the station keeping method being discussed for the longitude position of 90°W specified in Ref 3-2. The assumed parameter values were:

(1) F/m, 0.84×10^{-5} ft/sec^2

(2) $\lambda^1{}_{LIM}$, 2°

(3) Longitude of equatorial major axis, 37.5°W

Item (3) indicates that, for the specified longitude of the satellite, $\Lambda_o = 52.5°$. From Figure 3-23 the individual (steady state) corrective velocity impulse is 2.64 ft/sec, and the duty cycle is 0.035. The engine-on time per correction (T_{ON}) is thus determined as follows: $T_{ON} = \Delta V/F/m = 2.6/0.84 \times 10^{-5} = 3.1 \times 10^5$ seconds = 3.6 days, and the basic period between the steady state velocity corrections (P) is $P = T_{ON}/\text{duty cycles} = 3.1 \times 10^5/0.035 = 9.0 \times 10^6$ seconds = 104 days. Therefore (Figure 3-16), by using a series of n velocity impulses of magnitude ΔV spaced P seconds apart, the satellite will be limited to within ± 2° of the desired longitude for a total mission time t_M given by $t_M = P_o + (n + 1) P$. The associated total velocity impulse ΔV_T is given as follows

$$\Delta V_T = V_i + n \Delta V$$

From Figure 3-21, P_o is indicated to be about 38 days (3.3×10^6 seconds) for an Λ_o of 52°. Therefore, from Eq (3-3)

$$\Delta V_i \cong \left[\frac{P_o + P/2}{P}\right] \Delta V = \frac{3.3 \times 10^6 + 4.5 \times 10^6}{9.6 \times 10^6} \Delta V = 0.87 \Delta V$$

and therefore

$$\Delta V_T = (0.87 + n) \Delta V = (0.87 + n)\ 2.65$$

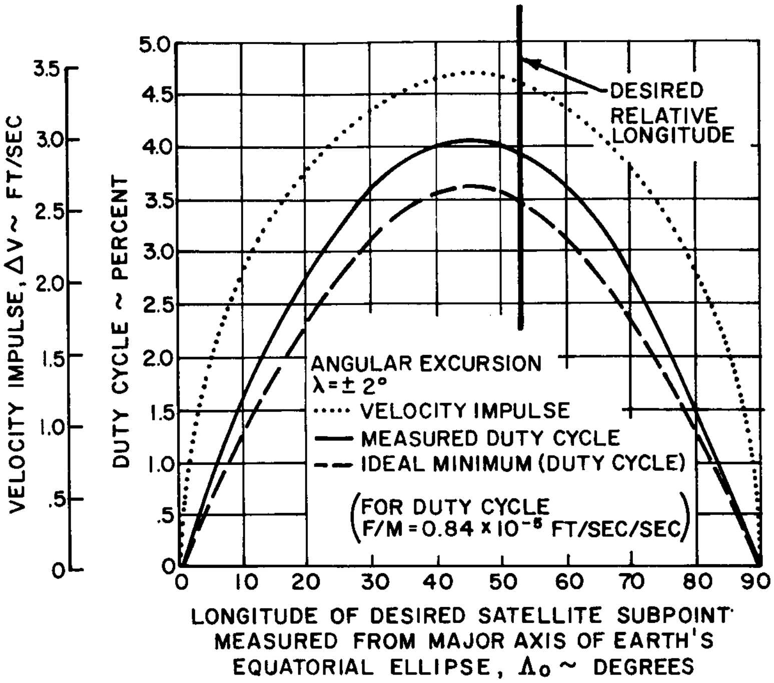

Figure 3-23. Impulse and Duty Cycle for Mean Motion Station Keeping Method

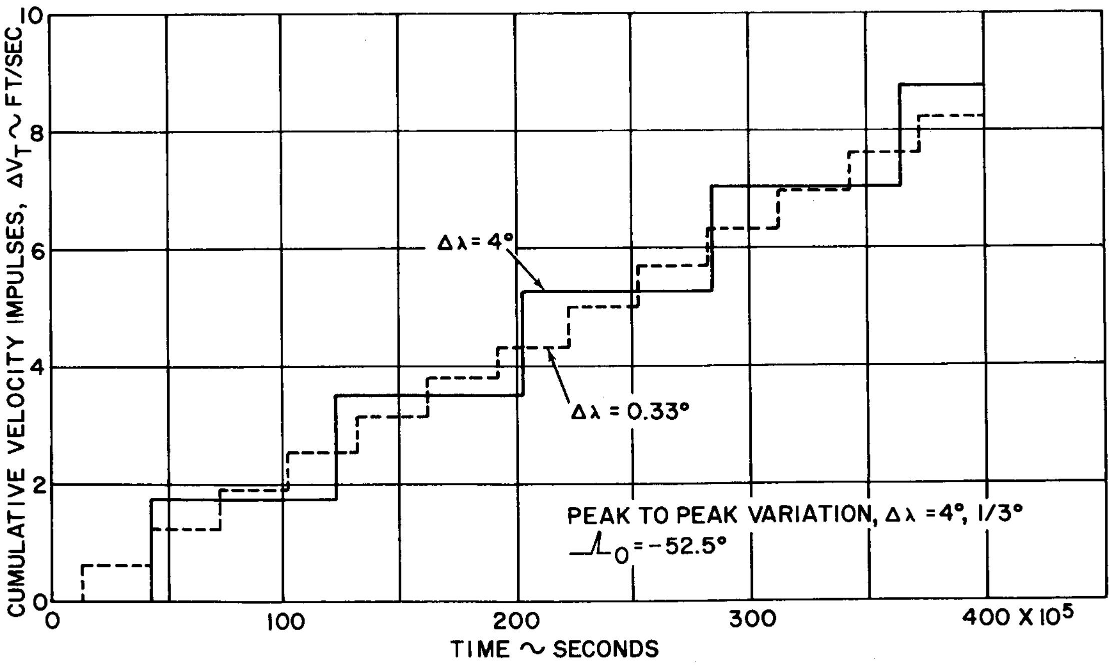

Figure 3-24. Cumulative Velocity Impulse vs Time for Peak to Peak λ Excursions

For $n = 2$, $\Delta V_T = 7.4$ ft/sec, and the maximum mission time, $t_M = P_o + (n + 1)\ P = 30.3 \times 10^6$ seconds, which is 0.96 year. (For $n = 3$, $\Delta V_T = 10.2$ ft/sec, and $t_M = 39.3 \times 10^6$ seconds, which is 1.24 years.)

Thus, for nearly a one year mission, a total velocity impulse or characteristic velocity of 7.4 ft/sec would be required for station keeping at the desired satellite longitude against the assumed terrestrial gravitational disturbing forces by the guidance method described. If a higher thrust force were used (such as that discussed in Section 2). the duty cycle would be proportionately reduced, but the velocity requirements would, of course, be the same.

b) More Frequent Use of a Smaller Corrective Impulse. One possible variation of the guidance method under study is the more frequent use of a smaller velocity impulse (shorter on time for the thruster with the same preset thrust level). This technique has one distinct advantage -- the long period, peak-to-peak excursions in longitude from the desired station (as opposed to any daily oscillations caused by orbit eccentricity) can be considerably reduced. Because less impulse is used with each correction, the satellite is forced back to the control boundary sooner by the disturbing accelerations than if relatively large impulses were used. The performance of such a technique would also be less affected by possible variations in system parameters.

In Figure 3-25 this peak to peak variation in longitude is plotted as a function of the impulse time, t_I, (with a fixed thrust level) for a longitude station ($\Lambda_o = -45°$) that represents the extreme guidance requirement for the station keeping and closely approximates the 90° W longitude station. As the individual impulse ΔV is reduced (the impulse is automatically applied more frequently, and there is essentially the same total impulse ΔV_T), the peak-to-peak variation in station is also reduced (see Figures 3-24 and 3-26). The computer results indicated that there is no significant change in the engine duty cycle for the different impulse times.

A typical computer run for the desired relative longitude of -52.5° is shown in Figure 3-26 where the excursions in longitude for this case of reduced ΔV are considerably less than those shown in Figure 3-22 and are biased towards the λ^1 equals $-\lambda^1{}_{LIM}$ boundary. A $\lambda^1{}_{LIM}$ boundary closer to the desired longitude could be chosen for such an approach.

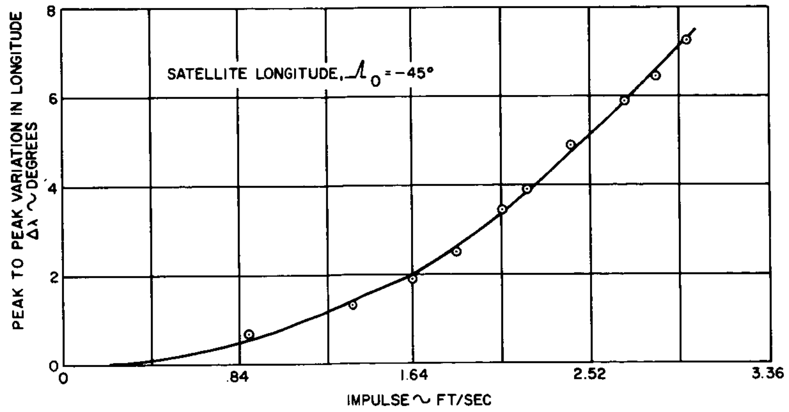

Figure 3-25. Peak to Peak Variation in Longitude vs Impulse

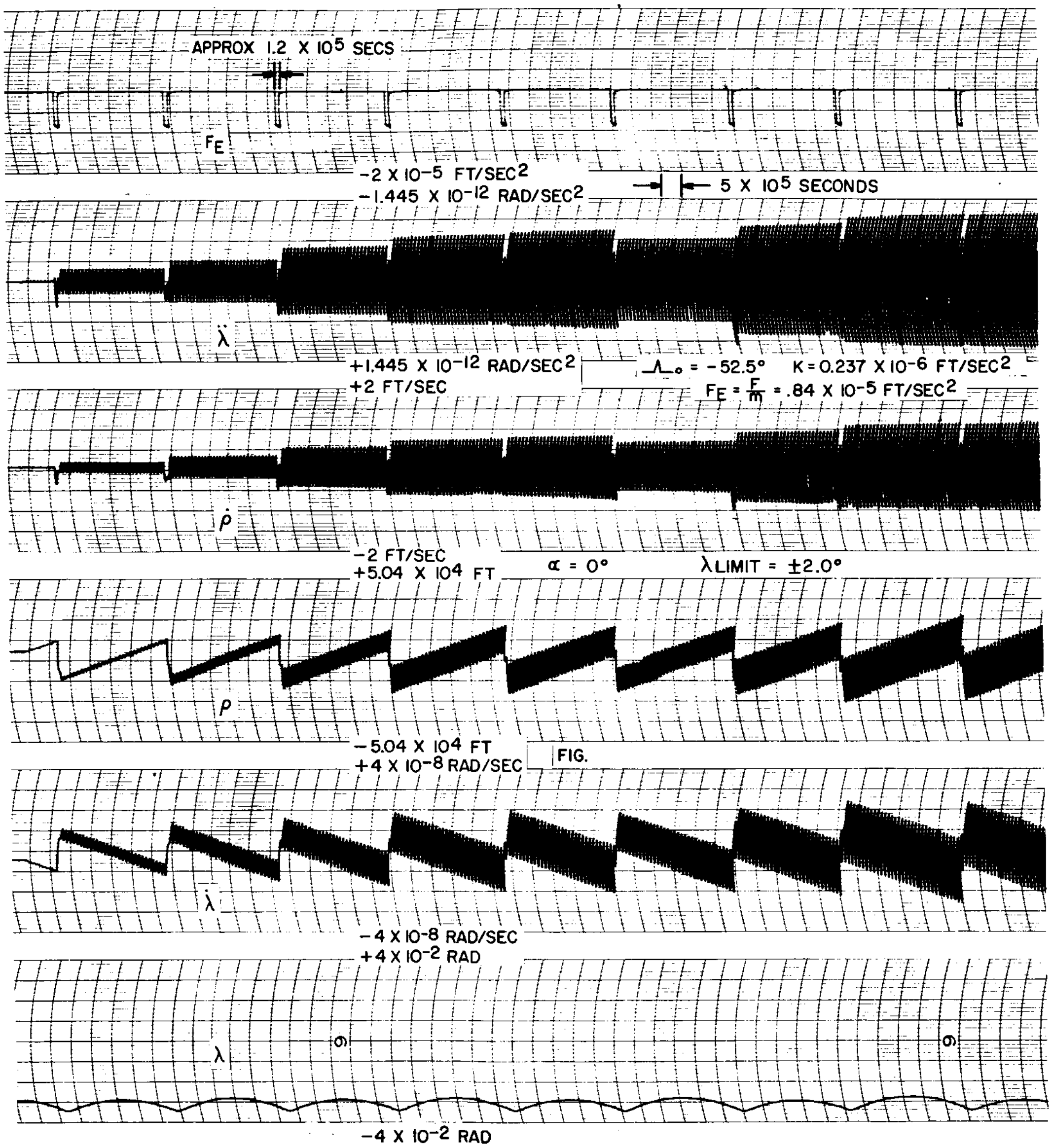

Figure 3-26. Relative Longitude of -52.5° - Typical Computer Run

c) Open-Loop Guidance Methods. A brief examination was made of possible guidance techniques for station keeping using a completely preprogrammed control sequence. It was found, however, that a more accurate knowledge of the disturbing gravitational forces than is now available would be required. With such preprogrammed techniques, satellite drift would be excessive unless some override provisions were made. The use of an adaptive process to enhance this approach may deserve further study.

4) Parametric Variations of System Components. The computer simulation setup was used to examine further the effects of variations in the parameters of the basic station keeping guidance system under study. The following results were obtained from this work.

A fixed bias on the measurement of the longitude angle results effectively in a bias or shift of the entire trace of λ^1; that is, peak-to-peak excursions in λ^1 and the period of these variations are essentially the same. The values given in Table 3-1 indicate only nominal variations in peak-to-peak longitude excursions for up to ±1° bias error in measurement of longitude (all other parameter values are as indicated). The longitude excursions could be altered in a different manner if the error in measuring longitude were randomly distributed, but it is felt that essentially the same conclusions would hold.

TABLE 3-1
EFFECTS OF BIAS ERRORS IN MEASUREMENT OF LONGITUDE(*)

Bias Error in Measurement of Longitude (degrees)	Peak to Peak Longitude Excursion (degrees)
1.0	4.32
0.5	4.40
0.25	4.33
0	4.06
-0.25	4.18
-0.5	4.17
-1.0	4.30

(*) Conditions included $\lambda_0 = -45°$, $F/m = 0.84 \times 10^{-5}$ ft/sec^2, and $\lambda^1_{LIM} = 2°$.

5) Injection Error Study. On attempted injection of the vehicle into a synchronous orbit, significant mean motion errors (or equivalently errors in the semimajor axis of the orbit) will exist. The effects of such errors were studied by considering initial longitude drift rates and their correction by the application of velocity impulses.

For this study, the terrestrial disturbing forces were neglected, and only transverse corrective thrusts were considered. Several different guidance thrust levels were considered in this study. Figure 3-27 shows a summary plot of the particular impulsetime, t_I,required for removal of given initial longitude drift rates,$\dot{\lambda}_0$, or equivalent initial mean velocity errors,ΔV_0. Curves for various acceleration levels are given, including an acceleration of 0.00284 ft/sec^2 representing a thrust of 0.044 pound on a 500-pound vehicle as studied in Section 2. An impulse time of 1.38 x 10^4 seconds (approximately 3.75 hours) is indicated to be required to correct the given mean motion error of 4.2°/day (Ref 3-2) with a corrective acceleration of 0.00284 ft/sec^2.

Figure 3-28 presents a summary plot of the longitude excursion λ^1, while various initial drift rates ($\dot{\lambda}_0$) are being removed by the indicated constant corrective acceleration levels. It is indicated that, in nulling the typical mean-motion error of 4.2°/day, a longitude excursion of 0.28° would occur if a corrective acceleration level of 0.00284 ft/sec^2 were used.

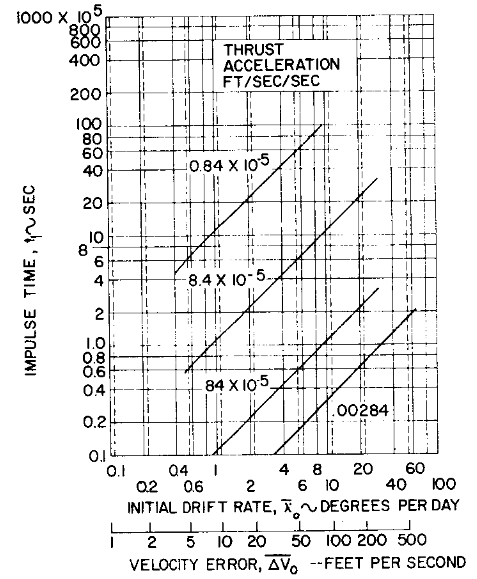

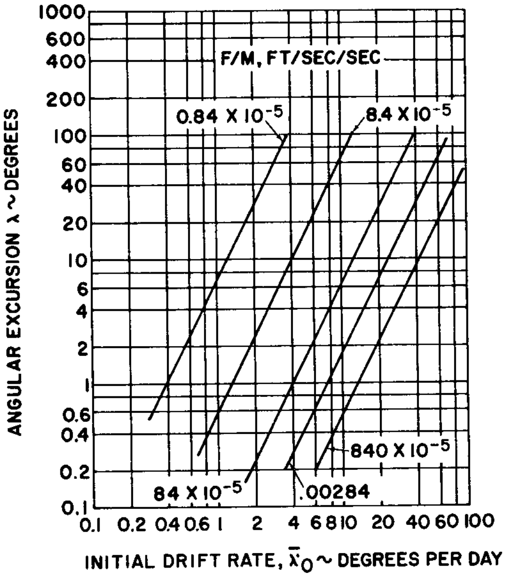

Figure 3-27. Impulse Time vs Initial Drift Rate or Velocity Error.

Figure 3-28. Longitude Excursion while Nulling Initial Drift Rate.

6) Orbit Eccentricity Caused by Constant Thrusting. Attention was given to the orbit eccentricities caused by thrust forces of various magnitudes and durations applied to vehicles in circular orbits. This work is related to the study of the effects of correcting the large velocity errors (or equivalent mean motion errors or longitude drift rates) that might exist after orbit injection. There are larger oscillations introduced in the variables λ°, ρ, and $\dot{\rho}$ following correction of injection errors with the higher thrust levels because of the larger eccentricity thereby introduced.

The eccentricity of an orbit can be measured by using the expression

$$e = \frac{r_a - r_p}{r_a + r_p}$$

where r_a = apocenter radius

r_p = pericenter radius

Measured in perturbation quantities, this equation becomes

$$e = \frac{\rho_{max} - \rho_{min}}{2r_o + \rho_{max} + \rho_{min}}$$

(Here, ρ_{max} is the value of ρ (t) at apogee and ρ_{min} is the value of ρ (t) at perigee.) Thus, the eccentricity is proportional to the peak-to-peak variation in the radius vector.

Figure 3-29 shows a corresponding plot of orbit eccentricities as a function of the input characteristic velocity ΔV for various levels of transverse thrust acceleration. The plots for each thrust acceleration are cyclic in ΔV. The associated period, expressed in terms of ΔV, is 0.726 $(F/m)/(F/m)_o$ where $(F/m)_o$ is equal to 0.84×10^{-5} ft/sec^2. Two and one-half cycles are shown in Figure 3-29 for the lowest thrust level. This cyclic response occurs because zero eccentricity is developed when transverse thrusting is employed for integral multiples of a day. The asymptote of the curves of Figure 3-29 represents the case of impulsive thrusting ($F = \infty$) to yield a given velocity impulse, ΔV. For this case (ΔV in foot per second), for a synchronous orbit

$$e = 2\Delta V/V \cong 2 \times 10^{-4}\ \Delta V$$

The significance of the curves of Figure 3-29 can be illustrated by considering a characteristic velocity of 39 ft/sec that represents the velocity correction required for the typical period error of 1000 seconds given in Ref 3-2. An eccentricity of 0.0075 is introduced when an 0.00284 ft/sec^2 corrective thrust acceleration is used for 3 3/4 hours to provide this characteristic velocity. This eccentricity would result in a daily longitudinal oscillation (λ_{max}) of ± 0.88° for injection near the line of apsides, since then λ_{max} (in degrees) is approximately equal to 115 e. Double this value could be experienced if injection were 90° removed from the line of apsides. Some modification of the correction procedure would probably be desirable in this case (as previously discussed in Section 3.B).

Figure 3-29 indicates that an eccentricity as high as 0.08 could result from use of a constant thrust acceleration level of 0.00284 ft/sec^2 to provide a characteristic velocity of 200 ft/sec, an expected upper limit for injection velocity error. An associated daily oscillation in longitude of 0.9 to 1.8° would occur, and for which compensation would probably again be required.

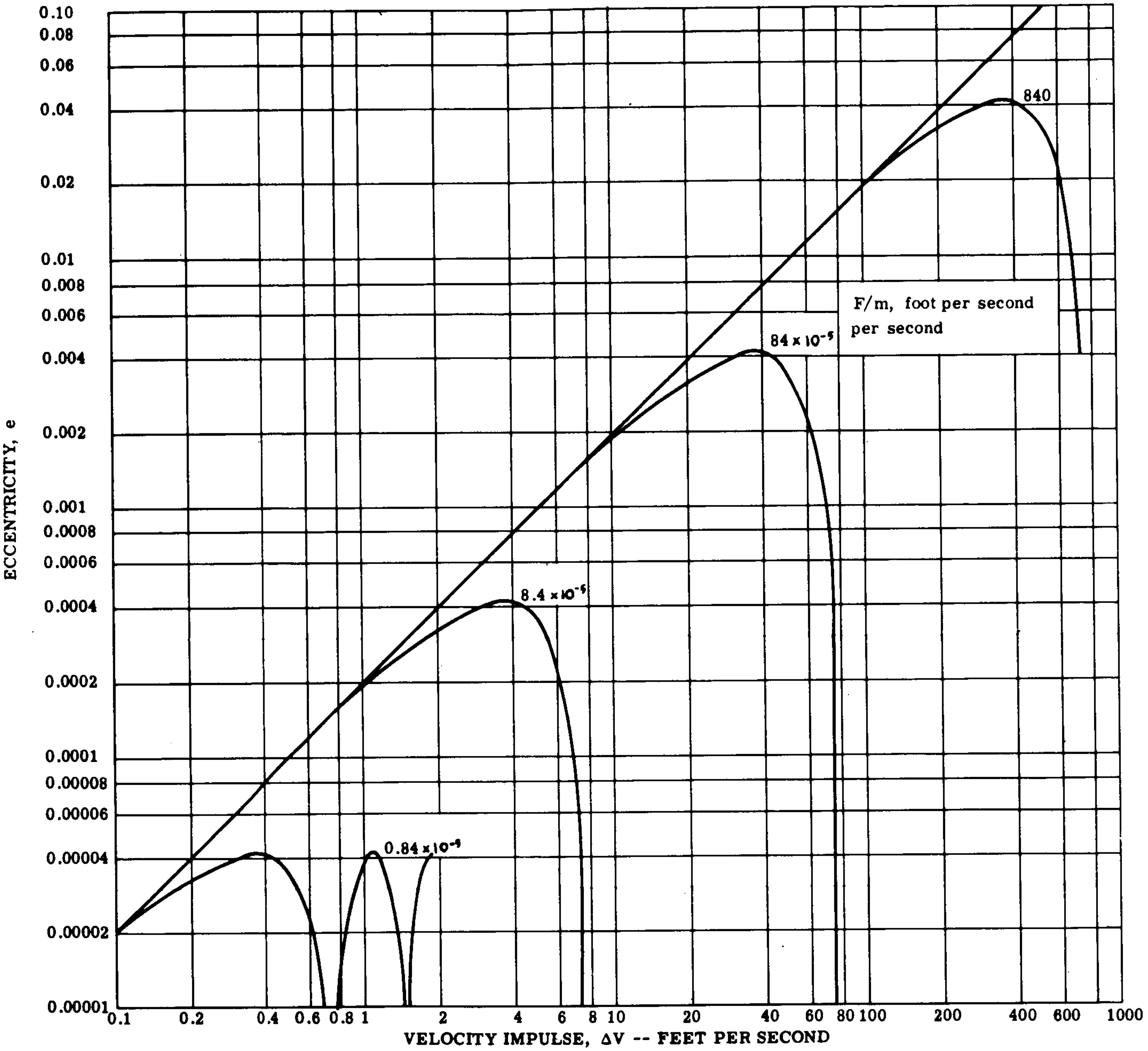

Figure 3-29. Eccentricity vs Impulse for Various Thrust Acceleration Levels

3. Conclusions

The second sectorial harmonic associated with the Earth's equatorial ellipticity can cause significant drift in the longitude location of the SMS. For such a vehicle, a station keeping guidance system that provides a corrective velocity impulse of 7.4 ft/sec/yr is required for the desired longitude station of 90° W longitude. The longitude drift effect is essentially caused by the transverse component of the perturbing force caused by the Earth's equatorial ellipticity; the radial component has a negligible effect. Radial acceleration causes a longitude drift rate of 1000°/day/ft/sec^2. The maximum radial acceleration caused by the second sectorial harmonic is indicated by Figure 3-30 to be 0.348×10^{-6} ft/sec^2. This would produce a longitude excursion of less than 0.2° over the period of a year. The tangential acceleration caused by the second sectorial harmonic causes excessive longitudinal excursions and must be corrected as indicated.

Transverse horizontal thrusting is the most effective way of controlling longitude excursions of the satellite. This technique results in a steady-state longitude drift rate, relative to the Earth, of -0.107°/day/ft/sec of characteristic velocity provided.

Radial thrust causes a transient longitude drift rate during thrust application. When the thrust force is removed, no steady-state $\lambda°$ is maintained. Radial thrust is, therefore, far less effective in producing longitude excursions than transverse thrusting with the same impulses.

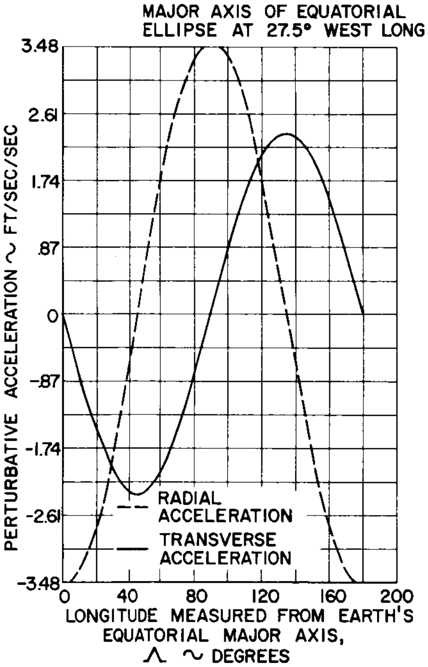

Figure 3-30. Disturbing Accelerations on the Satellite Caused by the Earth's Equatorial Ellipticity

Satisfactory longitude control against the disturbing accelerations caused by the terrestrial disturbing forces can be simply implemented by using a differential mean-motion correction scheme with thrust levels as low as 0.00013 pound for a 500-pound vehicle. The method of guidance involves using the engines for transverse thrusting when the satellite drifts by a preset amount (λ^1_{LIM}) from the desired latitude, and maintaining this thrust for a predetermined length of time. The total characteristic velocity required during a year of station keeping is not significantly affected for values of λ^1_{LIM} varying from 1 to 10°. The required velocity, however, is a function of the desired longitude station and ranges to a maximum of about 8.5 ft/sec/yr. The velocity impulse required for a year of station keeping at 90° W longitude (as specified in Ref 3-2) is 7.4 ft/sec.

The use of smaller velocity corrections at a higher repetition rate (yielding effectively the same total characteristic velocity for a year of station keeping) produces reduced peak-to-peak longitude excursions and makes such excursions less dependent on variations in disturbing force levels and initial longitude angles and rates.

Realizable tolerances on thrust level, thrust time, and longitude determination are compatible with the station keeping requirements to be met.

Orbit eccentricities developed through repetitive application of the nominal station keeping velocity corrections are not significant relative to longitude station keeping requirements.

An initial average velocity error of 39 ft/sec, corresponding to the typical 1000-second period error (Ref 3-2), will necessitate the use of guidance thrust devices with thrust capabilities greater than the minimum level permissible for station keeping against terrestrial disturbing forces in order that the initial satellite longitude drifts can be effectively controlled. If an effective acceleration level 0.00284 ft/sec^2 were used for about 3.8 hours to yield the indicated 39 ft/sec characteristic velocity, an initial longitude excursion of 1.1° would result while the mean motion error was being nulled. In addition, an orbit eccentricity of 0.00075 would be introduced, which would cause a corresponding daily oscillation in longitude of ±0.88°.

Following injection into synchronous orbit, an eccentricity of 0.013 is expected (Ref 3-2). Inopportune correction of the period error of 1000 seconds could effect a possible eccentricity increase of 0.00075 (Figure 3-30). The total residual eccentricity could then be 0.0205, which would result in a daily longitudinal oscillation drift of approximately ±2.35 to 4.7°. The residual eccentricity can be made acceptably small by applying the mean motion correction at the proper point in the orbit as discussed in Section 3.A.

D. LIST OF SYMBOLS

a = semimajor axis
a_e = Earth's mean equatorial radius, 2.0926×10^7 feet
e = eccentricity
F = magnitude of guidance thrust force, pounds
GHA = equivalent Greenwich hour angle
g' = true anomaly of disturbing body
h = altitude
h_{M_0} = initial hour angle of major axis
i = inclination
i' = relative inclination with respect to plane of disturbing body
$J^{(k)}$ = tesseral (j ± k) and sectorial (j=k) constants associated with the Earth's gravitational field
J_2 = Earth-shape constant related to the second gravitational harmonic caused by oblateness, 1.08×10^{-3}
$J_2^{(2)}$ = Earth-shape constant related to the second grafitational harmonic caused by equatorial ellipticity, 2.32×10^{-6}
K = $2K_2/r_o^4$, 0.235×10^{-6} ft/sec^2
K_1 = oblateness gravitational constant, 3.32×10^{27} ft/sec^2
K_2 = equatorial ellipticity gravitational constant, 4.26×10^{25} (foot)^5/sec^2
M_s = synchronous mean motion
m = mass
N = number of revolutions
n = mean motion
P = period
R = radius to disturbing body; disturbing function
R_b = range angle
r = satellite radius
r_s = synchronous radius, 1.38×10^8 foot
T = thrust
t = time
t_I = impulse time, seconds
U = force function
V = velocity or potential function
ΔV = incremental or impulsive velocity addition

$\overline{\Delta V}$ = magnitude of characteristic velocity (F/m) t_I, ft/sec
W = weight
X, Y, Z = inertial reference coordinates
$\bar{x}$ = time average over an orbit
$\dot{x}$ = the time derivative of a variable in inertial space
γ = flight path angle
Δ = incremental change
δ = guidance control variable
ϵ = additional velocity increment
θ = satellite true anomaly
Λ_o = longitude of desired satellite subpoint relative to the major axis of the equatorial ellipse
λ = longitude
λ_m = minor axis longitude
$\lambda_{R_1 o}$ = initial satellite longitude with respect to minor or major axis
$\Delta\lambda$ = longitude excursion
$\Delta\lambda_m$ = satellite longitude excursion measured from minor axis
$\lambda^{(k)}_{(j)}$ = longitude of principal axes for sectorial and tesseral harmonics
μ = gravitational constant of central body
μ_E = mass gravitational constant for the Earth, GM_E, 1.4077×10^{16} ft^3/sec^2
ρ, λ' = radial and longitudinal perturbation coordinates, respectively
ϕ = latitude
τ = time of perigee passage (epoch)
Ω = right ascension of ascending node
ω = angular velocity or argument of perigee
ω_o = angular velocity of Earth, 7.29×10^{-5} radian/sec

Subscripts

C = circularization
K = apogee kick
m = Moon or minor axis of Earth
o = initial or constant value
S = Sun or synchronous value
W = wait orbit
24 = synchronous orbit value

E. REFERENCES

3-1 "Proposal for Studies of Synchronous Meteorological Satellite System Problems," Republic Aviation Corporation Report No. RAC 826, Vol. III, 23 July 1962

3-2 NASA, "Statement of Work for Studies of Synchronous Meteorological Satellite System Problems," Goddard Space Flight Center, Contract NAS5-3189 with Republic Aviation Corporation, 31 January 1963

3-3 Lockheed Missiles and Space Company, "Syncom Booster Feasibility Study," Report No. LMSC A057612, 30 September 1962, Confidential

3-4 Musen, P., Bailie, A., and Upton, E., "Development of the Lunar and Solar Perturbations in the Motion of an Artificial Satellite," NASA TN-D-4941, January 1961

3-5 Kozai, Y., "On the Effects of the Sun and the Moon Upon the Motion of a Close Earth Satellite," Smithsonian Institution Astrophysical Observatory," Special Report No. 22, March 1960

3-6 Republic Aviation Corporation Proposal, "Radio-Microwave Powered 24-Hour Communication Satellite System," RAC 648-500, December 21, 1959

3-7 Brouwer, D., and Clemence, G.M., *Methods of Celestial Mechanics*, Academic Press, New York, N.Y., 1961

3-8 Smart, W.M., *Celestial Mechanics*, Longmans, Green and Co., London, 1953

3-9 Wyatt, S.P.,"The Effects of Radiation Pressure on the Secular Acceleration of Satellites,"Smithsonian Institution Astrophysical Observatory, Special Report No. 22, March 1961

3-10 Kozai, Y., "The Motion of a Close Earth Satellite," The Astronomical Journal, Vol. 64, No. 9, November 1959

3-11 Issak, I.G., "A Determination of the Ellipticity of the Earth's Equator From the Motion of Two Satellites," Astron. J., Vol. 66, No. 5, June 1961

3-12 Pines, S., and Wolfe, H., "Interplanetary Trajectory by the Encke Method Programmed for the IBM 707 and 7090," Republic Aviation Corporation Report No. RAC 656-451, 12 December 1960 (prepared under contract NASA - 109)

3-13 Kozai, Y., "Tesseral Harmonics of the Potential of the Earth as Derived from Satellite Motions," Smithsonian Institution Astrophysical Observatory Special Report No. 72, August 1961

3-14 Frick, R.H. and Garbey, T.B., "Perturbations of a Synchronous Satellite Due to Triaxiality of the Earth," J. Aerospace Sci., Vol. 29, No. 9, September 1962

3-15 Pines, S., Wolfe, H., and Richman, J., "Orbit Determination and General Purpose Differential Correction Program," Republic Aviation Corporation Report No. RAC 696, 25 April 1962 (contract NAS5-293)

SECTION 4 - CONTROL AND STATION KEEPING SYSTEM IMPLEMENTATION

The physical characteristics of the satellite equipments for attitude control and station keeping for a one year mission are given in Table 4-1. The 100, 500, and 1000 lb vehicles were considered for the 3-axis and gravity gradient configuration but only the 100 lb vehicle was considered for the spin configuration. The only significant changes in the systems for vehicles of different weight but of the same configuration are in the cold gas reaction torque system. The station keeping requirements correspond to a velocity impulse of 7 ft/sec.

With the exception of the spin vehicle system, adequate sensors and torquers are either available or being developed. Both the horizon sensor and the Sun sensor for the spin vehicle require fan shaped beams close to 180° wide and a few degrees in thickness. Although specific sensors were not located during the survey, the requirements for these units are not severe, making it possible to modify existing units to provide the fan shaped beams.

For meteorological sensor systems with 2 miles resolution, the present horizon sensors can be used to provide stabilization system rates compatible with the resolution. If better resolution is required, horizon sensors with better noise characteristics and null uncertainties must be developed. Pointing accuracy or basic instrument accuracy and reliability are two areas that need improving.

Control torque devices such as reaction wheels and gyros have performance characteristics which are superior to the sensor because they can be used to control the vehicle to tighter limits than the sensors can measure. Because these devices have rotating parts and bearings, they also have low reliability for a one year mission.

Integrating rate gyros fall into another category. Their random drift characteristics on Earth are better than required; their performance in space in a zero g condition should be comparable or better. The use of hydrodynamic gas spin bearings should improve gyro life; but little factual data on their use in space for long periods of time is available.

Because the reliability of some of the equipment is uncertain, using redundant units is advisable. The larger satellites will provide greater reliability as a result of the possibility of increased redundancy. Redundancy can also be accomplished by providing multiple functions with existing equipment. As an example, the rate gyros in the 3-axis control system are used primarily for acquisition. However, in case of a horizon sensor failure they can be used, by means of the command link and the full Earth pictures, to keep the vehicle properly oriented. Also, by means of the telemetry and command link, many of the normally automatic functions can be performed manually from the ground.

The cold gas system listed in the tabulation is the normal high pressure system with a 3000 psi storage tank, reducing and relief valves, and solenoid valves and nozzles. The cold gas system was used because the total required

TABLE 4-1
PHYSICAL CHARACTERISTICS OF SATELLITE EQUIPMENT

All Size Vehicles	Size	Peak Power (W)	Average Power (W)	Weight (lb)
	Typical 3-Axis Stabilization System			
Variable speed wheels(2)	8.75 in. dia x 3.75 in.	9 ea	4.5 ea	5 ea
Constant speed wheel	10.75 in. dia x 3.75 in.	36	18	10
Horizon sensor	6 in. x 6 in. x 6 in.	4	4	4
Sun sensor	2 in. dia x 9 in.	-	-	0.2
Rate gyros(3)	2.25 in. dia x 3.1 in ea	28 ea	8 ea	0.85 ea
Electronics	8 in. x 8 in. x 5 in.	75	26	12
100 lb vehicle - Cold gas system				
Nitrogen (3000 psi*)	-	-	-	5.3
Titanium tank	1463 cu in.	-	-	7.0
Valves (7) and Nozzles	1/2 cu in. ea	6 ea	-	1.0 total
100 lb vehicle total	2837 cu in.	259	81	52.05
500 lb vehicle - Cold gas system				
Nitrogen (3000 psi*)	-	-	-	24.0
Titanium tank	2587 cu in.	-	-	30
Valves (7) and Nozzles	1/2 cu in. ea	6 ea	-	1.0 total
500 lb vehicle total	3961 cu in	259	81	93.75
1000 lb vehicle - Cold gas system				
Nitrogen (3000 psi*)	-	-	-	41.5
Titanium tank	4474 cu in.	-	-	50.0
Valves (7) and Nozzles	1/2 cu in. ea	6 ea	-	1.0 total
1000 lb vehicle total	5848 cu in	259	81	131.25
	Typical Gravity Gradient Stabilization System			
Variable speed wheels(3)	8.75 in. dia x 3.75 in.	9 ea	4.5 ea	5 ea
Constant speed wheel	10.75 in. dia x 3.75 in.	36	18	10
Horizon sensor	-	-	-	-
Sun sensor	-	-	-	-
Rate gyros(3)	2.25 in. dia x 3.1 in. ea	28 ea	8 ea	0.85 ea
Star tracker	-	-	-	-
Electronics	5 in. x 7 in. x 8 in.	65	23	11
100 lb vehicle Cold gas system				
Nitrogen (3000 psi*)	-	-	-	4.6
Titanium tank	506 cu in.	-	-	7.0
Valves (7) and Nozzles	1/2 cu in. ea	6 ea	-	1.0 total
100 lb vehicle total	1835 cu in.	254	78.5	51.15

TABLE 4-1 (Cont'd)
PHYSICAL CHARACTERISTICS OF SATELLITE EQUIPMENT

	Size	Peak Power (W)	Average Power (W)	Weight (lb)
	Typical Gravity Gradient Stabilization System (Cont'd)			
500 lb vehicle				
Cold gas system				
Nitrogen (3000 psi*)	-	-	-	18.6
Titanium tank	2046 cu in.	-	-	22.0
Valves (7) and Nozzles	1/2 cu in. ea	6 ea	-	1.0 total
500 lb vehicle total	3375 cu in.	254	78.5	80.15
1000 lb vehicle				
Cold gas system				
Nitrogen (3000 psi*)	-	-	-	37.0
Titanium tank	4070 cu in.	-	-	45.0
Valves (7) and Nozzles	1/2 cu in. ea	6 ea	-	1.0 total
1000 lb vehicle total	5399 cu in.	254	78.5	121.55
	Typical Spin Stabilized System			
Wheels	-	-	-	-
Horizon sensor	5 in. x 5 in x 5 in.	4	4	4
Sun sensor	2 in. dia x 1.9 in.	-	-	0.2
Rate gyro (1)	2.25 in dia x 3.1 in.	28	8	0.85
Star tracker	5 in. dia x 10 in.	8	6.5	9
Electronics	5 in. x 5 in x 7 in.	10	7.2	5
100 lb vehicle				
Cold gas system				
Nitrogen (3000 psi*)	-	-	-	5.4
Titanium tank	594 cu in.	-	-	7.0
Valves (7) and Nozzles	1/2 cu in. ea	6 ea	-	1
100 lb vehicle total	1112 cu in.	92	25.7	32.45

* Includes 50% safety factor plus 0.5 lb for leakage.

impulse is not large enough to warrant using hot gas, and also because the reliability of cold gas systems is better.

A low pressure cold gas system which uses a subliming solid has a definite weight savings over the high pressure system, of approximately the weight of the stored propellant. The reducing and relief valves are eliminated, and the storage tank is much lighter because the gas pressures are in the 1 to 5 psi range. The system is still in the developmental stage and problems of condensation in the lines, maintenance of pressure by controlling the temperature of the solid, and filtering of small solid particles are not completely solved. The advantages of the system, however, warrant its consideration for future systems.

The nozzle geometry for the 500 lb 3-axis system is shown in Figure 4-1. Six nozzles are used for 3-axis attitude control instead of the 12 necessary to produce pure couples. The translation force produced when the yaw and pitch nozzles are operated in the proper direction to aid in the station keeping function of countering the drift produced by the Earth's equatorial ellipticity. By orienting these four nozzles in this direction, they can be used for correcting initial injection velocity excesses and for station keeping corrections, in addition to attitude control. The two roll nozzles produce a translation which disturbs the orbit; but because the total impulse is small, the disturbance is insignificant. The one nozzle at the center of mass is used for injection velocity error corrections which would require thrust in the forward direction opposite to the other four nozzles.

The electronics unit contains a static inverter for converting DC power to AC power which is used to operate the wheels and gyros. It also contains the control amplifiers for the variable speed wheels and gyros, the logic circuitry and the stabilization amplifiers. Modular construction would be used to permit changing small functional units for ease of maintenance.

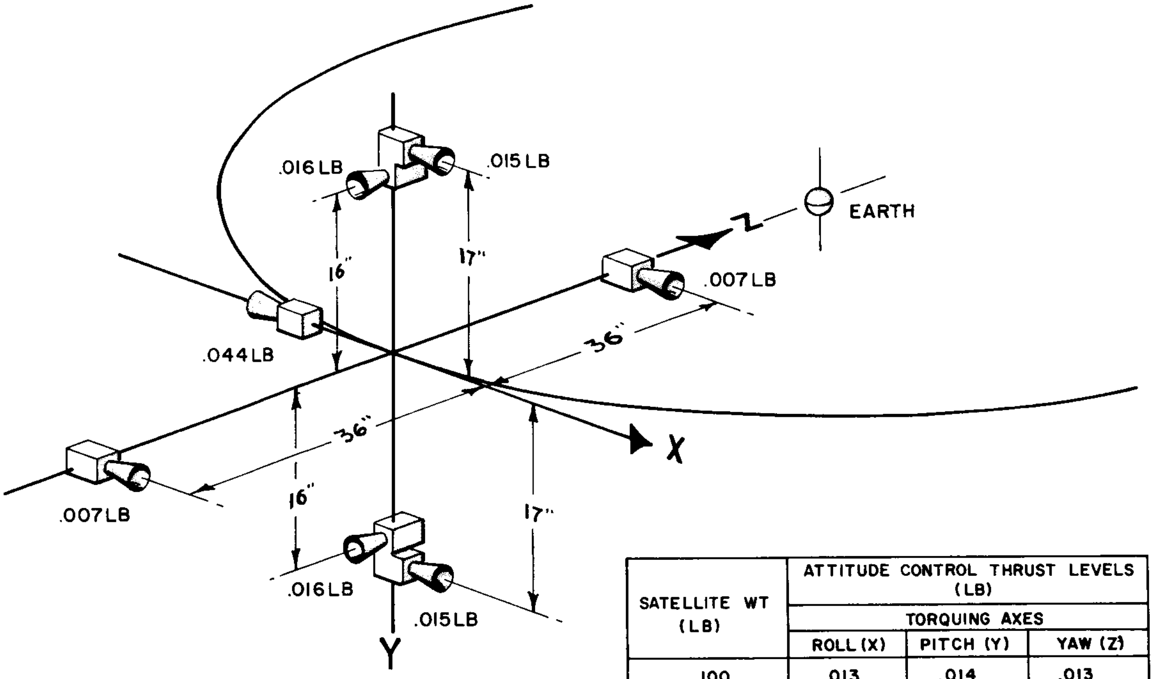

SATELLITE WT (LB)	ATTITUDE CONTROL THRUST LEVELS (LB)		
	TORQUING AXES		
	ROLL (X)	PITCH (Y)	YAW (Z)
100	.013	.014	.013
500	.016	.007	.015
1,000	.012	.007	.011

Figure 4-1. 500 lb 3-Axis Stabilized Nozzle Geometry

SECTION 5 - SYSTEM IMPLICATIONS OF ATLAS-AGENA INJECTION ERRORS

A. INJECTION ERROR CORRECTION

Atlas-Agena-spacecraft guidance inaccuracies result in injection errors that cause the final orbit to depart from the desired synchronous, equatorial, circular orbit. These errors are larger than those specified by Ref 5-1. The increased injection errors have the following 3σ values (Ref 5-2).

ΔV = 238 ft/sec

e = 0.025

Included in the 238 ft/sec velocity error is the incremental velocity (ΔV = 106 ft/sec) necessary to correct for an inclination error of 0.63°. It is not necessary to correct this inclination error, since the tolerable SMS latitude excursion is ±5° maximum, ±2° desirable. Hence, the Atlas-Agena-spacecraft injection errors requiring correction for the SMS mission are $\Delta V = 132$ ft/sec and $e = 0.025$. This velocity disparity is equivalent to a semimajor axis error of $|\Delta a| \leq 0.173$ Earth radii.

Eccentricity errors need not be reduced to zero. Daily longitude excursions which are less than the desired ±2° control boundary excursion employed to actuate the station keeping mode (see Section 4-3) are considered acceptable. Accordingly, an eccentricity error of 0.009 ($\Delta\lambda = \pm 1°$) is tolerable, provided final station injection occurs near the line of apsides. Regardless of the injection point location, however, an eccentricity residual of less than 0.009 ensures a daily longitude excursion of less than ±2°. Thus, injection correction mode must be calculated to eliminate randomly distributed semimajor axis errors and maintain $e \leq 0.009$. Practically, if Δa is reduced to about 0.001 Earth radii, then the associated residual mean motion error is acceptable when compared to the mean motion correction required during the subsequent station keeping mode.

Semimajor axis and eccentricity errors can be corrected by a single impulse provided

$$(a + \Delta a)(1 + e) \leq a \leq (a + \Delta a)(1 - e) \quad a = \text{synchronous radius for desired circular orbit}$$

Various combinations of Δa and e errors, which satisfy the foregoing, are contained within area AOB shown in Figure 5-1. A single nontransverse impulse will generally be required to correct any of these Δa, e combinations.

The application of transverse corrections does not appear favorable, however, because

(1) The attitude control system must then be capable of unrestricted pitch freedom about an axis parallel to the Earth's polar axis.

(2) The station guidance system becomes more complex.

(3) The ΔV requirements increase.

defined by the shaded area of Figure 5-1 can be rectified to tolerable limits ($\Delta a \approx 0$; $e \leq 0.009$) by the application of a single transverse velocity correction. This correction is applied near perigee in opposition to the direction of motion for $\Delta a > 0$, and near apogee in the direction of motion when $\Delta a < 0$.

Single impulse corrections are also applicable to restricted regions above the shaded area. If the perturbed orbit is initially eccentric, then a transverse impulse applied near the latus rectum ($\theta \approx 90°$) will cause a change in semimajor axis and perigee location without significantly altering the eccentricity. Hence, for modest initial eccentricities (e greater than some minimum value but < 0.009), the semimajor axis error can be rectified without introducing intolerable eccentricity errors.

Two transverse impulse maneuvers are required when $|\Delta a| > 0.06$ Earth radii and $e \approx 0$, and when $\Delta a \approx 0$ and $e > 0.009$. In the former case, the total characteristic velocity is equivalent to the Δa error. In the latter case, ΔV_{max} will be approximately 125 ft/sec.

Substantial off-station drift may accrue during the interval of time between injection and error correction. It is estimated that an initial tracking time of 5 hours will be required to determine the existing injection errors. A maximum wait time of 24 hours may be required to realize a favorable orbit position for the initiation of the corrective maneuver. Hence, a conservative estimate for initial off-station drift (ΔV = 132 ft/°) is 20°. On this basis, approximately 28 ft/sec of additional equivalent propellant is required to re-establish the desired station position within a minimum wait time of 2 weeks. On this 28 ft/sec, 14 ft/sec will be required on-station to halt the corrective drift.

It is emphasized that the foregoing injection correction scheme is predicated on accurate knowledge of the orbital parameters subsequent to injection, the application of known circumferential impulses, and linearized theory. The influence of orbit determination errors and errors inherent in the corrective process should not be critical, since these errors can be made small compared to the allowable residual injection errors.

B. ATTITUDE CONTROL

The effect of the larger Atlas-Agena injection errors on the vehicle attitude control system is to make it necessary to employ a separate hot gas system for injection error correction. Although a hot gas system could have been used to correct the injection errors given in the Work Statement, the weight saving would have been very small. Hence, in the interests of simplicity and reliability, it was decided to use high pressure cold gas for injection error correction in order to utilize the thrusters of the cold gas attitude control system.

The velocity increment of ± 160 ft/sec arising from use of the Agena vehicle, however, imposes a completely different set of conditions, and the weight saving realized with a hot gas system for this application is large, so that a hot gas system becomes the logical choice. A thrust level of 1 lb was chosen. This value is adequate for initial error correction, since using a larger value would result only in aggravating the problem of torques due to trimming out misalignment.

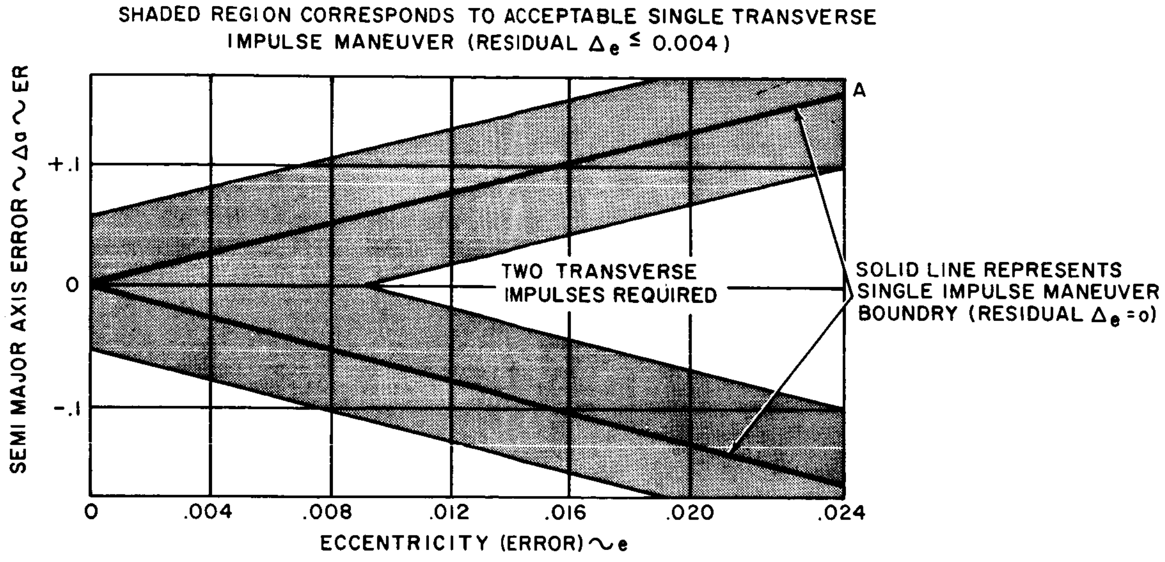

Figure 5-1. Single and Double Impulse Maneuver Boundaries

In the interest of overall system simplicity, it is therefore desirable to consider correction logic requirements based on applying small transverse velocity impulses. For certain Δa, e combinations, two velocity corrections are always necessary.

The propulsion system utilized to correct injection errors provides a constant acceleration of 0.06 ft/sec^2. Total thrusting time, for the maximum correction, is equivalent to approximately 8° of central angle. Based on the foregoing acceleration level and thrusting interval, it was found that the perturbative element changes (Δa, Δe) could be estimated with sufficient accuracy from linearized impulsive relations between ΔV, Δa, and Δe. These relations are (see subsection 4).

$$\frac{\Delta a}{a} \approx \frac{\Delta V}{V}$$

$$\Delta e \approx \frac{\Delta a}{a}\left[2 \cos \theta + (1 + \cos^2 \theta)\right]; \quad e_{max} = 0.025$$

Parameter θ represents the (mean) true anomaly of transverse thrust application, measured from perigee of the perturbed orbit. As the perturbed eccentricity approaches zero, perigee is undefined, and $\Delta e \approx \frac{\Delta a}{a}$. Each velocity correction is specified by the existing Δa error which, in turn, fixes the level of eccentricity error that can be removed.

The relation between Δe and Δa for perigee or apogee velocity corrections is idential to the boundary specified by the single impulse maneuvers within the accuracy of the scales shown in Figure 5-1. Any combination of Δa and e values, Since the preceeding discussions indicate that a restart capability will be required, a hydrogen peroxide hot gas system was selected. The results of independent estimates of system weight by Walter Kidde & Co. and Republic yield a system weight of approximately 30 lb.

The cold gas attitude control system proposed for the 500 lb, 3-axis stabilized vehicle uses 24 lb of high pressure cold gas contained in a 30 lb tank. The total impulse available is 1680 lb - sec, if the specific impulse of nitrogen is taken as 60 sec. Of this total, it was planned that 600 lb - sec of impulse would be used for correcting initial injection errors, in particular the 1000 sec period error given in the Work Statement. By eliminating the corresponding quantity of gas (10 lb) required to produce this thrust, then a saving in tank weight of approximately 12 lb can also be realized. A total weigh saving of 22 lb would thereby be effected. With this reduction in weight of the cold gas attitude control system, the addition of the 30 lb hot gas injection error correction system described above results in an attitude control system weight increase of only 8 lb.

C. REFERENCES

5-1. NASA, "Statement of Work for Studies of Synchronous Meteorological Satellite System Problems," Goddard Space Flight Center, Contract NAS5-3189 with Republic Aviation Corporation, 31 January 1963

5-2. Lockheed Missiles and Space Company, "Syncom Booster Feasibility Study," Report No. LMSC A057612, 30 September 1962 (Confidential)

APPENDIX A
DERIVATION OF COMPLETE MOMENT EQUATIONS

A. INTRODUCTION

The purpose of this appendix is to define the vehicle equations of motion when the satellite is in an Earth tracking mode. This mode occurs after acquisition where the satellite yaw axis has been aligned with the geocentric Earth vertical. A secondary purpose is to describe a method for simplification of the resulting equations of motion.

The simplification procedure considers the relative magnitude of comparable terms and the particular feed back or feed forward path of each term in the equations. The last consideration provides justification for eliminating terms on the basis of system stability and insures that no feedback or feed forward path has been eliminated, which could create system stability problems.

B. SATELLITE EQUATIONS OF MOTION FOR EARTH TRACKING

The resulting equations are to be used for simulation of the gyrocompass and the discrete-continuous control concepts, with the satellite in the Earth tracking mode. Because in the Earth tracking mode, the satellite attitude deviations are small, by definition, the final equations will be expressed in terms of small angles. To obtain a set of equations which are applicable to both control concepts (gyrocompass and discrete-continuous) small angle approximations will not be made of the vehicle yaw angle. The final equations, thus, are expressed in terms of small pitch and roll angles and large yaw angles.

In the following derivation, the small angle approximations are not made until the final equations are obtained. This insures that no terms are lost in the derivation. All symbols are defined in the List of Symbols.

The basic vector moment equation expressed in the body axis coordinate system (Figure A-1) is

$$\dot{\vec{H}}_B + \vec{\omega}_{IB_B} \times \vec{H}_B = \Sigma \vec{D}_B \qquad \text{(A-1)}$$

Here, $\overset{\circ}{\vec{H}}_B$ is the rate of change of vehicle angular momentum as seen in the body axis system. The angular velocity of the body axis coordinate system, in inertial space, $\vec{\omega}_{IB_B}$, may be expressed as a summation of angular velocities expressed in the body reference frame.

Thus,

$$\vec{\omega}_{IB_B} = \vec{\omega}_{IO_B} + \vec{\omega}_{OB_B} \qquad \text{(A-2)}$$

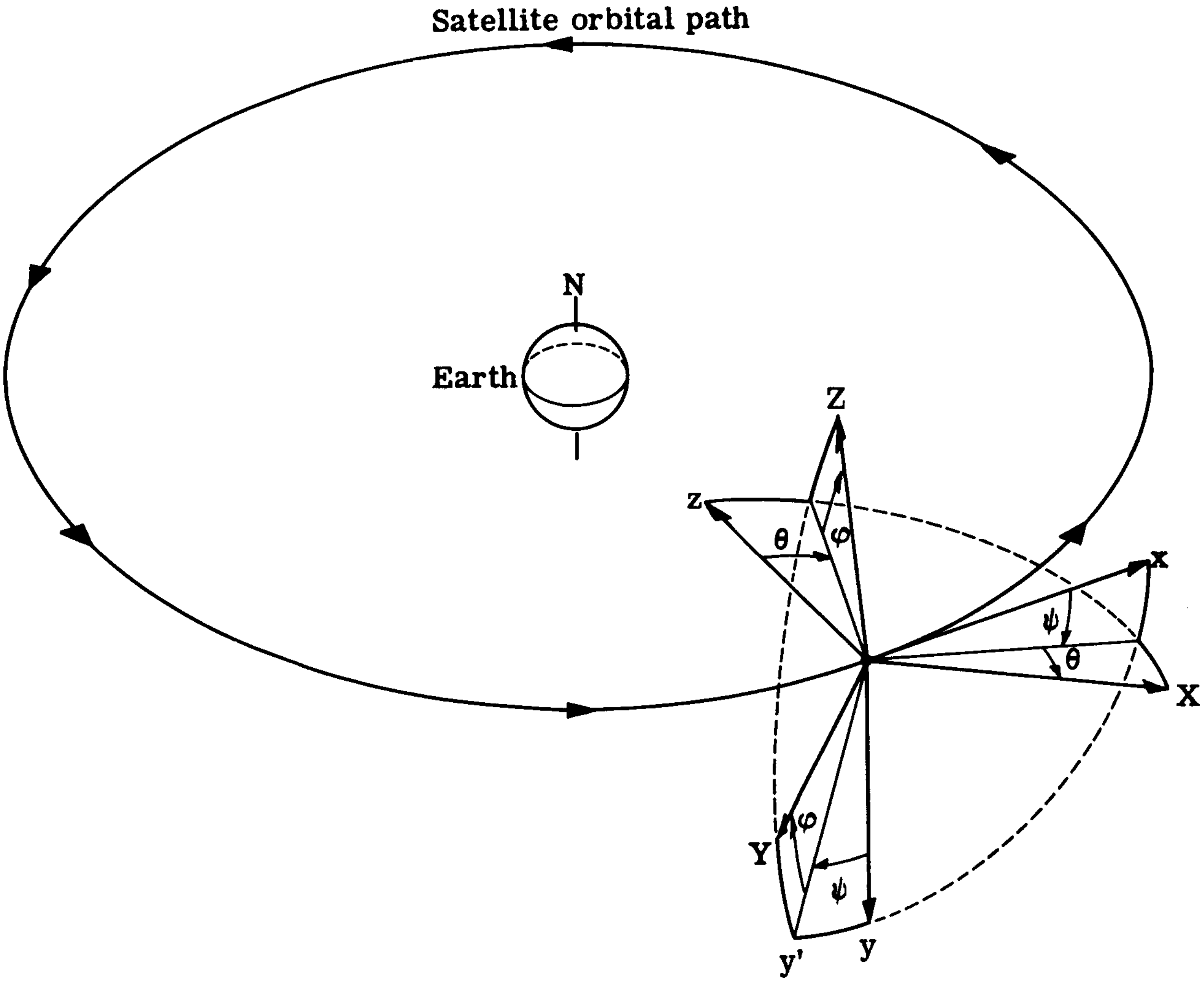
Satellite orbital path
N
Earth
Z
z
θ
φ
x
ψ
θ
X
Y
φ
ψ
y'
y

The vehicle-centered orbital-reference co-ordinate system (x, y, z) is referenced to the Earth and the orbital plane.

The body-axis co-ordinate system(X, Y, Z) is obtained from the reference orbital co-ordinate system by an angle sequence of yaw (ψ) about z, pitch (θ) about y' and roll (φ) about X.

Figure A-1. Coordinate Reference System

Since $\vec{\omega}_{IO}$ and $\vec{\omega}_{OB}$ are naturally expressible in coordinate frames other than the body frame, Eq A-2 can be expressed by the following.

$$\vec{\omega}_{IB_B} = Q_{BO}\vec{\omega}_{IO_O} + Q_{BE}\vec{\omega}_{OB_E} \tag{A-3}$$

where

$$\vec{\omega}_{IO_O} = \begin{bmatrix} 0 \\ -\omega_o \\ 0 \end{bmatrix} \tag{A-4}$$

$$\vec{\omega}_{OB_E} = \begin{bmatrix} \dot{\phi} \\ \dot{\theta} \\ \dot{\psi} \end{bmatrix} \tag{A-5}$$

$$Q_{BE} = \begin{bmatrix} 1 & 0 & -\sin\theta \\ 0 & \cos\phi & \sin\phi\cos\theta \\ 0 & -\sin\phi & \cos\phi\cos\theta \end{bmatrix} \tag{A-6}$$

$$Q_{BO} = \begin{bmatrix} \cos\theta\cos\psi & \cos\theta\sin\psi & -\sin\theta \\ \sin\phi\sin\theta\cos\psi - \cos\phi\sin\psi & \cos\phi\cos\psi + \sin\phi\sin\theta\sin\psi & \sin\phi\cos\theta \\ \sin\phi\sin\psi + \cos\phi\sin\theta\cos\psi & \cos\phi\sin\theta\sin\psi - \sin\phi\cos\psi & \cos\phi\cos\theta \end{bmatrix} \tag{A-7}$$

Substitution of Eqs A-4 through A-7 into Eq A-2 results in

$$\vec{\omega}_{IB_B} = \begin{bmatrix} -\omega_o\cos\theta\sin\psi + \dot{\phi} - \dot{\psi}\sin\theta \\ -\omega_o\cos\phi\cos\psi - \omega_o\sin\phi\sin\theta\sin\psi + \dot{\theta}\cos\phi + \dot{\psi}\sin\phi\cos\theta \\ -\omega_o\cos\phi\sin\theta\sin\psi + \omega_o\sin\phi\cos\psi - \dot{\theta}\sin\phi + \dot{\psi}\cos\phi\cos\theta \end{bmatrix} \tag{A-8}$$

Differentiating Eq 8 produces an expression for $\dot{\vec{\omega}}_{IB_B}$

$$\dot{\vec{\omega}}_{IB_B} = \begin{bmatrix} \omega_o\dot{\theta}\sin\theta\sin\psi - \omega_o\dot{\psi}\cos\theta\cos\psi + \ddot{\phi} - \ddot{\psi}\sin\theta - \dot{\psi}\dot{\theta}\cos\theta \\[1em] \omega_o\dot{\phi}\sin\phi\cos\psi + \omega_o\dot{\psi}\cos\phi\sin\psi - \omega_o\dot{\phi}\cos\phi\sin\theta\sin\psi \\ - \omega_o\dot{\theta}\sin\phi\cos\theta\sin\psi - \omega_o\dot{\psi}\sin\phi\sin\theta\cos\psi - \dot{\theta}\dot{\phi}\sin\phi \\ + \ddot{\theta}\cos\phi + \ddot{\psi}\sin\phi\cos\theta + \dot{\psi}\dot{\phi}\cos\phi\cos\theta - \dot{\psi}\dot{\theta}\sin\phi\sin\theta \\[1em] \omega_o\dot{\phi}\sin\phi\sin\theta\sin\psi - \omega_o\dot{\theta}\cos\phi\cos\theta\sin\psi - \omega_o\dot{\psi}\cos\phi\sin\theta\cos\psi \\ + \omega_o\dot{\phi}\cos\phi\cos\psi - \omega_o\dot{\psi}\sin\phi\sin\psi - \ddot{\theta}\sin\phi - \dot{\theta}\dot{\phi}\cos\phi \\ + \ddot{\psi}\cos\phi\cos\theta - \dot{\psi}\dot{\phi}\sin\phi\cos\theta - \dot{\psi}\dot{\theta}\cos\phi\sin\theta \end{bmatrix} \qquad \text{(A-9)}$$

Equations A-8 and A-9 are substituted into Eq A-1 considering

$$\dot{\vec{H}}_B = \begin{bmatrix} I_x & 0 & 0 \\ 0 & I_y & 0 \\ 0 & 0 & I_z \end{bmatrix} \dot{\vec{\omega}}_{IB_B} + \begin{bmatrix} J_{X_B} & 0 & 0 \\ 0 & J_{Y_B} & 0 \\ 0 & 0 & J_{Z_B} \end{bmatrix} \dot{\vec{\Omega}}_{IB_B} \qquad \text{(A-10)}$$

$$\dot{\vec{H}}_B = \begin{bmatrix} I_x & 0 & 0 \\ 0 & I_y & 0 \\ 0 & 0 & I_z \end{bmatrix} \dot{\vec{\omega}}_{IB_B} + \begin{bmatrix} \dot{h}_{c_x} \\ \dot{h}_{c_y} \\ \dot{h}_{c_z} \end{bmatrix}$$

where the satellite body axes are taken to be principal axes. The equations that result are the final equations of motion for large angles. Equations A-11 depict the simplified set for small pitch (θ) and roll (ϕ) angles and large yaw (ψ) angles.

$$\begin{aligned} D_{X_B} = {} & -I_x\omega_o\dot{\psi}\cos\psi + I_x\ddot{\phi} - I_x\dot{\psi}\dot{\theta} - I_x\theta\ddot{\psi} + \dot{h}_{c_x} + (I_y - I_z)\Big[-\omega_o^2\theta^2\phi\sin^2\psi \\ & + \omega_o^2\phi\cos^2\psi - 2\omega_o\phi\dot{\theta}\cos\psi + \phi\mathring{\theta}^2 - \phi\dot{\psi}^2 + \omega_o\mathring{\psi}\cos\psi - \omega_o\dot{\psi}\phi^2\cos\psi \\ & - \mathring{\theta}\mathring{\psi} + \dot{\theta}\dot{\psi}\phi^2 + 2\,\omega_o\theta\phi\dot{\psi}\sin\psi - \omega_o^2\theta\sin\psi\cos\psi + \omega_o^2\theta\phi^2\sin\psi\cos\psi \\ & + \omega_o\theta\mathring{\theta}\sin\psi - \omega_o\theta\mathring{\theta}\phi^2\sin\psi\Big] + \omega_o\theta\sin\psi h_{c_y} - \omega_o\theta\phi\sin\psi h_{c_z} \\ & - \dot{\psi}h_{c_y} + \mathring{\psi}\phi h_{c_z} - \omega_o\phi\cos\psi h_{c_y} - \omega_o\cos\psi h_{c_z} + \mathring{\theta}\phi h_{c_y} \\ & + \dot{\theta}h_{c_z} + I_x\,\omega_o\mathring{\theta}\theta\sin\psi \end{aligned} \qquad \text{(A-11)}$$

$$
\begin{aligned}
D_{Y_B} = {} & I_y\ddot{\theta} + I_y\phi\ddot{\psi} - I_y\omega_o\dot{\phi}\,\theta\sin\psi + I_y\omega_o\dot{\psi}\sin\psi - I_y\omega_o\dot{\theta}\sin\psi \\
& - I_y\omega_o\theta\phi\dot{\psi}\cos\psi + I_y\dot{\phi}\dot{\psi} + \dot{h}_{c_y} + (I_x - I_z)\big[\omega_o{}^2\theta\sin^2\psi \\
& - \omega_o{}^2\phi\sin\psi\cos\psi + \omega_o\phi\dot{\theta}\sin\psi - \omega_o\theta\dot{\phi}\sin\psi - \omega_o\dot{\psi}\sin\psi \\
& + \omega_o\dot{\psi}\theta^2\sin\psi + \omega_o\phi\dot{\phi}\cos\psi - \omega_o\phi\theta\dot{\psi}\cos\psi + \dot{\phi}\dot{\psi} - \phi\dot{\phi}\dot{\theta} \\
& - \theta\dot{\psi}^2 + \phi\theta\dot{\theta}\dot{\psi}\big] - \omega_o\theta\sin\psi\, h_{c_x} + \omega_o\sin\psi\, h_{c_z} + \omega_o\phi\cos\psi\, h_{c_x} \\
& - \phi\dot{\theta}h_{c_x} - \dot{\phi}h_{c_z} + \dot{\psi}h_{c_x} + \dot{\psi}\theta h_{c_z} - I_y\dot{\theta}\dot{\phi}\phi - I_y\dot{\psi}\dot{\theta}\theta\phi \\
& + I_y\omega_o\dot{\phi}\phi\cos\psi
\end{aligned}
$$

$$
\begin{aligned}
D_{Z_B} = {} & -I_z\omega_o\dot{\theta}\sin\psi - I_z\omega_o\phi\dot{\psi}\sin\psi - I_z\omega_o\theta\dot{\psi}\cos\psi + I_z\omega_o\dot{\phi}\cos\psi \\
& - I_z\phi\ddot{\theta} - I_z\dot{\phi}\dot{\theta} + I_z\ddot{\psi} + \dot{h}_{c_z} + (I_y - I_x)\big[\omega_o{}^2\theta\phi^2\sin^2\psi \\
& + \omega_o{}^2\sin\psi\cos\psi - \omega_o\dot{\theta}\sin\psi - \omega_o\phi\dot{\psi}\sin\psi - \omega_o\theta\phi\dot{\phi}\sin\psi \\
& + \omega_o\theta^2\phi\dot{\psi}\sin\psi - \omega_o\dot{\phi}\cos\psi + \omega_o\theta\dot{\psi}\cos\psi + \dot{\phi}\dot{\theta} + \phi\dot{\phi}\dot{\psi} \\
& - \theta\dot{\theta}\dot{\psi} - \phi\theta\dot{\psi}^2\big] - \omega_o\sin\psi\, h_{c_y} + \omega_o\theta\phi\sin\psi\, h_{c_x} + \omega_o\cos\psi\, h_{c_x} \\
& + \dot{\phi}h_{c_y} - \dot{\theta}h_{c_x} - \dot{\psi}\theta h_{c_y} - \dot{\psi}\phi h_{c_x} - I_z\dot{\psi}\dot{\theta}\theta - I_z\dot{\psi}\dot{\phi}\phi \\
& + I_z\omega_o\dot{\phi}\phi\theta\sin\psi
\end{aligned}
$$

C. LIST OF SYMBOLS

ψ, θ, ϕ = modified Euler angles defining the orientation of the satellite body with respect to the orbital reference frame (rotation sequence is yaw, pitch, and roll from the orbital frame to the body frame)

$D_{X_B}, D_{Y_B}, D_{Z_B}$ = external torques acting about the vehicle body axes

I_x, I_y, I_z = moments of inertia related to principle axes (body and principal axes are assumed coincident)

$h_{c_x}, h_{c_y}, h_{c_z}$ = angular moments of internal rotating equipment

$J_{X_B}, J_{Y_B}, J_{Z_B}$ = moments of inertia of internal rotating equipment

$\Omega_{X_B}, \Omega_{Y_B}, \Omega_{Z_B}$ = angular velocities of internal rotating equipment

ω_o = the orbital angular velocity

$\vec{H}_B$ = the vehicle angular momentum expressed in the body coordinate system

$\vec{\omega}_{IB_B}$ = the angular velocity of the body frame with respect to an inertial frame expressed in the body coordinate system

$\vec{\omega}_{IO_B}$ = the angular velocity of the orbital reference frame with respect to an inertial frame expressed in body coordinates

$\vec{\omega}_{OB_B}$ = the angular velocity of the body frame with respect to the orbital frame expressed in body coordinates

$\vec{\omega}_{IO_O}$ = the angular velocity of the orbital reference frame with respect to the inertial frame expressed in orbital coordinates

$\vec{\omega}_{OB_E}$ = the angular velocity of the body with respect to the orbital reference frame expressed in Euler coordinates

Q_{B_O} = an orthogonal transformation which transforms orbital coordinates to body coordinates

Q_{B_E} = a nonorthogonal transformation which transforms Euler coordinates to body coordinates

A dot $(\cdot)$ above a variable denotes its time rate of change as seen in the body coordinate system.

APPENDIX B
ANALYTICAL SIMPLIFICATION

A. SIMPLIFICATION OF TRACKING EQUATIONS

For the purpose of simplifying Eqs A-11, a block diagram (Figure B-1) is shown which depicts all the terms of Eqs A-11 as either feed back or feed forward components of the three single-axis control systems. The basic control systems for each axis were considered to be represented by the block diagram, the sketch below.

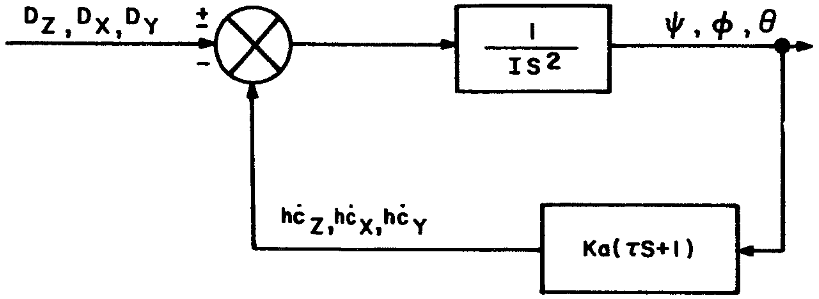

Single Axis Control Loop

The gain, K_a, may be expressed in terms of damping ratio (ξ), the lead time constant (τ) and the vehicle inertia (I) as

$$K_a = \frac{4I\xi^2}{\tau^2} \tag{B-1}$$

A typical value for K_a, based on a moment of inertia of 690 in.-lb-sec^2 (which represents the minimum inertia of the 500 lb-vehicle), a lead time constant of 10 seconds, and a desired damping ratio of 0.7 would be 12.1 in.-lb/radian.

The philosophy for equation simplification is to examine all feedback terms which parallel the basic control path and to compare the magnitude of the coupling terms to the basic control terms. As an example, consider the block diagram below, where the yaw control term has been separated into rate and attitude terms. Typical coupling terms are included which parallel each of the control feedback terms.

From this diagram, the characteristic equation is seen to be the following (in the Laplace notation):

$$I_x S^2 + \left[K_a \tau - I_z \dot{\theta}\theta - I_z \dot{\phi}\phi\right] S + \left[K_a - I_z \omega_o \dot{\theta}\right] \tag{B-2}$$

It is evident that if

$$K_a \tau >> I_z (\dot{\theta}\theta + \dot{\phi}\phi) \tag{B-3}$$

and

$$K_a >> I_z \omega_o \dot{\theta} \tag{B-4}$$

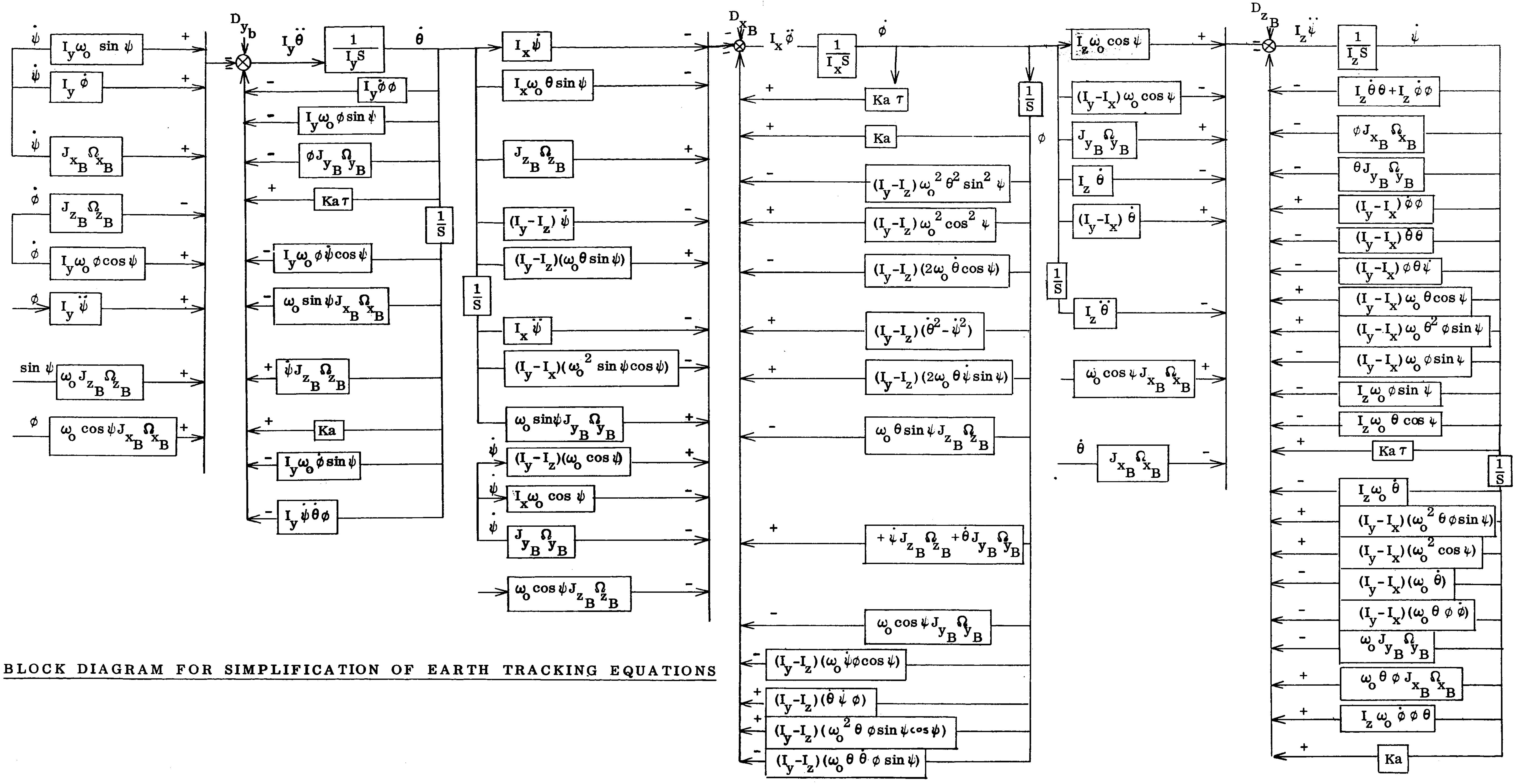
D_{y_b}
$I_y\ddot{\theta}$
$\frac{1}{I_yS}$
$\dot{\theta}$
$I_y\omega_o \sin\psi$
$I_y\dot{\phi}$
$J_{x_B}\Omega_{x_B}$
$J_{z_B}\Omega_{z_B}$
$I_y\omega_o\phi\cos\psi$
$I_y\ddot{\psi}$
$\omega_o J_{z_B}\Omega_{z_B}$
$\omega_o \cos\psi J_{x_B}\Omega_{x_B}$
$\sin\psi$
$I_y\dot{\phi}\phi$
$I_y\omega_o\phi\sin\dot{\psi}$
$\phi J_{y_B}\Omega_{y_B}$
$Ka\,\tau$
$I_y\omega_o\phi\dot{\psi}\cos\psi$
$\omega_o\sin\psi J_{x_B}\Omega_{x_B}$
$\dot{\psi}J_{z_B}\Omega_{z_B}$
Ka
$I_y\omega_o\dot{\phi}\sin\psi$
$I_y\dot{\psi}\dot{\theta}\phi$
$\frac{1}{S}$
D_{x_B}
$I_x\ddot{\phi}$
$\frac{1}{I_xS}$
$\dot{\phi}$
$I_x\dot{\psi}$
$I_x\omega_o\theta\sin\psi$
$J_{z_B}\Omega_{z_B}$
$(I_y-I_z)\dot{\psi}$
$(I_y-I_z)(\omega_o\theta\sin\psi)$
$I_x\ddot{\psi}$
$(I_y-I_x)(\omega_o^2\sin\psi\cos\psi)$
$\omega_o\sin\psi J_{y_B}\Omega_{y_B}$
$(I_y-I_z)(\omega_o\cos\psi)$
$I_x\omega_o\cos\psi$
$J_{y_B}\Omega_{y_B}$
$\omega_o\cos\psi J_{z_B}\Omega_{z_B}$
$Ka\,\tau$
Ka
ϕ
$(I_y-I_z)\omega_o^2\theta^2\sin^2\psi$
$(I_y-I_z)\omega_o^2\cos^2\psi$
$(I_y-I_z)(2\omega_o\dot{\theta}\cos\psi)$
$(I_y-I_z)(\dot{\theta}^2-\dot{\psi}^2)$
$(I_y-I_z)(2\omega_o\theta\dot{\psi}\sin\psi)$
$\omega_o\theta\sin\psi J_{z_B}\Omega_{z_B}$
$+\dot{\psi}J_{z_B}\Omega_{z_B}+\dot{\theta}J_{y_B}\Omega_{y_B}$
$\omega_o\cos\psi J_{y_B}\Omega_{y_B}$
$(I_y-I_z)(\omega_o\dot{\psi}\phi\cos\psi)$
$(I_y-I_z)(\dot{\theta}\dot{\psi}\phi)$
$(I_y-I_z)(\omega_o^2\theta\phi\sin\psi\cos\psi)$
$(I_y-I_z)(\omega_o\theta\dot{\theta}\phi\sin\psi)$
$I_z\omega_o\cos\psi$
$(I_y-I_x)\omega_o\cos\psi$
$J_{y_B}\Omega_{y_B}$
$I_z\dot{\theta}$
$(I_y-I_x)\dot{\theta}$
$I_z\ddot{\theta}$
$\omega_o\cos\psi J_{x_B}\Omega_{x_B}$
$\dot{\theta}$
$J_{x_B}\Omega_{x_B}$
D_{z_B}
$I_z\ddot{\psi}$
$\frac{1}{I_zS}$
$\dot{\psi}$
$I_z\dot{\theta}\theta+I_z\dot{\phi}\phi$
$\phi J_{x_B}\Omega_{x_B}$
$\theta J_{y_B}\Omega_{y_B}$
$(I_y-I_x)\dot{\phi}\phi$
$(I_y-I_x)\dot{\theta}\theta$
$(I_y-I_x)\phi\theta\dot{\psi}$
$(I_y-I_x)\omega_o\theta\cos\psi$
$(I_y-I_x)\omega_o\theta^2\phi\sin\psi$
$(I_y-I_x)\omega_o\phi\sin\psi$
$I_z\omega_o\phi\sin\psi$
$I_z\omega_o\theta\cos\psi$
$Ka\,\tau$
$I_z\omega_o\dot{\theta}$
$(I_y-I_x)(\omega_o^2\theta\phi\sin\psi)$
$(I_y-I_x)(\omega_o^2\cos\psi)$
$(I_y-I_x)(\omega_o\dot{\theta})$
$(I_y-I_x)(\omega_o\theta\phi\dot{\phi})$
$\omega_o J_{y_B}\Omega_{y_B}$
$\omega_o\theta\phi J_{x_B}\Omega_{x_B}$
$I_z\omega_o\dot{\phi}\phi\theta$
Ka

BLOCK DIAGRAM FOR SIMPLIFICATION OF EARTH TRACKING EQUATIONS

Figure B-I. Block Diagram for Simplification of Earth Tracking Equations

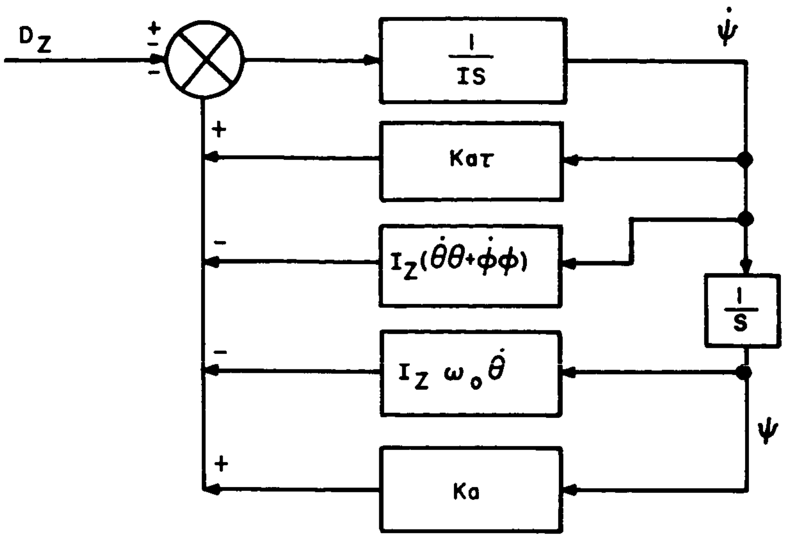

Single Axis Loop with Coupling Feedback

then the damped natural frequency and damping ratio are essentially unaffected by the presence of coupling terms. It is concluded, therefore, that coupling terms which parallel control feed back paths do not significantly change the loop stability if they are small compared to the control feed back terms. This philosophy has been applied to all feed back terms indicated in Figure B-1.

Terms of the equations which are feed forward in nature do not directly influence the stability of individual single-axis loops because they are not contained within the closed loop. These terms, however, do couple the three single axis loops and, thus, provide possible paths which could cause stability problems of the integrated 3-axis system. To achieve equation simplification, considering feed forward terms, it is possible to group these terms, as indicated in Figure B-1, such that they may be compared on a common basis.

Several of the feed forward terms have no basis for comparison and have been maintained in the final set of simplified equations. This approach keeps all possible feed back and feed forward paths, and only eliminates parallel terms in those cases where they are small by comparison.

B. NUMERICAL EXAMPLE OF SIMPLIFICATION

The maximum value of each term in Eqs A-11 or Figure B-1 was computed based on estimated performance requirements and previous experience with the basic system parameters and variables.

Parameters and variable maximum values used for the equation simplification are tabulated in Table B-1.

TABLE B-1
ESTIMATED MAXIMUM VALUES

I_x = 2500 in.-lb-sec^2

I_y = 4100 in.-lb-sec^2

I_z = 2500 in.-lb-sec^2

$\dot{\psi}_{max} = \dot{\theta}_{max} = \dot{\phi}_{max}$ = ± 10^{-3} rad/sec

Lead Time Constant = 10 sec

Control Gain (K_a) = 12.1 in.-lb/rad

Reaction Wheel Momentum = ± 10 in.-lb-sec

ω_o = 0.725×10^{-4} rad/sec

$\ddot{\phi}_{max} = \ddot{\psi}_{max} = \ddot{\theta}_{max}$ = 10^{-3} rad/sec^2

$\phi_{max} = \theta_{max}$ = ± 0.35 rad

ψ_{max} = ± π rad

As an example of the type of numerical comparisons which were made, consider the pitch axis of Figure B-1. The feed back terms dependent on $\dot{\theta}$ and θ will be shown as an illustration of the simplification comparisons.

1. Terms Dependent on $\dot{\theta}$

$$\text{eliminated since less than 1\% of primary term}\begin{cases} I_y\,\dot{\phi}\phi & = 1.43 \text{ in.-lb-sec} \\ I_y\,\omega_o\phi \sin\psi & = 0.104 \text{ in.-lb-sec} \\ J_{Y_B}\Omega_{Y_B}\phi & = 3.5 \text{ in.-lb-sec} \end{cases}$$

$K_a\tau$ = 121 in.-lb-sec

2. Terms Dependent on θ

$$\text{eliminated since less than 1\% of primary term}\begin{cases} I_y\omega_o\phi\dot{\psi}\cos\psi & = 1.04\text{x}10^{-4} \text{ in.-lb} \\ \omega_o \sin\psi\, J_{X_B}\Omega_{X_B} & = 7.25\text{x}10^{-4} \text{ in.-lb} \\ \dot{\psi}\, J_{E_B}\Omega_{E_B} & = 1\text{x}10^{-2} \\ I_y\,\omega_o\dot{\phi}\sin\psi & \equiv 2.97\text{x}10^{-4} \text{ in.-lb} \\ I_y\dot{\psi}\dot{\theta}\phi & = 1.44\text{x}10^{-3} \text{ in.-lb} \end{cases}$$

K_a = 12.1 in.-lb

The criterion used for eliminating terms was taken to be a value less than 1% of the value of the largest term in a set of comparable terms.

On the basis of the previous discussions, the final simplified tracking equations are the following

$$\begin{aligned}D_X = {} & I_x\ddot{\phi} + \mathring{h}_{c_x} + \dot{\psi}\phi h_{c_z} + \dot{\theta}\phi h_{c_y} - \omega_o\phi\cos\psi\, h_{c_y} - I_x\mathring{\psi}\mathring{\theta} + h_{c_z}\dot{\theta}\\ & - (I_y - I_z)\mathring{\psi}\dot{\theta} - I_x\theta\ddot{\psi} - h_{c_y}\dot{\psi} - \omega_o h_{c_z}\cos\psi + \omega_o\vartheta\sin\psi\, h_{c_y}\end{aligned}$$

$$\begin{aligned}D_Y = {} & I_y\ddot{\theta} + \dot{h}_{c_y} - \phi\dot{\theta}h_{c_x} + I_y\dot{\phi}\mathring{\psi} + \dot{\psi}h_{c_x} - \dot{\phi}h_{c_z} + I_y\phi\ddot{\psi}\\ & + \omega_o h_{c_z}\sin\psi + \omega_o\phi\cos\psi\, h_{c_x}\end{aligned}$$

$$\begin{aligned}D_Z = {} & I_z\ddot{\psi} - \phi\dot{\psi}h_{c_z} - \theta\dot{\psi}h_{c_y} + \dot{h}_{c_z} - h_{c_y}\omega_o\sin\psi - h_{c_x}\dot{\theta}\\ & + \omega_o\cos\psi\, h_{c_x} - I_z\phi\ddot{\theta} + I_z\omega_o\dot{\phi}\cos\psi + h_{c_y}\dot{\phi}\\ & - I_z\dot{\theta}\dot{\phi} + (I_y - I_x)\dot{\theta}\dot{\phi}\end{aligned}$$

APPENDIX C
THE INFLUENCE OF THE EARTH'S EQUATORIAL ELLIPTICITY ON THE NODAL AND INCLINATION PERTURBATIONS OF AN INCLINED 24-HOUR ORBIT

The Earth's force function in Earth radii units is given by (Ref 3-11)

$$U = \frac{\mu}{r}\left[1 + \sum_{n=2} \sum_{m=o}^{n} \frac{1}{r^n} J_n^{(m)} P_n^{(m)} (\sin \phi) \cos m (\lambda - \lambda_n^{(m)})\right]$$

where $$P_n^{(m)}(t) = \frac{1}{2^n n!} (1-t^2)^{m/2} \frac{d^{n+m}(t^2-1)^n}{dt^{n+m}}$$

The disturbing function, based on the $J_2^{(2)*}$, $J_3^{(1)}$, $J_3^{(3)}$, and $J_4^{(1)}$ sectorial and tesseral constants, which are indicated to be of equal magnitude, is written as

$$\begin{aligned} R = \frac{\mu}{r^3}\Big[& 3 J_2^{(2)} \cos^2 \phi (\cos 2\lambda \cos 2\lambda_2^{(2)} + \sin 2\lambda \sin 2\lambda_2^{(2)}) \\ & + \frac{3}{2} \frac{J_3^{(1)}}{r} (\cos \phi)(5 \sin^2 \phi - 1)(\cos\lambda \cos \lambda_3^{(1)} + \sin \lambda \sin \lambda_3^{(1)}) \\ & + \frac{15 J_3^{(3)}}{r} \cos^3 \phi (\cos 3\lambda \cos 3\lambda_3^{(1)} + \sin 3\lambda_3^{(1)}) \\ & + \frac{5}{2} \frac{J_4^{(1)}}{r^2} \cos \phi (7 \sin^3 \phi - 3 \sin \phi)(\cos \lambda \cos \lambda_4^{(1)} + \sin\lambda \sin\lambda_4^{(1)}\Big] \end{aligned}$$

Both latitude and longitude can be expressed in terms of Cartesian coordinates with respect to an inertially fixed reference system (see Figure 3-14); where

$$\cos \phi = \frac{\sqrt{x^2 + y^2}}{r} \qquad \sin 2\lambda = \frac{2\,xy}{x^2 + y^2}$$

$$\sin \phi = \frac{z}{r} \qquad \cos 2\lambda = \frac{x^2 - y^2}{x^2 + y^2}$$

$$\sin \lambda = \frac{y}{\sqrt{x^2 + y^2}} \qquad \sin 3\lambda = \frac{3x^2 y - y^3}{(x^2 + y^2)^{3/2}}$$

$$\cos \lambda = \frac{x}{\sqrt{x^2 + y^2}} \qquad \cos 3\lambda = \frac{x^3 - 3xy^2}{(x^2 + y^2)^{3/2}}$$

---

* $J_2^{(2)} = 2.32\text{x}10^{-6}$
$J_3^{(3)} = 3.95\text{x}10^{-6}$
$J_3^{(3)} = 2.64\text{x}10^{-6}$
$J_4^{(1)} = 1.91\text{x}10^{-6}$
$\lambda_2^{(2)} = 37.5°$ (longitude of major axis)
$\lambda_3^{(1)} = 22°$
$\lambda_3^{(3)} = 51.3°$
$\lambda_4^{(1)} = 163.5°$

The following equations are employed to transform the Cartesian coordinates into orbital parameters

$$\frac{x}{r} = \frac{1-\cos i}{2} \cos (\theta + \omega - \Omega + nt) + \frac{1+\cos i}{2} \cos (\theta + \omega + \Omega - nt)$$

$$\frac{y}{r} = \frac{1+\cos i}{2} \sin (\theta + \omega + \Omega - nt) - \frac{1-\cos i}{2} \sin (\theta + \omega - \Omega + nt)$$

$$\frac{z}{r} = \sin (\theta + \omega) \sin i$$

Consider a 24-hour circular satellite orbit ($\theta = n_s t$; $\omega = 0$). By appropriate substitution and simplification, the disturbing function becomes

$$R = \frac{\mu}{r_s^3} \Big[3J_2^{(2)} \Big\{ \frac{(1-\cos i)^2}{4} \cos (4n_s t - 2\Omega + 2\lambda_2^{(2)}) + \frac{(1+\cos i)^2}{4} \cos (2\Omega - 2\lambda_2^{(2)}) + \frac{\sin^2 i}{2} \cos (2\Omega - 2n_s t - 2\lambda_2^{(2)} \Big\}$$

$$+ \frac{5}{3} \frac{J_3^{(3)}}{r_s} \Big\{ 3 (1-\cos i)(1+\cos i) \Big[(1+\cos i) \cos (2n_s t - 3\Omega + 3\lambda_3^{(3)}) + (1-\cos i) \cos (4_n t - 3\Omega + 3\lambda_3^{(3)} \Big]$$

$$+ (1-\cos i)^3 \Big[2\cos 2 (2n_s t - \Omega) \cos (2n_s t - \Omega + 3\lambda_3^{(3)}) - \cos (2n_s t - \Omega - 3\lambda_3^{(3)}) \Big]$$

$$+ (1+\cos i)^3 \Big[2 \cos 2\Omega \cos (\Omega - 3\lambda_3^{(3)}) - \cos (\Omega + 3\lambda_3^{(3)}) \Big] \Big\}$$

$$+ \frac{3}{2} \frac{J_3^{(1)}}{r_s} \Big\{ (\frac{5}{2} \sin^2 i \Big[1 - \cos 2n_s t \Big] - 1) \frac{1-\cos i}{2} (2n_s t - \Omega + \lambda_3^{(1)}) + \frac{1+\cos i}{2} \cos (\Omega - \lambda_3^{(1)}) \Big\}$$

$$+ \frac{5}{2} \frac{J_4^{(1)}}{r_s} \Big\{ \sin n_s t \sin i (7 \sin^2 n_s t \sin^2 i - 3) (\frac{1-\cos i}{2} \cos (2n_s t - \Omega + \lambda_4^{(1)}) + \frac{1+\cos i}{2} \cos (\Omega - \lambda_4^{(1)} \Big\} \Big]$$

Nodal and inclination perturbations are given by the following planetary equations (Ref 3-6)

$$\frac{d\Omega}{dt} = \frac{1}{na^2 \sin i} \frac{\partial R}{\partial i}$$

$$\frac{di}{dt} = \frac{1}{na^2} \Big[- \frac{1}{\sin i} \frac{\partial R}{\partial \Omega} + \cot i \frac{\partial R}{\partial \omega} \Big]$$

Maximum element excursions are produced by the long period perturbations, hence, terms dependent on mean motion (n) are neglected. It is subsequently found that

$$\Delta\Omega = \frac{3n_s}{a^2\dot{\Omega}}\Big[-\frac{J_2^{(2)}}{4}(1+\cos i)\sin 2(\Omega-\lambda_2^{(2)}) + \frac{J_3^{(1)}}{2r_s}\sin(\Omega-\lambda_3^{(1)})(-\frac{5}{2}\sin^2 i+5\cos^2 i+\frac{1}{\sin i})$$

$$-\frac{5}{8}\frac{J_3^{(3)}}{r_s}(1+\cos i)^2\sin 3(\Omega+\lambda_3^{(3)})\Big]$$

$$\Delta i = \frac{-3n_s}{a^2\dot{\Omega}\sin i}\Big[\frac{J_2^{(2)}}{4}(1+\cos i)^2\cos 2(\Omega-\lambda_2^{(2)}) + \frac{J_3^{(1)}}{4r_s}\cos(\Omega-\lambda_3^{(1)})\Big\{(1+\cos i)(\frac{5}{2}\sin^2 i-1)$$

$$-(1-\cos i)\frac{5}{4}\sin^2 i\Big\} + \frac{5}{8r_s}J_3^{(3)}(1+\cos i)^3\cos 3(\Omega-\lambda_3^{(2)})\Big]$$